UNIVERSITÀ DEGLI STUDI DI SALERNO
DIPARTIMENTO DI INGEGNERIA INDUSTRIALE
VIA PONTE DON MELILLO 84084, FISCIANO
SALERNO

DOTTORATO IN SCIENZE MATEMATICHE, FISICHE E INFORMATICHE
CURRICULUM FISICA DEI SISTEMI COMPLESSI E DELL'AMBIENTE
CICLO XI NUOVA SERIE

PhD Thesis in

Gaussian and non-Gaussian resources in Quantum Information

CANDIDATE:
Gaetano Nocerino

SUPERVISOR:
Prof. Fabrizio Illuminati

COORDINATOR:
Prof. Patrizia Longobardi

2012-2013

Imago ergo sum

Enrico Baj, *La Patafisica*, Abscondita, Milano, 2009.

.....

Acknowledgments

I would like to express my gratitude to my supervisor, Prof. Fabrizio Illuminati, for having offered me the possibility to work in the Quantum Theory group of Salerno and for stimulating scientific discussions. I would also like to thank Prof. Silvio De Siena and Dott. Fabio Dell'Anno, for their availability. Their scientific guidance was really important. I would like to extend my gratitude to Dott. Alberto Porzio and Prof. Salvatore Solimeno for their exemplary critical spirit, with whom they have helped me to face the experimental work. I want to thank my partner Dott. Daniela Buono, for the useful discussions of physics and life.

CONTENTS

LIST OF TABLES

Part I

Introduction

This dissertation was carried out within the framework of the *Quantum Information* (**QI**). This recent branch of quantum physics, involving elements of quantum optics, can be schematically divided into four different and complementary subgroups: the protocol, the quantum states, the conditional measurements, and the dechoerence (see Figure 1). They are different because of the pursued objectives and of the problems facing; on the other hand, they are complementary, in the sense that in all areas of **QI** it is impossible to ignore even one of the four subgroups.

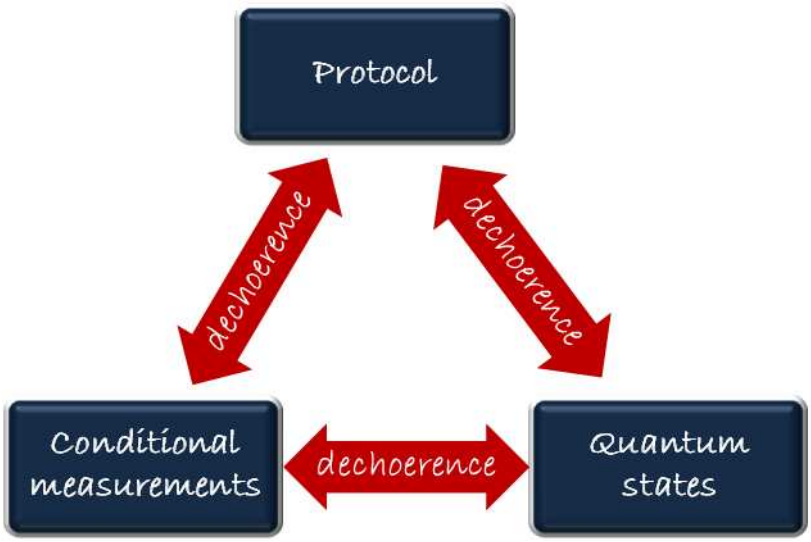

Figure 1: Schematic representation of the key elements of the Quantum Information.

In fact, the choice of the protocol automatically implies the preference of some quantum states (*resources*) compared to others. In turn, the preparation of quantum states is often made with conditional measures chosen *ad hoc*. Finally, all the measurements have non-unitary efficiencies and each quantum property, possessed by the resource and useful for the protocol, is afflicted by the effects of the external environment (*dechoerence*).

In this dissertation, we have consedered each of the four subgroups:

The protocol. – A protocol consists of a set of rules to follow in order to achieve a certain type of transmission of information. It defines the methods for the generation and preparation of the quantum states, compatibly to the interaction of the system with the external environment.

In this dissertation within of the 'protocol' subgroup, we have studied three fundamental tools of the **QI** expressed in terms of the *continuous variables* (**CV**) of the electromagnetic field:

- the teleportation protocol;

- the entanglement swapping protocol;
- Bell's theorem (which is the basis of some protocols such as the quantum cryptography).

We have dealt with the maximization of the efficiency of each protocol, by acting on the generation of the appropriate quantum states. In [1] Dell'Anno *et al* have shown that the squeezed Bell (**SB**) states are, to date, the more efficient theoretical states for the quantum teleportation. We have shown that even for the entanglement swapping protocol [2] and for the violation of the Bell's inequality [3], the **SB** states exhibit better performance than all the other **CV** quantum states.

Preparation of quantum states. – The quantum states represent the essential ingredient of each protocol. There are two important distinct classes: Gaussian and non-Gaussian states. The Gaussian states are described by a Gaussian characteristic function, all other states are non-Gaussian. Both the classes offer merits and defects, so the choice of using one or the other one depends on the type of used protocol and on the goals being sought. In this dissertation, we present an experimental scheme capable of generating, with good approximation, the **SB** states [4]. We have identified a scheme that is based on conditional measures performed on ancillary quantum states. We have started to study an ideal scheme (free by inefficiencies and decoherence), obtaining the reproduction of the **SB** states. Then we introduced the inefficiencies of detection, of the optical elements and of the conditional measurements. In the latter case, the scheme does not exactly reproduces the **SB** states, but tunable quantum states are obtained, which are very close to **SB** states. They exhibit a greater teleportation fidelity than all other realistic quantum states that we have analyzed.

In addition, in collaboration with Prof. Salvatore Solimeno and Dr. Alberto Porzio of University of Naples "Federico II", we have studied (the work is still at a preliminary stage) the non-Gaussianity introduced by fluctuations in the pump amplitude of the Optical Parametric Oscillator (**OPO**) below threshold and with non-degenerate polarization. We have solved the coupled Langevin equations of the three electromagnetic fields involved in the dynamic of the **OPO** system (*i.e.* pump, idler, and signal). We have considered the following fluctuating quantities [5]: optical length of the cavity **OPO**, the susceptibility of the crystal of second harmonic generation, the frequency and amplitude of the pump field. The solution is expressed in the phase space, in terms of the characteristic function or, equivalently, of the Wigner's function. We have calculated the fidelity of teleportation of a coherent state, when the output state of the fluctuating **OPO** is used as a resource for the teleportation. We have proved that such fluctuations lead to an increase of fidelity of teleportation with respect to the case not fluctuating (and gaussian). This suggests that the classic noise, introduced by the fluctuations, can increase the value of a quantum quantity such as the fidelity of teleportation,

making the non-Gaussian state, generated by **OPO** with fluctuating pump, better than the Gaussian case (non-fluctuating pump).

Conditional Measurements. – In the context of the **QI**, conditional measurements are used to prepare quantum states and to optimize the transfer of information, as required by the specific protocol. Often, in order to generate the states most suitable for a certain type of protocol, it is necessary to combine the input states with a set of other quantum states, said ancillary states. Then the latter are appropriately measured in order to obtain output states with the desired characteristics.

We propose a rather general formulation of the method of conditioning through ancillary measurements, in terms of the characteristic functions. In this formalism, we have expressed both density operators describing the involved states, both operators (**POVM**) describing the quantum measurements. Then, we have considered the case of simultaneous measurements of *single-photon*, of *homodyne detection*, and of *on/off type* (via ideal and realistic **POVM**). This approach is used for the calculation of the state actually generated by the experimental scheme of generation of the **SB** states.

Dechoerence. – The quantum properties are very sensitive to the interaction of the quantum systems with the external environment. In quantum optics even the vacuum is modeled as an set of infinite harmonic oscillators, each of which interacts with the considered physical system. This circumstance requires not to neglect the effects of deterioration that the environment determines on the physical systems. For this reason, a part of this dissertation is devoted to analysis of the evolution of some quantum quantities under the action of the dechoerence. In particular, we have studied how the effects of decoherence acting on the following quantities: the purity, the quantum correlations, the content of information, the fidelity of teleportation of a coherent state [6], and the Bell's inequality [7] of a bi-partite Gaussian state that is transmitted through a realistic channel.

As regards the correlations, we have studied the different types of correlations that can be observed in a bi-partite Gaussian state. The quantum correlations arise from the superposition principle of the quantum mechanics and from the collapse of the wave function (or, more generally, of the matrix density). Hence, the correlations are dependent not only by the state, but also by the measures which are performed on the state in order to derive informations. These different aspects cause different types of correlation, so they are related to different quantum markers. The issue is further complicated by the fact that for mixed states there is not a satisfactory measure of entanglement. However, there are some criteria which determine if the state is entangled or not. These demarcation criteria are: the criterion of Duan, of PHS and of EPR-Reid.

In this context, we have added the experimental verification to the theoretical study. In collaboration with the University of Naples "Federico II" and under the guidance of Dr. Alberto Porzio and of Prof. Salvatore Solimeno, we carried out

laboratory activities on [8]:

- Study of the generation of bi-partite Gaussian states produced by non-degenerate polarization, below threshold **OPO**;
- Thermal stabilization through the realization of an electronic circuit (with negative feedback control);
- Optimization of the electronic chain for the stabilization of the optical length of two optical cavities through the Pound-Drever-Hall technique;
- Study of the homodyne detection technique. In particular, we have used a single homodyne for the characterization of a bi-partite Gaussian state [78];
- Writing of programs, in LabviewPro8 language, for the management of rotators, laminae of delay and for faster acquisition of the collected data, and statistical analysis;
- Writing of programs, in Mathematica language, for the search of triple resonance temperature of the **OPO**;
- Simulation of a realistic transmission channel with an optical attenuator with variable absorption coefficient.

In this dissertation, we have reported the results of the laboratory activities. In particular, from the measurements performed for different absorption values, we have calculated the quantum properties of the state and found an excellent agreement with the theoretical expectations [6], even at high absorptions [9].

This dissertation is organized as follows:

In the Chapters 1 and 2, we have present a brief introduction on all the fundamental concepts of **QI** and of quantum optics, more often mentioned during the dissertation. We remark that in Chapter 1 it is reported the definition of the **SB** states and the formalization, in terms of the characteristic function formalism, of the method of the conditional measurements. In the Chapter 2 we present the main properties of a quantum state. Moreover, we discuss the problem of the entanglement quantification. We present also the **CV** teleportation protocol and the type of non-locality introduced by the Bell's inequality.

In the Chapter 3, we have explored the Bell's inequality using the Gaussian and non-Gaussian **CV** resources. In particular, we discuss two different approaches to inequality: the pseudospins approach (Sect. 3.1) and the Wigner's function approach (Sect. 3.2). In both formulations, the non-Gaussian **SB** resources prove to be less suitable for a *local* classical description. In the case of Gaussian resource (squeezed vacum state or twin beam), we emphasize the link between the state purity, the entanglement (valued through the criterion of Duan) and the violation of the Bell's inequality.

In the Chapter 4, we present the realistic entanglement swapping protocol with Gaussian and non-Gaussian resources. In the realistic protocol we consider the inefficiencies of detection and the interaction with the external environment. In any case, we show that the non-Gaussian **SB** states are the best resource for the entanglement swapping protocol, compared to other Gaussian (twin beam) and non-Gaussian (*e.g.* the photon-subtracted squeezed states) states [2].

In the Chapter 5, we propose an experimentally feasible scheme for the realization of the fundamental non-Gaussian **SB** resources. We show that in the ideal case, the proposed scheme creates exactly the **SB** states; in the realistic case, the producted states are very close to the **SB** states.

In the Chapter 6, we analyze the evolution of the "quantumness" of a Gaussian state, when the system interacts with the environment (Gaussian channel). We experimentally find that, even in presence of strong decoherence, the state generated by a sub—threshold **OPO** never disentangles, keeps breaking the quantum limit for the discord and, as resource for quantum teleportation of a coherent state, would allow, in principle, to realize quantum teleportation over an infinitely long Gaussian channel.

In the Chapter 7, we rough out the calculation of the characteristic function of the **OPO** with fluctuating pump. It exhibits a non-Gaussianity useful for the teleportation protocol of a coherent state.

Eventually, in Appendix A, we present a nice discussion about the beam splitter, which is an essential element both for laboratory activities of Quantum Optics, and as mathematical tool capable of modeling the interaction of a quantum state with a thermal bath (and therefore with the quantum vacuum).

CHAPTER 1

ELEMENTS OF QUANTUM INFORMATION

In this Chapter, we analyze the foundations of the Quantum Optics that are the basis of the main aspects of the modern Quantum Information. We start from some primitive concepts: representation of the quantum states (Sect. 1.1) through two different approaches (density matrix and characteristic function); observables and uncertainty principle (Sect. 1.2); Gaussian and non-Gaussian quantum states of the light radiation (Sect. 1.3). In particular, we discuss a general class of the non-Gaussian quantum states (the **SB** states), to which we will often refer in the following Chapters of this dissertation. In Sect. 1.4, we present a disquisition on the concept of the conditional measures, proposing a formalization of a rather general circumstances. In Sect. 1.5, we treat briefly the theory of the open quantum systems, specializing the results to the realistic transmissions.

1.1 Density Matrix *versus* Characteristic Function

In this Section, we review the basic properties of the density matrix and we discuss its connection with the characteristic function. We especially want to highlight the properties that will be used later.

Each observable physical quantity of a quantum system is represented by a Hermitian operator O. Its expectation value is

$$\langle O \rangle = \langle \psi \, | O | \, \psi \rangle \, , \tag{1.1}$$

where the ket $|\psi\rangle$ represents the wave function in the Dirac's operatorial formalism [10]. When the quantum system is in a mixture of states[1], it is not expressible with the simple ket $|\psi\rangle$. It becomes necessary to use the description of the state through the *density matrix* ρ. The expectation value of O, Eq.(1.1), is given by $\mathrm{Tr}[\rho O]$. The density matrix is a bounded positive Hermitian operator representing the state of the system. It is definited by convex sum of the projector operators $\Pi_n \equiv |\psi_n\rangle \langle \psi_n|$ of the normalized state $|\psi_n\rangle$ belonging to the Hilbert space $\mathcal{H}_S$ of the system,

$$\rho_S \equiv \sum\nolimits_n p_n \Pi_n \ , \tag{1.2}$$

[1] We will see that in nature there are no physical systems (strictly contained in the Universe) which can be described by simple kets. This is because no system is isolated from its environment. In fact for the interaction of the system with the vacuum, a pure state immediately becomes mixed. Otherwise, not all the mixed states are born pure.

However, the pure states are a useful abstraction and they can be seen as the states to which a realistic state tends *asymptotically* (at birth).

where the real coefficients $p_n = p(\Pi_n)$, represent a good probability measure over the Hilbert space describing the quantum system. In fact, p is a map of each projector operator, Π_n, to a real number, $p(\Pi_n)$, onto the interval $[0,1]$,

$$p : \Pi_n \rightarrow p(\Pi_n) \ ,$$

such that it satisfies the quantum version of the Kolmogorov probability axioms [11]:

- $\sum_n p_n = 1$;
- $p(\mathbb{O}) = 0$ and $p(\mathbb{I}) = 1$ with $\mathbb{O} = |0\rangle\langle 0|$ and $\mathbb{I} = \sum_{j=0}^{\infty} |j\rangle\langle j|$, being $|j\rangle$ Fock state, $j \in \mathbb{N}$;
- $p\left(\sum_j \Pi_j\right) = \sum_j p(\Pi_j)$.

The fundamental Gleason's theorem shows that all probability measure $p(\Pi_n)$ are of the form

$$p(\Pi_n) \equiv \mathrm{Tr}\left[\rho_S \Pi_n\right] \ ,$$

if the matrix ρ_S satisfies the following conditions

1. It is a unitary trace, $1 = \mathrm{Tr}[\rho_S] = p(\mathbb{I})$;
2. It is hermitian, $\rho_S = \rho_S^{\dagger}$;
3. It is semipositive, $\mathrm{Tr}[\rho_S \Pi_n] \geq 0 \ \forall n$.

The coefficients $p(\Pi_n)$ are also interpreted as the probability that the system, described by a mixture of states $\sum_n p_n |\psi_n\rangle\langle\psi_n|$, is in the state $|\psi_n\rangle$.

Now, we can introduce the measure of the purity of a quantum state. The state (1.2) is said *pure* if $\exists!\ n = \bar{n} : p_{\bar{n}} = 1$ for which $\rho_S = \Pi_{\bar{n}}$ being $p_n = 0$, $\forall n \neq \bar{n}$. The state is *mixed* if $\forall n$ we have that $p_n < 1$, in this case the sum in ρ_S, Eq.(1.2), can not be reduced to a single term. These properties of purity of a quantum state, combined with the conditions 1, 2 and 3, suggest the introduction of the following measure of purity:

$$\mu = \mathrm{Tr}\left[\rho_S^2\right] \ . \tag{1.3}$$

The Eq. (1.3) is an appropriate measure of purity. In fact, calculating the quantity ρ_S^2 we obtain:

$$\begin{aligned} \rho_S^2 &= \sum_{n,m} p_n p_m \Pi_n \Pi_m \\ &= \sum_n p_n^2 \Pi_n \end{aligned}$$

being $\Pi_n \Pi_m = \delta_{nm} \Pi_n$, and therefore the Eq. (1.3) reduces to

$$\begin{aligned} \mathrm{Tr}\left[\rho_S^2\right] &= \sum_n p_n^2 \\ &\leq 1 \, . \end{aligned}$$

In particular, $\mathrm{Tr}[\rho_S^2] = 1 \Leftrightarrow \rho_S$ is pure $(\exists! n = \bar{n} : p_{\bar{n}} = 1)$.

We consider a system S composed by N bosonic sub-systems described by annihilation operators a_k, with $k = 1, ..., N$, and such that the commutation relations are $[a_k, a_h^\dagger] = \delta_{kh}$ for $k, h = 1, ...N$. The system S is the union of the N sub-systems, labelled with S_k, so $S = \bigcup_{k=1}^N S_k$. It is described by vectors in the Hilbert space $\mathcal{H}_S = \bigotimes_{k=1}^N \mathcal{H}_k$, being $\mathcal{H}_k$ the Hilbert space of the sub-system $k-$th.

When it is known the density matrix, ρ_S, of the system, it is possible to determinate the density matrix of the sub-system k using the partial trace operation. It is defined as

$$\rho_k = \mathrm{Tr}_{1,...,k-1,k+1,...N}\left[\rho_S\right] \ , \tag{1.4}$$

where $\mathrm{Tr}_{1,...,k-1,k+1,...N}$ is the trace operation done on all N sub-systems excluding the $k-$th sub-system. The operators ρ_k satisfy all the properties of density matrices. They are called reduced density matrices and describe the sub-systems S_k.

Example 1 *Purity of a bi-partite quantum state − In the case bi-partite state, we have $\mathcal{H}_S = \mathcal{H}_1 \otimes \mathcal{H}_2$. We suppose that the overall state, given by the density matrix ρ_S, is the pure state $\rho_S = |\psi\rangle_{12\ 12} \langle\psi|$ with*

$$|\psi\rangle_{12} = \sum_{n_1, n_2} c_{n_1,n_2} |n_1\rangle_1 \otimes |n_2\rangle_2$$

written as a linear combination of two-mode Fock states of two modes and such that $\sum_{n_1,n_2} |c_{n_1,n_2}|^2 = 1$ for the normalization. We calculate the density matrix of the sub-system $1(2)$, using the definition of Eq.(1.4). We have

$$\begin{aligned} \rho_{1(2)} &= Tr_{2(1)}\left[\rho_S\right] \\ &= \sum_{n_1 n_2} |c_{n_1,n_2}|^2 \left|n_{1(2)}\right\rangle_{1(2)\ 1(2)} \left\langle n_{1(2)}\right| \ , \end{aligned}$$

so

$$\rho_{1(2)}^2 = \sum_{n_1 n_2} |c_{n_1,n_2}|^4 \left|n_{1(2)}\right\rangle_{1(2)\ 1(2)} \left\langle n_{1(2)}\right| \ ,$$

and

$$\mu = \mu_{1(2)} = Tr\left[\rho_{1(2)}^2\right] = \sum_{n_1,n_2} |c_{n_1,n_2}|^4 \, .$$

So we can deduce that the purity μ is limitate to 1. In particular, $\mu_1 = 1$ iff $\exists!$ $n_1, n_2 = \bar{n}_1, \bar{n}_2 : c_{\bar{n}_1,\bar{n}_2} = 1$ so the state $|\psi\rangle_{12} = |\bar{n}_1\rangle_1 \otimes |\bar{n}_2\rangle_2$ is factorizable in the tensor product of the state $|\bar{n}_1\rangle_1$ and $|\bar{n}_2\rangle$ of the two sub-systems. Otherwise, $\mu_1 < 1$, strictly; in latter case the state $|\psi\rangle_{12}$ is not factorizable and the systems 1 and 2 are called quantum correlated or entagled [12]. As will be established later, the purity can give indications on correlations between the two sub-systems of a pure bi-partite system.

Another representation of the quantum state is in terms of the phase space functions. The characteristic function is one of them. It is defined as

$$\chi_{\rho_S}(\boldsymbol{\alpha}) = \mathrm{Tr}\left[\rho_S D_N(\boldsymbol{\alpha})\right] \ , \tag{1.5}$$

where $\boldsymbol{\alpha}$ is the complex column vector $\boldsymbol{\alpha} = (\alpha_1, ...\alpha_N)^{\mathsf{T}}$, $\alpha_k \in \mathbb{C}$, and

$$D_N(\boldsymbol{\alpha}) = \bigotimes_{k=1}^{N} D_k(\alpha_k)$$

is the tensor product of N single mode dispacement operators

$$D_k(\alpha_k) = \exp\left\{\alpha_k a_k^\dagger - \alpha_k^* a_k\right\}.$$

Then the characteristic function is the expectation value of the multimode operator $D_N(\boldsymbol{\alpha})$ and, since $D_N(\boldsymbol{\alpha})$ is unitary, the magnitude of each of its eigenvalues is limited from 1. Hence $\left|\chi_{\rho_S}(\boldsymbol{\alpha})\right| \leq 1$ and its maximum value is given by $\chi_{\rho_S}(\mathbf{0}) = \mathrm{Tr}[\rho_S \mathbb{I}] = 1$ for the propriety 1 of the density matrix.

It is easy to prove some important properties of $\chi_{\rho_S}(\boldsymbol{\alpha})$. Let us O_1 and O_2 two generic operators acting on the Hilbert space $\mathcal{H}_S$, we have

$$\mathrm{Tr}\left[O_1 O_2\right] = \frac{1}{\pi^N}\int_{\mathbb{C}^N} d^{2N}\boldsymbol{\alpha}\, \chi_{O_1}(\boldsymbol{\alpha})\, \chi_{O_2}(-\boldsymbol{\alpha}) \ , \tag{1.6}$$

where $d^{2N}\boldsymbol{\alpha} = d\alpha_1 ... d\alpha_N d\alpha_1^* ... d\alpha_N^*$. To obtain this expression we have used the property $\mathrm{Tr}[D_k(\alpha_k)] = \pi\delta^{(2)}(\alpha_k)$ and the completeness of the set of displacement operators $D_N(\boldsymbol{\alpha})$, for which any generic operator O can be expressed as

$$O = \frac{1}{\pi^N}\int_{\mathbb{C}^N} d^{2N}\boldsymbol{\alpha}\, \chi_{\rho_S}(\boldsymbol{\alpha})\, D_N^\dagger(\boldsymbol{\alpha}) \ . \tag{1.7}$$

The Eq.(1.6) allows to evaluate the expectation value, with respect to state ρ_S, of an operator O acting on the Hilbert space $\mathcal{H}_S$

$$\begin{aligned} \langle O\rangle_{\rho_S} &\equiv \mathrm{Tr}\left[\rho_S O\right] \\ &= \frac{1}{\pi^N}\int_{\mathbb{C}^N} d^{2N}\boldsymbol{\alpha}\, \chi_{\rho_S}(\boldsymbol{\alpha})\, \chi_O(-\boldsymbol{\alpha}) \ , \end{aligned}$$

where $\chi_O(-\boldsymbol{\alpha}) = \mathrm{Tr}[OD_N(-\boldsymbol{\alpha})]$ is the characteristic function of the operator O. From Eq.(1.6), we can also rediscover the purity μ of the quantum state ρ_S expressed in the characteristic function formalism:

$$\begin{aligned}\mu &= \mathrm{Tr}\left[\rho_S^2\right] \\ &= \frac{1}{\pi^N}\int_{\mathbb{C}^N} d^{2N}\boldsymbol{\alpha}\chi_{\rho_S}(\boldsymbol{\alpha})\chi_{\rho_S}(-\boldsymbol{\alpha}) \\ &= \frac{1}{\pi^N}\int_{\mathbb{C}^N} d^{2N}\boldsymbol{\alpha}\left|\chi_{\rho_S}(\boldsymbol{\alpha})\right|^2 \end{aligned} \tag{1.8}$$

Using the property $\left|\chi_{\rho_S}(\boldsymbol{\alpha})\right| \leq 1$ we see that the *purity* is a positive quantity and it is bounded by 1 (so $0 \leq \mu \leq 1$).

Another useful property of the characteristic function is the simple connection with the expectation values of the moments of symmetrically ordereding operators of creation and annihilation. In fact,

$$(-)^l \frac{\partial^{l+m}}{\partial\alpha_k^l \partial\alpha_h^{*m}}\chi_{\rho_S}(\boldsymbol{\alpha})\Big|_{\boldsymbol{\alpha}=\mathbf{0}} = \mathrm{Tr}\left[\rho_S\left[\left(a_k^\dagger\right)^l a_h^m\right]_{\mathrm{Symm}}\right], \tag{1.9}$$

where the subscript $_{\mathrm{Symm}}$ indicates the symmetric order, so

$$\begin{aligned}\left[a^\dagger a\right]_{\mathrm{Symm}} &= \frac{1}{2}\left(a^\dagger a + aa^\dagger\right), \\ \left[a^\dagger a^2\right]_{\mathrm{Symm}} &= \frac{1}{3}\left(a^2a^\dagger + a^\dagger a^2 + aa^\dagger a\right), \\ &\textit{so on...}\end{aligned}$$

The Fourier transform of the characteristic function defines the so-called Wigner function [13, 14]:

$$W_{\rho_S}(\boldsymbol{\beta}) \equiv \frac{1}{\pi^{2N}}\int_{\mathbb{C}^N} d^{2N}\boldsymbol{\alpha}e^{\beta^*\alpha-\alpha^*\beta}\chi_{\rho_S}(\boldsymbol{\alpha}).$$

It can be expressed also through the parity operator $\mathfrak{P} = \bigotimes_{k=1}^N (-)^{a_k^\dagger a_k}$ of the photon number for the mode k; we have:

$$W_{\rho_S}(\boldsymbol{\beta}) = \left(\frac{2}{\pi}\right)^N \mathrm{Tr}\left[\rho_S D(\boldsymbol{\beta})\mathfrak{P}D^\dagger(\boldsymbol{\beta})\right]. \tag{1.10}$$

1.2 Osservables and uncertainty principle

In this Section we briefly discuss the connection between observable physical quantities and mathematical operators in quantum mechanics. In addition, we present a general derivation of the uncertainty principle of Heisenberg. Eventually,

we focus on quantum states that have minimum uncertainty, making some specific examples.

In quantum mechanics, observable quantities are described by Hermitian operators A, such that $A = A^\dagger$. What we measure of an observable operator are its average value $\langle A \rangle$, its variance $\langle \Delta A^2 \rangle$, or, in general, the higher moments. Such quantities can be calculated with the procedure introduced before: $\langle O \rangle = \mathrm{Tr}[O\rho]$ where ρ is the quantum state with respect to which to calculate the average value of the operator $O\,(= A,\, A^2 - A,\, ...)$. However, in contrast to the classical case, in quantum mechanics there is a restriction on the simultaneous observation of the variances of non-commuting observables. In fact, they do not admit common eigenvectors and thus it is impossible to measure simultaneously these observables with arbitrary accuracy. The application of the Scwarz's inequality, that is valid in any Hilbert space, has an important consequence about the possibility to measure two non-commuting observables A and B such that $[A, B] \neq 0$, known as *uncertainty principle of Heisenberg*. In order to prove this important theoretical and experimental limitation, we start from the Schwarz inequality

$$\begin{aligned} \left\langle \Delta A^2 \right\rangle \left\langle \Delta B^2 \right\rangle &\geq |\langle \sigma_{AB} \rangle|^2 + |\langle C_{AB} \rangle|^2 \\ &\geq |\langle C_{AB} \rangle|^2 \ , \end{aligned} \tag{1.11}$$

where $\sigma_{AB} = \frac{1}{2}\{A, B\} - \langle A \rangle \langle B \rangle$ is a measure of correlations between A and B, being $\{A, B\} = AB + BA$, and $C_{AB} = \frac{1}{2}[A, B]$. We can note that when the operators are Hermitian (as it is for the all obsevables), the operators σ_{AB} and C_{AB} are also Hemitian. Let consider the two vector

$$\begin{aligned} |\psi_1\rangle &= (A - \langle A \rangle)\,|\psi\rangle \\ |\psi_2\rangle &= (B - \langle B \rangle)\,|\psi\rangle \ . \end{aligned}$$

The operator of the type $O - \langle O \rangle$ has the same variance of the operator O but in the first case the average value is shifted by the amount $-\langle O \rangle$; so $\langle (O - \langle O \rangle) \rangle = 0$. The uncertainty relation is miminum when the two vectors are parallel in the Hilbert space, $|\psi_1\rangle = -i\lambda\,|\psi_2\rangle$, where λ is a complex number. In fact, in this way we have

$$(A + i\lambda B)\,|\psi\rangle = (\langle A \rangle + i\lambda \langle B \rangle)\,|\psi\rangle \ . \tag{1.12}$$

The state $|\psi\rangle$ that satisfies the Eq.(1.12) is called *minimum uncetainty state*. We can prove that the states $|\psi\rangle$, that satisfy this property, are Gaussian [15]. We can use the Eq. (1.12) in order to determine the relationship between variances of two observables. We have that

$$\begin{aligned} \left\langle \Delta A^2 \right\rangle &= -i\lambda \left(\langle \sigma_{AB} \rangle + i \langle C_{AB} \rangle \right) \ , \\ \left\langle \Delta B^2 \right\rangle &= \frac{i}{\lambda} \left(\langle \sigma_{AB} \rangle - i \langle C_{AB} \rangle \right) \ . \end{aligned}$$

Expliciting real part, λ_r, and imaginary part, λ_i, of the parameter $\lambda = \lambda_r + i\lambda_i$, the above relations become

$$\begin{aligned} \left\langle \Delta A^2 \right\rangle &= \lambda_i \left\langle \sigma_{AB} \right\rangle + \lambda_r \left\langle C_{AB} \right\rangle \ , \\ \left\langle \Delta B^2 \right\rangle &= \frac{1}{|\lambda|^2} \left\langle \Delta A^2 \right\rangle \ , \end{aligned}$$

with $\lambda_r \left\langle \sigma_{AB} \right\rangle - \lambda_i \left\langle C_{AB} \right\rangle = 0$. These relations imply the following cases:

1. $|\lambda| = 1$ and $\lambda_i \neq 0$. In this case $\langle \Delta A^2 \rangle = \langle \Delta B^2 \rangle$ and the corresponding state is a *minimum uncertainty state* with *equal variance* for both the observables. The coherent state (see next Section) belongs to this case. For it the two operators A and B are the observables, called *field operators* or *quadrature operators*, definited as linear combination of creation and annihilation operators

$$X \equiv \mathfrak{X}_0 = \frac{1}{\sqrt{2}} \left(a^\dagger + a \right) \ , \tag{1.13}$$

$$Y \equiv \mathfrak{X}_{\pi/2} = \frac{i}{\sqrt{2}} \left(a^\dagger - a \right) \ , \tag{1.14}$$

   where

$$\mathfrak{X}_\theta \equiv \frac{1}{\sqrt{2}} \left(a e^{-i\theta} + a^\dagger e^{i\theta} \right)$$

   is the generalized field operator, such that $[\mathfrak{X}_\theta, \mathfrak{X}_{\theta'}] = i \sin(\theta - \theta')$. We will often use these important observables of the electromagnetic field in the course of this dissertation.

2. $\lambda = \lambda_r$. In this case then $\langle \sigma_{AB} \rangle = 0$. The operators A and B are uncorrelated, with the variances given by

$$\begin{aligned} \left\langle \Delta A^2 \right\rangle &= \lambda_r \left\langle C_{AB} \right\rangle \ , \\ \left\langle \Delta B^2 \right\rangle &= \frac{1}{\lambda_r} \left\langle C_{AB} \right\rangle \ , \end{aligned}$$

   then $\lambda_r \gtrless 0$ implies $\langle \Delta A^2 \rangle \gtrless \frac{1}{2}[A, B]$ and $\langle \Delta B^2 \rangle \lesseqgtr \frac{1}{2}[A, B]$, simultaneously. This is case of the *squeezed vacuum state* [16] (see next Section). The uncertainty principle is respected, but it happens that the single observable exhibits variance smaller of the variance of the vacuum state, fixed by $|\langle C_{AB} \rangle| = \frac{1}{2}$.

3. $\lambda_r, \lambda_i \neq 0$. In this case we have:

$$\begin{aligned} \left\langle \Delta A^2 \right\rangle &= \frac{|\lambda|^2}{\lambda_r} \langle C_{AB} \rangle \ , \\ \left\langle \Delta B^2 \right\rangle &= \frac{1}{\lambda_r} \langle C_{AB} \rangle \ , \\ \langle \sigma_{AB} \rangle &= \frac{\lambda_i}{\lambda_r} \langle C_{AB} \rangle \ . \end{aligned}$$

i.e. the variances and the correlations are expressed as function of the average of the commutator $\langle C_{AB} \rangle$. This is the case of the like-position and -momentum operaotors (q, p), for which we have $C_{qp} = \frac{\hbar}{2}\mathbb{I}$ and $\lambda_r > 0$.

A quantum state which violates the Heisenberg's inequality is said *non-physical*.

1.3 Quantum states of **CV** light radiation

In this Section, we present some quantum states of **CV** light radiation in the characteristic function formalism, dividing them into two main classes: Gaussian and non-Gaussian class, respectively. At first, we define a generic Gaussian multimodal system, and then specialize the obtained results for the bi-partite case. Later we will briefly discuss two important Gaussian states: coherent states and thermal states. Then we will present a general class of states typically non-Gaussian: the **SB** states. Finally, we will analyze the variances of the quadrature operators (Eqs. (1.13−1.14)) with respect to the **SB** states.

1.3.1 The Gaussian States

In this subsection we introduce an important peculiarity of some states of light radiation: the Gaussianity. A quantum state is called *Gaussian* if its characteristic function has a Gaussian form.

We consider a bosonic system composed by N sub-systems and we introduce the column vector of the field quadratures for the $N-$modes of the field

$$\mathbf{K} \equiv (X_1, Y_1, ..., X_N, Y_N)^{\mathsf{T}} \, ,$$

as we have defined them in Eqs.(1.13) and (1.14), such that

$$\begin{aligned} [X_k, Y_{k'}] &= i\delta_{kk'} \ , \\ [X_k, X_{k'}] &= [Y_k, Y_{k'}] = 0 \ , \end{aligned}$$

or equivalently

$$[K_k, K_h] = i\Omega_{kh}, \quad (k, h = 1, ..., 2N) \ ,$$

where

$$\mathbf{\Omega} \equiv \bigoplus_{k=1}^{n} \boldsymbol{\omega} \ , \quad \boldsymbol{\omega} = \begin{pmatrix} 0 & 1 \\ -1 & 0 \end{pmatrix} \ ,$$

and $\bigoplus$ denotes the diret sum.

The state ρ is said to be a Gaussian state if the corresponding characteristic function is Gaussian,

$$\begin{aligned} \chi(\mathbf{\Lambda}) &= \mathrm{Tr}\left[\rho D_N(\boldsymbol{\alpha})\right] \\ &= \exp\left\{-\frac{1}{2}\mathbf{\Lambda}^{\mathsf{T}}\mathbf{\Omega}\boldsymbol{\sigma}\mathbf{\Omega}^{\mathsf{T}}\mathbf{\Lambda} - i\mathbf{\Lambda}^{\mathsf{T}}\mathbf{\Omega}\langle\mathbf{K}\rangle\right\} \ , \end{aligned}$$

with $\mathbf{\Lambda} = (\mathsf{a}_1, \mathsf{b}_1, ..., \mathsf{a}_N, \mathsf{b}_N)^{\mathsf{T}} \in \mathbb{R}^{2N}$ such that $\alpha_k = (\mathsf{a}_k + i\mathsf{b}_k)/\sqrt{2}$ and $\langle\mathbf{K}\rangle$, usually referred to as first moment, is the column vector of the average of the quadrature operators. The Gaussian states are completely characterized by the first and second moments of the field quadrature $\langle\mathbf{K}\rangle$ and $\boldsymbol{\sigma}$, respectively. Moreover, the quantities that characterize the quantum properties of the state are invariant with respect to a translation of the first moments. Therefore, the assumption $\langle\mathbf{K}\rangle = 0$ is lawful and, without loss of generality, it is possible to use the simple form

$$\chi(\mathbf{\Lambda}) = \exp\left\{-\frac{1}{2}\mathbf{\Lambda}^{\mathsf{T}}\mathbf{\Omega}\boldsymbol{\sigma}\mathbf{\Omega}^{\mathsf{T}}\mathbf{\Lambda}\right\}.$$

In spite of the infinite-dimensional Hilbert space, a complete description of an arbitrary Gaussian state is therefore obtainable via the finite-dimensional covariance matrix ($2N \times 2N$). We define the covariance matrix (**CM**), where the moments are calculated as in Eq.(1.11),

$$\sigma_{kh} \equiv (\boldsymbol{\sigma})_{kh} = \frac{1}{2}\langle\{K_k, K_h\}\rangle - \langle K_k\rangle\langle K_h\rangle \ .$$

We can observe that the diagonal elements ($k = h$) of $\boldsymbol{\sigma}$ are the autocorrelations of the quadrature operators, while the off-diagonal elements ($k \neq h$) are related to the correlations between quadratures of different modes. When the matrix elements, σ_{kh}, are calculated with respect to the vacuum state, the covariance matrix takes the diagonal form, $\boldsymbol{\sigma} = \boldsymbol{\sigma}_{vac} = \frac{1}{2}\mathbb{I}$ with $\frac{1}{2}$ the value of the vacuum variance.

The uncertainty relation imposes a restriction on the elements of the covariance matrix; in terms of the operators of quadrature it becomes

$$\boldsymbol{\sigma} + \frac{i}{2}\mathbf{\Omega} \geq 0, \tag{1.15}$$

and it expresses, in a compact form, the positivity of the density matrix of

the state[2]. This inequality is known as the uncertainty relation of Robertson-Schrodinger [17], [18].

In terms of quadrature operators of the field, we can write the average number of photon in a system of N sub-systems as

$$\sum_{k=1}^{N} \left\langle a_k^\dagger a_k \right\rangle = \frac{1}{2} \sum_{h=1}^{2N} \left(\sigma_{hh} + \langle K_h \rangle^2 \right) . \tag{1.16}$$

S we see that the diagonal terms σ_{hh} of the covariance matrix are proportional to the number of average photons in the mode k, hence to the energy of the itself mode**.**

The purity of state, defined in Eq.(1.8), can be easily expressed in terms of the covariance matrix. We have

$$\mu = \frac{1}{2^N \sqrt{\det \left[\boldsymbol{\sigma} \right]}} . \tag{1.17}$$

Hence a Gaussian state is pure iff

$$\det \left[\boldsymbol{\sigma} \right] = \frac{1}{2^{2N}} .$$

1.3.1.1 Bi-partite mixed case

We specialize the notations of the previous Section to the case of bi-partite mixed Gaussian states [8]. When $N = 2$, the overall Hilbert $\mathcal{H}$ space is given by tensor product of two Hilbert spaces $\mathcal{H}_A \otimes \mathcal{H}_B$. The covariance marix of system is a 4×4 square matrix which can be written as follows:

$$\boldsymbol{\sigma} = \begin{pmatrix} \mathbf{A} & \mathbf{C} \\ \mathbf{C}^\intercal & \mathbf{B} \end{pmatrix} . \tag{1.18}$$

$\mathbf{A}$ and $\mathbf{B}$, are the 2×2 square covariance matrices associated to the states of sub-systems A and B, respectively, while the 2×2 matrix $\mathbf{C}$ describes the correlations between the two sub-systems. Due to the Theorem of Williamson[3] [19] for the Gaussian states, it is possible to choose a generic symplectic transormation $\mathbf{S}_A \oplus \mathbf{S}_B$, $(\mathbf{S}_A, \mathbf{S}_B \in Sp\left(4, \mathbb{R}\right))$, that acts on $\boldsymbol{\sigma}$ and diagonalizes the matrices $\mathbf{A}$, $\mathbf{B}$, and $\mathbf{C}$:

$$\mathbf{A} \rightarrow \mathbf{S_A A S_A^\intercal} = \begin{pmatrix} n & 0 \\ 0 & n \end{pmatrix} ,$$

[2] A quantum state which violates the inequality (1.15) is said not physical:

$$\left\{ \boldsymbol{\sigma} + \frac{i}{2} \boldsymbol{\Omega} \geq 0 \right\} \Leftrightarrow \left\{ \text{phisical state} \right\} .$$

[3] The hypotheses of theorem dictates that the matrices $\mathbf{A}$, $\mathbf{B}$, and $\mathbf{C}$ must be square, real, and strictly positive.

$$\mathbf{B} \to \mathbf{S_B B S_B^\intercal} = \begin{pmatrix} m & 0 \\ 0 & m \end{pmatrix} ,$$

$$\mathbf{C} \to \mathbf{S_A A S_B^\intercal} = \begin{pmatrix} c_1 & 0 \\ 0 & c_2 \end{pmatrix} ,$$

The quantities, n, m, c_1 and c_2 are determined by the four local symplectic invariants

$$I_1 \equiv \det(A) = n^2 , \tag{1.19}$$

$$I_2 \equiv \det(B) = m^2, \tag{1.20}$$

$$I_3 \equiv \det(C) = c_1 c_2 , \tag{1.21}$$

$$I_4 \equiv \det(\boldsymbol{\sigma}) = \left(nm - c_1^2\right)\left(nm - c_2^2\right) . \tag{1.22}$$

Hence the covariance matrix is given in the *standard form*

$$\boldsymbol{\sigma} = \begin{pmatrix} n & 0 & c_1 & 0 \\ 0 & n & 0 & c_2 \\ c_1 & 0 & m & 0 \\ 0 & c_2 & 0 & m \end{pmatrix} . \tag{1.23}$$

In the Chapter 6 we will show some measured experimental matrices. They are producted by sub-threshold type-II **OPO** (Optical Parametric Oscillator). We will see that due to the symmetry of the Hamiltonian describing the **OPO**, the covariance matrices produced in the laboratory are exactly in the standard form Eq.(1.23). Moreover, at the time of their birth, states produced by an **OPO** show $n = m$, so the matrix is called symmetric and represents a bi-partite state where the energy is equally distributed between the two modes. In fact, with reference to the Eq.(1.16) we have

$$n = m \Rightarrow \left\langle a_1^\dagger a_1 \right\rangle = \left\langle a_2^\dagger a_2 \right\rangle .$$

The condition expressed by Heisenberg uncertainty principle Eq.(1.15) can be written in terms of the four symplectic invariants[4]

$$I_1 + I_2 + 2I_3 \leq 4I_4 + \frac{1}{4} . \tag{1.24}$$

The covariance matrix is also characterized by its symplectic eigenvalues

$$d_\pm = \sqrt{\frac{I_1 + I_2 + 2I_3 \pm \sqrt{\left(I_1 + I_2 + 2I_3\right)^2 - 4I_4}}{2}} . \tag{1.25}$$

[4]For this reason, a quantum state is physical when it verifies the inequality (1.24) and the assumptions of the Williamson's theorem.

The inequality (1.24) assumes a simple form in term of d_-:

$$d_- < \frac{1}{2}. \tag{1.26}$$

So the covariance matrix $\boldsymbol{\sigma}$ represents a physical state iff it is valid the inequality (1.24) or equivalently (1.26).

We also note that a pure Gaussian state is a minimum uncertainty state and that the covariance matrix relative to a pure state necessary has $\det[\boldsymbol{\sigma}] = I_4 = 1/16$ (see Eq. (1.17)) so that the case of $c_1 = -c_2 \equiv c$ implies $n = m$ (*fully symmetric states*), to ensure a *bona fide* covariance matrix, and for a pure state we have

$$c = \sqrt{n^2 - 1/4}. \tag{1.27}$$

Moreover, for the generic fully symmetric states $c \leq \sqrt{n^2 - 1/4}$, with the inequality saturated only by pure states.

1.3.1.2 Coherent and Thermal states

In this subsection, we report the characteristic functions of coherent states and thermal states. We do not discuss their physical properties in detail (for this purpose it is possible to consult the texts [20, 21]).

The displacement operator, first introduced, is strictly connected with Glauber-Surdashan's states or coherent states. In fact, th single mode coherent state $|\beta\rangle$ is defined as

$$|\beta\rangle = D(\beta)|0\rangle,$$

where $D(\beta) = \exp\{\beta\alpha^* - \beta^*\alpha\}$ is the singlemode displacement operator. The characteristic function is Gaussian, and it is given by

$$\chi_{coh}(\alpha) = \exp\left\{-\frac{1}{2}|\alpha|^2 + \alpha\beta^* - \alpha^*\beta\right\}.$$

The thermal state of N bosonic systems at thermal equilibrium is represented by density operator $\rho = \bigotimes_k^N \rho_k$ with

$$\rho_k = \frac{1}{1+\bar{n}_k}\sum_{h=0}^{\infty}\left(\frac{\bar{n}_k}{1+\bar{n}_k}\right)^h |m\rangle_{k\,k}\langle m|,$$

where $\bar{n}_k = \left(e^{\hbar\omega/k_BT} - 1\right)^{-1}$ is the average number of thermal photons in the $k-$th mode at temperature T, and $|m\rangle_k$ is the Fock state with photon number m. The characteristic function of the thermal state is $\boldsymbol{\chi}_{th}(\boldsymbol{\alpha}) = \prod_{k=1}^N \chi_k^{th}(\boldsymbol{\alpha}_k)$ with

$$\chi_k^{th}(\boldsymbol{\alpha}_k) = \exp\left\{-\frac{1}{2}(2\bar{n}_k + 1)|\alpha_k|^2\right\}. \tag{1.28}$$

By Eq. (1.28) we see that even the thermal state is Gaussian.

However, at the optical frequency ω, $\hbar\omega$ is always in the range 1.5 to 2.5 eV, so at the enviroment temperature $T \simeq 300K$, the averange number $\bar{n}$ is about 10^{-30}. The value of the $\bar{n}$ is very smaller compared at the average number of photons introduced by the other states involved in the schemes of this dissertation, in which the thermal state tends to vacuum state and its characteristic function is practically that of vacuum $\boldsymbol{\chi}_{vac}(\boldsymbol{\alpha}) = \prod_{k=1}^{N} \chi_k^{vac}(\boldsymbol{\alpha}_k)$ with

$$\chi_k^{vac}(\boldsymbol{\alpha}_k) = \exp\left\{-\frac{1}{2}|\alpha_k|^2\right\} .$$

1.3.2 Squeezed Bell state

In this subsection we discuss a important class of the bi-partite quantum states of the light radiation: the squeezed Bell (**SB**) states. They were introduced by Dell'Anno *et al* [1, 22], for finding the best resource for the **CV** teleportation protocol. They found that with an appropriate choice of the free parameters, the **SB** states represent, to date, the best available (quantum) resource. In the Chapter 5, this aspect will be discussed in greater depth, and will be proposed an optical scheme for their experimental generation; now, we see under what condition the **SB** state reproduces some known states as: squeezed vacuum, squeezed number, photon-added squeezed, and photon-subtracted squeezed states. The **SB** states are generally non-Gaussian, indeed only for a specific set of the free parameters the **SB** state recovers an Gaussian state. Its properties are characterized by the interplay between continuous-variable (**CV**) squeezing and discrete excited, single-photons.

The **SB** state is a pure bi-partite **CV** quantum state defined as

$$|\psi\rangle_{\mathbf{SB}} = S_{12}(\zeta)\left[c_1|0,0\rangle_{12} + c_2|1,1\rangle_{12}\right] , \tag{1.29}$$

where $S_{12}(\zeta) = \exp\left\{-\zeta a_1^\dagger a_2^\dagger + \zeta^* a_1 a_2\right\}$ is the bi-modal squeezing operator, $|n,n\rangle_{12}$ is the tensor product of the two Fock states $|n\rangle_1 \otimes |n\rangle_2$, and $|c_1|^2 + |c_2|^2 = 1$ for the normalization. In terms of the characteristic function it reads

$$\begin{aligned} & \chi_{\mathbf{SB}}(\alpha_1,\alpha_2) \\ = \; & \left\{c_1^2 + 2c_1c_2\,\mathrm{Re}\left[e^{i\theta}\xi_1\xi_2\right] + c_2^2\left(1-|\xi_1|^2\right)\left(1-|\xi_2|^2\right)\right\} \\ & \times \exp\left\{-\frac{1}{2}\left(|\xi_1|^2 + |\xi_2|^2\right)\right\}, \end{aligned} \tag{1.30}$$

where

$$\xi_k = \alpha_k \cosh r + \alpha_h^* e^{i\phi}\sinh r \;, \quad (k,h=1,2;\; k\neq h) \;.$$

With an appropriate choice of free parameters c_1 and c_2, we can recovered the following states [1]:

- squeezed vacuum state (or *twin beam* **TB**) [16]. If $c_1 = 1$, the **SB** state, Eqs.(1.29 and 1.30) becomes, respectively

$$\begin{aligned} |\psi\rangle_{\mathbf{TB}} &= S_{12}(\zeta)\,|0,0\rangle_{12}\ , \\ \chi_{\mathbf{TB}}(\alpha_1,\alpha_2) &= \exp\left\{-\frac{1}{2}\left(|\xi_1|^2+|\xi_2|^2\right)\right\}\ . \end{aligned}$$

  Only with this setting we get a Gaussian bi-partite state for all values of the squeezing parameter $r = |\zeta|$.

- squeezed number (**PN**) state of first excited Fock state : if $c_1 = 0$ we have

$$\begin{aligned} |\psi\rangle_{\mathbf{PN}} &= S_{12}(\zeta)\,|1,1\rangle_{12}\ , \\ \chi_{\mathbf{PN}}(\alpha_1,\alpha_2) &= \left(1-|\xi_1|^2\right)\left(1-|\xi_2|^2\right)\exp\left\{-\frac{1}{2}\left(|\xi_1|^2+|\xi_2|^2\right)\right\}\ . \end{aligned}$$

- photon-added (**PA**) squeezed state. If $c_1 = -\mathcal{N}e^{-i\theta}\tanh r$ we have

$$\begin{aligned} |\psi\rangle_{AS} &= \mathcal{N}_{AS}a_1^\dagger a_2^\dagger S_{12}(\zeta)\,|0,0\rangle_{12} \\ &= \mathcal{N}e^{-i\theta}S_{12}(\zeta)\left[-\tanh^2 r\,|0,0\rangle_{12}+e^{i\theta}\,|1,1\rangle_{12}\right]\ , \\ \chi_{AS}(\alpha_1,\alpha_2) &= \mathcal{N}^2\left\{\tanh^2 r-2\tanh r\,\mathrm{Re}\left[e^{-i\theta}\xi_1\xi_2\right]+\left(1-|\xi_1|^2\right)\left(1-|\xi_2|^2\right)\right\} \\ &\quad\times\exp\left\{-\frac{1}{2}\left(|\xi_1|^2+|\xi_2|^2\right)\right\}\ , \end{aligned}$$

  with $\mathcal{N} = \left[1+\tanh^2 r\right]^{-\frac{1}{2}}$ the normalization factor.

- photon-subtracted (**PS**) squeezed state. If $c_2 = \mathcal{N}e^{i\theta}\tanh r$ we have

$$\begin{aligned} |\psi\rangle_{\mathbf{PS}} &= \mathcal{N}_{\mathbf{PS}}a_1a_2S_{12}(\zeta)\,|0,0\rangle_{12} \\ &= \mathcal{N}e^{i\theta}S_{12}(\zeta)\left[-|0,0\rangle_{12}+e^{i\theta}\tanh r\,|1,1\rangle_{12}\right]\ , \\ \chi_{\mathbf{PS}}(\alpha_1,\alpha_2) &= \mathcal{N}^2\left\{1-2\tanh r\,\mathrm{Re}\left[e^{-i\theta}\xi_1\xi_2\right]+\tanh^2 r\left(1-|\xi_1|^2\right)\left(1-|\xi_2|^2\right)\right\} \\ &\quad\times\exp\left\{-\frac{1}{2}\left(|\xi_1|^2+|\xi_2|^2\right)\right\}\ . \end{aligned}$$

In ref [1], Dell'Anno *et al* have studied the properties of entanglement, of the affinity of squeezed vacuum, and of the non-Gaussianity as a function of the parameters c_1 and c_2. In particular, they have adopted the useful parametrization

$$\begin{aligned} c_1 &= \cos\delta, \\ c_2 &= \sin\delta, \end{aligned}$$

and in such way all the properties of the **SB** state are expressed as a function of the parameter δ.

1.3.3 Variances

In this subsection, we calculate the variances of the field quadrature operators of the **SB** state, Eq.(1.29) or (1.30). We will see that such variances depend on the parameters c_1, c_2, and ϕ_r (where ϕ_r is the phase of the parameter ζ) and that the minimization of the squeezed variance is obtained with the setting $c_1 = 1$ ($c_2 = 0$) and $\phi_r = 2\pi j$, ($j \in \mathbb{N}$), *i.e.* for the **TB** states.

We invoke the propertie of the characteristic function Eq. (1.9) for calculating the variances. We refer to a bi-partite state and for convenience we recall the definition of the field quadrature operators:

$$\begin{pmatrix} X_k \\ Y_k \end{pmatrix} = \frac{1}{\sqrt{2}} \begin{pmatrix} 1 & 1 \\ i & -i \end{pmatrix} \begin{pmatrix} a_k^\dagger \\ a_k \end{pmatrix}$$

with $k = 1, 2$. We introduce two other observables, $X_\varkappa$ and $Y_\varkappa$ with $\varkappa = c, d$, obtained by rotating the base of the operators a_1 and a_2:

$$\begin{pmatrix} c \\ d \end{pmatrix} = \frac{1}{\sqrt{2}} \begin{pmatrix} 1 & 1 \\ 1 & -1 \end{pmatrix} \begin{pmatrix} a_1 \\ a_2 \end{pmatrix} .$$

Then we define the field operators associated to the c, d by replacing a_k with $a_\varkappa$:

$$\begin{pmatrix} X_\varkappa \\ Y_\varkappa \end{pmatrix} = \frac{1}{\sqrt{2}} \begin{pmatrix} 1 & 1 \\ i & -i \end{pmatrix} \begin{pmatrix} a_\varkappa^\dagger \\ a_\varkappa \end{pmatrix} .$$

The importance of rotated operators $X_\varkappa, Y_\varkappa$ lies in the fact that the bi-modal squeezing operator $S_{12}(\zeta)$, expressed in the basis c, d, is factorized in product of two squeezing operators of single mode $\varkappa$, in fact

$$\begin{aligned} S_{12}(\zeta) &= \exp\left\{-\zeta a_1^\dagger a_2^\dagger + \zeta^* a_1 a_2\right\} \\ &= \exp\left\{-\frac{\zeta}{2}\left(c^\dagger + d^\dagger\right)\left(c^\dagger - d^\dagger\right) + \frac{\zeta^*}{2}(c+d)(c-d)\right\} \\ &= \exp\left\{-\frac{\zeta}{2}c^{\dagger 2} + \frac{\zeta^*}{2}c^2\right\} \exp\left\{-\frac{(-\zeta)}{2}d^{\dagger 2} + \frac{(-\zeta^*)}{2}d^2\right\} \\ &= S_1(\zeta) S_2(-\zeta) \ , \end{aligned}$$

being $[c, d] = 0$. This factorization has suggested to realize experimentally the bi-partite squeezed state $S_{12}(\zeta)|0,0\rangle_{12}$ suitably combining two single squeezed state $\bigotimes_{k=1,2} S_k\left((-)^{k+1}\zeta\right)|0\rangle_k$.

Using the Eq. (1.9), the averages and variances of field operators are given by

$$\begin{matrix} \langle X_k \rangle \\ i\langle Y_k \rangle \end{matrix} = \frac{1}{\sqrt{2}} \left(\frac{\partial \chi(\boldsymbol{\alpha})}{\partial \alpha_k^*} \pm \frac{\partial \chi(\boldsymbol{\alpha})}{\partial \alpha_k} \right) \Bigg|_{\boldsymbol{\alpha}=\mathbf{0}}$$

$$\begin{matrix}\langle \Delta X_k^2 \rangle \\ \langle \Delta Y_k^2 \rangle\end{matrix} = \pm\frac{1}{2}\left(\frac{\partial^2 \chi(\boldsymbol{\alpha})}{\partial \alpha_k^2} + \frac{\partial^2 \chi(\boldsymbol{\alpha})}{\partial \alpha_k^{*2}} \mp 2\frac{\partial^2 \chi(\boldsymbol{\alpha})}{\partial \alpha_k \partial \alpha_k^*}\right)\Big|_{\boldsymbol{\alpha}=\mathbf{0}}.$$

For the **SB** state the quadrature average is zero

$$\langle X_k \rangle = \langle Y_k \rangle = \langle X_\varkappa \rangle = \langle Y_\varkappa \rangle = 0 \ .$$

The variances of modes $k = 1, 2$ are given by

$$\left\langle \Delta X_k^2 \right\rangle = \left\langle \Delta Y_k^2 \right\rangle = \frac{1}{2}\left(c_1^2 + 3c_2^2\right)\cosh(2r) \ ,$$

while the variances of modes c and d are

$$\begin{aligned}\left\langle \Delta X_c^2 \right\rangle &= \left\langle \Delta Y_d^2 \right\rangle = \frac{1}{2}\left(c_1^2 + 3c_2^2\right)\left[\cosh(2r) - \cos(\phi_r)\sinh(2r)\right] \ , \\ \left\langle \Delta Y_c^2 \right\rangle &= \left\langle \Delta X_d^2 \right\rangle = \frac{1}{2}\left(c_1^2 + 3c_2^2\right)\left[\cosh(2r) + \cos(\phi_r)\sinh(2r)\right] \ .\end{aligned}$$

where we have $\zeta = re^{i\phi_r}$. We can see that the variances are not dependent on the phase difference θ between the parameters c_1 and c_2. Moreover, for a fixed value of $r\,(>0)$, the minimum of the squeezed variances $(\langle \Delta X_c^2 \rangle, \langle \Delta Y_d^2 \rangle)$ is obtained for $\phi_r = 2\pi j$, $(j \in \mathbb{N})$. In this case the above equations become

$$\begin{matrix}\langle \Delta X_c^2 \rangle \\ \langle \Delta Y_c^2 \rangle\end{matrix} = \begin{matrix}\langle \Delta Y_d^2 \rangle \\ \langle \Delta X_d^2 \rangle\end{matrix} = \frac{1}{2}\left(c_1^2 + 3c_2^2\right)e^{\mp 2r}.$$

Further minimizing the squeezed variance with respect to the free parameters c_1 and c_2, we obtain $c_1 = 1\,(\Rightarrow c_2 = 0)$ and the variances

$$\left\langle \Delta X_k^2 \right\rangle = \left\langle \Delta Y_k^2 \right\rangle = \frac{1}{2}\cosh(2r),$$

$$\begin{matrix}\langle \Delta X_c^2 \rangle \\ \langle \Delta Y_c^2 \rangle\end{matrix} = \begin{matrix}\langle \Delta Y_d^2 \rangle \\ \langle \Delta X_d^2 \rangle\end{matrix} = \frac{1}{2}e^{\mp 2r},$$

are precisely the variances of the quadrature of the mode c and d of the bi-partite squeezed vacuum state [16],[23]. This allows us to conclude that, in the search of the states with smallest variance, the Gaussian states are extremal with respect to all states that can be obtained by tuning the free parameters of the **SB** state, *i.e.* de-Gaussified states. When the parameter of squeezing r is null, we find the shot noise.

1.4 Quantum Measurements

The measurement theory is important in the applications of quantum information to measure light fields or to detect a part of the radiation. In this Section, we discuss some important measurements, the so-called *conditional measurements*,

that can be performed on a part of a system composed of several sub-systems. The formalism of the characteristic function is particularly suitable for this purpose. Therefore, we see how to represent the main measurements in quantum information through appropriate characteristic functions. Therefore we analyze in some details three different measurement techniques: *single-photon* (sp), *realistic Geiger* (on/off), and *homodyne detection* (Hom).

1.4.1 Conditional Measurement

We briefly recall the basis tools needed in order to describe in the most general way a quantum system and the possible measurements that can be performed on it.

We introduce a general class of quantum measurements in which an input state of N sub-systems is mapped into a output state of $0 < M < N$ sub-systems (see Fig.(1.1)). When the characteristics of the output state depend on measurements made on $N - M$ sub-systems we can say that the input system is composed of N correlated (*entangled*[5]) sub-systems . Therefore this type of measurements affect the final state and for this reason they are called *conditional measurements*. The $N - M$ measured sub-systems are called *ancilla* states.

In this feature of quantum physics there is the foundation of the holistic view of physical reality: perfect knowledge of the components of a system is not sufficient for knowledge of the entire system. The reason can be found in the existence of physical properties that are not localized on a single physical system, but are "distributed" between some systems. For example, the mass of a particle is a physical characteristic that is located exactly in the region space where the particle is. Otherwise, the *quantum entanglement* is a characteristic of system and it is distributed among the sub-systems that compose it. This is one of the most important novelties of quantum physics, compared to the classical one.

In this subsection we present a general experimental that allows to formalize the concept of conditional measurements made on one part (ancilla) of the system, using the operatorial approach (via matrix density), and the characteristic function formalism. In Fig.(1.1) we report a schematic diagram of a tipical conditional measurement device. We consider the system $S\left(=\bigcup_{k=1}^{N} S_k\right)$ as the set of N sub-systems S_k and suppose, without loss of generality, to measure the last $N - M$ sub-systems with three different measurements : *single-photon* (sp), *realistic Geiger* (on/off), and *homodyne detection* (Hom).

In particular, we can think to factorize the entire Hilbert space $\mathcal{H}_S$ as product of two Hilbert spaces: $\mathcal{H}_C$ involving the input computing state (C) and $\mathcal{H}_A$ involving the input ancilla states (A),

$$\mathcal{H}_S = \mathcal{H}_C \otimes \mathcal{H}_A \ .$$

[5] this fundamental aspect will be discussed in the next chapter.

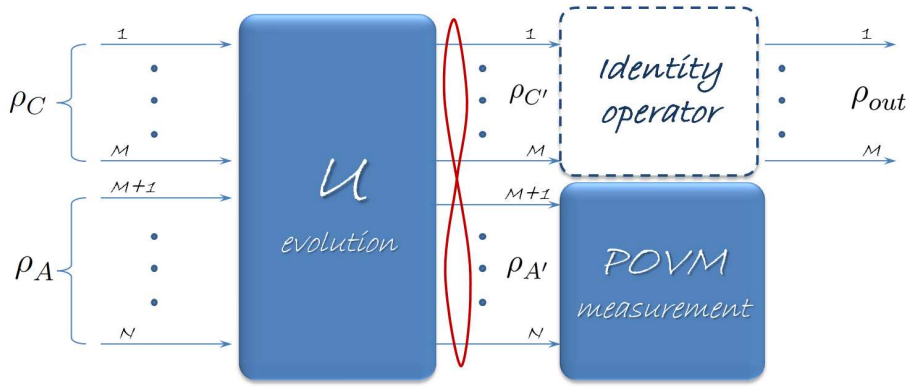

Figure 1.1: Schematic representation of the mechanism of conditional measurements: a system described by a factorizable density matrix undergoes the action of a unitary operator U representing passive optical devices. The action of U makes the state ρ_C (in $\mathcal{H}_C$) correlated with the ancilla state ρ_A (in $\mathcal{H}_A$). A measure described by operators **POVM** is realized on the ancillary system; while the system C' is left undisturbed. Because of the correlations introduced by the operator U, the state C' is modified by type-**POVM** measurements of A', thereby providing the desired output state ρ_{out} as result of the measurement process.

We suppose that the state of the system is described by the density matrix espressed as tensor product of the density matrices, ρ_C and ρ_A, of the sub-systems C and A, respectively. In this case the states ρ_C are non-correlated and no-interacting with the ancilla states ρ_A,

$$\rho_S = \rho_C \otimes \rho_A.$$

In this configuration it isn't possible to carry out conditional measurements. Generally, in the protocols of the quantum information the computational input and ancilla systems are subject to local unitary transformations U, which are implementated with beam splitters (see appendix), optical lens, phase shifters, attenuators and other passive optical devices. The operator U describes the pre-measurement evolution and it maps the density operator ρ_S in the density operator $\rho'_S = U\rho_S U^\dagger$. Under the action of U, the sub-systems described by ρ_C and ρ_A can become correlated, so that the overall system can not yet be factorized. However, it is useful to continue to distinguish the two Hilbert spaces $\mathcal{H}_{C'}$ and $\mathcal{H}_{A'}$ such as $\mathcal{H}_S = \mathcal{H}_{C'} \otimes \mathcal{H}_{A'}$ where $\mathcal{H}_{C'}$ denotes the new Hilbert space of the computing system and $\mathcal{H}_{A'}$ the new Hilbert space of ancilla system.

At this point we perform some measurements on the sub-system in the Hilbert space $\mathcal{H}_{A'}$ and suppose that the measurement outcomes form a set Ω. A general mathematical desciption of quantum observables can be carried out in terms of the normalized *positive operator value measures* (**POVM**) operator. A **POVM** is a application M which associates to each measurable sub-set $X \subseteq \Omega$ a po-

sivite operator $\mathsf{M}(X)$ acting on $\mathcal{H}_{A'}$. For every state described by density matrix $\rho_{A'} = \mathrm{Tr}_{C'}[\rho'_S]$, a **POVM** operator produces a probability distribution given by the map $X \rightarrow p(\mathsf{M}(X)) = \mathrm{Tr}[\rho_{A'}\mathsf{M}(X)]$. M satisfies the normalization condition $\mathsf{M}(\Omega) = \mathbb{I}$, so the $p(\mathsf{M}(X)) = \mathrm{Tr}[\rho_{A'}\mathsf{M}(X)]$ sums to unity. The real number $\mathrm{Tr}[\rho_{A'}\mathsf{M}(X)]$ is the probability of getting the measurement outcome x belonging to X, when the system is in the state $\rho_{A'}$ and a measurement of M is performed. For this reason we give the following definition

$$\Pr(X \rightarrow x) = \mathrm{Tr}[\rho_{A'}\mathsf{M}(X)] \equiv \left\{ \begin{array}{c} \text{The probability of obtaining } x \\ \text{as the result of the measurement } \mathsf{M} \\ \text{of } X \text{ made on the system described} \\ \text{by the density matrix } \rho_{A'} \end{array} \right\}. \tag{1.31}$$

The **POVM** operator is the generalization of the projector operator. A **POVM** operator M is called a projector value measure, or spectral measure, if $\mathsf{M}(X^2) = \mathsf{M}(X)$. When $\Omega = \mathbb{R}$, the spectral measures correspond to self-adjoint operators.

So, referring to Fig. (1.1), we have N correlated sub-systems and $N - M$ of them are measured. For our purposes, it is not important to know which type of correlation there is between the sub-systems and how it is structured between them. Our goal is to calculate the output state ρ_{out} after we have measured the $N - M$ ancillary states. We suppose that $N - M$ measurements are computed with different types of detectors. In particultar, we assume that A_1 sub-systems are measured by detectors of single photons (sp), the subsequent A_2 sub-systems are measured by *on/off* detectors that record presence (on) or absence (off) of photons, and the last A_3 sub-systems are measured by homodyne detectors. Overall $A_1 + A_2 + A_3 = N - M$. We assume that each measurement is realized simultaneously, i.e. the measurements are temporally *delta* correlated. Due of the $N - M$ measurements the output state is composed of M sub-systems, whose properties are directly linked to the results of each measurement. So influencing the measurement results we obtain a state ρ_{out} with suitable propieties to our specific purposes.

In the formalism of the density matrix, the output state ρ_{out}, *i.e.* the conditional density matrix, of the system C', given the result of the measurements performed on the sub-system A', is linked to the input state $\rho_{S'}$ through the following expression:

$$\rho_{out} = \frac{\mathrm{Tr}_{M+1,\ldots,N}[\rho_{S'}\mathsf{M}(\mathbf{D})]}{\mathrm{Tr}[\rho_{S'}\mathsf{M}(\mathbf{D})]}, \tag{1.32}$$

where

$$\mathsf{M}(\mathbf{D}) = \bigotimes_{k_1=M+1}^{M+A_1} \Pi_{k_1}^{(sp)} \otimes \bigotimes_{k_2=M+A_1+1}^{M+A_2} \Pi_{k_2}^{(on/off)} \otimes \bigotimes_{k_3=M+A_2+1}^{M+A_3=N} \Pi_{k_3}^{(Hom)}, \tag{1.33}$$

with $\Pi_{k_j}^{(D_j)}$ the **POVM** operators describing the measurement

$$\mathbf{D} \equiv (\mathbf{sp},\ \mathbf{on/off},\ \mathbf{Hom})$$

and such that

$$\Pi_{k_j}^{(D_j)} \left(\Pi_{k_{j'}}^{(D_j)}\right)^{\dagger} = \delta_{k_j k_{j'}} \Pi_{k_j}^{(D_j)} \ .$$

In the next subsection, we define exactly the operators $\Pi_{k_j}^{(D_j)}$ in Eq. (1.33). The denominator of the Eq.(1.32) ensures the normalization of the output state ρ_{out}, in fact density matrix ρ_{out} is composed by the remaining modes $1, ..., M$ and its trace becomes normalized to unity

$$\begin{aligned} \mathrm{Tr}_{1,...,M}\left[\rho_{out}\right] &= \frac{\mathrm{Tr}_{1,...,M}\left[\mathrm{Tr}_{M+1,...,N}\left[\rho_{S'}\mathsf{M}\left(\mathbf{D}\right)\right]\right]}{\mathrm{Tr}\left[\rho_{S'}\mathsf{M}\left(\mathbf{D}\right)\right]} \\ &= 1. \end{aligned}$$

From the definition (1.31) we can note that $\mathrm{Tr}[\rho_S \mathsf{M}(\mathbf{D})]$ is just the probability of having the events sp, on/off, and Hom as a result of the simultaneous measurement $\mathbf{D}$

$$\mathrm{Tr}\left[\rho_S \mathsf{M}\left(\mathbf{D}\right)\right] = \Pr\left\{\mathbf{D} \rightarrow (sp,\ on/off,\ Hom)\right\}$$

In terms of the characteristic function, the procedure of conditional measurements can be traslated in resolutions of integrals involving the characteristic function of the input state and of the characteristic function associated with operators describing the measurements. We prove that the characteristic function of the output state is given by

$$\chi_{out}\left(\boldsymbol{\alpha}_1, ..., \boldsymbol{\alpha}_M\right) = \frac{\mathcal{M}\left(\boldsymbol{\alpha}_1, ..., \boldsymbol{\alpha}_M\right)}{\mathcal{M}\left(\mathbf{0}, ..., \mathbf{0}\right)} \ , \tag{1.34}$$

where $\boldsymbol{\alpha}_k \equiv (\alpha_k, \alpha_k^*)$, $\mathbf{0} = (0, 0)$ and

$$\mathcal{M}\left(\boldsymbol{\alpha}_1, ..., \boldsymbol{\alpha}_M\right) = \int_{\mathbb{C}^{N-M}} d\boldsymbol{\alpha}_{M+1,...N} \chi_{\rho_{S'}}\left(\boldsymbol{\alpha}_1, ..., \boldsymbol{\alpha}_N\right) \mathcal{X}\left(\boldsymbol{\alpha}_{M+1}, ..., \boldsymbol{\alpha}_N\right), \tag{1.35}$$

with $d\boldsymbol{\alpha}_{M+1,...N} = d\boldsymbol{\alpha}_{M+1}...d\boldsymbol{\alpha}_N$, is the integration on the modes $M+1, ..., N$ of the input state $\chi_{\rho_{S'}}\left(\boldsymbol{\alpha}_1, ..., \boldsymbol{\alpha}_N\right)$ multiplied by the characteristic function describing the measurements performed on the modes $M+1, ..., N$,

$$\mathcal{X}\left(\boldsymbol{\alpha}_{M+1}, ..., \boldsymbol{\alpha}_N\right) \tag{1.36}$$

$$= \prod_{k_1=M+1}^{M+A_1} \chi_{k_1}^{(sp)}\left(\boldsymbol{\alpha}_{k_1}\right) \prod_{k_2=M+A_1+1}^{M+A_2} \chi_{k_2}^{(on/off)}\left(\boldsymbol{\alpha}_{k_2}\right) \prod_{k_3=M+A_2+1}^{N} \chi_{k_3}^{(Hom)}\left(\boldsymbol{\alpha}_{k_4}\right) \tag{1.37}$$

The $\chi_{k_j}^{(D_j)}\left(\boldsymbol{\alpha}_{k_j}\right)$, with $\boldsymbol{\alpha}_{k_j} \equiv \left(\alpha_{k_j}, \alpha_{k_j}^*\right)$, is the characteristic function describing the conditional measurements D_j. The function $\mathcal{M}(\mathbf{0}, ..., \mathbf{0})$, at the denominator of the Eq.(1.34), ensures the normalization of the function χ_{out}. It is the equivalent of

$$\Pr\{\mathbf{D} \rightarrow (sp,\ on/off,\ Hom)\} = \mathrm{Tr}\left[\rho_S \mathsf{M}(\mathbf{D})\right]$$

in the characteristic function formalism.

Proof. In order to prove the Eq.(1.34), we express the matrix density of the input state $\rho_{S'}$ in the form suggested by Eq.(1.7)

$$\rho_{S'} = \frac{1}{\pi^N} \int_{\mathbb{C}^N} d\boldsymbol{\beta}_{1...N} \chi_{\rho_{S'}}(\boldsymbol{\beta}_1, ..., \boldsymbol{\beta}_N) D_N(-\boldsymbol{\beta}) \ ,$$

where $d\boldsymbol{\beta}_{1...N} \equiv d\boldsymbol{\beta}_1 ... d\boldsymbol{\beta}_N$ and $D_N(-\boldsymbol{\beta}) = \bigotimes_{k=1}^N D_k(-\beta_k)$. Substituting it in the partial trace of the Eq.(1.32), we have

$$\begin{aligned}
\rho_{out} &= \frac{1}{\mathcal{N}} \mathrm{Tr}_{M+1,...,N}\left[\left(\int_{\mathbb{C}^N} d\boldsymbol{\beta}_{1...N} \chi_{\rho_{S'}}(\boldsymbol{\beta}_1, ..., \boldsymbol{\beta}_N) D_N(-\boldsymbol{\beta})\right) \mathsf{M}(\mathbf{D})\right] \\
&= \frac{1}{\mathcal{N}} \int_{\mathbb{C}^N} d\boldsymbol{\beta}_{1...N} \chi_{\rho_{S'}}(\boldsymbol{\beta}_1, ..., \boldsymbol{\beta}_N) \prod_{h=1}^{M} D_h(-\boldsymbol{\beta}_h) \\
&\quad \cdot \mathrm{Tr}_{M+1,...,N}\left[\prod_{k=M+1}^{N} D_k(-\boldsymbol{\beta}_k) \mathsf{M}(\mathbf{D})\right] \\
&= \frac{1}{\mathcal{N}} \int_{\mathbb{C}^M} d\boldsymbol{\beta}_{1...M} \mathcal{M}(\boldsymbol{\beta}_1, ..., \boldsymbol{\beta}_M) \prod_{h=1}^{M} D_h(-\boldsymbol{\beta}_h) \ , \qquad (1.38)
\end{aligned}$$

where the term $\mathcal{N}$ contains numerical factors and will be determined by the normalization of the output state. The function $\mathcal{M}(\boldsymbol{\beta}_1, ..., \boldsymbol{\beta}_M)$ in Eq.(1.38) is the result of integration on the complex variables $(\boldsymbol{\beta}_1, ..., \boldsymbol{\beta}_M)$ of the modes measured through the operator M:

$$\begin{aligned}
\mathcal{M}(\boldsymbol{\beta}_1, ..., \boldsymbol{\beta}_M) &= \int_{\mathbb{C}^{N-M}} d\boldsymbol{\beta}_{M+1...N} \chi_{\rho_{S'}}(\boldsymbol{\beta}_1, ..., \boldsymbol{\beta}_N) \\
&\quad \cdot \mathrm{Tr}_{M+1,...,N}\left[\prod_{k=M+1}^{N} D_k(-\boldsymbol{\beta}_k) \mathsf{M}(\mathbf{D})\right].
\end{aligned}$$

Using the factorization Eq.(1.33) of the operator $\mathsf{M}(\mathbf{D})$, we have

$$\begin{aligned}
& \mathrm{Tr}_{M+1,...,N}\left[\prod_{k=M+1}^{N} D_k\left(-\boldsymbol{\beta}_k\right)\Pi_M\right] \\
= & \prod_{k_1=M+1}^{M+A_1}\mathrm{Tr}_{k_1}\left[D_{k_1}\left(-\boldsymbol{\beta}_{k_1}\right)\Pi_{k_1}^{(sp)}\right]\cdot\prod_{k_2=M+A_1+1}^{M_2}\mathrm{Tr}_{k_2}\left[D_{k_2}\left(-\boldsymbol{\beta}_{k_2}\right)\Pi_{k_2}^{(on/off)}\right] \\
& \prod_{k_3=M+A_2+1}^{N}\mathrm{Tr}_{k_3}\left[D_{k_3}\left(-\boldsymbol{\beta}_{k_3}\right)\Pi_{k_3}^{(Hom)}\right] \\
\equiv & \mathcal{X}\left(\boldsymbol{\beta}_{M+1},...,\boldsymbol{\beta}_N\right)
\end{aligned}$$

as definited by Eqs.(1.35) and (1.36), being

$$\mathrm{Tr}_{k_j}\left[D_{k_j}\left(-\boldsymbol{\beta}_{k_j}\right)\Pi_{k_j}^{(D_j)}\right]=\mathrm{Tr}_{k_j}\left[D_{k_j}\left(\boldsymbol{\beta}_{k_j}\right)\Pi_{k_j}^{(D_j)}\right]\ ,$$

for reasons that will be clear after. In conclusion, the characteristic function of the output state becomes

$$\begin{aligned}
& \chi_{out}\left(\boldsymbol{\alpha}_1,...,\boldsymbol{\alpha}_M\right) \\
= & \mathrm{Tr}_{1,...,M}\left[\rho_{out}\prod_{h=1}^{M}D_h\left(\alpha_h\right)\right] \qquad (1.39) \\
= & \frac{1}{\mathcal{N}}\mathrm{Tr}_{1,...,M}\left[\int_{\mathbb{C}^M}d\boldsymbol{\beta}_{1...M}\mathcal{M}\left(\boldsymbol{\beta}_1,...,\boldsymbol{\beta}_M\right)\prod_{h=1}^{M}D_h\left(-\beta_h\right)\prod_{h=1}^{M}D_h\left(\alpha_h\right)\right] \\
= & \frac{1}{\mathcal{N}}\int_{\mathbb{C}^M}d\boldsymbol{\beta}_{1...M}\mathcal{M}\left(\boldsymbol{\beta}_1,...,\boldsymbol{\beta}_M\right)\mathrm{Tr}_{1,...,M}\left[\prod_{h=1}^{M}D_h\left(-\beta_h\right)\prod_{h=1}^{M}D_h\left(\alpha_h\right)\right] \\
= & \frac{1}{\mathcal{N}}\int_{\mathbb{C}^M}d\boldsymbol{\beta}_{1...M}\mathcal{M}\left(\boldsymbol{\beta}_1,...,\boldsymbol{\beta}_M\right)\prod_{h=1}^{M}\mathrm{Tr}_h\left[D_h\left(-\beta_h\right)D_h\left(\alpha_h\right)\right] \\
= & \frac{1}{\mathcal{N}}\mathcal{M}\left(\boldsymbol{\alpha}_1,...,\boldsymbol{\alpha}_M\right)\ , \qquad (1.40)
\end{aligned}$$

being

$$\mathrm{Tr}_h\left[D_h\left(-\beta_h\right)D_h\left(\alpha_h\right)\right]=\pi\delta^{(2)}\left(\alpha_h-\beta_h\right)\exp\left\{\frac{1}{2}\left(-\beta_h\alpha_h^*+\beta_h^*\alpha_h\right)\right\}.$$

We have included all numerical factors (as for example π) in normalization constant $\mathcal{N}$. It is determined by the normalization of state ρ_{out}, or equivalently of χ_{out}, in fact

$$\begin{aligned}
1 &= \chi_{out}\left(0,...,0\right) \\
&= \frac{1}{\mathcal{N}}\mathcal{M}\left(0,...,0\right) \\
&\Rightarrow \mathcal{N}=1/\mathcal{M}\left(0,...,0\right)\ .
\end{aligned}$$

Replacing the factor $\mathcal{N}$ in Eq.(1.40) we obtain the desired Eq.(1.34). ■

1.4.2 Single-Photon photodetectors

The measurement of single photons consists of a projective measurement acting on the $k-$mode of the system. The projector operator that describes this measurement of the field k is given by

$$\Pi_k^{(sp)} = |1\rangle_{k\,k}\langle 1| \ ,$$

and its characteristic function results

$$\begin{aligned}\chi_k^{(sp)}(\boldsymbol{\alpha}_k) &= \mathrm{Tr}_k\left[\Pi_k^{(sp)} D(\boldsymbol{\alpha}_k)\right] \\ &= {}_k\langle 1| D(\boldsymbol{\alpha}_k)|1\rangle_k \\ &= \left(1-|\alpha_k|^2\right) e^{-|\alpha_k|^2/2} \ ,\end{aligned}$$

being

$$< m|D(-\alpha)|n >= \left(\frac{n!}{m!}\right)^{1/2} \alpha^{m-n} e^{-|\alpha|^2/2} L_n^{m-n}\left(|\alpha|^2\right)$$

with $L_n^{m-n}(|\alpha|^2)$ Laguerre polynomials and $L_1^0(x) = L_1(x) = 1-x$. The characteristic functions $\chi_k^{(sp)}$ are invariant under flip of sign of $\boldsymbol{\alpha}_k$.

1.4.3 On/off photodetectors

To date, there are no detectors able to resolve the photon number. The reason lies in excitation mechanism of the photosensitive element of the detector. Generally, in a photodetector each incident photon excites a single atom, the generated signal is too weak and, therefore, must be amplified to produce a measurable signal. Added to this, there is the efficiency not unitary of the photodetectors. This implies that one cannot discriminate between a single photon or many photons as the outcomes of a measurement.

However, in a realistic scenario the detection associated to mode k can be modeled by the **POVM** operator, $\Pi_k^{(on)}(\eta_k)$, taking account simply the threshold detection of $n \geq 1$ photons, given by

$$\Pi_k^{(on)}(\eta_k) = \mathbb{I}_k - \Pi_k^{(off)}(\eta_k), \tag{1.41}$$

where

$$\Pi_k^{(off)}(\eta_k) = \sum_{m=0}^{\infty} (1-\eta_k)^m |m\rangle_{k\,k}\langle m| \,, \tag{1.42}$$

and η_k is non-unitary efficient photon detection.

The characteristic function is given by

$$\begin{aligned}\chi_k^{(on)}(\boldsymbol{\alpha}_k) &\equiv \mathrm{Tr}_k\left[\hat{D}_k(\boldsymbol{\alpha}_k)\,\Pi_k^{(on)}\right] \\ &= \pi\delta^{(2)}(\alpha_k) - \frac{1}{\eta_k}\exp\left\{-\frac{2-\eta_k}{2\eta_k}|\alpha_k|^2\right\},\end{aligned}$$

while

$$\begin{aligned}\chi_k^{(off)}(\boldsymbol{\alpha}_k) &= \mathrm{Tr}_k\left[\hat{D}_k(\boldsymbol{\alpha}_k)\,\Pi_k^{(off)}\right] \\ &= \frac{1}{\eta_k}\exp\left\{-\frac{2-\eta_k}{2\eta_k}|\alpha_k|^2\right\},\end{aligned}$$

such as

$$\chi_k^{(on)}(\boldsymbol{\alpha}_k) + \chi_k^{(off)}(\boldsymbol{\alpha}_k) = \pi\delta^{(2)}(\alpha_k).$$

Clearly the characteristic functions $\chi_k^{(on/off)}$ are invariant under flip of sign of $\boldsymbol{\alpha}_k$.

We can see that if the detection mechanism is free-losses, $\eta_k = 1$, the operators (1.41) and (1.42) read

$$\begin{aligned}\Pi_k^{(on)}(1) &= \mathbb{I}_k - |0\rangle_{k\,k}\langle 0| \ , \\ \Pi_k^{(off)}(1) &= |0\rangle_{k\,k}\langle 0| \ .\end{aligned}$$

The characteristic functions become

$$\begin{aligned}\chi_k^{(on)}(\boldsymbol{\alpha}_k)\Big|_{\eta=1} &= \pi\delta^{(2)}(\alpha_k) - \exp\left\{-\frac{1}{2}|\alpha_k|^2\right\}, \\ \chi_k^{(off)}(\boldsymbol{\alpha}_k)\Big|_{\eta=1} &= \exp\left\{-\frac{1}{2}|\alpha_k|^2\right\}.\end{aligned}$$

1.4.4 Homodyne photodetectors

In this sub-section we report the characteristic function of the operator that describes the homodyne measurement. This **CV** detection technique measures the quadratures of the field. In terms of the density matrix, the homodyne measurement is expressed by projectors on the quadrature eigenstates $|Y\rangle$ and $|X\rangle$, the its characteristc function is given by

$$\begin{aligned}\chi_k^{(Hom)}(\alpha_k) &= \mathrm{Tr}\left[\hat{D}_k(\boldsymbol{\alpha}_k)\,\Pi_k^{(Hom)}\right] \\ &= \begin{cases} \exp\left\{-\frac{i}{2}X_kY_k + iX_k\tilde{Y}_k\right\}\delta(Y_k) & \text{if } \Pi_k^{(Hom)} = |Y\rangle_{k\,k}\langle Y| \\ \exp\left\{-\frac{i}{2}X_kY_k - i\tilde{X}_kY_k\right\}\delta(X_k) & \text{if } \Pi_k^{(Hom)} = |X\rangle_{k\,k}\langle X| \end{cases},\end{aligned}$$

where $\alpha_k = 2^{-1/2}(x_k + iy_k)$, and $\tilde{X}_k$ and $\tilde{Y}_k$ the measured eigenvalues of the states $|x_k\rangle$ and $|y_k\rangle$, respectively. However, in the Chapter 6, this powerful technique for the reconstruction of quantum states of light radiation will be treated in more detail.

1.5 Quantum Open System

A quantum open system is a quantum system S interacting with external environment R, called *reservoir*, composed by a large number of sub-systems (beam of photons, heat bath, absorber transmission channels, etc...). The aim of quantum open system theory is to study the behaviour of the coupled system to environment and in particular the dissipation effect on the quantum system S. Decoherence indicates the detrimental effect on a quantum system that stochastically interacts with the external world. The state of system, initially pure, becomes mixed. In the density matrix language it translates into the fact that while a pure state is represented by an idempotent density matrix ρ_S ($\rho_S^2 = \rho_S$) this is not true for a decohered mixed state. The lossy transmission of an arbitrary optical quantum state between two sites is an irreversible decoherence process that can be described by using the open systems approach [24]. In it the enviroment is modeled as a reservoir (thermal bath) made up of infinite modes at thermal equilibrium.

We want to determine the evolution of the state ρ_S of the system $\mathcal{H}_S$. That is, for an initial density matrix $\rho_S(0)$ at time 0 on $\mathcal{H}_S$, we calculate the state $\rho_S(t)$ at time t on $\mathcal{H}_S$ (see Fig. (1.2)). We assume the following general conditions for the system S and the reservoir R:

- *weak coupling (Born approximation)* – the coupling between system and environment is such that the density matrix ρ_R of the environment is negligibly influenced by the interaction (the thermal bath state is stationary). This approximation allows to write the state $\rho_{SR}(t)$ of the global system as $\rho_{SR}(t) \approx \rho_S(t) \otimes \rho_R$;
- *Markovianity* – there are not memory effects neither on the system and the reservoir. It means that the state of the system at time t is not related to the state in the past (being the reservoir in a stationary state this already implies the absence of memory effect on the reservoir). This approximation implies that the time scale τ over which $\rho_S(t)$ changes appreciably under the influence of the bath is large compared to the time scale τ_R over which the bath forgets about its past, $\tau \gg \tau_R$.
- *Secularity (rotating wave approximation)*– the typical time scale τ_S of the intrinsic evolution of the system S is small compared to the relaxation time τ. For an optical field it implies that the reservoir reacts to the average field and not to its istantaneous value.

Then the evolution of the state is give by the map

$$\rho_S(0) \to \rho_S(t) = L_t(\rho_S(0)).$$

The state $\rho_S(t)$ at time t determines the future states $\rho_S(t')$ at time $t' > t$, without needing to know the whole past $\rho_S(t'')$, with $t'' < t$. Of course, the maps L_t are trace-preserving and positivity-preserving.

We note that in the absence of the external system the evolution of the state $\rho_S(0)$ is described by the unitary operator $U(t)$ such that the map L_t reads

$$\rho_S(0) \rightarrow \rho_S(t) = U(t)\,\rho_S(0)\,U^\dagger(t)\,.$$

We can see that if the initial state $\rho_S(0)$ is pure ($\mathrm{Tr}\left[\rho_S^2(0)\right] = 1$), under unitary evolution, the state $\rho_S(t)$ at time $t > 0$ remains pure

$$\begin{aligned}\mathrm{Tr}\left[\rho_S^2(t)\right] &= \mathrm{Tr}\left[U(t)\,\rho_S(0)\,U^\dagger(t)\,U(t)\,\rho_S(0)\,U^\dagger(t)\right] \\ &= \mathrm{Tr}\left[\rho_S^2(0)\right].\end{aligned}$$

More generally, the purity is conserved under unitary evolution. When there is interaction with reservoir and the map L_t reads

$$\begin{aligned}\rho_S(t) &= L_t\left(\rho_S(0)\right) \\ &= \mathrm{Tr}_R\left[U(t)\left(\rho_S(0)\otimes\rho_R\right)U^\dagger(t)\right].\end{aligned}$$

Hence $\rho_S(t)$ is given by partial trace operation over the degrees of freedom of the reservoir and becomes generally mixed although initially pure.

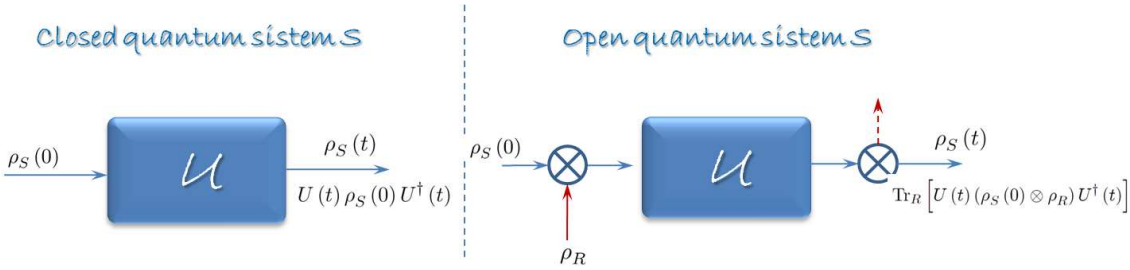

Figure 1.2: Schematic representation of a quantum system closed (left) and open (right). The closed system is characterized by an evolution that is not affected by the action of the external environment on the system. In contrast, an open system can not ignore the presence of the many enviromental modes.

In order to find the most general form of evolution of the state $\rho_S(0)$ in the bi-partite case, we write the interaction Hamiltonian as

$$H_{Int} = a^\dagger B(t)\,e^{i\omega_S t} + aB^\dagger(t)\,e^{-i\omega_S t}\,,$$

where $B(t) = \hbar\sum_k g_k b_k e^{-i\omega_k t}$ is the collective mode of the reservoir with constant of weak coupling g_k, annihilation operator of $k-$mode b_k such that $[b_k, b_h] = \delta_{kh}$, frequency ω_k, while ω_S is the frequency of the optical system S. The dynamics of the reduced density matrix $\rho_S(t)$ is described by following Kossakowski-Lindblad equation

$$\dot{\rho}_S(t) = \sum_{k=1,2}\frac{\Gamma_k}{2}\left\{(N_k+1)\,\mathcal{L}[a_k] + N_k\mathcal{L}\left[a_k^\dagger\right] - M_k^*\mathcal{D}[a_k] - M_k\mathcal{D}\left[a_k^\dagger\right]\right\}\rho_S(0)\,, \tag{1.43}$$

where Γ_k denotes the damping rate of the k–mode, the complex parameter $M_k \in \mathbb{C}$ is the correlation function of bath $k-$th, $N_k \in \mathbb{R}$ coincides with the average number of thermal photons in bath:

$$\begin{aligned} \langle b(\omega_k)\, b(\omega_h)\rangle_R &= M_k \delta(2\omega_S - \omega_k - \omega_h) \ , \\ \left\langle b^\dagger(\omega_k)\, b(\omega_h)\right\rangle_R &= N_k \delta(\omega_k - \omega_h) \ . \end{aligned}$$

M_k is usually referred to as the "squeezing" of the bath. N_k is instead a phenomenological parameter related to the purity of the asymptotic stationary state. The positivity of the density matrix imposes the constraint $|M_k|^2 \leq N_k(N_k+1)$. At thermal equilibrium, *i.e.* for $M_k = 0$, the parameter N_k coincides with the average number of thermal photons in bath.

$\mathcal{L}[O]$ and $\mathcal{D}[O]$ are Lindblad superatoroperators defined respectively by $\mathcal{L}[O]\rho \equiv 2O\rho O^\dagger - O^\dagger O\rho - \rho O^\dagger O$ and $\mathcal{D}[O]\rho \equiv 2O\rho O - OO\rho - \rho OO$ and describing, the former, losses and linear, phase insensitive, amplification processes and, the latter, phase dependent fluctuations.

Equation (1.43) is equivalent to the following equation for the characteristic function in terms of the quadrature variables X_k and Y_k :

$$\dot{\chi}_S(\mathbf{K},t) = -\sum_{k=1,2} \frac{\Gamma_k}{2} \left[(X_k, Y_k) \begin{pmatrix} \partial_{X_k} \\ \partial_{Y_k} \end{pmatrix} + (X_k, Y_k)\, \boldsymbol{\sigma}_k^{(\infty)} \begin{pmatrix} X_k \\ Y_k \end{pmatrix} \right] \chi_S(\mathbf{K},0) \ , \tag{1.44}$$

with

$$\boldsymbol{\sigma}_k^{(\infty)} = \begin{pmatrix} \frac{1}{2} + N_k + \mathrm{Re}[M_k] & \mathrm{Im}[M_k] \\ \mathrm{Im}[M_k] & \frac{1}{2} + N_k + \mathrm{Re}[M_k] \end{pmatrix} .$$

In optics the most common process leading to decoherence is the phase insensitive loss of photons through diffusion and absorption mechanisms. In this case, an optical two–mode field undergoing to a lossy transmission, R is made of an infinite number of modes at room temperature in thermal equilibrium. For this kind of reservoir we can assume $M_k = 0$ (no squeezing), $N_k \simeq 0$ (zero thermal photons), so that the evolution of system S is described by the equation

$$\dot{\rho}_S(t) = \sum_{k=1,2} \frac{\Gamma_k}{2} \mathcal{L}[a_k]\, \rho_S(0) \ . \tag{1.45}$$

From now on, we will consider symmetric channels $\Gamma_k = \Gamma$ (for $k = 1, 2$). The Eq.(1.45) can be translated into the formalism of the characteristic function obtaining the following Fokker-Planck equation for $\chi_S(\mathbf{K})$ [18],

$$\dot{\chi}_S(\mathbf{K};t) = \frac{\Gamma}{2} \left[(X_k, Y_k) \begin{pmatrix} \partial_{X_k} \\ \partial_{Y_k} \end{pmatrix} + \frac{1}{2}\left(X_k^2 + Y_k^2\right) \right] \chi_S(\mathbf{K};0) \tag{1.46}$$

with $\boldsymbol{\sigma}_k^{(\infty)} = \boldsymbol{\sigma}_{vac} = \frac{1}{2}\mathbb{I}$, ($\mathbb{I}$ is the 4×4 identity matrix) covariance matrix for the vacuum state. It sets the standard quantum limit SQL.

It is possible to show, [6], that the evolution of $\rho_S(t)$ corresponds to the transformation of the annihilation operators of $k-$mode given by

$$a_k(0) \rightarrow a_k(t) = e^{-\frac{1}{2}\Gamma t} a_k(0) + \left(1 - e^{-\frac{1}{2}\Gamma t}\right) v_k \ ,$$

or, equivalently, for the vector of the field quadratures $\mathbf{K}$,

$$\mathbf{K}(t) = e^{-\frac{1}{2}\Gamma t}\mathbf{K}(0) + \left(1 - e^{-\frac{1}{2}\Gamma t}\right)\mathbf{V}_k,$$

where $\mathbf{V} \equiv (X_{vac,1}, Y_{vac,1}, X_{vac,2}, Y_{vac,2})^\top$ is the vector of the field quadratures of the vacuum state and v_k is the annihilation operator of the vacuum field (bath with average number photon equal to zero) associated to the $k-$mode of the system. In terms of the **CM** we have

$$\boldsymbol{\sigma}(t) = \left(1 - e^{-\Gamma t}\right)\frac{1}{2}\mathbb{I} + e^{-\Gamma t}\boldsymbol{\sigma}(0) \ , \tag{1.47}$$

where $\boldsymbol{\sigma}(0)$ is the covariance matrix at $t = 0$.

This form is in all equal to the effects of a fictious beam–splitter (BS) that mimicks the channel losses and couples into the system the vacuum quantum noise through its unused port [6]. Being $U_k(\zeta) = \exp\left\{\zeta\left(a_k^\dagger v_k - v_k^\dagger a_k\right)\right\}$ the SU(2) transformation induced by the BS on the k–mode (with v_k the modal operator for the vacuum) and

$$T = e^{-\Gamma t}$$

the power transmission of the beam splitter ($\tan\zeta = \sqrt{(1-T)/T}$) the above equations become

$$\begin{aligned} a_{k,T} &= \sqrt{T}a_{k,1} + \left(1 - \sqrt{T}\right)v_k \\ \mathbf{K}_{k,T} &= \sqrt{T}\mathbf{K}_{k,1} + \left(1 - \sqrt{T}\right)\mathbf{V}_k. \end{aligned}$$

In terms of the **CM** $\boldsymbol{\sigma}$ reads

$$\boldsymbol{\sigma}_T = (1-T)\frac{1}{2}\mathbb{I} + T\boldsymbol{\sigma}_1. \tag{1.48}$$

In this form we can drop the temporal dependence and label the **CM** of the initial state as $\boldsymbol{\sigma}_{T=1} \equiv \boldsymbol{\sigma}_1$.

Complete absorption, corrisponding to $t \rightarrow \infty$ (infite transmission time) and/or $\Gamma \rightarrow \infty$ (infinite channel damping), implies $T \rightarrow 0$ and $\boldsymbol{\sigma}_T \rightarrow \frac{1}{2}\mathbb{I}$, i.e. the covariance matrix of the vacuum state becomes

$$\lim_{T\rightarrow 0}\boldsymbol{\sigma}_T = \frac{1}{2}\mathbb{I} \ .$$

In the lossless case $T = 1$, corrisponding to $t \to 0$ (no transmission) and/or $\Gamma \to 0$ (no damping), the covariance matrix does not change compared to the initial $\boldsymbol{\sigma}_1$.

In the case of the Gaussian bi-partite states, the Eq. (1.48) implies the following evolution for the **CM** elements

$$n_T = \frac{1}{2} + T\left(n - \frac{1}{2}\right) \ ,$$

$$m_T = \frac{1}{2} + T\left(m - \frac{1}{2}\right) \ ,$$

$$c_{1(2),T} = T c_{1(2)}$$

where n, m, and $c_{1(2)}$ are the covariance matrix elements expressed as in standard form (1.23). The purity μ of the state can be calculated as a function of the parameter T in the simple case of initial *symmetrical diagonal* state ($n = m$ and $c = c_1 = -c_2$). We suppose that the covariance matrix born pure (so that $c = \sqrt{n^2 - 1/4}$) and that is afflicted by losses represented by T. Then the evolution of the purity is

$$\mu_T \tag{1.49}$$

$$= \frac{1}{4\sqrt{\det\left[\boldsymbol{\sigma}_T\right]}} \tag{1.50}$$

$$= \frac{1/4}{\sqrt{\frac{1}{4^2} + \left(\frac{n}{2} - \frac{1}{4}\right)T + (n-1)\left(n - \frac{1}{2}\right)T^2 - (2n-1)^2 T^3 + \left(n - \frac{1}{2}\right)^2 T^4}} \tag{1.51}$$

We note that the vacuum state obtained for $T = 0$ (or $t \to \infty$ or $\Gamma \to \infty$) is a pure one, i.e. $\mu_0 = 1$, obviously. Then, we can see that $\mu_{T \neq 0,1} < \mu_0$ but we cannot assume a monothonic behaviour in T. We note that the state purity cannot be considered a general entanglement marker (see Exemple 1 in the sub-Section 1.1, also). As a matter of fact, any pair of physical system in a pure state has $\mu = 1$ even if the systems of the pair are disentanlged. So μ is a measure of the of decoherence that has afflicted the ideal state.

In the Figure (1.3), we plot the purity as a function of T for different initially pure states. In each of them, we can see that $\mu = 1$ for $T = 0, 1$ and that the minimum value $\mu|_{T=0.5}$ is inversely proportional to the matrix element n_1, *i.e.* to the energy of the initial state.

1.5.1 Squeezed Bell in lossy environment

In this subsection, we want to study the realistic **SB** state obtained when the effects of the losses and the dechoerence of the open system are consider. We consider an environment composed by thermal bath, and we simulate the lossy of the photons via two fictitious beam splitters (each one for the two beams). The

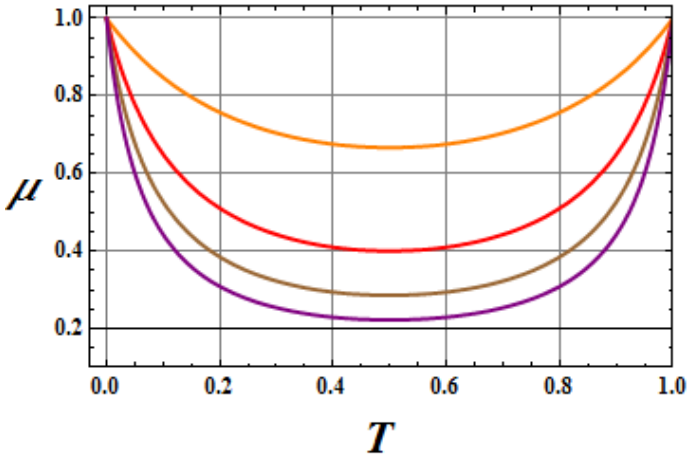

Figure 1.3: *(color online)* – The trend of the purity of quantum state as a function of the transmission coefficient T is shown. We plot the purity for different initially pure states with $c_1 = \sqrt{n_1^2 - 1/4}$: $n_1 = 1$ (orange line), $n_1 = 2$ (red line), $n_1 = 3$ (brown line), and $n_1 = 3$ (purple line). We can observe that $\mu_T = 1$ if $T = 0$ or 1, while the minimum value is at T = 0.5 and we have $\mu_{T=0.5}(n_1) = \frac{1}{n_1+0.5}$.

beam splitter 1 (2), BS_1 (BS_2), is illuminated by mode 1 (2) of the **SB** state and by the thermal state (of the reservoir) ρ_3^{th} $\left(\rho_4^{th}\right)$.

The density matrix of the output state is

$$\rho_{12}^{\mathbf{SB}} = \mathrm{Tr}_{34}\left[\hat{U}_{13}(T)\,\hat{U}_{24}(T)\,\hat{S}_{12}(\zeta)\,|C\rangle_{12}\;\rho_3^{th}\otimes\rho_4^{th}{}_{12}\,\langle C|\,\hat{S}_{12}^{\dagger}(\zeta)\,\hat{U}_{24}^{\dagger}(T)\,\hat{U}_{13}^{\dagger}(T)\right], \tag{1.52}$$

where $\hat{U}_{13}(T)$ and $\hat{U}_{24}(T)$ are the beam splitter operators that mix the modes $1-3$ and $2-4$, respectively, with trasmittivity T; the state $\hat{S}_{12}(\zeta)\,|C\rangle_{12}$ with $|C\rangle_{12} = c_1\,|00\rangle_{12} + c_2\,|11\rangle_{12}$, is the ideal **SB** state; ρ_k^{th} are the density matrix of the thermal state of modes $k = 3, 4$:

$$\rho_k^{th} = \frac{1}{1+\bar{n}_k}\sum_{m_k=0}^{\infty}\left(\frac{\bar{n}_k}{1+\bar{n}_k}\right)^{m_k}|m_k\rangle_{k\;k}\,\langle m_k|\,,$$

with $|m_k\rangle_k$ is the Fock state of the $k-$mode, with photon number m_k. In the formalism of the characteristic function, we have

$$\chi_{\mathbf{SB}}(\boldsymbol{\alpha}_1,\boldsymbol{\alpha}_2;T) = \mathrm{Tr}_{12}\left[\rho_{12}^{\mathbf{SB}}D_1(\alpha_1)\,D_2(\alpha_2)\right], \tag{1.53}$$

with $\rho_{12}^{\mathbf{SB}}$ given by Eq.(1.52). We prefer calcutate the (1.53) with a alternative strategy. We start from the characteristic funcions of the ideal **SB** state $\chi_{\mathbf{SB}}(\boldsymbol{\alpha}_1;\boldsymbol{\alpha}_2)$,

$$\begin{aligned}\chi_{\mathbf{SB}}(\boldsymbol{\alpha}_1,\boldsymbol{\alpha}_2) &= \left\{c_1^2 + 2c_1c_2\,\mathrm{Re}\left[e^{i\theta}\xi_1\xi_2\right] + c_2^2\left(1-|\xi_1|^2\right)\left(1-|\xi_2|^2\right)\right\}\\ &\quad\times\exp\left\{-\frac{1}{2}\left(|\xi_1|^2+|\xi_2|^2\right)\right\}\,,\end{aligned} \tag{1.54}$$

where

$$\begin{aligned} 1 &= c_1^2 + c_2^2, \quad \text{with } c_1, c_2 \in \mathbb{R} \\ \xi_k &= \alpha_k \cosh r + \alpha_h^* e^{i\phi} \sinh r \qquad (k, l = 1, 2; k \neq l)\,, \end{aligned}$$

and of the thermal state $\chi_{th}(\boldsymbol{\alpha}_3; \boldsymbol{\alpha}_4)$,

$$\chi_{th}(\boldsymbol{\alpha}_3; \boldsymbol{\alpha}_4) = \exp\left\{-\frac{1}{2}(2\bar{n}+1)\left(|\alpha_3|^2 + |\alpha_4|^2\right)\right\}\,.$$

We assumed that the average number of thermal photons $\bar{n}$ is the same for both modes. Befor the two fictitious beam splitters, the overall state is given by

$$\chi_{preBS}(\boldsymbol{\alpha}_1; \boldsymbol{\alpha}_2; \boldsymbol{\alpha}_3; \boldsymbol{\alpha}_4) = \chi_{\mathbf{SB}}(\boldsymbol{\alpha}_1; \boldsymbol{\alpha}_2)\, \chi_{th}(\boldsymbol{\alpha}_3; \boldsymbol{\alpha}_4)\,.$$

The beam splitters act on the state through a SU(2) trasformation such as

$$\alpha_{1,2} \longrightarrow \sqrt{T}\alpha_{1,2}, \tag{1.55}$$

$$\alpha_{3,4} \longrightarrow \sqrt{1-T}\alpha_{1,2}, \tag{1.56}$$

where we have trace out the modes $\boldsymbol{\alpha}_{3,4}$, putting $\boldsymbol{\alpha}_{3,4} = 0$ in the characteristic functions. In terms of the quantity $\xi_{1,2}$, the (1.55) and (1.56) involve the following trasformation

$$\xi_{1,2} \longrightarrow \sqrt{T}\xi_{1,2}.$$

Finally, the characteristic function of the realistic **SB** state becomes

$$\begin{aligned} &\chi_{\mathbf{SB}}(\boldsymbol{\alpha}_1, \boldsymbol{\alpha}_2; T) \\ = \;& e^{-\frac{1}{2}\left[T\left(|\xi_1|^2+|\xi_2|^2\right)+(2\bar{n}_k+1)(1-T)\left(|\alpha_1|^2+|\alpha_2|^2\right)\right]} \\ & \times \left\{c_1^2 + 2c_1c_2T\,\mathrm{Re}\left[e^{i\theta}\xi_1\xi_2\right] + c_2^2\left(1-T|\xi_1|^2\right)\left(1-T|\xi_2|^2\right)\right\}. \end{aligned}$$

For the reasons set out before we can put $\bar{n}_k \simeq 0$, so we have

$$\begin{aligned} &\chi_{\mathbf{SB}}(\boldsymbol{\alpha}_1, \boldsymbol{\alpha}_2; T) \\ = \;& e^{-\frac{1}{2}\left[T\left(|\xi_1|^2+|\xi_2|^2\right)+(1-T)\left(|\alpha_1|^2+|\alpha_2|^2\right)\right]} \\ & \times \left\{c_1^2 + 2c_1c_2T\,\mathrm{Re}\left[e^{i\theta}\xi_1\xi_2\right] + c_2^2\left(1-T|\xi_1|^2\right)\left(1-T|\xi_2|^2\right)\right\}. \end{aligned} \tag{1.57}$$

With a appropriate choice of parameters c_1 and c_2, from this function (1.57) we can obtain the corresponding realistic versions of the squeezed vacuum, squeezed number, photon-added squeezed and photon subtracted sqeezed states. For exemple, putting $c_2 = 0$, we have the evolution of the squeezed vacuum state $\hat{S}_{12}(\zeta)\,|00\rangle_{12}$ in terms of the characteristic function

$$\chi_{\mathbf{TB}}(\boldsymbol{\alpha}_1; \boldsymbol{\alpha}_2; T) = e^{-\frac{1}{2}\left[T\left(|\xi_1|^2+|\xi_2|^2\right)+(1-T)\left(|\alpha_1|^2+|\alpha_2|^2\right)\right]}.$$

1.5.2 Realistic Variances

In this subsection, we calculate the averages and the variances of the quadratures using the realistic **SB** state described by the characteristic function (1.57). Even in case of a real channel, we have that the averages of the quadratures are zero

$$\langle X_k \rangle = \langle Y_k \rangle = \langle X_{\varkappa} \rangle = \langle Y_{\varkappa} \rangle = 0 \ ,$$

while the variances of modes $k = 1, 2$ are given by

$$\left\langle \Delta X_k^2 \right\rangle = \left\langle \Delta Y_k^2 \right\rangle = \frac{1}{2} \left[1 - T + T \left(c_1^2 + 3c_2^2 \right) \cosh\left(2r\right) \right] \ ,$$

and the variances of modes c and d are

$$\begin{aligned} \left\langle \Delta X_c^2 \right\rangle &= \left\langle \Delta Y_d^2 \right\rangle = \frac{1}{2} \left\{ 1 - T + T \left(c_1^2 + 3c_2^2 \right) \left[\cosh\left(2r\right) - \cos\left(\phi_r\right) \sinh\left(2r\right) \right] \right\} \ , \\ \left\langle \Delta Y_c^2 \right\rangle &= \left\langle \Delta X_d^2 \right\rangle = \frac{1}{2} \left\{ 1 - T + T \left(c_1^2 + 3c_2^2 \right) \left[\cosh\left(2r\right) + \cos\left(\phi_r\right) \sinh\left(2r\right) \right] \right\} \ . \end{aligned}$$

The same procedure of minimization, used in the ideal case, leads to the condition

$$\phi_r = 2k\pi \ , \text{ with } k \in \mathbb{N} \ ,$$

So we have

$$\begin{aligned} \left\langle \Delta X_c^2 \right\rangle &= \left\langle \Delta Y_d^2 \right\rangle = \frac{1}{2} \left\{ 1 - T + T \left(c_1^2 + 3c_2^2 \right) e^{-2r} \right\} \ , \\ \left\langle \Delta Y_c^2 \right\rangle &= \left\langle \Delta X_d^2 \right\rangle = \frac{1}{2} \left\{ 1 - T + T \left(c_1^2 + 3c_2^2 \right) e^{2r} \right\} \ . \end{aligned}$$

Further minimizing the squeezed variance with respect to the free parameters c_1 and c_2, we obtain $c_1 = 1 \left(\Rightarrow c_2 = 0\right)$ and the variances become

$$\left\langle \Delta X_k^2 \right\rangle = \left\langle \Delta Y_k^2 \right\rangle = \frac{1}{2} \left[1 - T + T \cosh\left(2r\right) \right] \ ,$$

for $k = 1, 2$ and

$$\left\langle \Delta X_c^2 \right\rangle = \left\langle \Delta Y_d^2 \right\rangle = \frac{1}{2} \left\{ 1 - T \left(1 - e^{-2r} \right) \right\} \ , \tag{1.58}$$

$$\left\langle \Delta Y_c^2 \right\rangle = \left\langle \Delta X_d^2 \right\rangle = \frac{1}{2} \left\{ 1 - T \left(1 - e^{2r} \right) \right\} \ , \tag{1.59}$$

for the modes c and d. So, in the realistic case, the lower limit for the squeezed variance is $\left(1 - T\right)/2$, correspondent to $r \to \infty$. When T tends to 1 (ideal case), the variances (1.58) and (1.59) tend to ideal values given by $e^{-2r}/2$ and $e^{+2r}/2$, respectively, and their lower limit approaches zero. For $T \to 0$ (maximally absorption case) the variances tend to the vacuum state variances $\left(\frac{1}{2}\right)$, regardless of the value of r.

1.5.2.1 Effective parameter of squeezing

We can think of using the relations (1.58) and (1.59) to obtain a effective parameter of squeezing r'. In fact, because of decoherence at the exit of the source of squeezed vacuum, the effective parameter of squeezing is not r but a parameter r' which takes account of the losses, by means of coefficient T (see Fig. (1.4)).

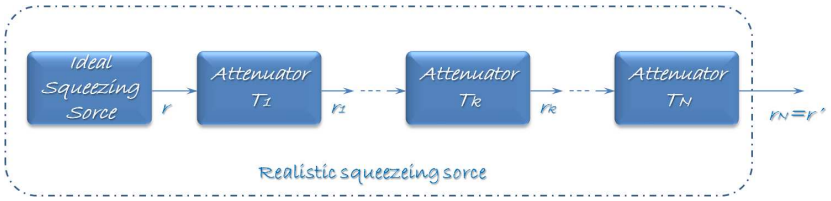

Figure 1.4: Schematic representation of a squeezed vacuum source subjected to the degrading action of the external environment. A vacuum squeezed source with ideal parameter of squeezing r, subjected to N attenuating stages, with attenuation coefficients T_k, respectively, is equivalent to a single source of ideal squeezing with squeezing parameter $r' = -\frac{1}{2}\ln\left[1 - \left(\prod_{k=1}^{N} T_k\right)\left(1 - e^{-2r}\right)\right]$.

Thus, the relation between the observable realistic parameter of squeezing r', after the losses, and the parameter of squeezing r of the ideal squeezed vacuum state is given by

$$\begin{aligned}\left\langle \Delta X_c^2 \right\rangle &= \frac{1}{2}\left[1 - T\left(1 - e^{-2r}\right)\right] \\ &= \frac{1}{2}e^{-2r'}.\end{aligned}$$

The inverse relation is

$$\begin{aligned}r' &= -\frac{1}{2}\ln\left[2\left\langle \Delta X_c^2 \right\rangle\right] \\ &= -\frac{1}{2}\ln\left[1 - T\left(1 - e^{-2r}\right)\right]. \end{aligned} \tag{1.60}$$

We also note that the relation (1.60) confirms the 'multiplicative nature' of the attenuation coefficients of the more sequential. In fact, observing the Fig. (1.4), let r be the parameter of squeezing of the squeezed vacuum source and N the number of consecutive attenuating stages, each characterized by an attenuation coefficient $0 < T_k < 1$, $(k = 1, ..., N)$ and a parameter of squeezing r_k. Then the final parameter of squeezing $r' = r_N$ is given by

$$r_N = -\frac{1}{2}\ln\left[1 - T_N\left(1 - e^{-2r_{N-1}}\right)\right],$$

where the generic parameter r_k is

$$r_k = -\frac{1}{2}\ln\left[1 - T_k\left(1 - e^{-2r_{k-1}}\right)\right],$$

with $r_0 = r$.

Substituting these recurrence relations we obtain that the entire system is equivalent to a single block with a effective parameter of squeezing r' equal to

$$r' = -\frac{1}{2}\ln\left[1 - T_{eff}\left(1 - e^{-2r}\right)\right],$$

where

$$T_{eff} = \prod_{k=1}^{N} T_k.$$

Then, a squeezed vacuum source with parameter of squeezing r, which transmits in a lossy environment, is fully equivalent to a vacuum squeezed source with rescaled parameter r' given by Eq.(1.60). The link between r and $r\prime$ is shown in Fig. (1.5) for different values of the effective transmittivity.

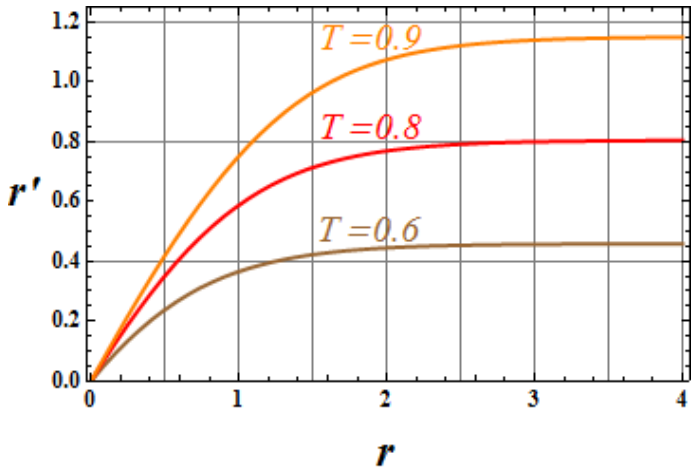

Figure 1.5: *(color online)* − Behavior of the parameter of effective squeezing r' as a function of the parameter r of the ideal squeezed source for three different values of the transmissivity: $T_{eff} = 0.6$ (brown line), $T_{eff} = 0.8$ (red line), and $T_{eff} = 0.9$ (orange line) .

We can note that if the observed realistic squeezing parameter r' goes to zero, then the ideal squeezing parameter r goes to zero as well $\forall T_{eq}$. There is no value of $r > 0$ and T_{eq} such that the observed squeezing r' is null. This implies that the decoherence attenuates the size of squeezing but cannot make it null.

CHAPTER 2

QUANTUMNESS

In this Chapter, we present a quick overview of the main quantum features, whose classical systems are lacking. The main peculiarity of quantum systems is the principle of superposition of states, *i.e.* the possibility to describe a physical system through a *simultaneous superposition* of more possible configurations. From this principle it descends large part of the purely quantum physical characteristics, *i.e.* the *quantumness* of a physical system. We are primarily interested in bi-partite bosonic systems treatable with the approach of the continuous variables (**CV**).

In this scenario, the quantumness of a bi–partite **CV** state can be tested by two classes of markers. The first is intimately related to the the state itself and includes inequalities that fix bounds for distinguishing among different types of entangled and un–entangled states. They are called entanglement criteria and are usually named by the authors that have theoretically found them. They are the Duan, EPR–Reid (Einstein-Podolsky-Rosen–Reid) and PHS (Peres-Horodecki-Simon) criteria.

The second has been translated into the quantum context from the classical information theory and is related to the amount of quantum information carried by the state. It includes quantitative measures such as mutual information, von Neumann entropy, and quantum discord.

Another useful indicator of quantumness of a state is the teleportation fidelity of a coherent state. In fact, in [25] it is shown that when the fidelity $\mathcal{F}$ is higher than the classical limit ($\mathcal{F} > \mathcal{F}_{class} = 0.5$), the resource that realizes the teleportation protocol is certainly quantum.

Finally, we discuss the Bell's non-locality. We see that when an inequality, called *Bell's inequality*, is violated then the physical system can not be described by classical theory.

The Chapter is organized as follows: in Section 2.1 we define the entanglement and discuss briefly about the difficult problem inherent in its quantification. In particular, we analyze the case of pure (sub-sect. 2.1.1) and mixed (sub-sect. 2.1.2) bi-partite states. In the second case (mixed states), we discuss the criteria of Duan, EPR-Reid, and PHS for Gaussian bi-partite states described by the covariance matrix written in the standard form Eq. (1.23). In Sect. 2.2 we present the **CV** protocol of quantum teleportation of Braunstein, Kimble [26], and Vaidman [27] in the characteristic function formalism. The analysis in this Section has a twofold utility:

i. for Gaussian resources, the fidelity provides indications on the quantumness

(entanglement) of the resource state;

ii. for non-Gaussian (**SB**) resources the fidelity of teleportation is maximized.

In Section 2.3 we discuss the mutual information and quantum discord. Finally, in Section 2.4 we present the non-locality of some bi-partite states expressed by the Bell's inequality.

2.1 Entanglement

As we have already said, a quantum state, described by density matrix ρ_S acting in $\mathcal{H}_S$, is called *separable* if it can be represented as the tensor product of its two sub-systems,

$$\rho_S = \rho_A \otimes \rho_B, \tag{2.1}$$

where ρ_A acts in $\mathcal{H}_A$ and ρ_B acts in $\mathcal{H}_B$ such that $\mathcal{H}_S = \mathcal{H}_A \otimes \mathcal{H}_B$. When the system is separable, the measurement results of the quantity A in $\mathcal{H}_A$ are not tied to the measurement results of the quantity B in $\mathcal{H}_B$. The knowledge of ρ_A prescinds from knowledge of ρ_B. In this case we can write that

$$\langle AB \rangle_{\rho_S} = \langle A \rangle_{\rho_A} \langle B \rangle_{\rho_B} \ ,$$

i.e. the correlation $\langle AB \rangle_{\rho_S}$ between the observables A and B, in the overall state ρ_S, corresponds to the product of the expectation values of the operators themselves. If $\rho_S \neq \rho_A \otimes \rho_B$, the state is non-factorizable and the quantity

$$\langle AB \rangle_{\rho_S} - \langle A \rangle_{\rho_A} \langle B \rangle_{\rho_B} \ , \tag{2.2}$$

no longer disappears. In this case, the two sub-systems are correlated and a measurement performed on a sub-system influences the measurements made on the other. The knowledge of ρ_A can not ignore the knowledge of ρ_B. A non-separable state is called *entangled* [12].

Although several entanglement measures $E(\rho)$ have been proposed, it has not been found a general solution to the problem of a quantitative measure of entanglement for a generic quantum state. However all researchers in this field seem to agree on the following three conditions that a good entanglement measurament $E(\rho)$ must comply [28]:

1. $E(\rho_S) = 0$ iff ρ_S is separable, *i.e.* if the density matrix can be writen as $\rho_S = \sum_j p_j \rho_j^{(A)} \otimes \rho_j^{(B)}$;
2. $E(\rho_S)$ should not increse under local operations and classical communication procedures (LOCC), i.e. $E\left(U_{AB}\rho_S U_{AB}^{\dagger}\right) = E(\rho_S)$, with $U_{AB} = U_A \otimes U_{AB}$. We intuitively know that such procedures (LOCC) cannot add non-locality characteristics to the system;

3. Convexity: $E(\alpha\rho_1 + (1-\alpha)\rho_2) \leq \alpha E(\rho_1) + (1-\alpha) E(\rho_2)$, with $\alpha \in [0,1]$;

Sometimes one impose further requirements:

4. Additivity: $E(\rho_1 \otimes \rho_2) = E(\rho_1) + E(\rho_2)$;

5. Continuity: $E(\rho_S)$ is a continuous function of ρ_S,

   or

5'. Asymptotic continuity: $E(\rho_S)$ is a continuous function of the fidelity for n copies of the same pure state $|\psi\rangle$ in the asymptotic limit $n \to \infty$.

The main problem resides in the fact that, in general, a measure of entanglement, which satisfies all these conditions was not found. Several measures that do not satisfy all the properties have been proposed, but the request of ordering is not always respected. Given two different quantum states ρ_A and ρ_B, subjected to two different (non-optimal) entanglement measures E_1 and E_2, the following unpleasant circumstance can happen

$$\begin{aligned} E_1(\rho_A) &< E_1(\rho_B), \\ E_2(\rho_A) &> E_2(\rho_B). \end{aligned}$$

2.1.1 Pure bi-partite states: Schmidt's decomposition and von Neumann entropy

The problem of the entanglement measure is solved for bi-partite pure states [29]. For these states the non-zero correlation, Eq. (2.2), implies entanglement. The authors of reference [29] showed that the von Neumann entropy of the partial traces of the sub-systems of the pure bi-partite system is a good entanglement measure. In fact, referring to the situation discussed in Example 1 of subsection 1.1, we write the wave function of the state AB into the form given by the *Schmidt decomposition* [30]

$$|\psi\rangle_{AB} = \sum_{k=1}^{d} \lambda_k |\phi_k\rangle_A \otimes |\eta_k\rangle_B \ ,$$

with $\sum_{k=1}^{d} |\lambda_k|^2 = 1$. The number of nonzero amplitudes λ_k is known as the *Schmidt number* (or *Schmidt rank*) and gives unique information on the separability of the state only in the case of bi-partite pure states. In fact, the Schmidt number of a state is greater than 1 if and only if it is entangled: the state is maximally entangled and its Schmidt coefficients λ_k are all equal to $d^{-1/2}$ (the Schmidt number is maximum). We can write the density matrices of the two sub-systems

A and B as

$$\rho_A = \sum_k |\lambda_k|^2 |\phi_k\rangle_{A\ A} \langle\phi_k| , \tag{2.3}$$

$$\rho_B = \sum_k |\lambda_k|^2 |\eta_k\rangle_{B\ B} \langle\eta_k| , \tag{2.4}$$

hence the partial traces of a maximally entangled state give the maximally chaotic states in their respective Hilbert space.

This link between entanglement of a system and chaos of its sub-systems suggests to introduce the von Neumann entropy as a entanglement measure. Another consideration is related to the analogy between irreversible processes in thermodynamic systems and quantum ones [29]. In fact, as it is impossible to build a *perpetuum mobile* because the entropy can not decrease in thermodynamic processes, in the same way the entanglement of a quantum system can not increase by local operations (condition 2 for an entanglement measure).

So, introducing the von Neumann entropy [30] of the system ρ,

$$S_{vN}(\rho) = -\mathrm{Tr}\left[\rho \ln \rho\right] , \tag{2.5}$$

the entanglement measure is given by

$$\begin{aligned} E(\rho_{AB}) &= S_{vN}(\rho_k) \\ &= -\mathrm{Tr}_k\left[\rho_k \ln \rho_k\right] , \end{aligned}$$

where ρ_k, $k = A, B$, is the (reduced) density matrix of the sub-system k. For the states (2.3) and (2.4) we have

$$S_{vN}(\rho_A) = S_{vN}(\rho_B) = \begin{cases} -\sum_k |\lambda_k|^2 \ln |\lambda_k|^2 & \text{for } \lambda_k \neq 0 \\ 0 & \text{for } \lambda_k = 0 \end{cases} .$$

It ranges from zero, for separable states ($\lambda_{\bar{k}} = 1$ and $\lambda_{k\neq\bar{k}} = 0$), to one for maximally entangled states ($\lambda_k = d^{-1/2}$, $\forall k$).

2.1.2 Mixed bi-partite Gaussian states: entanglement criteria

For mixed states there isn't a entanglement measure that satisfies all the conditions given above. There are, however, criteria of separability which do provide sufficient conditions for entanglement. However, in some circumstances, for bi-partite Gaussian states such criteria become necessary and sufficient. In this sub-Section we analyze some main criteria: the Peres-Horodecki-Simon [31], Duan [32], and EPR-Reid [33] criterion. At first, we give the analogous of the Eq.(2.1) for mixed states.

A bi-partite quantum state is separable iff its density operator can be written as a convex combination of the tensor product of density operators relative to the two different sub–spaces [121]

$$\rho = \sum_j p_j \rho_j^{(A)} \otimes \rho_j^{(B)}, \tag{2.6}$$

where $\sum_j p_j = 1$ while $\rho_j^{(k)}$ are the density matrices of sub-system $k = A, B$.

2.1.2.1 The Peres-Horodecki-Simon (PHS) criterion

The criterion of separability PHS uses the notion of positive map. We consider the map

$$\mathcal{L} : O_1 \to \tilde{O}_1 \ ,$$

that associates the operator O_1 to the operator $\tilde{O}_2 = \mathcal{L}(O_1)$. The map $\mathcal{L}$ is called positive if it sends positive operators into positive operators. A transformation that has physical sense, in addition to being positive, must also satisfy the following requirement:

> *if the transformation is applied to a only part of the system and the other part is left undisturbed, after processing the overall state must still be described by defined positive density operators.*

This requirement is satisfied if the map is completely positive. In formulas, the map $\mathcal{L}$ is completely positive if

$$\mathcal{L} \otimes \mathcal{I}_2 : O_1 \otimes O_2 \to \tilde{O}_1 \otimes O_2,$$

is positive for the generic operator O_1 acting on the sub-system 1, and $\mathcal{I}_2$ is the identity map acting on the sub-system 2.

A map positive, but not completely positive, allows to evaluate the separability of the state. In fact, we consider the tensor product state $\rho^{(A)} \otimes \rho^{(B)}$, where $\rho^{(k)}$ is the density matrix of the sub-system $k = A, B$, such that

$$\mathcal{L} \otimes \mathcal{I}_A : \rho^{(A)} \otimes \rho^{(B)} = \mathcal{L}\left(\rho^{(A)}\right) \otimes \rho^{(B)} \geq 0, \tag{2.7}$$

then the positive map sends product (separable) states in positive operators. Otherwise, if the state is non-separable there is a positive map $\mathcal{L}$ for which the Eq. (2.7),

$$\mathcal{L} \otimes \mathcal{I}_A : \rho^{(A)} \otimes \rho^{(B)},$$

is not positive. The PHS criterion makes use of the partial transpose ($\mathcal{PT}$) map, that realizes the operation of transposition of the density matrix with respect to only one of the two density matrices $\rho^{(A)}$ or $\rho^{(B)}$, *e.g.* $\rho^{(A)}$. So we have:

$$\mathcal{PT} : \rho_{AB} \to \sum_j p_j \left(\rho_j^{(A)}\right)^{\mathsf{T}} \otimes \rho_j^{(B)},$$

where we have assumed *a priori* that the state has factorized form Eq. (2.6). Because $\left(\rho_j^{(A)}\right)^{\mathsf{T}}$ is non-negative and preserves the unity of the trace, it is still a density matrix. It follows that if the state ρ_{AB} is separable then $\rho_{AB}^{\mathcal{PT}} = \mathcal{PT}\left(\rho_{AB}\right)$ should still represent a physical state so that any eigenvalue of $\rho_{AB}^{\mathcal{PT}}$ is non-negative. On the contrary if $\rho_{AB}^{\mathcal{PT}}$ exhibits negative eigenvalues, it no more represents a physical state and the system does not admit the form hypothesized *a priori* (2.6). In this case, the factorized form of Eq. (2.6) is not adequate for the state ρ_{AB}.

Thus, all separable states have a non-negative partially transposed density operator. From this consideration it is possible to deduce a necessary condition for separability or, viceversa, a sufficient condition for entanglement. In view of this the criterion is sometime referred to as the *ppt* criterion (*positivity* under *partial transposition*) [119, 120, 31]. In the following we prefer to indicate it as the PHS criterion. It can be proven that it becomes a necessary and sufficient condition for Gaussian states [31]. In terms of the characteristic function χ_{AB} of a bi-partite system, the map $\mathcal{PT}$ corresponds to the transformation

$$\mathcal{PT} : \chi_{AB}\left(X_a, Y_a, X_b, Y_b\right) \rightarrow \chi_{AB}\left(X_a, -Y_a, X_b, Y_b\right),$$

which is given by a change of sign of out–of–phase quadrature (usually indicated as Y). Partial transposition is, therefore, a "local time reversal" which inverts the Y quadrature of only one sub-system, $Y_a \rightarrow -Y_a$. It is defined as "time reversal" (or mirror reflection) in the phase space, also:

$$\mathcal{PT} : \mathbf{K} \rightarrow \mathbf{\Lambda}_A \mathbf{K},$$

with $\mathbf{\Lambda}_A \equiv \mathrm{diag}(1, -1, 1, 1) \equiv \mathbf{Z} \oplus \mathbb{I}$,

$$\mathbf{Z} \equiv \begin{pmatrix} 1 & 0 \\ 0 & -1 \end{pmatrix}, \tag{2.8}$$

and $\mathbb{I}$ is the 2×2 identity matrix. In these terms, the PHS criterion can be stated as follows:

> *if the state ρ_{AB} is separable, then when the map PT is applied the its characterereristic function $\chi_{AB}\left(\mathbf{K}\right)$ turns into one specularly reflected $\chi_{AB}\left(\mathbf{\Lambda}_A \mathbf{K}\right)$ in the phase space.*

Both $\chi_{AB}\left(\mathbf{K}\right)$ as $\chi_{AB}\left(\mathbf{\Lambda}_A \mathbf{K}\right)$ are good characteristic functions. The specular reflection of the type $\mathbf{\Lambda}_A$ is, therefore, a symmetry in the subspace of separable states [31]. This transformation acts, of course, also on the correlation matrix (1.23)

$$\boldsymbol{\sigma} \rightarrow \mathbf{\Lambda}_A \boldsymbol{\sigma} \mathbf{\Lambda}_A.$$

In terms of the covariance matrix, the (separability) PHS criterion can be expressed by the inequality

$$\mathbf{\Lambda}_A \boldsymbol{\sigma} \mathbf{\Lambda}_A + \frac{i}{2}\Omega \geq 0 \ ,$$

or equivalently

$$\boldsymbol{\sigma} \geq -\frac{i}{2}\mathbf{\Lambda}_A \Omega \mathbf{\Lambda}_A \ .$$

In terms of the symplectic invariants, Eqs. (1.19-1.22), partial transposition implies the transformations

$$\begin{aligned} \tilde{I}_{1,2,4} &= I_{1,2,4}, \\ \tilde{I}_3 &= -I_3, \end{aligned}$$

where I_j and $\tilde{I}_j$ are related to the correlation matrix $\boldsymbol{\sigma}$ and $\mathbf{\Lambda}_A \Omega \mathbf{\Lambda}_A$, respectively. As a result, a separable bi-partite Gaussian state must obey the uncertainty relation for $\boldsymbol{\sigma}$ and for $\mathbf{\Lambda}_A \Omega \mathbf{\Lambda}_A$

$$\tilde{\Delta}\left(\boldsymbol{\sigma}\right) \leq 4I_4 + \frac{1}{4} \ ,$$

with $\tilde{\Delta}\left(\boldsymbol{\sigma}\right) = \Delta\left(\mathbf{\Lambda}_A \Omega \mathbf{\Lambda}_A\right) = I_1 + I_2 - 2I_3$. Then, the condition of separability of the PHS criterion becomes: *a bi-partite Gaussian state is separable iff*

$$n^2 + m^2 + 2\left|c_1 c_2\right| - 4\left(nm - c_1^2\right)\left(nm - c_2^2\right) \leq \frac{1}{4} \ , \tag{2.9}$$

$$I_1 + I_2 + 2\left|I_3\right| - 4I_4 \leq \frac{1}{4} \tag{2.10}$$

and it is entangled otherwise.

We also note that the PHS criterion is invariant under symplectic transformations. Finally, using the symplectic eigenvalues, defined in Eq.(1.25), the criterion of separability becomes [18]

$$\tilde{d}_{\pm} \geq \frac{1}{2} \ ,$$

where

$$\tilde{d}_{\pm} = \sqrt{\frac{\tilde{\Delta}\left(\boldsymbol{\sigma}\right) \pm \sqrt{\tilde{\Delta}\left(\boldsymbol{\sigma}\right) - 4I_4}}{2}} \ .$$

PHS criterion relies on the possibility of describing independently the two sub-systems. If any *true quantum* correlation is set between Y_1 and Y_2 a sign flip on Y_1 (or Y_2) will affect the sign of c_1 (or c_2) in Eq. (1.23) making $\rho_{AB}^{\mathcal{PT}}$ no more physical.

2.1.2.2 The Duan criterion

For every **CV** entangled state there exists a pair of EPR–like conjugate operators defined by [32]

$$u = |a|\, x_1 + \frac{1}{a} x_2 \text{ and } v = |a|\, p_1 - \frac{1}{a} p_2 \ , \tag{2.11}$$

with a an arbitrary non–zero real number and $[x_j, p_{j'}] = \frac{i}{2}\delta_{jj'}$ $(j, j' = 1,\ 2)$ and where subscript 1 (2) refers to the entangled sub-systems. In the ideal case the variances of the above operators reduce to zero and the entangled system is in a co–eigenstate of the above operators. Of course, these eigenstates of the whole system, would require an infinite amount of energy and so they are not physical. Then, for discussing the birth of non–classical correlation between sub–systems 1 and 2, we will consider states for which the variance of EPR–like operators will reduce below the standard quantum limit (SQL) signalling the presence of non–classical features. By calculating the total variance of such a pair of operators on ρ_{AB}, a separable state of the form of Eq. (2.6), it can be proven [32] that the inequality

$$\left\langle (\Delta \widehat{u})^2 \right\rangle_{\rho_{AB}} + \left\langle (\Delta \widehat{v})^2 \right\rangle_{\rho_{AB}} \geq a^2 + \frac{1}{a^2} \ , \tag{2.12}$$

sets a lower bound for separable states. Contrarily to the PHS criterion (see Sect. 2.1.2.1) inequality (2.12) has been formulated as a sufficient condition for separability so that it is a necessary condition for entanglement of a generic **CV** state.

As shown in [32] it becomes a necessary and sufficient condition for entangled **CV** Gaussian states. The sufficient and necessary condition can be expressed in terms of the covariance matrix elements iff the matrix itself is expressed in the form of Eq. (10) of Ref. [32]

$$\boldsymbol{\sigma} = \begin{pmatrix} n_1 & 0 & c_1 & 0 \\ 0 & n_2 & 0 & c_2 \\ c_1 & 0 & m_1 & 0 \\ 0 & c_2 & 0 & m_2 \end{pmatrix} \ , \tag{2.13}$$

with the matrix elements satisfying the constrains (11a) and (11b) of Ref. [32] that, for the SQL equal to $\frac{1}{2}$, read

$$\begin{aligned} \frac{n_1 - 1/2}{m_1 - 1/2} &= \frac{n_2 - 1/2}{m_2 - 1/2} \ , \\ |c_1| - |c_2| &= \sqrt{(n_1 - 1/2)\,(m_1 - 1/2)} - \sqrt{(n_2 - 1/2)\,(m_2 - 1/2)} \ . \end{aligned} \tag{2.14}$$

In this case the EPR operators pair of Eq. (2.11) are written as

$$u = a_0 x_1 + \mathrm{sgn}\,(c_1)\, \frac{1}{a_0} x_2 \text{ and } v = a_0 p_1 - \mathrm{sgn}\,(c_2)\, \frac{1}{a_0} p_2 \ ,$$

where $a_0 = \sqrt{\frac{m_1-1/2}{n_1-1/2}} = \sqrt{\frac{m_2-1/2}{n_2-1/2}}$. With the sufficient and necessary Duan criterion given by

$$a_0^2 (n_1 + n_2 - 1) + \frac{m_1 + m_2 - 1}{a_0^2} - 2 (|c_1| - |c_2|) < 0 \ . \tag{2.15}$$

We note that, as proved in Ref. [32], any Gaussian state can be transformed into the form (2.13) by local linear unitary Bogoliubov operations, i.e. by acting independently on one or both the sub-systems by applying local squeezing and/or rotations.

In a more general context it is possible to write the sufficient but not necessary criterion for a generic **CM** in the standard form of Eq. (1.23) as

$$(2n-1)\, a^2 + \frac{(2m-1)}{a^2} - 2 (c_1 - c_2) < 0 \ ,$$

where a can be set by $a^2 = \sqrt{\frac{m-1/2}{n-1/2}}$ to minimize the left hand side of the inequality:

$$\sqrt{(2n-1)(2m-1)} - (c_1 - c_2) < 0 \ . \tag{2.16}$$

We note that, while for symmetric states ($m = n$) $|a| = 1$ the EPR pair consists of two orthogonal field quadratures, this is not true, in general.

The Duan criterion is strictly related to the Heisenberg principle for the single sub–system. If the state is separable the indeterminacy on a single operator is disjoint from the indeterminacy of the twin operator on the second sub–system; so that the total indeterminacy cannot violate the Heisenberg limit. This has nothing to do with conditional measurement and with the possibility of gaining information on one sub–system measuring the other. As we will see this approach leads to a stricter criterion: the so–called EPR−Reid criterion.

2.1.2.3 The EPR−Reid criterion

A stronger bound can be found by analysing a bi–partite state under the shadow of conditional measurements. This concept descends directly from the original EPR *gedanken* experiment [34]. For this reason this criterion is usually indicated as the EPR criterion and was firstly introduced by Reid in 1989 [33], in the very early days of quantum information. It describes the ability to deduce the expectation value of an observable on a sub–system by measuring the EPR companion observable on the second sub–system. Contrarily to the Duan and PHS criteria EPR-Reid one sets, by principle, only a sufficient condition for assessing entanglement.

Mathematically this criterion can be deduced by calculating the conditional variance for an observable on sub–system A given the result of a measurement on sub–system B and comparing it with the standard quantum limit:

$$V_{a|b} < 1/2 \ , \tag{2.17}$$

with

$$V_{a|b} = \left\langle \Delta \mathfrak{X}_a^2 \right\rangle \left(1 - C_{ab}^2\right),$$

where C_{ab} is the correlation coefficient related to the simultaneous measurements of the field generalized quadrature $\mathfrak{X}_a \mathfrak{X}_b$:

$$C_{ab} \equiv \frac{\langle \Delta \mathfrak{X}_a \mathfrak{X}_b \rangle}{\sqrt{\langle \Delta \mathfrak{X}_a^2 \rangle \langle \Delta \mathfrak{X}_b^2 \rangle}}. \tag{2.18}$$

For Gaussian states the Eq. (2.17) can be written in terms of **CM** elements:

$$n^2 \left(1 - \frac{c_1^2}{nm}\right)\left(1 - \frac{c_2^2}{nm}\right) < \frac{1}{4}\,. \tag{2.19}$$

We note that, being based on conditional variances (and thus on conditional states) this last criterion is not symmetric under the exchange of the two sub-systems. So that the criterion itself can be recast if sub–system A is measured and the conditional variance on B is given

$$m^2 \left(1 - \frac{c_1^2}{nm}\right)\left(1 - \frac{c_2^2}{nm}\right) < \frac{1}{4}\,.$$

The two definitions of the EPR criterion can make it ambiguous if one of the relations are not satisfied. This is not the case of balanced systems ($m = n$). Moreover, it can be proved that no pure state can asymmetrically violate the EPR criterion. It is easy to see that the above two expressions for the EPR criterion are invariant for symplectic transformations like the PHS one (see Eq. (2.9)). In particular,

$$\frac{I_4}{I_2} < \frac{1}{4} \quad \left(\frac{I_4}{I_1} < \frac{1}{4}\right)$$

For a pure state $I_4 = 1/16$ so that the two definitions lead to

$$\begin{aligned} I_2 &> \frac{1}{4} \\ I_1 &> \frac{1}{4}\,, \end{aligned}$$

Being for the uncertainty principle, written for the single sub–system, $I_{1,2} \geq 1/4$ for a pure state they cannot be violated asymmetrically.

2.1.2.4 Witnesses

All the above criteria (2.9), (2.16), and (2.19) cannot be used other than as bounds. They are not suitable for measuring entanglement in a quantitative way. They are only useful to determine the quality of the correlations when the conditions of separability are violated.

However, it may be useful to introduce the concept of witness that provides a method to verify whether a certain state is entangled or not [35]. We have the following *theorem of entanglement witness*:

> *A density matrix ρ_{AB} is entangled if and only if there exists a hermitian operator W, acting on the Hilbert space of ρ_{AB}, with the properites*
>
> - $\mathrm{Tr}[\rho_{AB}W] < 0$;
> - $\mathrm{Tr}[\rho_{AB}^{sep}W] \geq 0$, *for all separable states* ρ_{AB}^{sep}.
>
> *The operator W is called an entanglement witness.*

This is a necessary and sufficient condition for separability. A state ρ_{AB} is entangled if and only if there exists an entanglement witness that detects it. Entanglement witnesses do not really solve the problem of separability because we have to construct all possible entanglement witnesses for checking wether ρ_{AB} is entangled or not.

Another problem is to find the "best" entanglement witness, called *optimal entanglement witness*. In order to get a little more in detail, we define

$$\Omega_W = \{\rho_{AB} \geq 0 : \mathrm{Tr}\left[\rho_{AB}W\right] < 0\},$$

the set of all "detected" entangled states by W. So an entanglement witness W_1 is *finer* than W_2 if and only if $\Omega_{W_2} \subset \Omega_{W_1}$, that is the set of states Ω_{W_2} classified as entangled by W_2 is strictly contained in the set of states Ω_{W_1} judged by W_1. In other words, the ability to detect entangled states of W_1 is greater than W_2. Then, an entanglement witness is *optimal* if there exists no other entanglement witness which is finer. This means a finer entanglement witness can detect more states and an optimal one detects all states that are possible. Moreover, there is a unique correspondence between positive maps and entanglement witnesses [36]. The map $\mathcal{PT}$, viewed in the sub-sect. 2.1.2.1, is an explicit example of such correspondence.

Then, we can consider the inequalities obtained for the PHS, Duan, and EPR–Reid criteria (Eqs. (2.9), (2.16) and (2.19), respectively) as three entanglement witnesses, one for each criterion.:

$$\begin{aligned}
w_{PHS} &= 4\left(nm - c_1^2\right)\left(nm - c_2^2\right) + \frac{1}{4} - \left(n^2 + m^2\right) - 2\left|c_1 c_2\right| \ , \\
w_{DUAN} &= 2\sqrt{\left(n - \frac{1}{2}\right)\left(m - \frac{1}{2}\right)} - \left(c_1 - c_2\right) \ , \\
w_{EPR} &= n^2\left(1 - \frac{c_1^2}{nm}\right)\left(1 - \frac{c_2^2}{nm}\right) - \frac{1}{4} \ .
\end{aligned} \tag{2.20}$$

In summary, for a Gaussian bi–partite state the three criteria (see Eqs. (2.9), (2.16), and (2.19)) reduce to

$$\rho \text{ is entangled } \begin{cases} \Longleftrightarrow & w_{PHS} < 0 \\ \Longleftarrow & \begin{cases} w_{DUAN} < 0 \\ w_{EPR} < 0 \end{cases} \end{cases} . \tag{2.21}$$

The three w's don't satisfy the requirements for being a measure of entanglement. For example they don't verify the basic axiom stating that a good measure should be equal to 0 for any separable state [37].

However, once the state ρ is entangled w_{PHS}, w_{DUAN} and w_{EPR} provide suitable markers for evaluating how far the state is from being separable. Somehow measuring the robustness of the entanglement. In the Chapter 6, we will verify experimentally the effects of decoherence on entanglement "detected" by these witness. According to the definition of optimal entanglement witness given above and according to what said for each criterion, it is already possible to assert that the w_{PHS} and w_{DUAN} witnesses are better than w_{EPR} witness.

We note that for *diagonal* fully symmetric states ($n = m$ and $c_1 = -c_2 = c$ in Eq. (1.23)) w_{PHS}, w_{DUAN} and w_{EPR} read

$$\begin{aligned} w_{PHS} &= 4\left(n^2 - c^2\right)^2 + \frac{1}{4} - 2n^2 - 2c^2 \ , \\ w_{DUAN} &= \left(n - \frac{1}{2}\right) - c \ , \\ w_{EPR} &= n^2\left(1 - \frac{c^2}{n^2}\right)^2 - \frac{1}{4} \ ; \end{aligned}$$

and the two bounds ($c > n - 1/2$) for w_{PHS} and w_{DUAN} coincide while the bound for w_{EPR} is $c > \sqrt{n\left(n - \frac{1}{2}\right)}$ so that the EPR criterion is stricter than the PHS and Duan ones for any allowed value of n. We'll see it in more detail in Fig. (2.2) reported in the next Section.

2.2 Quantum Teleportation protocol with **CV**

The teleportation fidelity can be a useful indicator of quantumness of the states involved in the protocol. In particular, it is possible to show that in the case of Gaussian resources, the teleportation fidelity of a coherent state exceeds the maximum classical level, set to $\mathcal{F}_{class} = 0.5$, only if the resource is entagled. So

$$\{\mathcal{F} > 0.5\} \Rightarrow \{\text{resource is entangled state}\} \, ,$$

the inverse logical implication is not guaranteed. In this sense, therefore, the fidelity gives precise indications on quantumness of a state.

Instead, in order to find the quantum resources that maximizes the fidelity of teleportation, it is necessary to take into account non-Gaussian resources. In this Section, we discuss the importance of the **SB** states [22]. They exhibit a fidelity of teleportation exceeds that of all quantum states known to date. In Chapter 5, we propose a feasibility study for the experimental realization of **SB** states. In this Section we give a description of the **CV** teleportation protocol BKV [38] in terms of the characteristic functions of the quantum states involved.

As a matter of fact, the quality of a teleportation protocol can be evaluated by looking at the fidelity between the teleportated output state ρ_{out} and input state ρ_{in}:

$$\mathcal{F} = \mathrm{Tr}\left[\rho_{in}\rho_{out}\right]$$

that in terms of the characteristic functions reads

$$\mathcal{F} = \frac{1}{2\pi}\int dx_2 dy_2 \chi_{in}\left(x_2, y_2\right)\chi_{out}\left(-x_2, -y_2\right) \tag{2.22}$$

where χ_{in} and χ_{out} represent the respective characteristic functions in phase space and where $\alpha_k = \left(x_k + iy_k\right)/\sqrt{2}$. In this Section we refer always to the teleportation of a coherent state. The results obtained with other input states (for example the Fock states) are not dissimilar to the coherent state case, for a suitable settings of the free parameters of the quantum resource involved [22].

The output characteristic function χ_{out} can be directly obtained by appropriate manipulation of the characteristic functions of the resource states and of the input state of the protocol [75].

A scheme of teleportation is described in Fig. (2.1).

The input state ρ_{in} is initially separated from two-mode entangled resource ρ_{res}, so that the overall initial state is $\rho_0 = \rho_{in} \otimes \rho_{res}$ and the its characteristic function is given by

$$\chi_0\left(\alpha; \alpha_1; \alpha_2\right) = \chi_{in}\left(\alpha\right)\chi_{res}\left(\alpha_1; \alpha_2\right) \ .$$

where

$$\chi_{in}\left(\alpha\right) = e^{-\frac{1}{2}|\alpha|^2 + (\alpha\beta^* - \alpha^*\beta)}$$

is the characteristic function of the coherent state of amplitude β. At a first step Alice combines the input mode "in" with one of the entangled mode, let's say mode "1", at a balanced beam splitter, so that the characteristic function of the whole state becomes

$$\begin{aligned} & \chi_0^{'}\left(x'_{in}, y'_{in}; x'_1, y'_1; x_2, y_2\right) \\ = \ & \chi_{in}\left(\frac{x'_{in} + x'_1}{\sqrt{2}}, \frac{y'_{in} + y'_1}{\sqrt{2}}\right)\chi_{res}\left(\frac{x'_{in} - x'_1}{\sqrt{2}}, \frac{y'_{in} - y'_1}{\sqrt{2}}; x_2, v_2\right) \ . \end{aligned}$$

Then Alice performs a Bell measurement on her state consisting of two simultaneous homodyne measurements of the quadratures at beam splitter (50:50) outputs

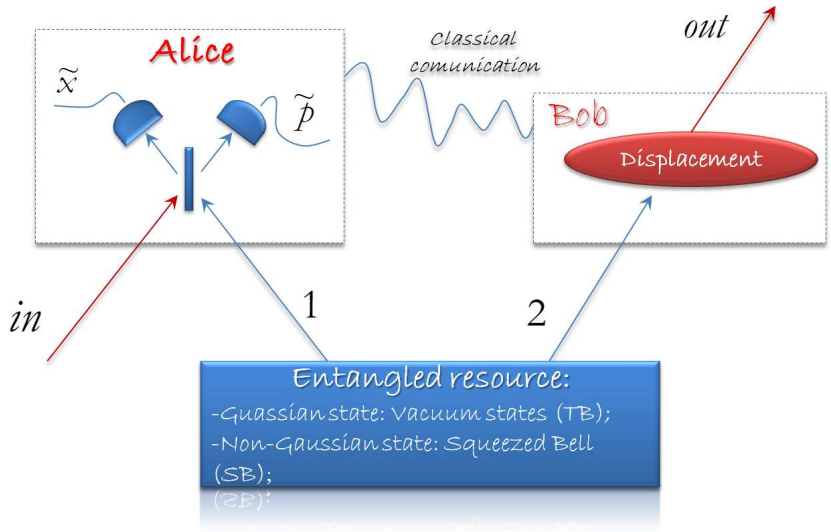

Figure 2.1: Schematic representation of a BKV CV quantum teleportation protocol. In the first step, the input mode is mixed by Alice with one of the two modes of the entangled resource; the ensuing state is then subject to a ideal (or realistic) Bell measurement. The result of the measurement is communicated to Bob through a classical channel. In the second step, a unitary transformation (displacement), determined by the previous measurement, is applied to the second mode of the entangled resource, that is affected by dechoerence during the propagation in a noisy channel. The ensuing output state is the final teleported state.

y'_{in} and x'_1. If the results of the Bell measurements are $y'_{in} = \tilde{y}$ and $x'_1 = \tilde{x}$, the characteristic function transforms into

$$\chi_{Bm}(x_2, y_2) = \frac{\mathcal{P}^{-1}(y, x)}{(2\pi)^2} \int dx'_{in} dy'_1 e^{i\left(x'_{in}\tilde{y} - \tilde{x}y'_1\right)} \chi_0^{'}(x'_{in}, 0; 0, y'_1; x_2, y_2),$$

where

$$\mathcal{P}(y, x) = \frac{1}{(2\pi)^2} \int dx'_{in} dy'_1 e^{i\left(x'_{in}\tilde{y} - \tilde{x}y'_1\right)} \chi_0^{'}(x'_{in}, 0; 0, y'_1; 0, 0)$$

is the distribution function of the outcomes $\tilde{y}$ and $\tilde{x}$ [22]. After recovering the classical information, Bob performs on mode 2 the displacement $\lambda = (\tilde{x} + i\tilde{y})$. It can be proved that the characteristic function of the teleportated state is

$$\chi_{out}(x_2, y_2) = \chi_{in}(x_2, y_2)\, \chi_{res}(x_2, -y_2; x_2, y_2), \tag{2.23}$$

So the fidelity of teleportation, Eq. (2.22), takes the simple form

$$\mathcal{F} = \frac{1}{2\pi} \int dx_2 dy_2 \chi_{in}(x_2, y_2)\, \chi_{in}(-x_2, -y_2)\, \chi_{res}(-x_2, y_2; -x_2, -y_2)\ . \tag{2.24}$$

In a realistic scenario, the propagation occurs with loss of photons and the modes involved in the teleportation protocol interact with the thermal modes of the external environment. The characteristic function of the output state, Eq. (2.23), becomes [22]

$$\begin{aligned} \chi_{out}(x_2, y_2) &= \chi_{in}(gTx_2, gTy_2)\, \chi_{res}\left(gTx_2, -gTy_2; e^{-\tau/2}x_2, e^{-\tau/2}y_2\right) \\ &\quad \times \exp\left\{-\frac{1}{2}\Gamma_{\tau,R}\left(x_2^2 + y_2^2\right)\right\}, \end{aligned}$$

where $\tau = \Upsilon t$, with damping rate Υ, the scale factor T expresses the effects of imperfections in Bell's measurements, g is the gain factor of the displacement, $\lambda = g(\tilde{x} + i\tilde{y})$, that Bob performs on mode 2 and the thermal phase-space covariance $\Gamma_{\tau,R}$ is defined as

$$\Gamma_{\tau,R} = \left(1 - e^{-\tau}\right)(1 + n_{th}) + g^2 R^2,$$

where n_{th} is the average number of thermal photons and $R = 1 - T$ is the reflectivity that quantifies the weight of the effects of decoherence.

The ideal case is rediscovered by placing $R = 0\,(T = 1)$, $\Upsilon = 0\,(\tau = 0)$, and $g = 1$.

2.2.1 Gaussian resources

In this subsection we analyze the fidelity of teleportation protocol of a coherent state by using Gaussian quantum resources. We highlight its ability to be entanglement marker by comparing it with the criteria presented in the Section

2.1.2. In fact, $\mathcal{F}$ for a Gaussian resource depends only on the entanglement quality of the used resource.

When the resource of teleportation is a Gaussian state, the fidelity (2.24) can be written in simple matrix form [25]

$$\mathcal{F} = \frac{1}{\sqrt{\det\left[\mathbf{\Gamma}\right]}} \ ,$$

where

$$\mathbf{\Gamma} = 2\boldsymbol{\sigma}_{coh} + \mathbf{ZAZ} + \mathbf{B} - \mathbf{ZC} - \mathbf{C}^{\mathsf{T}}\mathbf{Z} \ ,$$

and $\boldsymbol{\sigma}_{coh} = \frac{1}{2}\mathrm{diag}(1,1)$ is the covariance matrix of the coherent state, $\mathbf{A}$, $\mathbf{B}$, and $\mathbf{C}$ are the three 2×2 matrices that define the covariance matrix of the resource Eq.(1.18)[1], and the matrix $\mathbf{Z}$ is given in Eq.(2.8). In terms of the **CM** in Eq. (1.23), $\mathcal{F}$ is given by

$$\mathcal{F} = \frac{1}{\sqrt{\left(1+m+n-2c_1\right)\left(1+m+n+2c_2\right)}} \ . \tag{2.25}$$

It is possible to show that the teleportation protocol of a coherent state, fully based on classical strategies, provides $\mathcal{F} \leq 1/2$. Then, one can simply prove that

$$\mathcal{F} > \mathcal{F}_{class} = 1/2$$

implies that the resource is entangled. In this sense, the value of $\mathcal{F}$ becomes an indicator of the quality of the entanglement. We note that for *diagonal* states ($n = m$ and $c_1 = -c_2 = c$) we have

$$\mathcal{F} = \frac{1}{1+2n-2c} \tag{2.26}$$

$$= \frac{1}{2+w_{DUAN}} \ . \tag{2.27}$$

In this particular case, perfect fidelity would be obtained for $n = c$, or for $w_{DUAN} = -2$ that would implies an unphysical **CM** so that Gaussian resources, as the state produced by OPOs, cannot guarantee perfect teleportation. In fact, the purity imply the limit Eq. (1.27)

$$c \leq \sqrt{n^2 - 1/4}. \tag{2.28}$$

We want to highlight an imprecision that is often reported in the literature in this regard. In fact, it is said that when the squeezing parameter r tends to infinity ($n \simeq c \to \infty$), we obtain a perfect fidelity. In this way the impossibility of perfect fidelity ($\mathcal{F} = 1$) is attributed to the practical impossibility of achieving infinite values of r. This is not exactly correct: $\mathcal{F} = 1$ is unable to occur due to the

[1] $\mathbf{A} \equiv \mathrm{diag}(n,n)$, $\mathbf{B} \equiv \mathrm{diag}(m,m)$ and $\mathbf{C} \equiv \mathrm{diag}(c_1,c_2)$

limitations imposed by the purity of the state, Eq.(2.28). Nevertheless it remains true that for large n, c the factor $1/4$ in Eq.(2.28) becomes negligible with respect to n.

Moreover, $\mathcal{F} > 1/2$, see Eq.(2.26), give $c > n - 1/2$ and coincides with both the Duan and PHS bounds for such *diagonal* states. We note that, similarly to the Duan (Eq. (2.16)) but contrarily to the PHS and EPR criteria (Eqs. (2.9) and (2.19)) $\mathcal{F}$ is not invariant under symplectic transformations.

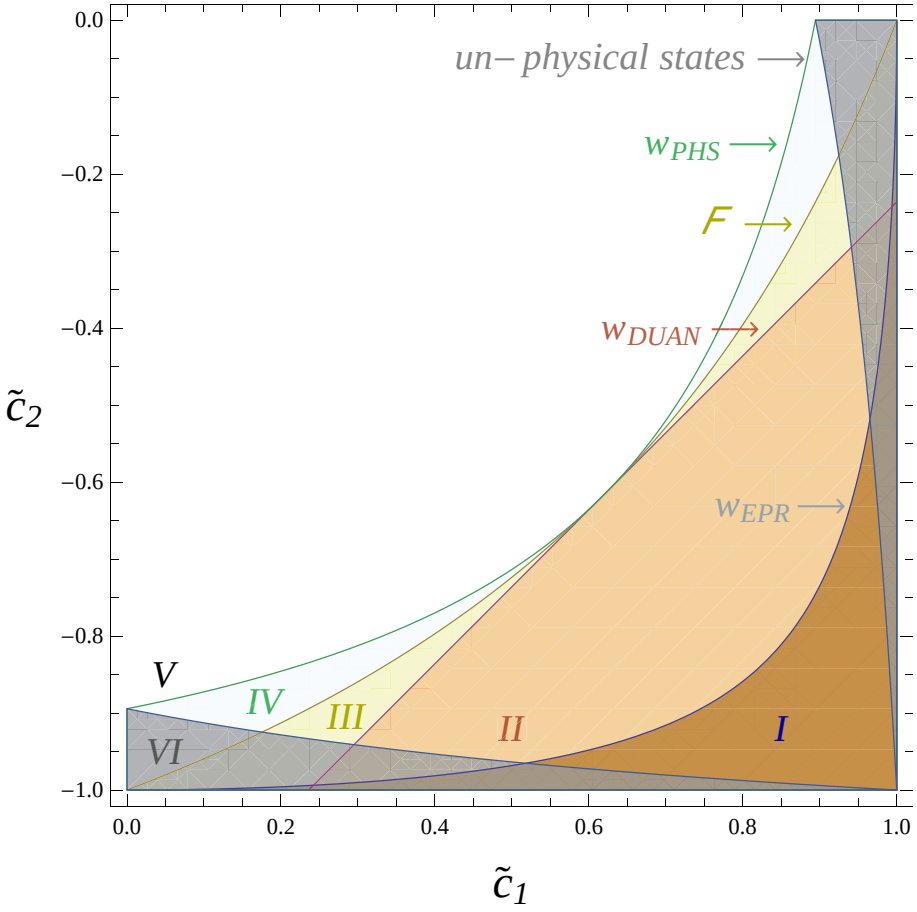

Figure 2.2: Region plot (*color online*) of the different entaglement witnesses of Eq. (2.20) and teleportation fidelity (Eq. (2.25)) as an entanglement marker. The *light blue* (labelled with (II)) area indicates un-physical **CM** (*i.e.* violating inequality (1.24)). The different criteria highlight different region of entanglement (see text for details).

As already mentioned, only the PHS criterion can be written for a generic **CM** as a sufficient and necessary condition while the Duan and the EPR one set only sufficient bounds. In order to discuss the relations between the different bounds and the teleportation fidelity, as an entanglement marker, it is possible to draw a

region plot, similar to the one drawn in Ref. [39] for a different case. In Fig. 2.2, we have visualized the different bounds set by the three entanglement witnesses of Eq. (2.20)) and the region for which $\mathcal{F} > 1/2$ (see Eq. (2.25)). The plot has been computed considering a **CM** in the standard form of Eq. (1.23) with $m = n$ (balanced system). The axes report the value of $\tilde{c}_1$ (below) and $\tilde{c}_2$ (left), the two correlation terms of the covariance matrix normalized to $c_{MAX} = \sqrt{n^2 - 1/4}$ so that $\tilde{c}_1 = -\tilde{c}_2 = 1$ will represent a pure maximally entangled state (i.e. the state showing the maximum quantum correlation for a given total energy of the system). We note that fully symmetric states, that we indicated as *diagonal* states, lay on the plot diagonal (top–left to bottom–right). These states, besides their symmetry, represent states that can be obtained at the output of a lossy propagation, described by Eq. (1.47), of an initially pure state. On the contrary, states outside the diagonal, having $\tilde{c}_1 \neq -\tilde{c}_2$, cannot be obtained by propagating pure states.

The *light gray* (labelled with (*VI*)) area indicates un–physical states, i.e. **CM** violating inequality (1.24).

The state lying on the diagonal starting in $\tilde{c}_1 = -\tilde{c}_2 = 1$ satisfies the conditions (see Eq. (2.14)) for which the Duan criterion become also necessary so that the coincidence between the Duan and the PHS bounds, along the diagonal, is not a surprise. Being both necessary and sufficient they coincide. For these *diagonal* states entanglement (seen as non–separability property) implies $\mathcal{F} > 1/2$. So that entanglement is a pre–requisite for using the state as a resource in the teleportation of a coherent state.

There are two pairs of interesting regions in the plot that deserve some comments. The first one, encompassing area labelled as (*III*) and (*IV*) in the plot (*light green* and *yellow*), represents regions where the states violate the PHS bound ($w_{PHS} < 0$) while they do not the Duan one ($w_{DUAN} \geq 0$). This apparent ambiguity can be solved noting that the **CM** represented by these regions does not respect the condition (2.14) so that the non–negativity of w_{DUAN} does not imply a separability of the state. On the other hand for such states $w_{PHS} < 0$ implying that they are effectively entangled and that their density matrix ρ cannot factorize into a convex combination of the tensor product of density operators relative to the two different sub–systems. By transforming by local squeezing operations, as outlined in Ref. [32], these **CM** into a form that respect conditions (2.14) it is possible to see that the transformed states show $w_{DUAN} < 0$. We have numerically done a few tests on such *odd* matrices, verifying that once taken into that form, the states violate the Duan bound (2.15) as well, so confirming that the Duan and PHS criterion are equivalent. We note that, being the latter written in a more general form, it is more useful from the practical point of view. Moreover, such a matrix transformation take states lying outside of the diagonal on the plot, completely out from the plot itself. Indeed, the transformed **CM** has the form given in Eq. (2.13) different from the one in Eq. (1.23) and represented in the plot.

We also note that the referred transformation change also the EPR operators pair (see Eq (2.11)).

The second interesting region, labelled with (IV) (*light green*) in Fig. 2.2, represents states that, although entangled, cannot be used for teleporting coherent states. **CM** lying inside this area will not give $\mathcal{F} > 1/2$. It is interesting to note that such states fall also inside the region for which the Duan criterion (2.16) is not fulfilled. As above mentioned, once the relative **CM** is transformed into the form (2.13) by local squeezing the transformed state will fulfill the Duan criterion in the form (2.15) so that, in this new scenario, the system is surely entangled. At the same time, if this novel state is used as a quantum resource for teleportation of a coherent state it will give $\mathcal{F} > 1/2$ [25] so that the local squeezing acts as entanglement unveiling. The initial state lying in this area is entangled for PHS, being $w_{PHS} < 0$, but, form the point of view of teleportation, entanglement manifests itself in an useless way. This entanglement can be made useful by locally transforming the two sub-systems.

We can see that the EPR criterion (region (I), *light brown*) offers a more restrictive condition with respect to the other two criteria even for diagonal states.

Region (II) (*salmon*) represents the bound fixed by the Duan criterion as a sufficient but not necessary condition. While region (V) (*white*) represents separable states.

2.2.2 Non-Gaussian Resources: Squeezed Bell states

In order to find the best resource for the **CV BKV** teleportation, we can reasonably conjecture that the use of non-Gaussian resources may be more efficient. In fact, for the Gaussian resources, type the squeezed vacuum state, the parameter of squeezing is the only free parameter to be manipulated in the procedure of maximizing of the teleportation fidelity. For the non-Gaussian resources the possibility of having additional degrees of freedom could be profitable, in principle. Of course, apart from additional degrees of freedom it is necessary that the state is an efficient resource for the success of the teleportation protocol. In literature, the authors of the reference [40, 41, 42] have shown that non-Gaussian states, used as a resource for teleportation, exhibit higher fidelity compared to the Gaussian. In particular, in [1], Dell'Anno et al. have proposed a new class of sculptured resources, the **SB** states, defined in Sect.(1.3.2), which interpolates between different degaussified states, and can be optimized acting on an independent free parameter in addition to the squeezing. At present, these states are the best theoretically drawn resource of teleportation. The various Gaussian and degaussified states are defined from a theoretical point of view by applying squeezing and ladder operators on the two-mode vacuum. Inside this theoretical context the teleportation fidelity is improved, in a significant range of the parameters, by the optimized **SB** states if compared both to Gaussian and other non-Gaussian resources, in-

cluding the (theoretically defined) photon-subtracted squeezed states. This has been verified for different inputs (including coherent states, squeezed states, and squeezed number states), and also if losses are present [1],[22]. The deep reason is that the optimized **SB** states realize the best balance among three properties that influence the teleportation fidelity: entanglement content, non-Gaussianity, and squeezed-vacuum affinity [1]. In particular, the third property (squeezed-vacuum affinity) is crucial; expressed in a simple way, it means that a resource must contain a contribution, with a relevant weight, given by the two-mode vacuum, plus symmetric non Gaussian corrections.

There are essentially two alternative strategies to generate experimentally non-Gaussian states. It is possible to generate non-Gaussian states from Gaussian ones by performing conditional measurements or, introducing non-linearities in the source.

In the Chapter 5 we will use the first strategy proposing a new class of bipartite non-Gaussian states, which approximates, well also in realistic conditions, the class of the **SB** states. The scheme has the advantage of being versatile, in the sense that a tuning of the free experimental parameters allows the generation of many non-Gaussian states, as photon-added (**PA**) squeezed states, photon-subtracted (**PS**) squeezed states, squeezed number states (**PN**) and, obviously, also Gaussian Twin Beams (**TB**). Furthermore, the free experimental parameters can be exploited to optimize, in different situations, the performance in the realization of quantum protocols. So, one can generate powerful nonclassical resources for quantum information, quantum communication and quantum computation.

In the Chapter 7, we will exploit the second strategy for the generation of the non-Gaussian states. We will solve the Langevin equations describing the dynamics of the Optical Parametric Oscillators (**OPO**) without to neglect, as done to date in the literature, the sources of noise (as pump amplitude and phase fluctuations, deviation from the cavity resonance, $\delta\chi$ and fluctuation of the non–linear coupling parameter). All the quantum processes are driven by a classical pump field and the quantum noise coupled into the cavity through loss mechanisms. The presence of these extra noise sources modifies the statistical properties of the state and switches unexpected, in a quite **OPO**, cross–correlations. We will see that as a first consequence of the presence of extra noise terms the generated state looses its Gaussian character so that its characteristic function becomes slightly non-Gaussian. Moreover, the fidelity of various **CV** teleportation schemes will be evaluated by giving for granted the Gaussian character of the resources provided by physical **OPO** sources. Thus, it is rather intuitive that loosing the Gaussian character the fidelity that the state can provide changes. In particular, we found that the fidelity increases in presence of extra fluctuations.

2.3 Mutual Information and Quantum Discord

Recent studies have shown that some particular classes of separable correlated states, traditionally considered classical, show quantum features useful for application in quantum technology [43].

The von Neumann entropy satisfies several important mathematical properties. In the scenario of statistical theory of particular importance is the *subadditivity*:

$$H(AB) \leq H(A) + H(B)$$

where $H(X)$ is the Shannon entropy (the classical analogue of the von Neumann entropy $S_{vN}(\rho)$ defined in Eq.(2.5)) associated to the statistical distribution of the variable X ("X, Y" indicates the joint probability distribution and "$X|Y$" the conditional distribution of Y given the value of X). It is evident, then, we can use the property of subadditivity to quantify the separability of a quantum state. Any correlation between two random variables A and B can be measured by their *mutual information* defined by two equivalent expressions:

$$\begin{aligned} I(A;B) &\equiv H(A) + H(B) - H(A,B) \\ &\equiv H(A) - H(A|B) = H(B) - H(B|A) \ . \end{aligned} \tag{2.29}$$

The mutual information quantifies the information that one have on the overall state observing the system in its entirety, and evaluating the information that is possible to extract separately observing the two sub-systems.

These two definitions translate into the quantum language by substituting H with $S_{vN}(\rho)$. They do not coincide anymore if non-classical correlations are present between the two systems [44, 45]. Moreover, while the translation of the first one into the quantum language is straightforward and univocal, this is not true for the second one.

The first of the two definitions (2.29), is unambiguously referred to as the quantum mutual information [123] between state 1 and 2 (ρ representing the state of the bi–partite system as a whole)

$$\mathcal{I}(\rho_{12}) \equiv S_{vN}(\rho_1) + S_{vN}(\rho_2) - S_{vN}(\rho_{12}) \ . \tag{2.30}$$

being ρ_k the reduced density matrix, $\rho_k = \mathrm{Tr}_{h \neq k}[\rho_{hk}]$, associated to the sub-system $k = 1, 2$. In a bi-partite system, described by a density matrix ρ, $\mathcal{I}(\rho)$ quantifies the total correlation between the sub-systems ρ_1 and ρ_2. When the state ρ_{12} is separable, i.e. the density matrix is factorizable as $\rho_{12} = \rho_1 \otimes \rho_2$, then the sub-additivity property becomes $S_{vN}(\rho_1 \otimes \rho_2) = S_{vN}(\rho_1) + S_{vN}(\rho_2)$ and the mutual information is null, $\mathcal{I}(\rho_1 \otimes \rho_2) = 0$. So it is strictly $= 0$ for separable states, while it is > 0 for entangled states.

It can be written in terms of the covariance matrix invariants (see Sect. 1.3.1.1) and symplectic eigenvalues (see Eqs. (1.19),(1.20),(1.21) and (1.22))

$$\mathcal{I}(\boldsymbol{\sigma}) = f\left(\sqrt{I_1}\right) + f\left(\sqrt{I_2}\right) - f\left(d^+\right) - f\left(d^-\right) \ , \tag{2.31}$$

with

$$f(x) = (x + 1/2)\ln(x + 1/2) - (x - 1/2)\ln(x - 1/2) \ . \tag{2.32}$$

The second definition of Eq. (2.29), translated into the quantum world, necessarily involves the conditional state of a sub-system after a measurement performed on the other one. So that, the symmetry between the two sub-systems is broken. Since the conditional entropy $H(A|B)$ requires us to specify the state of B given the state of A, its definition, in quantum theory is ambiguous until the to–be–measured observables on A are selected so that the conditional state of B can be defined.

This discrepancy has lead to the concept of quantum discord $\mathcal{D}(\rho_{12})$ [46]. A non zero quantum discord signals the presence of quantum features in the correlation between the two sub–systems notwithstanding their separabile or entangled nature. $\mathcal{D}(\rho_{12})$ is a measure of all genuine quantum correlations. It is defined as a difference between total correlations as given by the quantum information in Eq.(2.30) and the classical correlation,

$$\mathcal{D}(\rho_{12}) = \mathcal{I}(\rho_{12}) - \mathcal{C}(\rho_{12}),$$

where $\mathcal{C}(\rho)$ is the amount of genuinely classical correlation, given by

$$\mathcal{C}(\rho_{12}) = S_{vN}(\rho_1) - \inf_{\left\{\mathsf{M}_2^{(k)}\right\}} \left\{S_{vN}\left(\rho_{1|2}\right)\right\} \ ,$$

where $S_{vN}\left(\rho_{1|2}\right) = \sum_k p^{(k)} S_{vN}\left(\rho_1^{(k)}\right)$ is the conditional entropy of sub-system 1 and $\inf_{\left\{\mathsf{M}_2^{(k)}\right\}} \left\{S_{vN}\left(\rho_{1|2}\right)\right\}$ represents the minimal value of the entropy with respect to a complete set of local measurement $\left\{\mathsf{M}_2^{(k)}\right\}$ performed on the sub-system 2..

Originally the quantum discord was defined mainly for finite dimensional systems. Very recently [44, 45] the concept of discord has been extended to the domain of **CV** system, in particular, to the analysis of the quantum correlation of bi-partite system described by two-mode Gaussian states. Closed formulas have been derived for bi-partite thermal squeezed states [44] and for all two-mode Gaussian states [45].

For a Gaussian state described by the covariance matrix (1.23), $\mathcal{D}$ becomes

$$\mathcal{D}(\boldsymbol{\sigma}) = f(\sqrt{I_2}) - f\left(d^+\right) - f\left(d^-\right) + f\left(\frac{\sqrt{I_1} + 2\sqrt{I_1 I_2} + 2I_3}{1 + 2\sqrt{I_2}}\right) \ . \tag{2.33}$$

We note that, as for the EPR criterion, in quantum discord there is an asymmetry in the exchange of the two sub–systems. Again this is due to the use of the concept of conditional states. We can note some properties [47]: $\mathcal{D} \geq 0$, which is a direct consequence of the concavity of the conditional entropy [48]. Discord is invariant under local unitary transformations, i.e.

$$\mathcal{D}(\rho_{12}) = \mathcal{D}\left((U_1 \otimes U_2)\,\rho_{12}\,(U_1 \otimes U_2)\right);$$

$\mathcal{D} = 0$ iff the state is a classical state.

2.4 Bell's Non-locality

In 1935, EPR [34] presented an insidious problem, to date not fully resolved, suggesting a dilemma between two mutually exclusive assertions. They showed, in fact, that the quantum correlations (which we have previously called EPR-correlations) are incompatible with a local theory of the physical world. Therefore in order to not declare false the assumption of locality, quantum theory must be regarded as non-complete theory. EPR proposed a solution in terms of hidden variables, *i.e.* they supposed that some (hidden) variables had been neglected and that only after they have been inserted into the theory, it is possible to have a complete and unambiguous description of the physical world. The discussion that has succeeded the paper [34] is quite articulated and complex, and often involve aspects of the metaphysics field. Major contributions were made by Borh [49], Bohm [50], Jarrett [52], Bell [51], Clauser-Horn-Shimon-Holt (CHSH) [53], and others (see for exemple [54, 55, 56, 57]).

In particular, in 1964 Bell published a theorem that allows us to distinguish between quantum mechanics theory and all variables-hidden theories that restore the classical mechanics theory, proposing an inequality (*Bell's inequality*), whose violation is obtained if and only if the system can not be described by hidden-variables classical theories. In other words, a system that violates Bell's inequality admits only a purely quantum, and non-local description.

In order to discuss the Bell's inequality we consider a bi-partite system (composed by sub-systems 1 and 2). We suppose that two different experiments can be performed on each system, indicated by A, A' (for subsystem 1), and by B, B' (for subsystem 2). The measurement outcome of the experiment $A(B)$ is labelled by $s_A(s_B)$, and it has values dichotomous $s_{A,B} = \pm 1$. Let:

$$\textbf{(1)}\ \ p\left(s_A, s_B|A, B\right) \equiv \left\{ \begin{array}{c} \text{the probability that the results} \\ \text{of the joint measurements } A \text{ and } B \\ \text{are respectively } s_A \text{ and } s_B \end{array} \right\};$$

$$\textbf{(2)}\ \ p\left(s_A, |A, B, s_B\right) \equiv \left\{ \begin{array}{c} \text{the probability that the outcome} \\ \text{of the measurement performed} \\ \text{on the system 1 is } s_A \\ \text{when the measurements performed} \\ \text{on 1 and 2, respectively, are } A \text{ and } B, \text{ and the} \\ \text{result of the experiment on 2 is } s_B; \end{array} \right\}.$$

The fundamental hypothesis, on which it is based the Bell's theorem is based , is the factorization (or *Bell's locality*) of the probability $p\left(s_A, s_B|A, B\right)$ as

$$p\left(s_A, s_B|A, B\right) = p\left(s_A|A\right) p\left(s_B|B\right),$$

i.e the results of measurements on the two systems are independent (and uncorrelated). If this hypothesis is true, the lack of correlation in one of the possible

types of measurement may not exceed the lack of correlation in the remaining three types. For example:

$$\sum_{\substack{s_A,s_B=\pm \\ :s_A\neq s_B}} p\left(s_A,s_B|A,B\right) \leq \sum_{\substack{s_A,s_B=\pm \\ :s_A\neq s_B}} p\left(s_A,s_B|AB'\right)+p\left(s_A,s_B|A'B\right)+p\left(s_A,s_B|A'B'\right). \tag{2.34}$$

The hypothesis of factorization incorporates two different conditions:

- **(I) Sub-hypothesis of Outcome Indipendence.** The (statistical) results of the measurement performed on the sub-system 1 does not depend on those performed on the system 2. In terms of the conditional probabilities of above type **(1)** and **(2)**, we have:

$$\begin{aligned} p\left(s_A|A,B,s_B\right) &= p\left(s_A|A,B\right) \rightarrow \text{independence from the results } s_B \text{ and} \\ p\left(s_B|A,B,s_A\right) &= p\left(s_B|A,B\right) \rightarrow \text{independence from the results } s_A. \end{aligned}$$

This assumption of indipendence of the results obtained on each sub-systems adheres to the idea that the separability of two space-time events is a sufficient condition for regarding as distinct and independent events. Under this hypothesis, the assumption of factorization is strengthened. This assumption, typical of the classical mechanics, claims that a composed system is equivalent, at least in principle, to the sum of the parts. The outcome s_A of the experiment on the first sub-system provides no additional information regarding the outcome of the experiment on the other one.

- **(II) Sub-hypothesis of Type-context Indipendence.** The results of measurement on a sub-system does not depend on the type of measurement performed on the other sub-system:

$$\begin{aligned} p\left(s_A|A,B\right) &= p\left(s_A|A\right) \rightarrow \text{independence from the measurement } B \text{ and} \\ p\left(s_B|A,B\right) &= p\left(s_B|B\right) \rightarrow \text{independence from the measurement } A. \end{aligned}$$

The locality is related at the impossibility of simultaneous (or superluminal) actions at a distance.

Jarrett (1984) and Bell (1990) demonstrated that the factorization hypothesis is equivalent to the logical union of the two Sub-hypotheses **(I)** and **(II)**.

When inequality is verified, two circumstances may occur: *i.* there is not correlation $\Rightarrow p\left(s_A,s_B|A,B\right)=p\left(s_A|A\right)p\left(s_B|B\right)$; *ii.* there is correlation. In the latter case, the factorization hypothesis becomes

$$p\left(s_A,s_B|A,B\right)=\int d\boldsymbol{\lambda} p\left(s_A|A;\boldsymbol{\lambda}\right)p\left(s_B|B;\boldsymbol{\lambda}\right)\mathfrak{S}\left(\boldsymbol{\lambda}\right),$$

where the function $\mathfrak{S}(\boldsymbol{\lambda})$ expresses the *classic correlation*, as a function of the hidden variables $\boldsymbol{\lambda} = (\lambda_1, ...\lambda_N)$ that complete the description of describe the system.

Now, since the inequalities of the type (2.34), called *Bell's inequalities*, are empirically violated, then the factorization hypothesis is falsified in both cases. In this (quantum) circumstance, we can say that no theory that satisfies the principles of the Bell's locality is suitable for a correct description of the world.

In the scientific community there is not unanimous agreement about the role that the individual sub-hypotheses of separability and locality have on the violation of Bell's inequality. The main problems lie in the definitions of locality, separability and causality and in their connections with the principle of relativity of Einstein. In fact, for relativity theory:

- *no object or signal can be transmitted at superluminal speed* and

- *the simultaneity of distinct events depends on the reference system.*

Here we adopt the definition of locality given by EPR and then put on trial by the violation of Bell's inequality. EPR (and Bell) assume local causality, namely. They consider that the interactions between objects are pointlike (local) interactions whose immediate effects are confined to a single location and the actions at one location do not immediately have effect at a separate location. This assumption, when combined with the conclusions of special relativity, implies that no "effect" can travel faster than the speed of light in vacuum. This notion of locality is very close to (but not exactly the same as) the meaning of relativistic causality, which imposes important restrictions on the theory but, however it does not exclude the possibility of some kind of effect superluminal, such as the *quantum collapse*. In other words, an object or a signal, that travels faster than light, violates special relativity and involves encountering an unpleasant paradox of the arrow of time; on the contrary the collapse of the density matrix after a measurement (which assigns the *result* and *type* of the measure) respects still the causality.

We emphasize that the quantum correlations emerge from the superposition principle of states of quantum mechanics and from the instantaneous quantum collapse of the density matrix caused by a appropriate measurement. For this reason, such quantum correlations do not violate relativistic causality. In a schematic form:

$$\text{local relativistic causality} \equiv \left\{ \begin{array}{c} \text{no physical entity (object and/or signal)} \\ \text{can travel faster than light in the vacuum,} \\ \text{and simultaneous events} \\ \text{does not exist in absolute} \end{array} \right\},$$

$$\text{EPR-Bell local causality} \equiv \left\{ \begin{array}{c} \text{the interaction between objects are pointlike} \\ \text{(local) interactions whose immediate effects} \\ \text{are confined to the space-time regions} \\ \text{of the objects themselves.} \end{array} \right\}.$$

The first notion of causality no concerns the violation of Bell's inequality. This is because the quantum collapse of the state does not fall under the relativistic causality assertion (being neither an object nor a signal). The two quantum correlated sub-systems are a *single* system. Therefore, to think that the measurement of a part of it has effects on the entire system is reasonable (there isn't simultaneity of distinct events, because there are not two distinct events). Otherwise, the EPR-Bell locality is falsified by the Bell's inequality.

CHAPTER 3

EVALUATION OF THE BELL'S INEQUALITY

In this Chapter we explore the Bell's inequality specializing the observation introduced in Sect. 2.4 to the case of Gaussian and non-Gaussian **CV** states. In particular, we discuss two different approaches to inequality: the first is that of the pseudospins (Sect. 3.1) and the second is that of the Wigner function (Sect. 3.2).

3.1 Bell-CHSH's inequality in the psuedospin representation

Chen et al. [58] introduced a pseudospin operator $\mathbf{S} = (S_x, S_y, S_z)$ for a nonlocality **CV** test with a direct analogy to a spin-1/2 system:

$$\begin{aligned} S_z &= \sum_{n=0}^{\infty} |2n+1\rangle \langle 2n+1| - |2n\rangle \langle 2n|, \\ S_x &= S_+ + S_-, \\ S_y &= S_+ - S_-, \end{aligned}$$

where

$$S_+ = \sum_{n=0}^{\infty} |2n+1\rangle \langle 2n|, \qquad S_- = \sum_{n=0}^{\infty} |2n\rangle \langle 2n+1|,$$

and $|n\rangle$ is the Fock state with average photon number $n\,(\in \mathbb{N})$. The Bell's function $\mathcal{B}$ is the value of expectation of the operators $E(\theta_1, \theta_2)$ [53, 58]

$$\mathcal{B} = E(\theta_1, \theta_2) + E(\theta_1', \theta_2) + E(\theta_1, \theta_2') - E(\theta_1', \theta_2'), \tag{3.1}$$

where

$$E(\theta_1, \theta_2) = \left\langle s_{\theta_1}^{(1)} \otimes s_{\theta_2}^{(2)} \right\rangle,$$

and

$$s_{\theta_k}^{(k)} = S_z^{(k)} \cos\theta_k + \left(S_+^{(k)} + S_-^{(k)} \right) \sin\theta_k.$$

The inequalities of the type (2.34) are expressed in terms of the Bell's function $\mathcal{B}$, and become

$$|\mathcal{B}| \leq 2.$$

Hence a local state verifies the above condition.

So, we must calculate the quantity

$$\begin{aligned} E(\theta_1,\theta_2) &= \left\langle s^{(1)}_{\theta_1}\otimes s^{(2)}_{\theta_2}\right\rangle \qquad (3.2)\\ &= \cos\theta_1\cos\theta_2\left\langle S^{(1)}_z\otimes S^{(2)}_z\right\rangle+\cos\theta_1\sin\theta_2\left\langle S^{(1)}_z\otimes\left(S^{(2)}_+ + S^{(2)}_-\right)\right\rangle \\ &\quad +\sin\theta_1\cos\theta_2\left\langle\left(S^{(1)}_+ + S^{(1)}_-\right)\otimes S^{(2)}_z\right\rangle \\ &\quad +\sin\theta_1\sin\theta_2\left\langle\left(S^{(1)}_+ + S^{(1)}_-\right)\otimes\left(S^{(1)}_+ + S^{(1)}_-\right)\right\rangle. \qquad (3.3)\end{aligned}$$

For the sake of generality, we calculate the averages in Eq. (3.3) with respect to the generic (pure) bi-partite state

$$|\psi\rangle=\sum_{n=0}^{\infty}C_n\,|n,n\rangle\,, \qquad (3.4)$$

where $\sum_{n=0}^{\infty}|C_n|^2=1$ for the normalization, and $|n,n\rangle=|n\rangle\otimes|n\rangle$ is the bi-modal Fock states. We can see that the terms

$$\left\langle S^{(1)}_z\otimes\left(S^{(2)}_+ + S^{(2)}_-\right)\right\rangle,$$
$$\left\langle\left(S^{(1)}_+ + S^{(1)}_-\right)\otimes S^{(2)}_z\right\rangle$$

of the Eq.(3.3) vanish. Thus the function $E(\theta_1,\theta_2)$ becomes

$$\begin{aligned} E(\theta_1,\theta_2) &= \cos\theta_1\cos\theta_2\sum_{n=0}^{\infty}\left(|C_{2n+1}|^2+|C_{2n}|^2\right)+\sin\theta_1\sin\theta_2\sum_{n=0}^{\infty}\mathrm{Re}\left[2C_{2n}C^*_{2n+1}\right] \\ &= \cos\theta_1\cos\theta_2+\sin\theta_1\sin\theta_2\sum_{n=0}^{\infty}\mathrm{Re}\left[2C_{2n}C^*_{2n+1}\right].\end{aligned}$$

3.1.0.1 Squeezed Vacuum state case

For the squeezed vacuum (**TB**) states the coefficients C_n in the Eq.(3.4) reads [21]

$$C_n^{(\mathbf{TB})}=\frac{\tanh^n r}{\cosh r}, \qquad (3.5)$$

and the function $E(\theta_1,\theta_2)$ becomes

$$E(\theta_1,\theta_2)=\cos\theta_1\cos\theta_2+\sin\theta_1\sin\theta_2\tanh 2r,$$

as has been proven in [58]. Choosing $\theta_1=0$, $\theta_1'=\pi/2$, and $\theta_2=-\theta_2'$ the Bell's function $\mathcal{B}$ results

$$\mathcal{B}(\theta_2)=2\left(\cos\theta_2+\sin\theta_2\tanh 2r\right),$$

and maximizing with respect to θ_2, we have

$$\begin{aligned}\mathcal{B}_{\max}(r) &\equiv \max_{\theta_2}\mathcal{B}(\theta_2)\\ &= 2\sqrt{1+\tanh^2(2r)}.\end{aligned}$$

Then, the squeezed vacuum bi-partite state (Eq. (3.4) with $C_n = C_n^{(\mathbf{TB})}$) exhibits a violation of the Bell's inequality soon as the parameter of squeezing is different from zero ($r > 0$). This confirms the connection between entanglement and violation of Bell's inequality for pure states. In fact, Gisin and Peres [59] proved that every violation of the inequality is necessary and sufficient condition of the entanglement for pure states. The maximum of violation $\max_r \mathcal{B}_{\max}(r)$ occurs for r tending to infinity, and assumes the value $\mathcal{B}_{\max}(r)|_{r\to\infty} = 2\sqrt{2}$. In this case, in fact, the **TB** state tends to the maximally EPR-correlated state.

3.1.0.2 Squeezed Bell state case

Now we analyze the case of the **SB** states,

$$\begin{aligned}|\psi_{\mathbf{SB}}\rangle &= S_{12}(\zeta)\left[c_1|00\rangle + c_2|11\rangle\right]\\ &= S_{12}(\zeta)\left[c_1 + c_2 a_1^\dagger a_2^\dagger\right]|00\rangle,\end{aligned}$$

with $S_{12}(\zeta) = \exp\left\{-\zeta a_1^\dagger a_2^\dagger + \zeta^* a_1 a_2\right\}$, $\zeta = re^{i\phi}$, $c_1 = \cos\delta$, and $c_2 = \sin\delta$. It is convenient to use the two-mode Bogoliubov transformations,

$$S_{12}(\zeta)\, a_1^\dagger S_{12}^\dagger(\zeta) = S_{12}^\dagger(-\zeta)\, a_1^\dagger S_{12}(-\zeta) = c a_1^\dagger + e^{-i\phi} s a_2, \tag{3.6}$$

$$S_{12}(\zeta)\, a_2^\dagger S_{12}^\dagger(\zeta) = S_{12}^\dagger(-\zeta)\, a_2^\dagger S_{12}(-\zeta) = c a_2^\dagger + e^{-i\phi} s a_1, \tag{3.7}$$

where $c = \cosh r$, $s = \sinh r$, and $r = |\zeta|$; so we can write the state $|\psi_{\mathbf{SB}}\rangle$ in the form

$$\begin{aligned}&|\psi_{\mathbf{SB}}\rangle = \left[c_1 + c_2\left(c a_1^\dagger + e^{-i\phi} s a_2\right)\left(c a_2^\dagger + e^{-i\phi} s a_1\right)\right] S_{12}(r)|00\rangle\\
&= \sum_{n=0}^{\infty}\left[c_1 C_n^{(\mathbf{TB})} + e^{-i\phi} c_2 cs(2n+1)\right]|n,n\rangle + c_2 c^2 \sum_{n=0}^{\infty} C_n^{(\mathbf{TB})}(n+1)|n+1,n+1\rangle\\
&\quad + e^{-2i\phi} c_2 s^2 \sum_{n=0}^{\infty} C_n^{(\mathbf{TB})} n|n-1,n-1\rangle\\
&= \sum_{n=0}^{\infty}\Big[c_1 C_n^{(\mathbf{TB})} + e^{-i\phi} c_2 cs C_n^{(\mathbf{TB})}(2n+1) + e^{-2i\phi} c_2 s^2 C_{n+1}^{(\mathbf{TB})}(n+1)\\
&\quad + c_2 c^2 C_{n-1}^{(\mathbf{TB})} n(1-\delta_{n,0})\Big]|n,n\rangle\\
&= \sum_{n=0}^{\infty} C_n^{(\mathbf{SB})}|n,n\rangle\end{aligned}$$

Thus, the coefficients C_n of the state (3.4) for the **SB** state become

$$C_n^{(\mathbf{SB})} = c_1 C_n^{(\mathbf{TB})} + e^{-i\phi} c_2 cs\,(2n+1) + e^{-2i\phi} c_2 s^2 C_{n+1}^{(\mathbf{TB})}\,(n+1) + c_2 c^2 C_{n-1}^{(\mathbf{TB})} n\,(1-\delta_{n,0})$$

where $\delta_{n,0}$ is the Kronecker's Delta function. The funciton $E(\theta_1,\theta_2)$ results, then,

$$E(\theta_1,\theta_2) = \cos\theta_1\cos\theta_2 + \sin\theta_1\sin\theta_2 \sum_{n=0}^{\infty} \mathrm{Re}\left[2C_{2n}^{(\mathbf{SB})} C_{2n+1}^{(\mathbf{SB})*}\right]. \tag{3.8}$$

Unlike the case **TB**, for the **SB** state the expression of $E(\theta_1,\theta_2)$, Eq. (3.8), is rather long and for clarity we do not report it explicitly. Of course the case $\delta = 0$ returns the results obtained above for the **TB**. Using the Eq. (3.8) in the Eq. (3.1), we can then compare the function $\mathcal{B}$ for all states obtainable by **SB**, after the maximization on the free parameters. For this purpose, we observe that the function $\mathcal{B}$ depends on the squeezing parameter $\zeta = re^{i\phi}$, the relative weight δ of the Fock states $|00\rangle$ and $|11\rangle$, and the angles of orientation θ_1, θ_2 of the measurements, *i.e.* $\mathcal{B} = \mathcal{B}(r,\phi,\delta,\theta_1,\theta_2,\theta_1',\theta_2')$. However, following [58] we fix some values of orientations $\theta_1,\theta_2,\theta_1',\theta_2'$:

$$\begin{aligned} \theta_1 &= 0 \qquad \theta_1' = \pi/2 \\ \theta_2 &= \theta \qquad \theta_2' = -\theta. \end{aligned}$$

So we obtain $\mathcal{B} = \mathcal{B}(r,\phi,\delta,\theta)$, and the maximization procedure is made on the parameters (ϕ,δ,θ), *i.e.*

$$\max_{\phi,\delta,\theta} \mathcal{B}(r,\phi,\delta,\theta) \equiv \mathcal{B}_{opt}^{(\mathbf{SB})}(r).$$

We can see that the result of the maximization provides the following settings:

$$\phi = \pi,$$
$$\delta_{opt} = \delta(r) \quad \text{and} \quad \theta_{opt} = \theta(r).$$

Now, we compare $\mathcal{B}_{opt}^{(\mathbf{SB})}(r)$ with the Bell's functions of other quantum states (**TB**, **TB**, **PA**, **TB**, and **PN**), reported in Table (3.1).

In Fig. (3.1) we compare the following Bell's functions: $\mathcal{B}_{opt}^{(\mathbf{SB})}(r)$ for the optimized **SB** state (*blue solid line*), $B_{opt}^{(\mathbf{PS})}(r)$ for the **PS** state (*green dot-dashed line*), $B_{opt}^{(\mathbf{TB})}(r)$ for the **TB** state (*orange dashed line*), $B_{opt}^{(\mathbf{PA})}(r)$ for **PA** state (*purple dotted line*), and $B_{opt}^{(\mathbf{PN})}(r)$ for the **PN** state (*red double dot-doshed line*). We can observe that the optimized **SB** states are more non-local than everyone state. In particular, we note that $\mathcal{B}_{opt}$ reaches the maximum value, $2\sqrt{2}$, for r tends to infinity, asymptotically, and for $r = 0$ with $\delta = \pi/2$, *i.e.* when the **SB** state becomes the well-known Bell state $\frac{1}{\sqrt{2}}(|00\rangle + |11\rangle)$. However, for $r \to \infty$ all states are approaching the same violation.

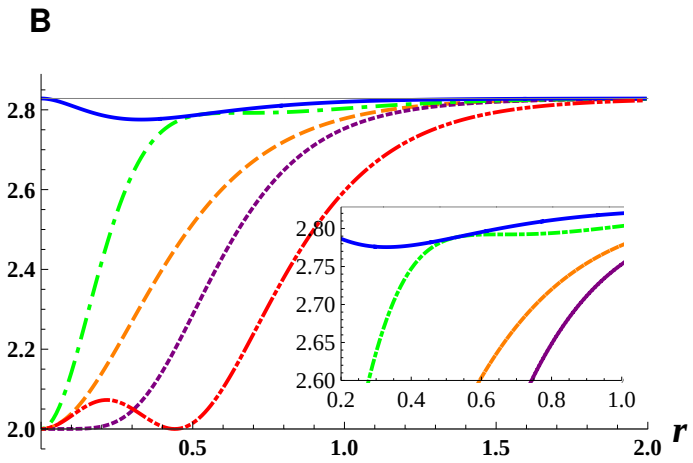

Figure 3.1: *(color online)*—In Figure it is shown the Bell's function of the optimized state (*blue solid line*), the **PS** state (*green dot-dashed line*), the **TB** state (*orange dashed line*), **PA** state (*purple dotted line*), and **PN** state (*red double dot-dashed*) for r ranging from 0 to 2. The small figure in the bottom right emphasizes the trends for $r \in [0.2, 1.0]$.

state	$B_{opt}(r)$
TB	$B_{opt}^{(TB)}(r) = \max_{\theta} B_{opt}(r, 0, \theta)$
PS	$B_{opt}^{(PS)}(r) = \max_{\theta} B_{opt}\left(r, \delta^{(PS)}, \theta\right)$
PA	$B_{opt}^{(PA)}(r) = \max_{\theta} B_{opt}\left(r, \delta^{(PA)}, \theta\right)$
PN	$B_{opt}^{(PN)}(r) = \max_{\theta} B_{opt}(r, \pi/2, \theta)$

Table 3.1: Definition of the Bell's functions optimized for the **TB**, **PS**, **PA**, and **PN** states.

3.2 Bell-CHSH's inequality in the Wigner representation

Another approach consists in considering the connection between the Wigner's function of the state and the parity measurement performed on the quantum state displaced by α_k. In order to show this correspondence we refer to the experimental proposal by Banaszek [60], [61]. We consider the diagram of measurement shown in Fig. 3.2.

The two modes of a bi-partite generic quantum state, represented by the density matrix ρ_{in}, impingue two high transmissivity beam splitters (BS_1 and BS_2) where they are mixed with two coherent states, $|\alpha_1\rangle$ and $|\alpha_2\rangle$, coming in two other ports of beam splitters. This arrangement (highly transmitter beam splitter, and interaction with coherent states) produces the displacement of the two input modes. Subsequently, the output states of the beam splitters are detected by two photodetectors able to resolve the photon number (n_1 and n_2, respectively). Now,

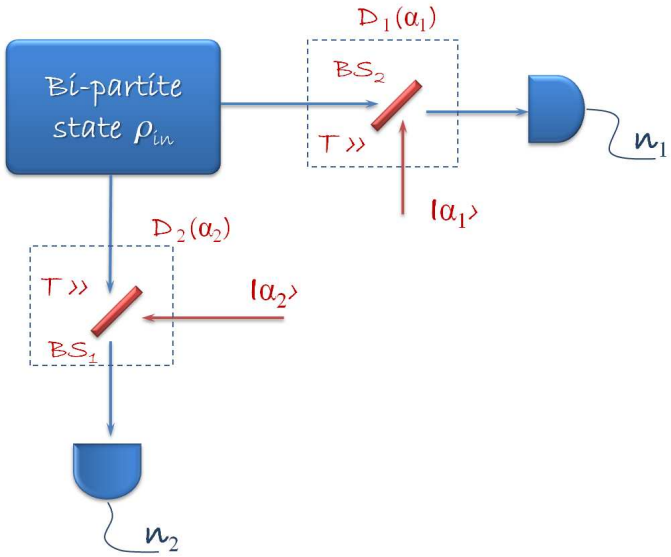

Figure 3.2: Schematic representation of the parity measurement. The BS_1 and BS_2 have the transmission coefficient close to one. Strong coherent states impact into the free ports. Two photodetectors are able to resolve the photon number.

we can assign to each event the value $+1$ or -1, depending on whether an even or an odd number of photons has been registered. This measurement is described by a pair of projection operators for the single mode:

$$\begin{aligned}\Pi^{(+)}(\boldsymbol{\alpha}) &= D(\boldsymbol{\alpha})\sum_{n=0}^{\infty}|2n\rangle\langle 2n|D^{\dagger}(\boldsymbol{\alpha}),\\ \Pi^{(-)}(\boldsymbol{\alpha}) &= D(\boldsymbol{\alpha})\sum_{n=0}^{\infty}|2n+1\rangle\langle 2n+1|D^{\dagger}(\boldsymbol{\alpha}),\end{aligned}$$

where $\boldsymbol{\alpha}=(\alpha,\alpha^{*})$. If we consider the difference of the operators above we obtain

$$\begin{aligned}\Pi^{(+)}(\boldsymbol{\alpha})-\Pi^{(-)}(\boldsymbol{\alpha}) &= D(\boldsymbol{\alpha})\sum_{n=0}^{\infty}\left(|2n\rangle\langle 2n|-|2n+1\rangle\langle 2n+1|\right)D^{\dagger}(\boldsymbol{\alpha})\\ &= D(\boldsymbol{\alpha})(-1)^{\hat{n}}D^{\dagger}(\boldsymbol{\alpha}),\end{aligned}$$

where $\hat{n}=a^{\dagger}a$ is the number photon operator. In fact, we note that the expectation value of $\sum_{n=0}^{\infty}\left(|2n\rangle\langle 2n|-|2n+1\rangle\langle 2n+1|\right)$ with respect to a quantum state with photon number m is given by

$$\begin{aligned}\left\langle\sum_{n=0}^{\infty}\left(|2n\rangle\langle 2n|-|2n+1\rangle\langle 2n+1|\right)\right\rangle &= \langle m|\sum_{n=0}^{\infty}\left(|2n\rangle\langle 2n|-|2n+1\rangle\langle 2n+1|\right)|m\rangle\\ &= \begin{cases}+1 \text{ if } m \text{ is even}\\ -1 \text{ if } m \text{ is odd}\end{cases}.\end{aligned}$$

Expressing the relation above for the bi-partite case we define the operator

$$\mathfrak{W}(\boldsymbol{\alpha}_1, \boldsymbol{\alpha}_2) = \bigotimes_{k=1}^{2} D_k(\boldsymbol{\alpha}_k)(-)^{\hat{n}_k} D_k^{\dagger}(\boldsymbol{\alpha}_k).$$

In this way, we express the correlations between the two modes in terms of a dichotomous variable ($+1 \rightarrow$ even, and $-1 \rightarrow$ odd) by measuring the expectation value of the operator $\mathfrak{W}(\boldsymbol{\alpha}_1, \boldsymbol{\alpha}_2)$ respect to the state ρ_{in}:

$$\langle \mathfrak{W}(\boldsymbol{\alpha}_1, \boldsymbol{\alpha}_2) \rangle = \mathrm{Tr}\left[\rho_{in} \bigotimes_{k=1}^{2} D_k(\boldsymbol{\alpha}_k)(-)^{\hat{n}_k} D_k^{\dagger}(\boldsymbol{\alpha}_k) \right]. \tag{3.9}$$

The Bell's function $\mathcal{B}$ can be expressed in terms of this expectation value, conditioning suitably the different values of the displacements. For example [60],

$$\mathcal{B} = \langle \mathfrak{W}(\mathbf{0}, \mathbf{0}) \rangle + \langle \mathfrak{W}(\boldsymbol{\alpha}_1, \mathbf{0}) \rangle + \langle \mathfrak{W}(\mathbf{0}, \boldsymbol{\alpha}_2) \rangle - \langle \mathfrak{W}(\boldsymbol{\alpha}_1, \boldsymbol{\alpha}_2) \rangle. \tag{3.10}$$

The local theories impose the bound

$$|\mathcal{B}| \leq 2. \tag{3.11}$$

The quantity (3.9) is exactly the definition of the Wigner function $W(\boldsymbol{\alpha}_1, \boldsymbol{\alpha}_2)$ describing the state ρ_{in} (see Eq. (1.10)). It is also the Fourier transform of the characteristic function, and contains all the information about the quantum state ρ_{in}. The description of ρ_{in} through the Wigner function is equivalent to that of the characteristic function. So, we have

$$W(\boldsymbol{\alpha}_1, \boldsymbol{\alpha}_2) \equiv \frac{4}{\pi^2} \langle \mathfrak{W}(\boldsymbol{\alpha}_1, \boldsymbol{\alpha}_2) \rangle.$$

This correspondence allows us to calculate the four expectation values of the Eq. (3.10), once we know the Wigner function of the state, that is once we know the state ρ_{in} to be analyzed. Otherwise, to determine (3.10), we should do a repeated measures with the scheme of Fig. (3.2), and then a statistical analysis of the results considering all the necessary constraints. In other words, the use of the Wigner function allows us to "simulate" the measurement apparatus.

If the correlation function $\mathfrak{W}(\boldsymbol{\alpha}_1, \boldsymbol{\alpha}_2)$ is measured for the combination $\alpha_1 = \sqrt{\mathcal{I}}$, $\alpha_2 = -\sqrt{\mathcal{I}}$, with $\mathcal{I}$ magnitude of the displacement, we can write the quantity $\mathcal{B}$ as

$$\mathcal{B} = \langle \mathfrak{W}(\mathbf{0}, \mathbf{0}) \rangle + \left\langle \mathfrak{W}(\sqrt{\mathcal{I}}, \mathbf{0}) \right\rangle + \left\langle \mathfrak{W}(\mathbf{0}, -\sqrt{\mathcal{I}}) \right\rangle - \left\langle \mathfrak{W}(\sqrt{\mathcal{I}}, -\sqrt{\mathcal{I}}) \right\rangle. \tag{3.12}$$

3.2.0.3 Bi-partite Gaussian state case

For a bi-partite Gaussian state, described by the covariance matrix σ,

$$\sigma = \begin{pmatrix} n & 0 & c & 0 \\ 0 & n & 0 & -c \\ c & 0 & n & 0 \\ 0 & -c & 0 & n \end{pmatrix}, \tag{3.13}$$

the quantity (3.10) becomes

$$\mathcal{B}(\mathcal{I}, n, c) = \frac{1 + 2\exp\left\{-\frac{n}{n^2-c^2}\mathcal{I}\right\} - \exp\left\{-\frac{n+c}{n^2-c^2}2\mathcal{I}\right\}}{4(n^2-c^2)}.$$

The maximal violation in respect to the displacement amplitude is given by

$$\tilde{\mathcal{B}}(n, c) \equiv \max_{\mathcal{I}} \mathcal{B}(\mathcal{I}, n, c).$$

We obtain the maximum value of $\mathcal{B}$, *i.e.* the maximal violation of the inequality (3.11), by solving the equation with respect to $\mathcal{I}$

$$\frac{\partial \mathcal{B}(\mathcal{I}, n, c)}{\partial \mathcal{I}} = 0.$$

We find that the maximum is given for $\mathcal{I}$ equal to

$$\widetilde{\mathcal{I}}(n, c) = \frac{1}{4(n+2c)\mu} \ln\left[\frac{n+c}{n}\right].$$

So $\tilde{\mathcal{B}}$ reads

$$\begin{aligned} \tilde{\mathcal{B}}(n, c) &= \mu\left[1 + 2\left(\frac{n+c}{n}\right)^{-\frac{n}{n+c}} - \left(\frac{n+c}{n}\right)^{-2\frac{n+c}{n+2c}}\right] \\ &= \mu\left[1 + 2(1+C_{ab})^{-\frac{1}{1+C_{ab}}} - (1+C_{ab})^{-2\frac{1+C_{ab}}{1+2C_{ab}}}\right] \\ &= \mu\left[1 + (1+2C_{ab})(1+C_{ab})^{-2\frac{1+C_{ab}}{1+2C_{ab}}}\right] \\ &= \tilde{\mathcal{B}}(\mu_s, C_{ab}), \end{aligned}$$

where

$$\mu = \frac{1}{4(n^2-c^2)} = \frac{\mu_s^2}{1-C_{ab}^2}$$

is the purity of the overall state, μ_s is the purity of sub-system ($\mu_s \equiv \mu_a = \mu_b = 1/(2n)$) and

$$C_{ab} \equiv \frac{\langle \Delta X_a X_b \rangle}{\sqrt{\langle \Delta X_a^2 \rangle \langle \Delta X_b^2 \rangle}} = \frac{c}{n}$$

is the correlation coefficient defined in EPR-Reid criterion, Eq. (2.18). Now, we want to prove the following equivalence for pure states:

Proposition 2 *For pure Gaussian bi-partite states, described by the covariance matrix of the form (3.13), the following three conditions are equivalent:*

(I) *The sub-systems a and b are correlated if only if the correlation coefficient is such that* $C_{ab} > 0$*;*

(II) *Duan's criterion: The system ab is entangled if only if* $w_{DUAN} \equiv \left(n - \frac{1}{2}\right) - c < 0$*;*

(III) *Bell's violation: The Bell's locality is violated if only if* $\left|\tilde{\mathcal{B}}\left(\mu, C_{ab}\right)\right| > 2$.

In particular, we show that for pure states the system is entangled if only if it violates the Bell'inequality.

Proof. *We observe that because the state is pure we have that*

$$1 = \frac{\mu_s^2}{1 - C_{ab}^2} \Longrightarrow \mu_s^2 = 1 - C_{ab}^2. \tag{3.14}$$

In order to prove the equivalence of the three above assertions, it is sufficient to verify the implication system:

$$\left\{ \begin{array}{c} (\mathbf{I}) \Longleftrightarrow (\mathbf{II}) \\ (\mathbf{I}) \Longleftrightarrow (\mathbf{III}) \end{array} \right\},$$

that implies $(\mathbf{II}) \Longleftrightarrow (\mathbf{III})$**.**
$(\mathbf{I}) \Longrightarrow (\mathbf{II})$*. If* $C_{ab} > 0$ *(and* $C_{ab} < 1$ *for definition) then*

$$1 - C_{ab} < \sqrt{\left(1 - C_{ab}\right)\left(1 + C_{ab}\right)} \tag{3.15}$$

is verified. We note that the above inequality corresponds to the Duan's condition. In fact, the condition $w_{DUAN} < 0$ *is equivalent to*

$$\begin{aligned} \left(n - \frac{1}{2}\right) - c &< 0 \\ n\left(1 - \frac{1}{2n} - \frac{c}{n}\right) &< 0 \\ 1 - \mu_s - C_{ab} &< 0. \end{aligned}$$

Recalling that $\mu_s = \sqrt{\left(1 - C_{ab}\right)\left(1 + C_{ab}\right)}$*, Eq. (3.14), it is proved that if the condition (3.15) is true then the Duan's condition* $1 - \sqrt{\left(1 - C_{ab}\right)\left(1 + C_{ab}\right)} - C_{ab} < 0$ *is verified,* i.e. *the state is entangled.*
$(\mathbf{I}) \Longleftarrow (\mathbf{II})$*. We solve the Duan's inequality* $1 - \sqrt{1 - C_{ab}^2} - C_{ab} < 0$*. It is immediate to verify that the solutions are: (1)* $C_{ab} < 0 \cap C_{ab} > 1$ *(impossible), and (2)* $C_{ab} > 0 \cap C_{ab} < 1$*. The solution (2) is compatible with the domain of*

definition of correlation coefficient C_{ab} and it is equivalent to the assertion (**I**).
(**I**) $\Longleftrightarrow$ (**III**). *If only if the sub-systems a and b are correlated ($C_{ab} > 0$) then the system ab violates the Bell'inequality,* i.e. *the Bell's function of the pure state (ps)* $\tilde{\mathcal{B}}_{\rm ps}$

$$\tilde{\mathcal{B}}_{ps}\left(C_{ab}\right) = \tilde{\mathcal{B}}\left(\mu_s, C_{ab}\right)\Big|_{\mu_s = 1 - C_{ab}^2} \tag{3.16}$$

$$= \left[1 + \left(1 + 2C_{ab}\right)\left(1 + C_{ab}\right)^{-2\frac{1+C_{ab}}{1+2C_{ab}}}\right] \tag{3.17}$$

assumes values greater than 2. *From Eq. (3.17), we can see* $\tilde{\mathcal{B}}_{\rm ps} = 2$ *if only if* $C_{ab} = 0$, *and* $\nexists C_{ab} = \bar{C}_{ab} \in [0,1] : \tilde{\mathcal{B}}_{\rm ps} < 2$. *Indeed,* $\forall\ C_{ab} \in\ ]0,1]$, *we have* $\tilde{\mathcal{B}}_{\rm ps} > 2$. *In particular, for* $C_{ab} = 1$, *we have*

$$\tilde{\mathcal{B}}_{\rm ps}^{\max} = \lim_{C_{ab}\to 1} \tilde{\mathcal{B}}_{\rm ps}\left(C_{ab}\right) = 1 + \frac{3}{2^{4/3}} \simeq 2.19,$$

according to the reported maximum value in [61].
In conclusion, we have shown that, for pure states, the entanglement is a necessary and sufficient condition to the violation of Bell's theorem. In other words, a pure entangled state does not allow a phisical description in terms of hidden variable theories. ■

In the mixed states case, we can see the uniqueness relationship between entanglement and Bell's violation no longer exists. In the following, we clarify this link. In particular, we prove that given a mixed system, $\mu_s^2 < 1 - C_{ab}^2$, with the correlation coefficient C_{ab}, it is possible to distinguish three different regimes. In Fig. (3.3) it is reported the region plot of $\tilde{\mathcal{B}}$, w_{DUAN} in terms of C_{ab} and μ_s. We distinguish three main regions. These regions are bounded by three purities μ_s of sub-systems, defined as

$$\begin{aligned}
\mu_D &\equiv 1 - C_{ab}, \\
\mu_B &\equiv \left[\frac{2\left(1 - C_{ab}^2\right)}{1 + \left(1 + 2C_{ab}\right)\left(1 + C_{ab}\right)^{-2\frac{1+C_{ab}}{1+2C_{ab}}}}\right]^{1/2}, \\
\mu_P &\equiv \left[1 - C_{ab}^2\right]^{1/2}.
\end{aligned}$$

They are defined by the states that occur the Duan's criterion (μ_D), Bell's inequality (μ_B) and the uncertainty principle (μ_P), with the sign of equality.

We report schematically the three areas in table:

Region	w_{DUAN}	$\tilde{\mathcal{B}}\left(\mu_s, C_{ab}\right)$
I	> 0	< 2
II	< 0	< 2
III	< 0	> 2

Observing the Fig. (3.3) we identify the following regions:

(White area) **Region** I) It is populated by states such that $\mu_s < \mu_D$. This area includes *separable* states ($w_{DUAN} > 0$) and *compatible* with the hidden variables theory ($\tilde{\mathcal{B}}(\mu_s, C_{ab}) < 2$).

(White Pink area) **Region** II) It is populated by states such that $\mu_D < \mu_s < \mu_B$. This area includes *entangled* states ($w_{DUAN} < 0$) and *compatible* with the hidden variables theory ($\tilde{\mathcal{B}}(\mu_s, C_{ab}) < 2$).

(Salmon area) **Region** III) It is populated by states such that $\mu_B < \mu_s < \mu_P$. This area includes *entangled* states ($w_{DUAN} < 0$) and *incompatible* with the hidden variables theory ($\tilde{\mathcal{B}}(\mu_s, C_{ab}) > 2$).

(Brown area) **no-physical Region** It is populated by no-physical states with $\mu_s > \mu_P$.

It is clear that there aren't separable states that violate the Bell's inequality. Instead, a locally describable state (*i.e.* compatible with a theory in hidden variables) can also be entangled. This confirms the existence of different forms of quantum correlations and localities. Clearly, there are quantum states (belonging to the region II) that, although they admit a local-classical description, they exhibit quntum behaviors as the entanglement.

At this point, we can evaluate the Bell's function of a bi-partite system subjected to the attenuated action of a passive Gaussian channel. We start (at $t = 0$) from an initially pure state and we analyze the evolution of $\tilde{\mathcal{B}}$ (at $t > 0$) as a function of the coefficient of transmissivity T. For this purpose, we resume the behavior of the elements of the covariance matrix as a function of T:

$$\begin{aligned} n_T &= \frac{1-T}{2} + Tn_1, \\ c_T &= Tc_1, \end{aligned}$$

where n_1 and c_1 are the matrix elements of the initial state. So the Bell's function $\tilde{\mathcal{B}}$ becomes a function $\tilde{\mathcal{B}}_T$ depending on the initial (pure) state and on the transmissivity T of the channel.

In Fig. (3.4), we can observe that when a state, that initially violate the inequality ($\tilde{\mathcal{B}} > 2$), is transmitted through a passive Gaussian channel, it ends up with verify the Bell's inequality ($\tilde{\mathcal{B}} < 2$). In particular, we see that a more energetic quantum state, more quickly loses its Bell's non-local. This fact is not surprising: a more energetic quantum state is closer to a classical state with respect to one less energetic. In other terms, the quantum coherence properties of a very energetic state are more perishable compared to those of a less energetic state [62].

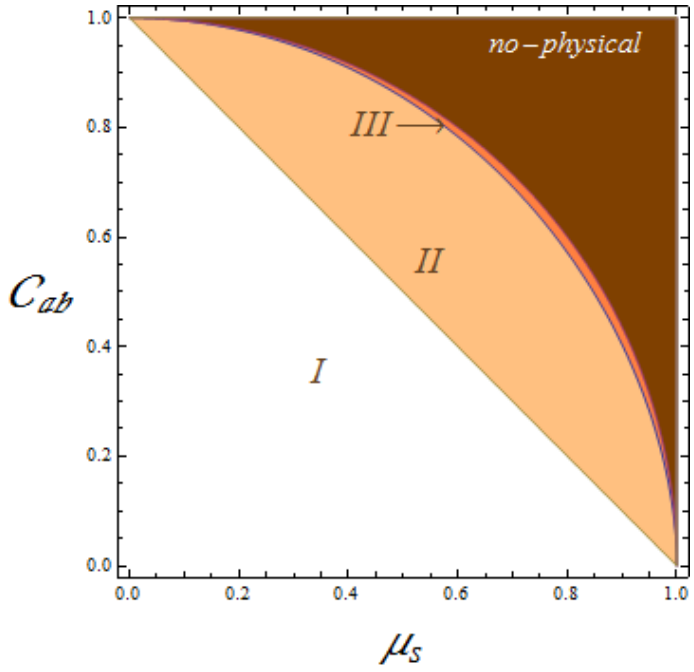

Figure 3.3: (Color online) Region plot of $\tilde{\mathcal{B}}$ as function of purity μ_s and the correlation coefficient C_{ab}. The brown area indicates unphysical states.

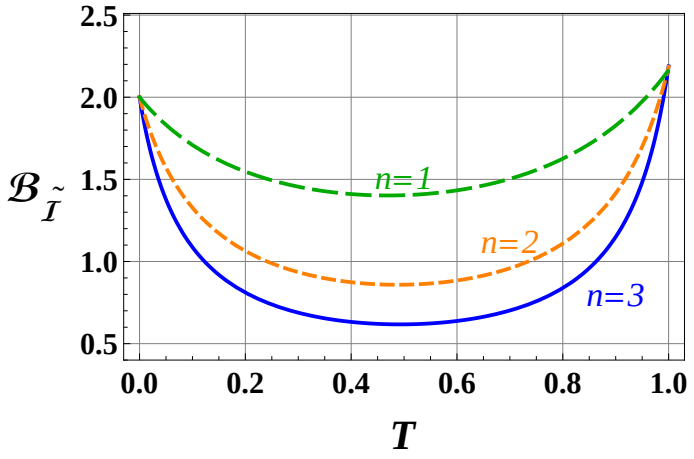

Figure 3.4: (Color online) Evolution of the Bell's function, in a realistic transmission channel, for different initial pure states.

CHAPTER 4

ENTANGLEMENT SWAPPING PROTOCOL WITH NON-GAUSSIAN RESOURCES

The **CV** entanglement swapping protocol has the task to establish quantum correlations between two remote parties through the entanglement transfer. It plays a fundamental role in long-distance quantum communications [63], e.g. in the building of quantum repeaters connecting distant communicating parties [64]. In general, the efficient teleportation of entanglement is a necessary requirement for the realization of a quantum information network based on multi-step information processing [65]. The experimental demonstration of **CV** van Loock and Braunstein (vLB) entanglement swapping protocol [66] has been already achieved [67, 68]. A detailed analysis of the optimal Gaussian entanglement swapping has been performed in Ref. [69].

We study the **CV** entanglement swapping protocol using non-Gaussian states as entangled input states and/or resources. We express the swapping protocol in the characteristic function representation, taking into account losses and decoherence due to the inefficiencies of the detectors. As a criterion for quantifying the performance of the swapping protocol, we exploit, both in the ideal and in the realistic instance, the fidelity of teleportation of single-mode coherent states using two-mode swapped states as entangled resources. Therefore, we analyze a cascaded quantum information scheme, including as a first step an ideal or realistic swapping protocol, and subsequently an ideal teleportation protocol. Specifically, the swapping protocol is feeded by a general class of optimized non-Gaussian states, *i.e.* the **SB** states introduced in Sect.1.3.2. By means of a controllable free parameter, such a class of entangled states allows a continuous tuning from Gaussian twin beams to (maximally non-Gaussian) squeezed number (**PN**) states, and contains as intermediate states as photon-added (**PA**) squeezed states and photon-subtracted (**PS**) squeezed states. The final teleportation fidelity is optimized over the free experimental parameters. The exploitation of non-Gaussian **SB** resources yields a sensible enhancement of the performance levels of the entanglement swapping protocol both in the ideal and in the realistic instances.

4.1 Entanglement Swapping protocol

In this Section, we exploit the characteristic function formalism for the description of the realistic **CV** entanglement swapping protocol, which is schematically depicted in Fig. 4.1.

The task of entanglement swapping protocol is the transfer of the entanglement between a couple of modes, e.g. 1 and 2, prepared in a entangled state, to the couple of modes, e.g. 1 and 4, initially unentangled; such a task is accomplished by exploiting a further resource entangled in the modes 3 and 4, a Bell measurement, and a final unitary transformation. A schematic picture of the **CV** swapping protocol is depicted in Fig. 4.1. Specifically, mode 2 of the input two-mode entangled state is mixed to mode 3 of the entangled resource at a balanced beam splitter. A Bell measurement, consisting in homodyne detections, is performed on the obtained state of mode 2 and 3. In order to model a non-ideal measurement, or equivalently to simulate the inefficiencies of the photodetectors, a further fictitious beam splitter is placed in front of each ideal detector [70]. After the realistic Bell measurement, the result is transmitted to the locations of modes 1 and 4 through classical channels. It is assumed that both the input state and the resource are produced close to the Charlie's location (Bell measurement), and far from Alice's and Bob's locations (remote users). Therefore, it is supposed that the modes 2 and 3 are not affected by the decoherence due to propagation; on the contrary, the modes 1 and 4 propagate through noisy channels, e.g. optical fibers, towards Alice's and Bob's locations, respectively. At these locations, according to the result of the Bell measurement, unitary displacements are performed on mode 1 of the input state and on mode 4 of the resource. The resulting two-mode swapped (entangled) state of modes 1 and 4 is the output state of the protocol.

Let $\rho_0 = \rho_{12}^A \otimes \rho_{34}^B$ the input biseparable four-mode state; such a state is described, in the phase space $(x_i, y_i)\,, i = 1, \ldots 4$, by the characteristic function $\chi_0(x_1, y_1; x_2, y_2; x_3, y_3; x_4, y_4)$:

$$\begin{aligned} \chi_0(\alpha_1; \alpha_2; \alpha_3; \alpha_4) &= \mathrm{Tr}[\prod_{j=1}^{4} D_j(\alpha_j)\rho_0] \\ &= \chi_{12}(\alpha_1; \alpha_2)\ \chi_{34}(\alpha_3; \alpha_4)\,, \end{aligned} \tag{4.1}$$

where Tr denotes the trace operation, $D_j(\alpha_j)$ denotes the displacement operator of mode j $(j = 1, \ldots, 4)$, χ_{12} is the characteristic function of the two-mode input state, and χ_{34} is the characteristic function of the two-mode resource. By introducing the quadrature operators $X_j = \frac{1}{\sqrt{2}}(a_j + a_j^\dagger)$ and $Y_j = \frac{i}{\sqrt{2}}(a_j^\dagger - a_j)$, and the corresponding phase space variables $x_j = \frac{1}{\sqrt{2}}(\alpha_j + \alpha_j^*)$ and $y_j = \frac{i}{\sqrt{2}}(\alpha_j^* - \alpha_j)$, the characteristic function can be written in terms of x_j, y_j, *i.e.* $\chi_0(\alpha_1; \alpha_2; \alpha_3; \alpha_4) \equiv \chi_0(x_1, y_1; x_2, y_2; x_3, y_3; x_4, y_4)$. The first step of the protocol consists of the Bell measurement at the first user's location. The mode 2 and 3 are mixed at a balanced beam splitter; the effects of the inefficiencies of the photodetectors and of the photon losses are simulated by two additional fictitious beam splitters, with transmissivity T_j^2 (reflectivity $R_j^2 = 1 - T_j^2$), $j = 2, 3$, placed in front of the detectors. Let us denote by $\tilde{x}$ and $\tilde{y}$ the homodyne measurements of the first quadrature of the mode 3 and of the second quadrature of the mode 2, respectively. The re-

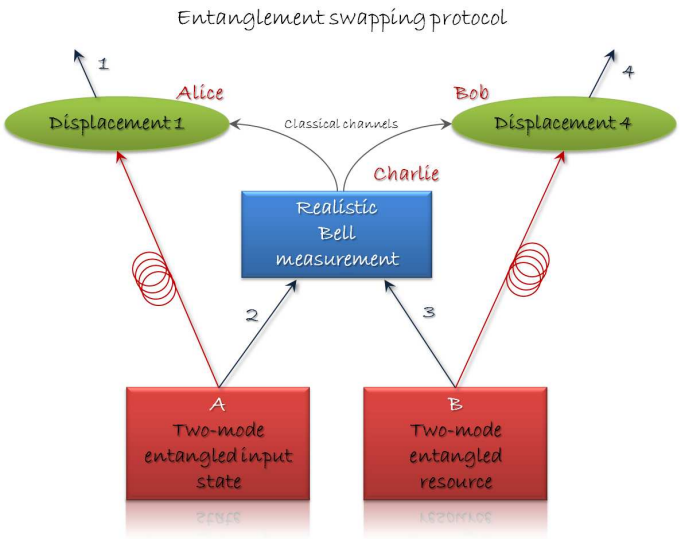

Figure 4.1: (Color online) Pictorial representation of the non-ideal CV entanglement swapping protocol. Initially, two parties, i.e. Alice and Bob, share entangled states with a third party, i.e. Charlie; Alice shares the input two-mode entangled state of modes 1 and 2 with Charlie, and Bob shares the two-mode entangled resource of modes 3 and 4 with Charlie. In the first step, at Charlie's location, the mode 2 of the input two-mode entangled state is mixed with the mode 3 of the entangled resource; the ensuing state is then subject to a realistic Bell measurement (imperfect photodetection). The result of the measurement is communicated by Charlie to Alice and Bob through classical channels. The modes 1 and 4 propagate towards the corresponding locations through noisy channels, i.e. optical fibers. In the second step, two unitary transformations, determined by the previous measurement, are applied by Alice and Bob to mode 1 and 4, respectively. The ensuing output state of modes 1 and 4 is the final swapped (entangled) state. Such a state is shared by the two final users Alice and Bob.

alistic Bell measurement is described in full details, by using the formalism of the characteristic function, in Ref. [22]. Here we give the final expression of the characteristic function $\chi_{Bm}(x_1, y_1; x_4, y_4)$ associated with the whole measurement process:

$$\begin{aligned}\chi_{Bm}(x_1, y_1; x_4, y_4) &= \frac{\mathcal{P}^{-1}(\tilde{y}, \tilde{x})}{(2\pi)^2} \int d\xi d\upsilon \, e^{i\xi\tilde{y} - i\tilde{x}\upsilon} \\ &\times \chi_{12}\left(x_1, y_1; \frac{T_2\xi}{\sqrt{2}}, \frac{T_3\upsilon}{\sqrt{2}}\right) \chi_{34}\left(\frac{T_2\xi}{\sqrt{2}}, -\frac{T_3\upsilon}{\sqrt{2}}; x_4, y_4\right) \\ &\times \exp\left[-\frac{R_2^2}{4}\xi^2 - \frac{R_3^2}{4}\upsilon^2\right], \end{aligned} \tag{4.2}$$

where the function $\mathcal{P}(\tilde{y}, \tilde{x})$ is the distribution of the measurement outcomes $\tilde{y}$ and $\tilde{x}$, *i.e.*

$$\begin{aligned}\mathcal{P}(\tilde{y}, \tilde{x}) &= \frac{1}{(2\pi)^2} \int d\xi d\upsilon \, e^{i\xi\tilde{y} - i\tilde{x}\upsilon} e^{-\frac{R_2^2}{4}\xi^2 - \frac{R_3^2}{4}\upsilon^2} \\ &\times \chi_{12}\left(0, 0; \frac{T_2\xi}{\sqrt{2}}, \frac{T_3\upsilon}{\sqrt{2}}\right) \chi_{34}\left(\frac{T_2\xi}{\sqrt{2}}, -\frac{T_3\upsilon}{\sqrt{2}}; 0, 0\right). \end{aligned} \tag{4.3}$$

Afterwards, modes 1 and 4 propagate in noisy channels, like optical fibers, towards Alice's and Bob's locations, respectively. The dynamics of a multimode system subject to decoherence is described, in the interaction picture, by the following master equation for the density operator ρ :

$$\partial_t \rho \;=\; \sum_{i=1,4} \frac{\Gamma_i}{2} \left\{ n_{th,i} L[a_i^\dagger]\rho + (n_{th,i} + 1) L[a_i]\rho \right\}, \tag{4.4}$$

where the Lindblad superoperators are defined as $L[\mathcal{O}]\rho \equiv 2\mathcal{O}\rho\mathcal{O}^\dagger - \mathcal{O}^\dagger\mathcal{O}\rho - \rho\mathcal{O}^\dagger\mathcal{O}$, Γ_i is the mode damping rate, and $n_{th,i}$ is the number of thermal photons of mode i. Because of the effect of decoherence due to propagation in the noisy channels, the characteristic function (4.2) rewrites:

$$\begin{aligned}&\chi_t(x_1, y_1; x_4, y_4) \;= \\ &\chi_{Bm}(e^{-\frac{1}{2}\Gamma_1 t}x_1, e^{-\frac{1}{2}\Gamma_1 t}y_1; e^{-\frac{1}{2}\Gamma_4 t}x_4, e^{-\frac{1}{2}\Gamma_4 t}y_4) \\ &\times \; e^{-\frac{1}{2}\sum_{i=1,4}(1 - e^{-\Gamma_i t})\left(\frac{1}{2} + n_{th,i}\right)(x_i^2 + y_i^2)}. \end{aligned} \tag{4.5}$$

Being related to the technical specifics of the experimental apparatus, e.g. the efficiency of the photodetectors, the characteristics as the length of the channels (fibers), the temperature of the environment, we will assume to possess full knowledge on the following quantities: T_j (equivalently R_j, $j = 2, 3$), Γ_i and $n_{th,i}$ ($i = 1, 4$). Therefore, we will consider T_j, Γ_i and $n_{th,i}$ fixed to certain values. In the last step of the protocol, two displacements λ_1 and λ_4 are performed at Alice's

and Bob's locations; a displacement $\lambda_1 = -g_1(\tilde{x} - i\tilde{y})$ is performed on mode 1, and a displacement $\lambda_4 = g_4(\tilde{x} + i\tilde{y})$ is performed on mode 4. The real parameters g_1 and g_4 are the gain factors of the displacement transformations [80]. After such transformations, the characteristic function writes:

$$\begin{aligned}\chi_D(x_1, y_1; x_4, y_4) &= e^{-i\sqrt{2}\tilde{x}(g_1 y_1 - g_4 y_4) - i\sqrt{2}\tilde{y}(g_1 x_1 + g_4 x_4)} \\ &\quad \times \chi_t(x_1, y_1; x_4, y_4)\,. \end{aligned} \tag{4.6}$$

Finally, in order to obtain the output characteristic function $\chi_{out}(x_1, y_1; x_4, y_4)$, describing the output state of the entanglement swapping protocol, one must take the average of all the possible outcomes $\tilde{y}$ and $\tilde{x}$ of the Bell measurements:

$$\chi_{out}^{(swapp)}(x_1, y_1; x_4, y_4) = \int d\tilde{x} d\tilde{y} \mathcal{P}(\tilde{y}, \tilde{x}) \chi_D(x_1, y_1; x_4, y_4), \tag{4.7}$$

where $\tau_i = \Upsilon_i t$. The above integral yields the final expression for the characteristic function associated with the swapped resource:

$$\begin{aligned}&\chi_{out}^{(swapp)}(x_1, y_1; x_4, y_4) = \\ &\chi_{12}\left(e^{-\frac{\tau_1}{2}} x_1, e^{-\frac{\tau_1}{2}} y_1; T_2(g_1 x_1 + g_4 x_4), T_3(-g_1 y_1 + g_4 y_4)\right) \\ &\chi_{34}\left(T_2(g_1 x_1 + g_4 x_4), -T_3(-g_1 y_1 + g_4 y_4); e^{-\frac{\tau_4}{2}} x_4, e^{-\frac{\tau_4}{2}} y_4\right) \\ &e^{-\frac{1}{2}(1-e^{-\tau_1})\left(\frac{1}{2} + n_{th,1}\right)(x_1^2 + y_1^2) - \frac{1}{2}(1-e^{-\tau_4})\left(\frac{1}{2} + n_{th,4}\right)(x_4^2 + y_4^2)} \\ &e^{-\frac{R_2^2}{2}(g_1 x_1 + g_4 x_4)^2 - \frac{R_3^2}{2}(-g_1 y_1 + g_4 y_4)^2}\,, \end{aligned} \tag{4.8}$$

In order to give an immediate correspondence, we list in Tab. 4.1 all the parameters associated with the experimental apparatus, that appear in Eq. (4.8). Such parameters are taken as fixed constants; indeed, we assume a complete knowledge about the technological components and devices that are the building blocks of the protocol.

g_i , $i = 1, 4$	gains associated with unitary displacements
T_i (R_i) , $i = 2, 3$	transmissivities (reflectivities) of beam splitters
Υ_i , $i = 1, 4$	damping factors
$n_{th,i}$, $i = 1, 4$	average numbers of thermal photons
$\tau_i \equiv \Upsilon_i t$, $i = 1, 4$	dimensionless times

Table 4.1: Parameters characterizing the experimental apparatus.

In the instance of ideal protocol ($R_i = 0\,, T_i = 1\,, \tau_i = 0$) and for $g_1 = 0$, $g_4 = 1$, Eq. (4.8) reduces to:

$$\begin{aligned} &\chi_{out}^{(swapp)}(x_1, y_1; x_4, y_4) = \\ &\chi_{12}\,(x_1, y_1; x_4, y_4)\ \chi_{34}\,(x_4, -y_4; x_4, y_4)\ . \end{aligned} \tag{4.9}$$

This last formula offers a clear interpretation of the task of the swapping protocol. For instance, assuming the entangled resource to be a twin beam with squeezing parameter r_{34}, in the limit of large r_{34} the function $\chi_{34}\,(x_4, -y_4; x_4, y_4)$ tends to one; correspondingly, the output characteristic function χ_{out} coincides with χ_{12}, with the complete swapping of mode 2 with the mode 4.

4.2 Swapping protocol with Non-Gaussian entangled states

In order to analyze the performance of the swapping protocol implemented with Gaussian or non-Gaussian resources for the swapping of input Gaussian or non-Gaussian entanglement, we exploit the following criterion: we study the performance of the two-mode entangled states, at the output of the swapping protocol (swapped states), using them as entangled resources of a protocol of teleportation of an input single-mode coherent state. Thus, given the input two-mode entangled state $\chi_{12}(x_1, y_1; x_2, y_2)$ and the two-mode entangled resource $\chi_{34}(x_3, y_3; x_4, y_4)$, we compute the two-mode entangled output (swapped) state of the swapping protocol $\chi_{out}^{(swapp)}(x_1, y_1; x_4, y_4)$, given by Eq. (4.8) for the realistic protocol (or Eq. (4.9) for the ideal protocol). Then such a two-mode entangled state is used as a resource for the ideal teleportation protocol of input single-mode coherent states. So, we compute the single-mode state output (teleported) state of the teleportation protocol $\chi_{out}^{(telep)}(x_4, y_4)$, given by the formula:

$$\chi_{out}^{(telep)}(x_4, y_4) \;\; = \;\; \chi_{in}^{(coh)}(x_4, y_4)\, \chi_{out}^{(swapp)}(x_4, -y_4; x_4, y_4), \tag{4.10}$$

where $\chi_{in}^{(coh)}(x_4, y_4)$ is the characteristic function of the input coherent state of complex amplitude β. Finally, we compute the fidelity of teleportation:

$$\mathcal{F}_{X^{sw}Y} \;\; = \;\; \frac{1}{2\pi} \int dx_4 dy_4\ \chi_{in}^{(coh)}(x_4, y_4) \chi_{out}^{(telep)}(-x_4, -y_4)\,, \tag{4.11}$$

where the subscript $X^{sw}Y$ specifies the features of the swapped entangled state used as a resource, *i.e.* it stands for X resource swapped with Y resource, with $X, Y = \mathbf{TB}, \mathbf{PS}, \mathbf{SB}$. Concerning the achievements of current quantum technology, a reasonable hypothesis is the assumption of on-demand availability of Gaussian **TB** with finite squeezing, and hardly, costly producible non-Gaussian

states. Therefore, we may assume to have at disposal many copies of **TB** and few copies of **SB** states. With such a constraint, the most convenient approach would be to swap the non-Gaussian entanglement, and thus to use the **TB** and the **SB** states as resources and input states of the swapping protocol, respectively. For example, in a long-distance communication scheme, the entanglement swapping and entanglement purification protocols can be performed to transfer the non-Gaussian entanglement along the quantum channel, divided into several segments. On the other hand, by removing the above constraint, one would have on-demand availability of **TB** states. In this desirable instance, one could use **SB** states both as input and as resources of the swapping protocol. In conclusion, we will compute the fidelity $\mathcal{F}_{\mathbf{SB}^{sw}\mathbf{SB}}$, which contains as particular cases all the fidelities of interest, *i.e.* $\mathcal{F}_{\mathbf{SB}^{sw}\mathbf{TB}}$, $\mathcal{F}_{\mathbf{PS}^{sw}\mathbf{TB}}$, and $\mathcal{F}_{\mathbf{TB}^{sw}\mathbf{TB}}$. We fix the phases ϕ_{hk} and θ_{hk} at the optimal values $\phi_{hk} = \pi$ and $\theta_{hk} = 0$. With such a choice, the dependence of the fidelity $\mathcal{F}_{\mathbf{SB}^{sw}\mathbf{SB}}$ on the two gains g_1 and g_4 simplifies to only one degree of freedom $\tilde{g} = g_1 + g_4$, which is an optimizable parameter. In particular, the optimized fidelities are defined as:

$$\mathcal{F}^{(opt)}_{X^{sw}Y} = \max_{\mathcal{P}} \mathcal{F}_{X^{sw}Y} \,, \tag{4.12}$$

where $\mathcal{P}$ denotes the set of free parameters available for optimization. In the most general case, *i.e.* **SB** resources swapped with **SB** resources, the free parameters available for optimization are $\mathcal{P} = \{\delta_{12}, \delta_{34}, \tilde{g}\}$.

4.2.1 Ideal swapping protocol

We consider the ideal swapping protocol. Before proceeding in the analysis, let us assume some simplifications and assumptions. Without any loss of generality, as in Refs.[1, 22], we fix the phases of the **SB** states: specifically, we put the non-Gaussian phases $\theta_{12} = \theta_{34} = 0$ and the squeezing phases $\phi_{12} = \phi_{34} = \pi$ in Eq. (1.29). Due to such a choice, the dependence of the teleportation fidelity on the two gains g_i $(i = 1, 4)$ reduces to the unique parameter $\tilde{g} = g_1 + g_4$ both the ideal and in the realistic instances.

Here, we report some analytical results for the teleportation fidelities in the instance of ideal swapping protocol, *i.e.* $\tau_1 = \tau_4 = 0$, $n_{th,1} = n_{th,4} = 0$, $R_2 = R_3 = 0$ $(T_2 = T_3 = 1)$. We assume the Gaussian **TB** resources as on-demand swapping resources, and non-Gaussian **SB** states as the resources to be swapped. In order to provide significant examples, we report the analytical expressions for $\mathcal{F}_{\mathbf{TB}^{sw}\mathbf{TB}}$ and $\mathcal{F}_{\mathbf{SB}^{sw}\mathbf{TB}}$. Given the general analytical expression for $\mathcal{F}_{\mathbf{SB}^{sw}\mathbf{SB}}$, the fidelity $\mathcal{F}_{\mathbf{TB}^{sw}\mathbf{TB}}$ can be computed by letting $\delta_{12} = \delta_{34} = 0$:

$$\begin{aligned} \mathcal{F}_{\mathbf{TB}^{sw}\mathbf{TB}} \;=\; & \left\{ 1 + \frac{1}{4}(1+\tilde{g})^2 (e^{-2r_{12}} + e^{-2r_{34}}) \right. \\ & \left. + \frac{1}{4}(1-\tilde{g})^2 (e^{2r_{12}} + e^{2r_{34}}) \right\}^{-1} . \end{aligned} \tag{4.13}$$

For fixed r_{12} and r_{34}, $\mathcal{F}_{\mathbf{TB}^{sw}\mathbf{TB}}$ can be maximized over the free parameter $\tilde{g}$; the optimal value $\tilde{g}_{opt}$ and the corresponding optimized fidelity $\mathcal{F}^{opt}_{\mathbf{TB}^{sw}\mathbf{TB}}$ write

$$\tilde{g}_{opt} = \frac{1-e^{-2(r_{12}+r_{34})}}{1+e^{-2(r_{12}+r_{34})}}, \tag{4.14}$$

$$\mathcal{F}^{(opt)}_{\mathbf{TB}^{sw}\mathbf{TB}} = \frac{1+e^{-2(r_{12}+r_{34})}}{(1+e^{-2r_{12}})(1+e^{-2r_{34}})}, \tag{4.15}$$

By looking at Eq. (4.15), it appears evident that the fidelity $\mathcal{F}^{(opt)}_{\mathbf{TB}^{sw}\mathbf{TB}}$ is invariant under the exchange of r_{12} with r_{34}. In the limit of $r_{34} \to \infty$ Eq. (4.15) reduces to the well known relation:

$$\mathcal{F}_{\mathbf{TB}} = [1+e^{-2r_{12}}]^{-1}, \tag{4.16}$$

corresponding to teleportation with twin beam resources of squeezing r_{12}. Moreover, it is worth noticing that, for growing values of the quantity $(r_{12}+r_{34})$, see Eq. (4.14), the optimal parameter $\tilde{g}_{opt}$ rapidly goes to one.

If we let $\delta_{34}=0$ in $\mathcal{F}_{\mathbf{SB}^{sw}\mathbf{SB}}$, we get $\mathcal{F}_{\mathbf{SB}^{sw}\mathbf{TB}}$:

$$\begin{aligned}
&\mathcal{F}_{\mathbf{SB}^{sw}\mathbf{TB}} = \mathcal{F}_{\mathbf{TB}^{sw}\mathbf{TB}} \times \\
&\Big\{1+\frac{e^{-4r_{12}}}{8}\mathcal{F}^2_{\mathbf{TB}^{sw}\mathbf{TB}}\left[(1+\tilde{g})^2 - e^{4r_{12}}(1-\tilde{g})^2\right]\sin^2\delta_{12} \\
&+\frac{e^{-2r_{12}}}{2}\mathcal{F}_{\mathbf{TB}^{sw}\mathbf{TB}}\left[(1+\tilde{g})^2(\cos\delta_{12}-\sin\delta_{12})\right. \\
&\left.-e^{4r_{12}}(1-\tilde{g})^2(\cos\delta_{12}+\sin\delta_{12})\right]\sin\delta_{12}\Big\}\,,
\end{aligned} \tag{4.17}$$

where $\mathcal{F}_{\mathbf{TB}^{sw}\mathbf{TB}}$ is given by Eq. (4.13). Obviously, for $\delta_{12}=0$ Eq. (4.17) reduces to Eq. (4.13).

At fixed $\tilde{g}$, the maximization of the fidelity (4.17) yields the optimal angle $\delta^{(opt)}_{12}$ given by the relation

$$\begin{aligned}
&\tan 2\delta^{(opt)}_{12} = \frac{1}{\Delta}\left[e^{-2r_{12}}G^2_+ - e^{2r_{12}}G^2_-\right]\left\{4e^{2(r_{12}+r_{34})} + (e^{2r_{12}}+e^{2r_{34}})\right. \\
&\left.\times\left[G^2_+ + e^{2(r_{12}+r_{34})}G^2_-\right]\right\}
\end{aligned}$$

where

$$\begin{aligned}
\Delta &= G^2_+\left[4e^{2r_{34}}+G^2_+\right] + e^{2(2r_{12}+r_{34})}G^2_-\left[1+4e^{2r_{34}}G^2_-\right] \\
&\quad +G^2_+G^2_-\left(e^{4r_{12}}+4e^{2(r_{12}+r_{34})}+e^{4r_{34}}\right),
\end{aligned}$$

and

$$G_\pm = (1\pm\tilde{g})\,.$$

Note that, if we let $\tilde{g}=1$ in Eq. (4.18), and take the limit of the corresponding reduced expression for $r_{34}\to\infty$, then we recover the optimal angle given by

$\tan 2\delta_{12}^{(opt)} = [1+e^{-2r_{12}}]$ associated with optimized teleportation of input coherent states with (non-swapped) **SB** states used as resources (see Ref. [1]). Finally the optimized fidelity $\mathcal{F}_{\mathbf{SB}^{sw}\mathbf{TB}}^{(opt)}$ is given by:

$$\mathcal{F}_{\mathbf{SB}^{sw}\mathbf{TB}}^{(opt)} = \max_{\tilde{g}} \mathcal{F}_{\mathbf{SB}^{sw}\mathbf{TB}}\Big|_{\delta_{12}=\delta_{12}^{(opt)}} . \tag{4.18}$$

Furthermore, if the angle δ_{12} is a specific function of r_{12}, *i.e.* $\delta_{12} = \delta_{12}(r_{12})$ the **SB** states reduce to the **PS** states, and the optimized fidelity is simply given by

$$\mathcal{F}_{\mathbf{PS}^{sw}\mathbf{TB}}^{(opt)} = \max_{\tilde{g}} \mathcal{F}_{\mathbf{SB}^{sw}\mathbf{TB}}\Big|_{\delta_{12}=\delta_{12}(r_{12})} . \tag{4.19}$$

The optimization over $\tilde{g}$ in Eqs. (4.18) and (4.19) is carried out numerically.

Now, we analyze the behavior of teleportation fidelity associated with entangled resources swapped with Gaussian **TB** resources. In Fig. 4.2, we plot the optimized fidelities $\mathcal{F}_{\mathbf{SB}^{sw}\mathbf{TB}}^{(opt)}$, $\mathcal{F}_{\mathbf{PS}^{sw}\mathbf{TB}}^{(opt)}$, and $\mathcal{F}_{\mathbf{SB}^{sw}\mathbf{TB}}^{(opt)}$ as functions of r_{12} , at a fixed value of r_{34}; we also report for comparison the corresponding fidelities $\mathcal{F}_{\mathbf{SB}}^{(opt)}$, $\mathcal{F}_{\mathbf{PS}}^{(opt)}$, and $\mathcal{F}_{\mathbf{SB}}^{(opt)}$ associated with the same non-swapped resources.

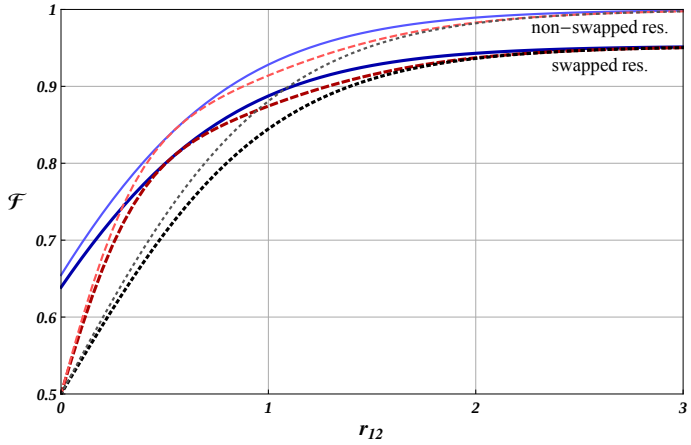

Figure 4.2: (Color online) Optimized fidelity of teleportation $\mathcal{F}_{X^{sw}TB}^{(opt)}$ with $X = SB$ (full line), $X = PS$ (dashed line), and $X = TB$ (dotted line), as a function of the squeezing parameter r_{12} of the swapped input state, and at fixed $r_{34} = 1.5$ of the swapping TB resource. For comparison, we also report the plots of the teleportation fidelities associated with the corresponding non-swapped resources (same plot style, but with tinier and lighter lines). While the fidelities associated with non-swapped resources saturate to one, the fidelities associated with swapped resources saturate to a lower level, depending on the swapping squeezing parameter r_{34}.

Obviously, for large value of the swapping squeezing parameter r_{34}, the fidelities $\mathcal{F}_{X^{sw}\mathbf{TB}}^{(opt)}$ tend to the ideal fidelities $\mathcal{F}_{X}^{(opt)}$. Indeed, the saturation level,

exhibited for large values of the squeezing of the swapped resource r_{12}, is higher, and tends to the ideal value one, for growing r_{34}.

In order to emphasize the improvement in the teleportation performance when non-Gaussian resources are used, in Ref. [1] it is introduced a suitable relative fidelity defined as:

$$\Delta\mathcal{F}_{\mathbf{SB}}^{(X)} = \frac{\mathcal{F}_{\mathbf{SB}}^{(opt)} - \mathcal{F}_{X}^{(ref)}}{\mathcal{F}_{X}^{(ref)}}\,, \tag{4.20}$$

where $\mathcal{F}_{\mathbf{SB}}^{(opt)}$ is the optimized fidelity of teleportation associated with a **SB** resource, and $\mathcal{F}_{X}^{(ref)}$ is the reference (optimized) fidelity associated to a resource X. In order to quantify the enhancement in the teleportation performance when (swapped) non-Gaussian **SB** resources are used with respect to reference swapped resources, we generalize Eq. (4.20) and define the following relative fidelity:

$$\Delta\mathcal{F}_{\mathbf{SB}^{sw}X}^{(Y^{sw}Z)} = \frac{\mathcal{F}_{\mathbf{SB}^{sw}X}^{(opt)} - \mathcal{F}_{Y^{sw}Z}^{(ref)}}{\mathcal{F}_{Y^{sw}Z}^{(ref)}}\,, \tag{4.21}$$

where $\mathcal{F}_{\mathbf{SB}^{sw}X}^{(opt)}$ is the optimized fidelity of teleportation associated with a **SB** resource swapped with a resource X, and $\mathcal{F}_{Y^{sw}Z}^{(ref)}$ is the reference (optimized) fidelity of teleportation associated with a resource Y swapped with a resource Z. In particular, we analyze the behavior of $\Delta\mathcal{F}_{\mathbf{SB}^{sw}\mathbf{TB}}^{(\mathbf{TB}^{sw}\mathbf{TB})}$ and $\Delta\mathcal{F}_{\mathbf{SB}^{sw}\mathbf{TB}}^{(\mathbf{PS}^{sw}\mathbf{TB})}$. These quantities are plotted in Fig. 4.3 as functions of the squeezing parameter r_{12} of the swapped resource.

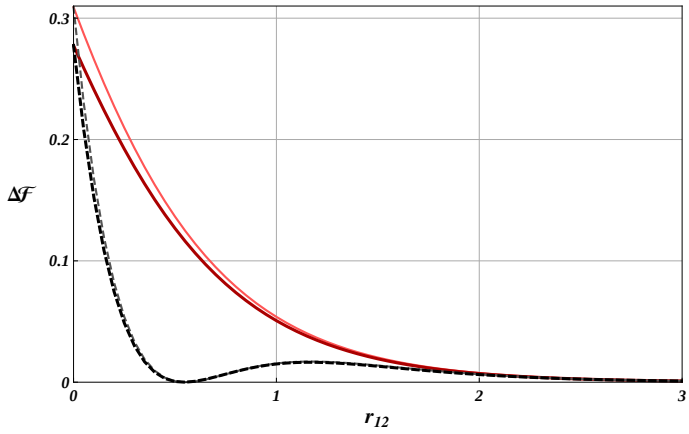

Figure 4.3: (Color online) Relative teleportation fidelities $\Delta\mathcal{F}_{SB^{sw}TB}^{(Y^{sw}TB)}$ with $Y = TB$ (full line) and $Y = PS$ (dashed line), as a function of the squeezing parameter r_{12} of the swapped input state, and at fixed $r_{34} = 1.5$ of the swapping TB resource. For comparison, we also report the relative fidelities $\Delta\mathcal{F}_{SB}^{(X)}$ associated with the corresponding non-swapped resources (same plot style, but with tinier and lighter lines).

It is worth noticing that the percentage improvement corresponding to swapped resources is practically equal to that corresponding to non-swapped resources. A high enhancement is obtained with respect to the Gaussian instance. Moreover, the swapped **SB** resources perform better that the swapped **PS** resources too, especially for low values of r_{12}; however, a significant improvement is also evident for $r_{12} \in [1, 2]$. In Figs. 4.4 and 4.5, there are given the three-dimensional plots of $\Delta\mathcal{F}^{(Y^{sw}\mathbf{TB})}_{\mathbf{SB}^{sw}\mathbf{TB}}$, with $Y = \mathbf{TB}$ and $Y = \mathbf{PS}$ respectively, as functions of r_{12} and r_{34}. $\Delta\mathcal{F}^{(\mathbf{TB}^{sw}\mathbf{TB})}_{\mathbf{SB}^{sw}\mathbf{TB}}$, see Fig. 4.4, is monotone both as a function of r_{12} and as a function of r_{34}. However the performance supremacy of swapped **SB** resources is evident with respect to swapped **TB** resources for low values of r_{12} as $r_{34} \neq 0$.

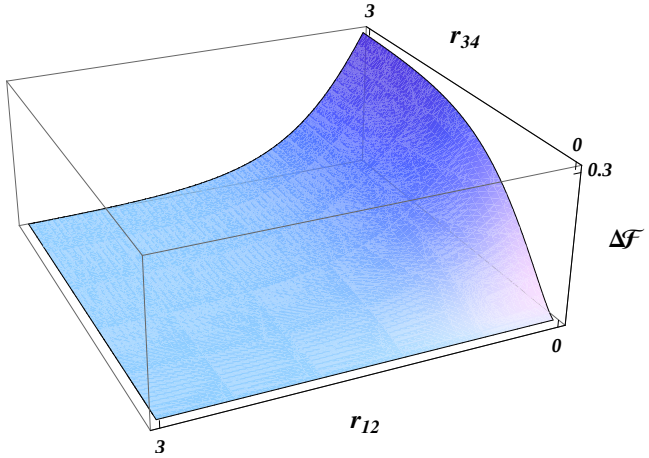

Figure 4.4: (Color online) Three-dimensional relative teleportation fidelity $\Delta\mathcal{F}^{(TB^{sw}TB)}_{SB^{sw}TB}$ as a function of the squeezing parameter r_{12} of the swapped input resource, and of the squeezing parameter r_{34} of the swapping TB resource. $\Delta\mathcal{F}^{(TB^{sw}TB)}_{SB^{sw}TB}$ is monotone in r_{12} and r_{34}.

Looking at Fig. 4.5, *i.e.* $\Delta\mathcal{F}^{(\mathbf{PS}^{sw}\mathbf{TB})}_{\mathbf{SB}^{sw}\mathbf{TB}}$, we see that the swapped **SB** resources perform better than the swapped **PS** resources for low values of r_{12}; then the improvement, *i.e.* the relative fidelity, vanishes (as the resources coincide) for a specific value of r_{12}, depending on r_{34}; at last, for growing r_{12}, $\Delta\mathcal{F}^{(\mathbf{PS}^{sw}\mathbf{TB})}_{\mathbf{SB}^{sw}\mathbf{TB}}$ exhibits a revival till it goes to zero for large r_{12}.

Let us now assume that also the swapping resource can be a non-Gaussian resource as well. Then, we consider the optimized fidelities $\mathcal{F}^{(opt)}_{X^{sw}X}$ with $X = \mathbf{SB}, \mathbf{PS}, \mathbf{TB}$. Although we have computed the analytical expression for $\mathcal{F}_{X^{sw}X}$, the optimization of these fidelities is carried out numerically. In Fig. 4.6, $\mathcal{F}^{(opt)}_{X^{sw}X}$ is plotted as a function of r_{12}, for a fixed value of r_{34}. As expected, a sensible enhancement of the teleportation fidelity can be observed for the fully non-Gaussian instances with respect to the fully Gaussian instance; such an improvement is more pronounced for the case of swapped **SB** resources. In Fig. 4.7, the relative teleportation fidelities $\Delta\mathcal{F}^{(\mathbf{TB}^{sw}\mathbf{TB})}_{\mathbf{SB}^{sw}\mathbf{SB}}$ and $\Delta\mathcal{F}^{(\mathbf{PS}^{sw}\mathbf{PS})}_{\mathbf{SB}^{sw}\mathbf{SB}}$ are plotted as functions of r_{12}.

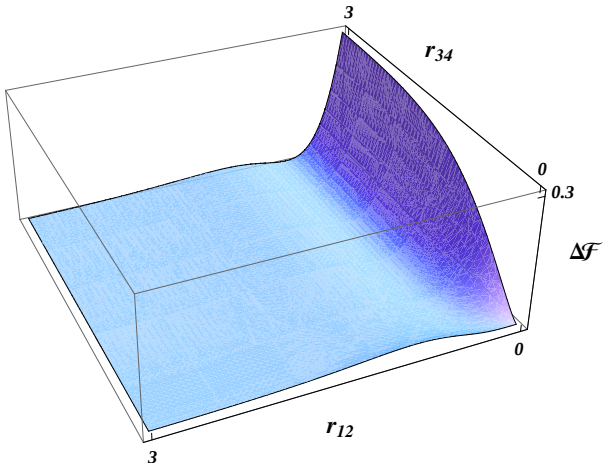

Figure 4.5: (Color online) Three-dimensional relative teleportation fidelity $\Delta\mathcal{F}_{SB^{sw}TB}^{(PS^{sw}TB)}$ as a function of the squeezing parameter r_{12} of the swapped input resource, and of the squeezing parameter r_{34} of the swapping TB resource.

The relative fidelities clearly show a marked enhanced performance of swapped **SB** resources with respect to swapped **PS** and **TB** resources. Remarkably, in the fully non-Gaussian instance, the optimized (swapped) **SB** resources never collapse onto optimized (swapped) **PS** resources; correspondingly, the relative fidelity never vanishes.

4.2.2 Realistic swapping protocol

Let us now investigate the behavior of the swapped resources in the instance of realistic swapping protocol. As previously discussed, we assume to know the values of the parameters associated with imperfections and decoherence effects. From an operational point of view, the knowledge of these parameters is equivalent to assume a control on the characteristics of the experimental apparatus, including the inefficiency of the photo-detectors and the length and damping rate of the noisy channels. Fixed the parameters associated with the experimental apparatus, the optimization of the fidelities is carried out numerically. In Fig. 4.8, we plot the optimized fidelities $\mathcal{F}_{X^{sw}Y}^{(opt)}$ for several choices of the swapped resource X and of the swapping resource Y. We observe that the (swapped) **SB** resources perform better than the (swapped) **PS** and **TB** resources, even when they are swapped with **TB** resources. Indeed, $\mathcal{F}_{\mathbf{SB}^{sw}\mathbf{SB}}$ shows the best performance for any value of r_{12} (at fixed r_{34}). Furthermore, also $\mathcal{F}_{\mathbf{SB}^{sw}\mathbf{TB}}$ maintains above $\mathcal{F}_{\mathbf{PS}^{sw}\mathbf{PS}}$, $\mathcal{F}_{\mathbf{PS}^{sw}\mathbf{TB}}$, and $\mathcal{F}_{\mathbf{TB}^{sw}\mathbf{TB}}$ for any r_{12}. Let us notice that the **PS** resources perform better than the **TB** resources for low values of r_{12}, and as the squeezing parameter grows, both the fidelities $\mathcal{F}_{\mathbf{PS}^{sw}\mathbf{PS}}$ and $\mathcal{F}_{\mathbf{PS}^{sw}\mathbf{TB}}$ decrease going even below the fully Gaussian instance $\mathcal{F}_{\mathbf{TB}^{sw}\mathbf{TB}}$. In order to emphasize the percentage improvement obtained in

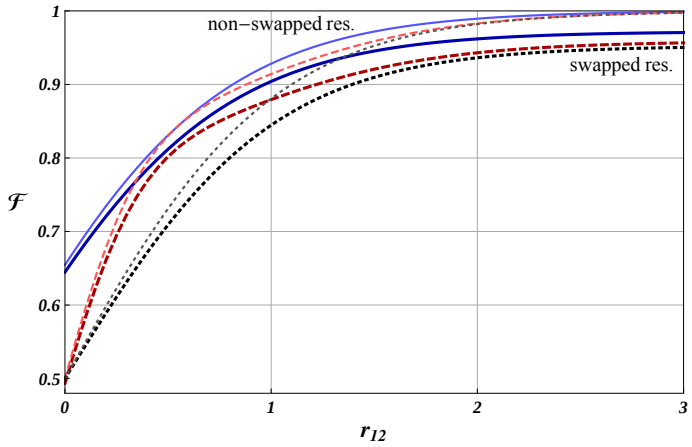

Figure 4.6: (Color online) Optimized fidelity of teleportation $\mathcal{F}^{(opt)}_{X^{sw}X}$ with $X = SB$ (full line) $X = PS$ (dashed line) and $X = TB$ (dotted line), as a function of the squeezing parameter r_{12} of the swapped input state, and at fixed $r_{34} = 1.5$ of the swapping resource. For comparison, we also report the plots of the teleportation fidelities associated with the corresponding non-swapped resources (same plot style, but with tinier and lighter lines). The swapped SB resources show a sensibly higher saturation level with respect to the swapped PS and TB resources.

the instance of **SB** input states and/or resources, in Fig. 4.9, we plot the relative fidelity $\Delta\mathcal{F}^{(Y^{sw}Z)}_{\mathbf{SB}^{sw}X}$ for several choices of the swapping and swapped resources.

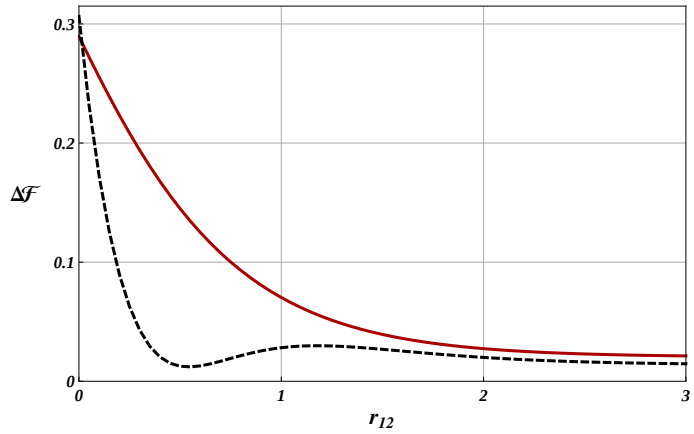

Figure 4.7: (Color online) Relative teleportation fidelities $\Delta\mathcal{F}_{SB^{sw}SB}^{(X^{sw}X)}$ with $X = TB$ (full line) and $X = PS$ (dashed line), as a function of the squeezing parameter r_{12} of the swapped input state, and at fixed $r_{34} = 1.5$ of the swapping resource. $\Delta\mathcal{F}_{SB^{sw}SB}^{(PS^{sw}PS)}$ never vanishes for any r_{12}.

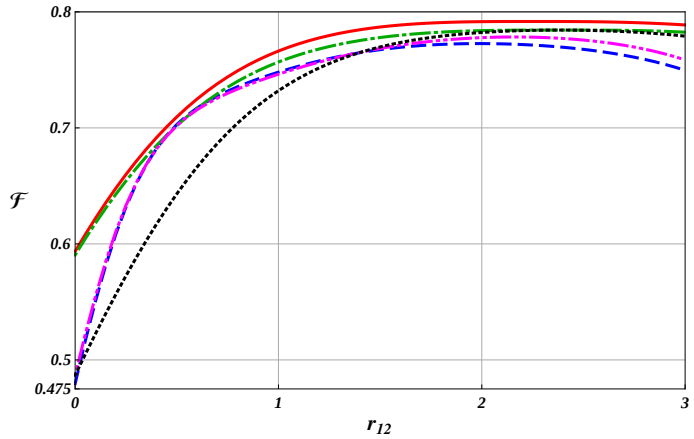

Figure 4.8: (Color online) Optimized fidelity of teleportation $\mathcal{F}_{X^{sw}Y}^{(opt)}$ with $X = Y = SB$ (full line), $X = Y = PS$ (dashed line), $X = SB$, $Y = TB$ (dot dashed line), $X = PS$, $Y = TB$ (double-dot dashed line), and $X = Y = TB$ (dotted line), as a function of the squeezing parameter r_{12} of the swapped input state, and at fixed $r_{34} = 1.5$ of the swapping resource. The parameters of the experimental apparatus are fixed as: $\tau_1 = 0.1$, $n_{th,1} = 0$, $\tau_4 = 0.2$, $n_{th,4} = 0$, $R_2 = \sqrt{0.05}$, $R_3 = \sqrt{0.05}$. The swapped SB resources show a sensibly higher saturation level with respect to the swapped PS and TB resources.

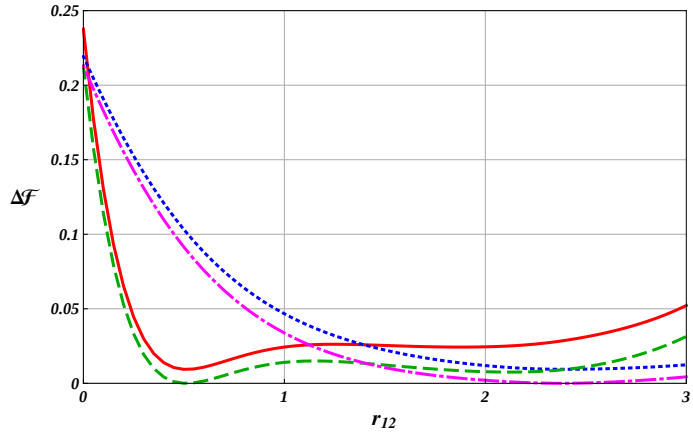

Figure 4.9: (Color online) Relative teleportation fidelities $\Delta\mathcal{F}_{SB^{sw}X}^{(Y^{sw}Z)}$ with $X = SB$, $Y = Z = PS$ (full line), $X = SB$, $Y = Z = TB$ (dotted line), $X = Z = TB$, $Y = PS$ (dashed line), $X = Y = Z = TB$ (dot-dashed line), as a function of the squeezing parameter r_{12} of the swapped input state, and at fixed $r_{34} = 1.5$ of the swapping resource. The parameters of the experimental apparatus are fixed as in Fig. 4.8.

CHAPTER 5

TUNABLE NON-GAUSSIAN RESOURCES BY ANCILLARY SQUEEZING AND CONDITIONING.

Based on the encouraging theoretical results shown in the previous chapter, the ultimate goal would be thus to build an experimental set up that is able to generate the new quantum states that contain the **SB** states (seen in the sub-Sect. 1.5.1 and 1.3.2), with enhanced performance with respect to, e. g., the (experimentically generated) photon-subtracted state [26, 71]. However, before proceeding to do that, some preliminary steps are required. First of all, one must be able to introduce a basic scheme of generation, taking into account further imperfections introduced by a real generation with respect to the pure theoretical instance. Then, one must check if, despite these imperfections, the performance of the generated state gives an appreciable advancement that justifies the experimental effort. After this preliminary analysis, one must design more in details the experimental device, and then one must provide a method to reconstruct the states (being the generated states non Gaussian, this last step is not trivial). Only once these steps have been performed one can possibly proceed to organize an experiment.

Then, we introduce the basic scheme of generation and perform the preliminary analysis, while in a subsequent article we will face with the design of the experimental device, and the method of reconstruction of the states. Therefore, here we introduce an experimental scheme to generate a new class of non-Gaussian states. This class approximates, in realistic conditions, the class of the (theoretically defined) **SB** states. The scheme shows a versatile character, in the sense that a variation of the free experimental parameters allows the generation of known non-Gaussian states, as Photon-Added (**PA**) squeezed states, Photon-Subtracted (**PS**) squeezed states, squeezed photon-number states (**PN**) (and, obviously, also Gaussian Twin Beams (**TB**)). Furthermore, the free experimental parameters can be exploited to optimize, in different situations, the performance in the realization of quantum protocols.

The usefulness of a state is estimated by investigating its performance as a resource for the quantum teleportation of a coherent state [27, 26] (see Sect. 2.2). Based on this criterion, we show that the optimized state generated by our realistic scheme provides, in a significant range of the parameters, a better performance than the other realistically generated states, including the **PS** state.

The Chapter is organized as follows. In Section 5.1 we introduce, in two steps, the basic generation scheme of the new class of entangled states: at first we consider a very ideal case of generation in order to emphasize the connection with

State	Definition
PS squeezed state	$N_{PS}\ a_1 a_2 S_{12}(\zeta)\|0,0>_{12}$
PA squeezed state	$N_{PA}\ a_1^\dagger a_2^\dagger S_{12}(\zeta)\|0,0>_{12}$
Squeezed number states	$S_{12}(\zeta)\|1,1>_{12}$
Twin Beam	$S_{12}(\zeta)\|0,0>_{12}$

Table 5.1: Theoretical (operatorial) definition of particular states included in the SB class.

the theoretical **SB** states, and then we discuss the realistic instance. In Section 5.2 we investigate the usefulness of the states introduced in Section 5.1 by checking their performance as resources of the teleportation protocol, both in ideal and in realistic generation.

5.1 Generation schemes and corresponding states

The (normalized) form of the **SB** states which have been Sect. 1.3.2 is

$$|\Psi>_{\mathbf{SB}} \equiv S_{12}(-r)\left\{\cos\delta|0,0>_{12}+\sin\delta|1,1>_{12}\right\}, \tag{5.1}$$

where $|0,0>_{12}$ and $|1,1>_{12}$ denote the tensor products of the two vacua and of the two one-photon states, respectively, associated to the modes $1,2$, $S_{12}(-r)$ is the two-mode squeezing operator, and δ is a free parameter allowing optimization (a more general form of the **SB** states could include a relative phase between the two terms inside the braces, but this inclusion results to be not stricly necessary). At some suitably chosen values of the parameter δ, the **SB** superposition coincides with **PA** states, with **PS** states, with **PN** states, and with **TB** [1], where addition/subtraction, as well the number state, are referred to the case of 1 photon. In TABLE 5.1, we present anew a listeof the theoretical definitions of all these states.

In this Section we introduce a scheme to generate a general class of non-classical, two-mode states of the electromagnetic field which provides the best approximation to the shape and/or to the performance of the theoretically defined **SB** states. The whole class can be experimentally obtained manipulating, by linear optical components and conditional measurements, two independent (two–mode) squeezed states. The basic generation scheme is illustrated in Fig. 5.1.

In this scheme we start by two independently generated Gaussian twin beams, $|\zeta>_{12}= S_{12}(\zeta)|0,0>_{12}$ and $|\xi>_{34}= S_{34}(\xi)|0,0>_{34}$, i. e. by the initial proto-state

$$|\zeta>_{12}|\xi>_{34}= S_{12}(\zeta)S_{34}(\xi)|\mathbf{0}>_{1234}, \tag{5.2}$$

where $|\mathbf{0}>_{1\ldots n}= \bigotimes_{k=1}^{n}|0>_k$ is the tensor product of n vacuum states. The twin beams feed the input ports of two beam splitters of transmissivity T_1 and T_2,

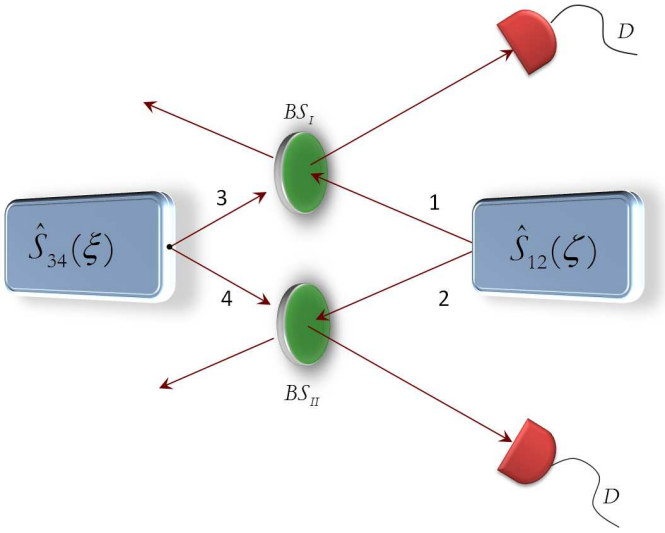

Figure 5.1: Sketch of the ideal scheme for generating the class of states of Eq. (5.4): two independently generated two-mode squeezed vacuum states, $|\zeta\rangle_{12}$ and $|\xi\rangle_{34}$, mix onto two beam splitters BS_I and BS_{II} of transmissivity T_1 and T_2, respectively. State generation is triggered by two simultaneous detections realized by the single photon projective detectors (D_3 and D_4).

respectively. Specifically, modes $1, 3$ mix themselves at the beam splitter (BS_I), and modes $2, 4$ at the beam splitter (BS_{II}). The resulting state is the four-mode entangled state $|\Phi>_{1234}$ described by:

$$\begin{aligned} |\Phi>_{1234} &= U_{13}(\kappa_1)U_{24}(\kappa_2)|\zeta>_{12}|\xi>_{34} \\ &= U_{13}(\kappa_1)U_{24}(\kappa_2)S_{12}(\zeta)S_{34}(\xi)|\mathbf{0}>_{1234}. \end{aligned} \tag{5.3}$$

Here the squeezing operators, with complex squeezing parameters $\zeta = r\exp\{i\,\phi_\zeta\}$ $(i = 1,\ j = 2)$ and $\xi = s\exp\{i\,\phi_\xi\}$ $(i = 3,\ j = 4)$, respectively, are given by $S_{ij}(\mu) = \exp\left\{-\mu\hat{a}_i^\dagger\hat{a}_j^\dagger + \mu^*\hat{a}_i\hat{a}_j\right\}$ $(\mu = \zeta,\ \xi)$. Furthermore, the beam-splitter operators are given by $U_{lk}(\kappa_l) = \exp\left\{\kappa_l\left(a_l^\dagger a_k - a_l a_k^\dagger\right)\right\}$, $l = 1, 2$, $k = 3, 4$, where $\tan\kappa_l = \sqrt{(1-T_l)/T_l}$.

The basic idea is that, starting by the four-mode state $|\Phi>_{1234}$, the conditional measurements provided by the simultaneous "cliks" of detectors D_3, D_4, and the restriction to suitable ranges of the beam-splitters parameters and of the squeezing parameters, will lead to the generation of two-mode states which well approximate the theoretical **SB** states. Obviously, the experimental generation implies non ideal conditions, including inefficiency of detection, and losses. However, here we will proceed by steps. At first, we consider the ideal situation, i. e. *single-photon conditional measurements* without inefficiency and losses. This allows, to the benefit of the reader, to describe the basic elements of the scheme, and

the connection with the theoretical **SB** states. In a second step, we discuss the full realistic instance: we add detection inefficiency and losses, whose values are choosen as those at present experimentally accessible.

5.1.1 Single-photon conditional measurements

We will discuss this simplified instance a little big more in details, in order to make more clear the connection between the theoretically defined **SB** states and the generated **SB** states obtainable by our scheme (for further details on the postselection procedure in this ideal instance, see Sect. 1.4). At first we suppose that losses are not present, that the detectors are perfectly photon-resolving, and that the apparatus is able to perform simultaneous detections of single photons in modes 3 and 4. Thus, simultaneous detections project the state of Eq. (5.3) onto the *tunable state* (**T**)

$$|\Psi_{\mathbf{T}}>=\mathcal{N}_{34}<1,1|U_{13}(\kappa_1)U_{24}(\kappa_2)S_{12}(\zeta)S_{34}(\xi)|\mathbf{0}>_{1234}, \tag{5.4}$$

with $\mathcal{N}$ a normalization constant.

Varying the free parameters, κ_1, κ_2, r, s, ϕ_ζ, ϕ_ξ we can obtain different Gaussian or degaussified states. On the other hand, being the role of the two beam splitters inside the scheme indistinguishable, transmissivities T_1, T_2, and thus parameters κ_1, κ_2, can be taken equal ($T_1 = T_2 \equiv T$). Indeed, we will see that the simplified instances: $\kappa_1 = \kappa_2 = \kappa \in \mathbf{R}$, and ξ real, are sufficient for our purposes. We fix also $\phi_\zeta = \pi$; thus, $S_{12}(\zeta) \equiv S_{12}(-r)$. Furthermore, we will make the assumption that $\kappa^2 << 1$, and that the value of the strength $|\xi|(\equiv s)$ of the ancillary squeezing S_{34} is at most of the same order of κ^2 (this will be clarified by the procedure below). Therefore, we exploit beam splitters with a high transmissivity $T = \cos^2|k|$, and the ancillary squeezing S_{34} with a weak squeezing strength. As a consequence of such assumptions, the unitary operators $U_{13}(\kappa)$, $U_{24}(\kappa)$ can be expanded in power series and truncated to order κ^2, while $S_{34}(|\xi|)$ can be truncated to order $|\xi|$.

Therefore, we have:

$$\begin{aligned}
&|\Phi\rangle_{1234} \approx \\
&\left[1+\kappa(a_1^\dagger a_3 - a_1 a_3^\dagger) + \frac{\kappa^2(a_1^\dagger a_3 - a_1 a_3^\dagger)^2}{2} + \mathcal{O}(\kappa^3)\right] \times \\
&\left[1+\kappa(a_2^\dagger a_4 - a_2 a_4^\dagger) + \frac{\kappa^2(a_2^\dagger a_4 - a_2 a_4^\dagger)^2}{2} + \mathcal{O}(\kappa^3)\right] \times \\
&\left[1+(-\xi(a_3^\dagger a_4^\dagger - a_3 a_4) + \mathcal{O}(\xi^2))\right] \times \\
&S_{12}(-r)|0,0,0,0\rangle_{1234}.
\end{aligned} \tag{5.5}$$

Next, the postelection strategy is applied. Specifically, by using coincidence photodetection, the conditional measurements of simultaneous detections of single photons in mode 3 and 4 project the non-normalized state Eq. (5.5) onto $_{34} < 1,1|\Phi >_{1234}$, which writes:

$$_{34} < 1,1|\Phi >_{1234} \approx (-\xi + \kappa^2 a_1 a_2) S_{12}(-r)|0,0>_{12} . \tag{5.6}$$

Due to our assumptions on κ^2 and $|\xi|$, in the above equation we have implicitly neglected terms proportional to $|\xi|\kappa^2$, *i.e.* contributions of the form $\xi\kappa^2(a_1^\dagger a_1 + a_2^\dagger a_2) S_{12}(\zeta)|0,0>_{12}$, and of higher degree. Using the two-mode Bogoliubov transformations

$$\begin{aligned} & S_{12}^\dagger(-r)\, a_i\, S_{12}(-r) = \cosh r\, a_i + \sinh r\, a_j^\dagger, \\ & (i \neq j = 1,2)\,, \end{aligned} \tag{5.7}$$

Eq. (5.6) yields the non-normalized state:

$$\begin{aligned} & S_{12}(-r)\, \left\{ (-\xi + \kappa^2 \sinh r \cosh r)|0,0\rangle_{12} \right. \\ & \left. + \kappa^2 \sinh^2 r |1,1>_{12} \right\}\,, \end{aligned} \tag{5.8}$$

whose form, apart from normalization, reduces to that of the **SB** state (5.1). Performing normalization, we obtain:

$$|\psi_T>_{12} = S_{12}(-r)\, \{c_{00}|0,0>_{12} + c_{11}|1,1>_{12}\}\,, \tag{5.9}$$

$$c_{00} = \frac{-\lambda + \sinh r \cosh r}{[(-\lambda + \sinh r \cosh r)^2 + (\sinh^2 r)^2]^{1/2}}, \tag{5.10}$$

$$c_{11} = (1 - c_{00}^2)^{1/2}\,, \tag{5.11}$$

where $\lambda = \xi/\kappa^2$. Obviously, the state can be written in the form (5.1), where it is simple to see that (recall that $|\xi| = s$)

$$\delta = \arctan\left(\frac{\kappa^2 \sinh^2 r}{s + \kappa^2 \sinh r \cosh r} \right)\,. \tag{5.12}$$

Note that, being the expression (5.9) of the state generated by the scheme of Fig. 5.1 practically identical to that of the theoretical state (5.1), the particular cases of the **PA**, **PS**, **PN** and **TB** states generated in this ideal instance can be obtained by choosing the experimental parameters in such a way that δ (Eq. (5.12)) is led to assume, from time to time, the corresponding special values described in [1].

The ideal instance here discussed allows to well understand the general idea, showing that the basic scheme can generate states close to theoretical **SB** states. On the other hand, the constraint that the shape of the generated states must be just that of the **SB** states is not strictly necessary for our aims, the previous

procedure being only addressed to emphasize the connection with the theoretical **SB** states. In fact, we aim simply to generate states which perform better than **TB** and generated **PS** squeezed states. If our scheme, in some conditions, generates a state that is not of the **SB** form (5.1), but that satisfies this last requirement, it is not a problem. Therefore, in the analysis of Section III, while retaining the condition $\kappa^2 << 1$, we will allow instead the parameter s to assume any value.

We now move to discuss the inclusion of unavoidable experimental imperfections to gain insight on a realistic realization of our scheme.

5.1.2 Realistic State

In realistic experimental conditions the state $|\Psi_T>$ takes trace of decoherence mechanisms which affect the squeezing sources: cavity output coupling and propagation losses [72, 73].

In this context, the four-mode squeezed vacuum proto–state $|\zeta>_{12}|\xi>_{34}$ becomes the four-mode squeezed thermal state described by the input density matrix

$$\rho_{1234} = S_{12}(\zeta)\, S_{34}(\xi)\, \rho^{th}_{1234} S^{\dagger}_{12}(\zeta)\, S^{\dagger}_{34}(\xi)\,, \tag{5.13}$$

where $\rho^{th}_{1234} = \bigotimes_{k=1}^{4} \rho^{th}_{k}$, with ρ^{th}_{k} the density matrix of the thermal state associated to the k–mode. On the other hand, at typical temperatures (300 K) the thermal density matrix ρ^{th}_{1234} tends to the vacuum state, so that ρ_{1234} coincides practically with the projection operator associated to the previous pure state $|\Phi>_{1234}$ (see Sect. 1.3.1.2, at the end of the characteristic function formalism).

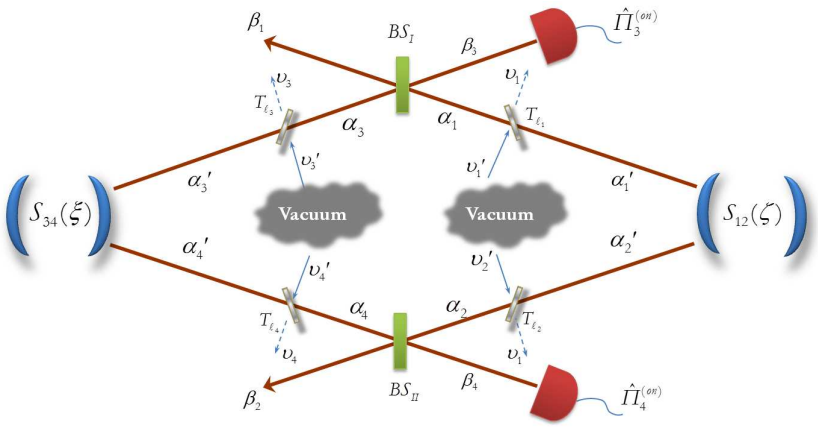

Figure 5.2: Realistic scheme: two independently generated two-mode squeezed vacuum states, $|\zeta\rangle_{12}$ and $|\xi\rangle_{34}$, mix into two beam splitters BS_I and BS_{II} of transmissivity T_1 and T_2, respectively. Four fictitious beam splitters with transmissivity T_ℓ, mimic decoherence mechanisms. In a realistic scenario single photon projective measurements are replaced by POVMs ($\Pi_3^{(on)}$ and $\Pi_4^{(on)}$) with quantum efficiencies $\eta < 1$.

A possible realistic scheme is sketched in Fig. 5.2. We model the decoherence mechanisms by introducing four fictitious beam-splitters (each one for every starting mode) with equal transmissivity $T_\ell\,(=1-R_\ell)$. Each beam-splitter has the empty port illuminated by a vacuum mode υ_k. As already mentioned, at room temperature the thermal contribution to the decoherence is negligible, and thus we must simply replace the state $|\Phi>_{1234}$ of Eq. (5.3) with the state

$$|\Phi'>_{1234}=\bigotimes_{k=1}^{4}\widehat{U}_k\left(T_\ell\right)|\Phi>_{1234}, \tag{5.14}$$

where the beam splitter operator that mixes mode $\hat{a}_k$ with the respective vacuum $\hat{v}_k$ is given by $U_k\left(T_\ell\right)=\exp\left\{\kappa_\ell\hat{a}_k^\dagger\hat{v}_k-\kappa_\ell^*\hat{a}_k\hat{v}_k^\dagger\right\}$, and κ_ℓ is such that $\tan\kappa_\ell=\sqrt{\left(1-T_\ell\right)/T_\ell}$. Now we proceed with the postselection procedure (also in this case, see Sect. 1.4 for further details).

The detection associated to mode $k=3,4$, is now modeled by the POVM $\Pi_k^{(on)}(\eta_k)$, taking account simply of the threshold detection of $n\geq 1$ photons, and given by

$$\Pi_k^{(on)}(\eta_k)=\mathbb{I}_k-\Pi_k^{(off)}(\eta_k), \tag{5.15}$$

where

$$\Pi_k^{(off)}(\eta_k)=\sum_{m=0}^{\infty}\left(1-\eta_k\right)^m|m>_k\,{}_k<m|, \tag{5.16}$$

and η_k is the $k-$mode non-unit detection efficiency. So that the relative density matrix becomes

$$\rho_{\mathbf{T}}^{(on)}\left(T_\ell,\eta_3,\eta_4\right)=\frac{\mathrm{Tr}_{34}\left[\rho'_{1234}\otimes\Pi_3^{(on)}(\eta_k)\otimes\Pi_4^{(on)}(\eta_k)\right]}{\mathcal{N}_{\mathbf{T}}^{(on)}\left(\eta_3,\eta_4\right)}, \tag{5.17}$$

where ρ'_{1234} is the density matrix relative to the state $|\Phi'>_{1234}$, and the normalization constant

$$\mathcal{N}_{\mathbf{T}}^{(on)}\left(\eta_3,\eta_4\right)=\mathrm{Tr}_{1234}\left[\rho_{1234}\otimes\Pi_3^{(on)}(\eta_k)\otimes\Pi_4^{(on)}(\eta_k)\right], \tag{5.18}$$

depending on η_3,η_4, represents the success rate in a real scenario [74]. Applying this scheme, we can obtain approximately **SB** states, **PS** and **TB** states under a realistic situation of presence of losses $(T_\ell<1)$ and of not perfect quantum efficiencies $(\eta_3,\eta_4<1)$, simply by inserting the values of the ancillary parameters which provide these states in the theoretical instance [1]:

$$\begin{aligned}
\rho_{\mathbf{PS}}^{(on)}\left(T_\ell,\eta_3,\eta_4\right) &= \rho_{\mathbf{T}}^{(on)}\left(T_\ell,\eta_3,\eta_4\right)\Big|_{s=0,\kappa\simeq 0},\\
\rho_{\mathbf{SB}}^{(on)}\left(T_\ell,\eta_3,\eta_4\right) &= \rho_{\mathbf{T}}^{(on)}\left(T_\ell,\eta_3,\eta_4\right)\Big|_{s\simeq\kappa^2\ll 1,\phi=\pi},\\
\rho_{\mathbf{TB}}^{(on)}\left(T_\ell,\eta_3,\eta_4\right) &= \rho_{\mathbf{T}}^{(on)}\left(T_\ell,\eta_3,\eta_4\right)\Big|_{\xi=\zeta\equiv\varepsilon}.
\end{aligned}$$

In addition, it is to be considered a further practical restriction: due to decoherence, the effective value of the squeezing parameters is reduced. In fact, in Sect.1.5.2.1 , we show that the real squeezing parameter r' is related to the free-losses parameter r according to

$$r' = -\frac{1}{2}\ln\left[1 - T_\ell\left(1 - e^{-2r}\right)\right]. \tag{5.19}$$

So, *e.g.*, if in the block scheme (Fig. 5.1) the squeezing is fixed at $r = 2$ ($\simeq 17.4$ dB), the realistic scheme, affected by 15% losses ($T_\ell = 0.85$), corresponds to a beam with r' of about 0.90 ($\simeq 7.81$ dB).

Once established the generation scheme, and the form of the generated states, the criterion we will assume in the next Section to test their usefulness will be their efficiency (measured by fidelity) in implement quantum protocols as quantum teleportation. However, we will compare only fidelities associated to optimized **SB** states, **PS** states and **TB**. In fact, the performance of the **PA** states and, more, of the **PN** states when used as resources in quantum teleportation protocols is even worst than that of the Gaussian **TB**: the deep reason is that these states do not satisfy the crucial requirement of Gaussian affinity [1].

5.2 Generated states as resources

Preliminaries – In this Section we seek to optimize the fidelity of the BKV teleportation protocol for a coherent state [27, 26] using, as the bi–partite entangled resource, the states generated by the proposed scheme. To this end, it is convenient to express the above depicted class of states in the formalism of the characteristic function ([75]), particularly suited for analyzing non-Gaussian states, because it simplifies the computational strategies, in particular if the non Gaussian state is used as a resource for the BKV teleportation protocol [1].

In Sect 1.4 we have shown the relationship between the characteristic function of the output state and the the conditional measurement type performed on the initial state. Here, we are interested to specialize the results of Sect. 1.4 to the case of conditional measures performed on the 2-modes of the initial 4-modes state. Furthermore, conditional measures are of the same type: single-photon projector or on / off POVM. Then, given a four–mode state represented by the characteristic function $\boldsymbol{\chi}_{1234}(\boldsymbol{\beta}_1;\boldsymbol{\beta}_2;\boldsymbol{\beta}_3;\boldsymbol{\beta}_4)$, the state achieved after conditional measurements on the two ancillaries modes (3 and 4) (depicted by detectors D in Fig.5.1) is given by the characteristic function $\boldsymbol{\chi}_{\mathbf{T}}^{(D)}(\boldsymbol{\beta}_1;\boldsymbol{\beta}_2)$,

$$\begin{aligned}
&\boldsymbol{\chi}_{\mathbf{T}}^{(D)}(\boldsymbol{\beta}_1;\boldsymbol{\beta}_2) = \frac{1}{\mathcal{N}\pi^2}\times \\
&\int d^2\boldsymbol{\beta}_3 d^2\boldsymbol{\beta}_4 \boldsymbol{\chi}_{1234}(\boldsymbol{\beta}_1;\boldsymbol{\beta}_2;\boldsymbol{\beta}_3;\boldsymbol{\beta}_4) \\
&\times\chi_3^{(D)}(\boldsymbol{\beta}_3)\,\chi_4^{(D)}(\boldsymbol{\beta}_4),
\end{aligned} \tag{5.20}$$

where $\boldsymbol{\beta}_k$ is a vector of the complex coherent amplitude, $d^2\beta_k = d\beta_k d\beta_k^*$, while $\boldsymbol{\chi}_{1234}(\boldsymbol{\beta}_1;\boldsymbol{\beta}_2;\boldsymbol{\beta}_3;\boldsymbol{\beta}_4)$ is the characteristic function of the initial state. It will correspond to $|\Phi>_{1234}$ (see Eq.(5.3)), for the ideal scheme, or to $|\Phi'>_{1234}$ (see Eq. (5.14)), for the realistic scheme. In the above formula, $\chi_k^{(D)}(\boldsymbol{\beta}_k)$ denotes the characteristic function of the conditional measurement realized by detectors D on the modes $k = 3, 4$ (its definition is provided in Sect. 1.4).

We note now that we can consider the following states:

- *Theoretical states* – the ones given by their operatorial definition (see TABLE I) and not always exactly attainable by our scheme. Their performance has been considered in [1, 22] both in absence and with the presence of losses.
- *Generated states: ideal case* – the ones outing our scheme when we assume that losses are absent, detectors are perfectly photon-resolving, and projective measurements are performed.
- *Generated states: realistic case* – the ones outing our scheme when losses are considered, and only on/off measurements are allowed, described by a non–ideal POVM.

In the next Section we will discuss then at first the performance of the generated states in the ideal instance, by making also a comparison with the performance of the theoretically defined states. Later, we discuss the performance of the generated states in realistic conditions. As announced, we measure the performance of a given state by considering the teleportation fidelity. In the formalism of the characteristic function, the teleportation fidelity is given by [75]

$$\mathcal{F} = \frac{1}{\pi}\int d^2\boldsymbol{\lambda}\chi_{in}(\boldsymbol{\lambda})\chi_{out}(-\boldsymbol{\lambda}), \tag{5.21}$$

where $\boldsymbol{\lambda}$ is the vector of the complex coherent amplitude for a generic state, and $d^2\lambda = d\lambda d\lambda^*$. Being the input state a coherent state $|\alpha>$, the characteristic function χ_{in} is

$$\chi_{in}(\boldsymbol{\lambda}) = e^{-\frac{1}{2}|\lambda|^2 + 2i\Im[\lambda\alpha^*]}, \tag{5.22}$$

while for the output state we have [1]

$$\chi_{out}(\boldsymbol{\lambda}) = \chi_{coh}(\boldsymbol{\lambda})\chi_{res}(\boldsymbol{\lambda}^*;\boldsymbol{\lambda}), \tag{5.23}$$

where $\chi_{res}(\boldsymbol{\lambda}^*;\boldsymbol{\lambda})$ denotes the characteristic function of the two-mode entangled state used as resource for the protocol. From time to time, it will be specialized to the characteristic function of each considered state.

However, we have focused our proposal on both an approximation ($\kappa^2 << 1$), and on the possibility of an improvement provided by an optimization procedure. The only unconditioned parameter is the strength r of the squeezing operator

$S_{12}(\xi)$; once fixed r, the fidelity for the state outing our generation scheme will depend on the two squeezing parameters, and on transmissivity: $\mathcal{F}_{\mathbf{T}}(\zeta, \xi, T)$. Thus, the optimization must be performed with respect to the phases (ϕ_ζ, ϕ_ξ) of the two squeezing operators, the transmissivity T (recall that $T_1 = T_2 = T$) and the strength s of $S_{34}(\xi)$. In the following we will show that optimization with respect to phases and transmissivity are compatible with the assumptions exploited in order to generate **SB** states.

In general, at fixed squeezing intensity $|\zeta| = r$ for mode $1, 2$ (see Fig. 5.1), we define the optimal fidelity as

$$\mathcal{F}_{opt}(r) = \max_{\phi_\zeta, \xi, T} \mathcal{F}_{\mathbf{T}}(\zeta, \xi, T) = \mathcal{F}_{\mathbf{T}}(r, \phi_{\zeta,opt}, \xi_{opt}, T_{opt}), \tag{5.24}$$

where $\phi_{\zeta,opt}$, $\xi_{opt} = \xi_{opt}(\zeta)$ and $T_{opt} = T^{(opt)}(\zeta)$ are the parameters of the phase of ζ, of the ancillary squeezing, and of the transmissivity that optimize the fidelity $\mathcal{F}_{\mathbf{T}}(\zeta, \xi, T)$.

Starting from this rather general formula, we have at first solved the optimization problem with respect to the squeezing phases; in fact, the analysis of several cases shows that the optimization procedure always returns $\phi_\zeta = \phi_\xi = \pi$, thus implying that the optimal building bricks for our scheme (see Fig. 5.1) are two independent two–mode squeezed states with $\zeta = -r$, and $\xi = -s$; this agrees, for the first phase, with the position assumed *a priori* when we implemented our scheme in the previous Section. From now on, we modify our notation for the squeezing operators by replacing the dependence of fidelity on ζ, ξ with the dependence only on r, s: $S_{12}(-r), S_{34}(-s)$. The optimization on T must take into account the role that the transmissivity plays in setting the distillation success rate (see Eq. (5.18)). Furthermore, the result of this analysis must be congruent with the assumption $\kappa^2 << 1$ (i. e. *high transmissivity* $T = \cos^2|k|$) that is needed for our generation scheme. We have found that the fidelity is monotonically increasing with T. The optimal value would have thus been obtained for $T \to 1$, a limiting value that, however, will make the success rate to drop to zero. Therefore, we set, in all what follows, $T = 0.99$ (a value experimentally obtainable), and drop the dependence on T. In this way, we satisfy the assumption $\kappa^2 \sim 0.01 << 1$ and, *de facto*, we realize optimization with respect to transmissivity.

Finally, regarding optimization with respect to the ancillary parameter s, as we have announced in the previous Section we allow this parameter to cover a wide range, and we identify, from time to time, the value of s that, at any given r, maximizes the fidelity. We will see that, when the ideal generation is considered, this value corresponds to **SB** states for not too large values of r, while for values of r which exceed a given threshold this is no more true; despite this, the generated states associated to the maxima perform better than **TB** and **PS** states. In the realistic instance, obviously, we do not mind to compare the optimized states with the **SB** states, but focus our attention only on their performance.

5.2.1 Ideal case of the single-photon measurement

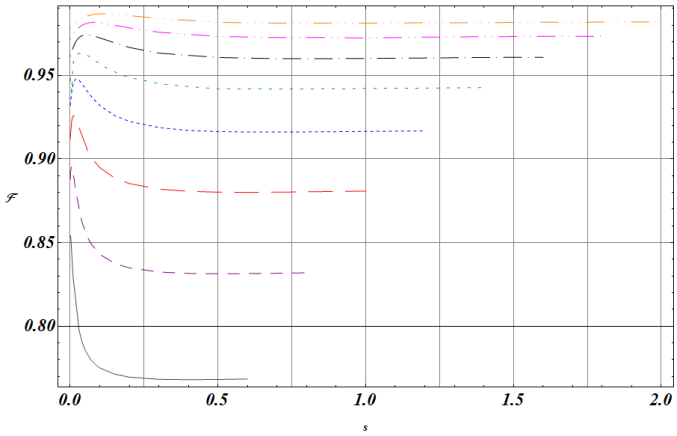

Figure 5.3: (Color on line) Fidelity of teleportation of the state generated from our scheme in the ideal instance (single-photon conditional measurements) plotted vs. s ($\leq r$), the ancillary squeezing parameter, for different values of the main squeezing parameter r: (a) $r = 0.6$ (brown full line); (b) $r = 0.8$ (purple dashed line); (c) $r = 1$ (red large–dashed line); (d) $r = 1.2$ (blue dotted line); (e) $r = 1.4$ (green large–dotted line); (f) $r = 1.6$ (black dotted–dashed line); (g) $r = 1.8$ (magenta double dotted–dashed line); (h) $r = 2$ (orange triple dotted–dashed line). The point at $s = 0$ corresponds to the fidelity relative to the PS squezed state generated in ideal conditions, while at $s = r$ we obtain the fidelity relative to the TB, as well generated in ideal conditions

As a testbench for the proposed scheme, we have considered the teleportation fidelity, Eq.(5.24), for the most ideal case where the detectors D, Fig. 5.1, realize simultaneus projective single photon measurements, and the system is loss free. The resulting state is, then, pure and described by the wave function given in Eq. (5.4).

Fig. 5.3 shows plots for the teleportation fidelity using, as a resource, states that can be generated by the most ideal version of the proposed scheme. In particular, we have plotted the fidelity vs. s ($\leq r$), the squeezing of the ancillary modes $(3, 4)$, for eight different values of r ($= 0.6$, 0.8 , 1, 1.2, 1.4, 1.6, 1.8, and 2). For every curve, the value at $s = 0$ corresponds to the fidelity for the generated **PS** state, while $s = r$ corresponds to the fidelity obtained with **TB**.

It can be seen that for every r there is a maximum in the fidelity that moves toward higher s for increasing r; at the same time the maximum becomes less pronounced. We see that:

- For low main squeezing the optimal resource state is obtained for s close to 0. In particular, for the first lower values $r = 0.6, 0.8, 1$ the generated **SB**

r	s
0.6	0.00057
0.8	0.0046
1.0	0.011
1.2	0.022
1.4	0.036
1.6	0.056
1.8	0.082
2.0	0.12

Table 5.2: Values of s corresponding to the maximum performance of the generated states for the considered values of r.

state, as approximated by our scheme, provides the best performance (the strength s does not exceed the order of magnitude of $\kappa^2 \sim 0.01$, see TABLE II).

- For values of r greater than 1 the generated state corresponding to the maximum deviates increasingly, as r grows, from the **SB** state (the value of s exceeds sensibly the order of magnitude of $\kappa^2 \sim 0.01$, see TABLE II); however, this state still performs better than **TB** and generated **PS** states.

- In this same region **TB** states performs better than generated **PS** (and **SB**) states.

We now compare the optimal fidelity that can be obtained by the class of states we have introduced, i.e. the value for the maximum in Fig. 5.3 (see Eq. (5.24), with that of the *theoretical* states. In Fig. 5.4 we plot the optimal fidelity corresponding to states generated in the ideal case vs. r, and we compare it to the fidelity of the theoretically defined **TB**, **PS**, and **SB** states. In the same figure we also report the fidelity of the **PS** states ($s = 0$) generated in the ideal case.

On one hand, we can see that, in this pretty ideal contest, the best teleportation fidelity, for all the considered range of r, is achieved by the (optimized) theoretical **SB** states as found in Ref. [1]. On the other hand, the optimal fidelity for the class of states we have introduced gets closer to that of the theoretical **SB** states as r increases. It has to be stressed that while the fidelities of the theoretical states and of the generated **PS** state can be analitycally computed as functions of r, the optimal fidelity for the whole class of generated states must be computed numerically point by point, so that the plot of this optimized fidelity, if seen in greater details, looks as a broken–line.

In the plot range $0 < r \lesssim 2$, representing experimentally feasible levels of squeezing, we can distinguish two different regimes:

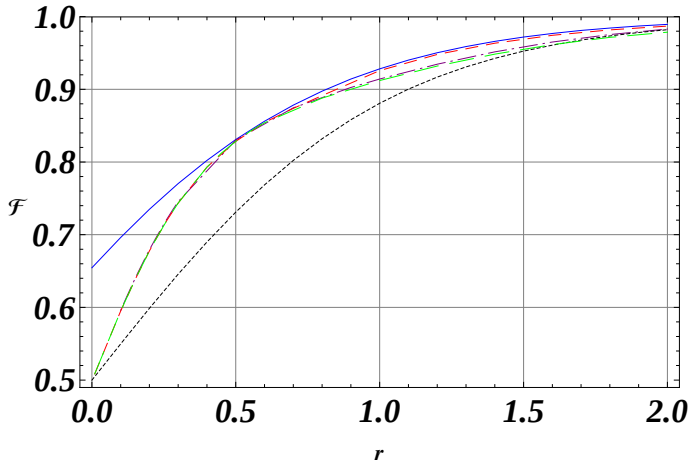

Figure 5.4: (Color online) Comparison between the optimized fidelity on the class of generated states in the ideal instance of generation (red dashed), the fidelity of the PS squeezed state generated in the ideal instance (green large–dashed), the optimized fidelity of the theoretical SB states (cyan continuous), the fidelity of the theoretical PS squeezed states (purple dotted–dashed), and the fidelity of the theoretical TB (black dotted).

a) $r \lesssim 0.5$ – the procedure of maximization Eq. (5.24) gives $s \simeq 0$, *i.e.* the best teleportation resource generated by the presented scheme is given by states that well approximate the generated **PS** states. On the other hand, the three curves corresponding to the optimal fidelity on generated states, to the fidelity of generated **PS** states and to to the fidelity of theoretical **PS** states, respectively, are superimposed and lye in between the fidelity of the optimized theoretical **SB** state (above) and the fidelity of **TB** (below).

b) $r > 0.5$ – the performance of the optimized resource generated by the scheme overcomes both that of the genrated **PS** state and that of the theoretical **PS** state, while offering a performance very close to that of the optimized theoretical **SB** state. In Fig. 5.5 we report the behaviours in the range $1 \leq r \leq 2$.

As an example, if we fix $r = 1.6$, we obtain the value 0.974 (at $s = 0.056$) for the optimized fidelity of the generated states. While, for the same r, the fidelities, given by theoretical resources, are 0.977 (optimized theoretical **SB** state), 0.965 (theoretical **PS** state), and 0.961 (**TB**). Therefore, in the ideal generation the performance of the generated states is very close to that of the theoretical ones.

5.2.2 Realistic lossy scenario

As pointed out previously, a realistic scenario for the generation of these class of states can be modeled by accounting for an inefficient photon detection and a lossy environment for the starting pair of two–mode squeezed states. In what

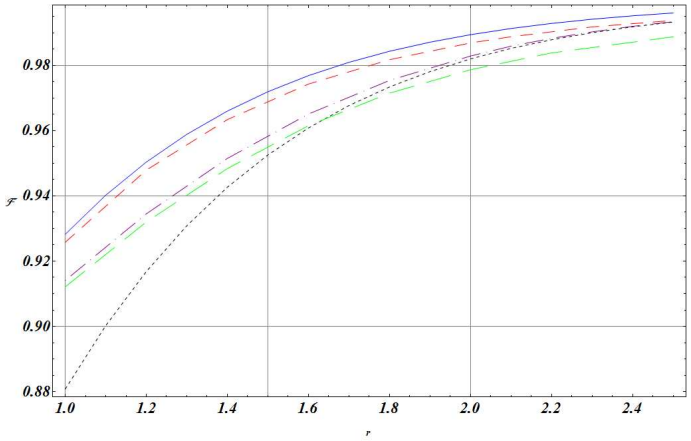

Figure 5.5: (Color online) Details of Fig. 5.4 in the range $1 \leq r \leq 2$ for: the optimized fidelity on the class of generated states in the ideal instance of generation (red dashed), the fidelity of the PS squeezed state generated in the ideal instance (green large–dashed), the optimized fidelity of the theoretical SB states (cyan continuous) the fidelity of the theoretical PS squeezed states (purple dotted–dashed), and the fidelity of the theoretical TB (black dotted).

follows we have considered the value $\eta = 0.15$ for the detection efficiency (that is the value at present obtainable in real experiments) .

In Fig. 5.6 we have plotted the optimized teleportation fidelity of the generated states, (that depends on the squeezing strengths r, s) assuming at first an overall level of (fictitious) transmissivity $T_\ell = 0.85$ (i. e. a level of loss equal to 0.15) in Eq. (5.14). In the figure we have plotted the optimized fidelity as a function of the squeezing parameter s ($\leq r$), for r assuming the same values of Fig. 5.3. We can observe that:

a) the behavior of the fidelities does not change very much apart from a smoothing of the curves around their maximum;

b) as expected, the fidelities further deteriorate due to the combined effect of non–ideal single photon detection processes and losses.

In this first plot the level of losses equal to 0.15 has been taken as a reference, being at present this level experimentally accessible by properly choosing optical components for the squeezing source. On the other hand, very recently an outstanding source with an overall loss of less than 0.08 has been reported [76]. In view of this result, we are led to investigate the behavior of the fidelities when the level of losses is varied. Therefore, we fix again the detection efficiency to be $\eta = 0.15$, we select for the squeezing parameter r the value $r = 1.6$, and we report, in Fig. 5.7, the optimized fidelity on the generated states as a function of the loss parameter (denoted by ℓ). The plot is compared with the curves relative to the fidelity associated to the generated **PS** state and to the fidelity associated

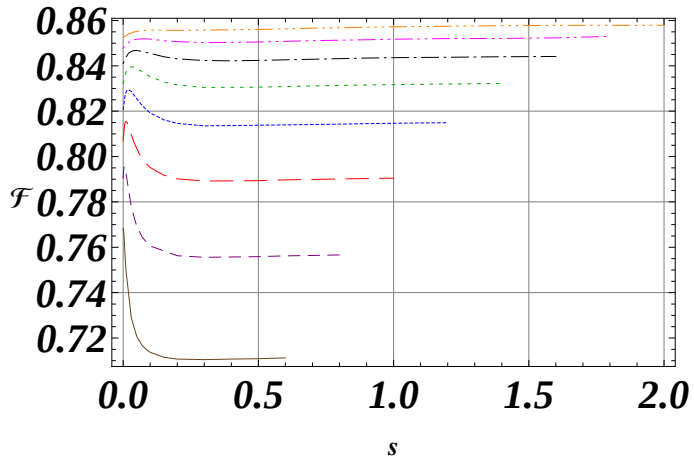

Figure 5.6: (Color online) Fidelity of teleportation of the generated state in a realistic lossy scenario (level of losses equal to 0.15, i. e. $T_\ell = 0.85$, and $\eta = 0.15$). The fidelity depends on the squeezing parameters s, r, and has been plotted vs. s ($\leq r$) for the same values of r used in Fig. 5.3: (a) $r = 0.6$ (brown full line); (b) $r = 0.8$ (purple dashed line); (c) $r = 1$ (red large–dashed line); (d) $r = 1.2$ (blue dotted line); (e) $r = 1.4$ (green large–dotted line); (f) $r = 1.6$ (black dotted–dashed line); (g) $r = 1.8$ (magenta double dotted–dashed line); (h) $r = 2$ (orange triple dotted–dashed line).

to **TB**, where also in these last two cases we have fixed $\eta = 0.15$, $r = 1.6$. As it can be seen, for losses up to $\ell = 0.30$ the optimized state that can be obtained by our scheme can lead to the best fidelity. It has to be noted that, at a fixed r, the value of s corresponding to the maximum does not change very much. In the reported case this value is included in the interval $(0.048, 0.050)$.

Summing up, as remarked in point b) above the values of the fidelities in this realistic instance sensibly deteriorate. On the other hand, for values of r between 1.2 and 1.6 the optimized fidelities takes again appreciable values which looks better than those obtained when generated **PS** states and **TB** are exploited. Furthermore, as we see by the Fig. 5.7, a (foreseeable) improving in the control of losses could improve the performance to levels comparable with those of the theoretical instance.

In conclusion, our preliminary analysis shows that our scheme can generate non Gaussian states which performs better than other generated states, including the **PS** squeezed states. In a forthcoming work we will design in details the experimental set up needed to realize our scheme. To this end, we will consider the two possible instances: continuous wave and pulsed regime. In the same work we will show how we will reconstruct the generated states by performing suitable homodyne detections.

Obviously, at the end of this route we aim to obtain our most ambitious goal,

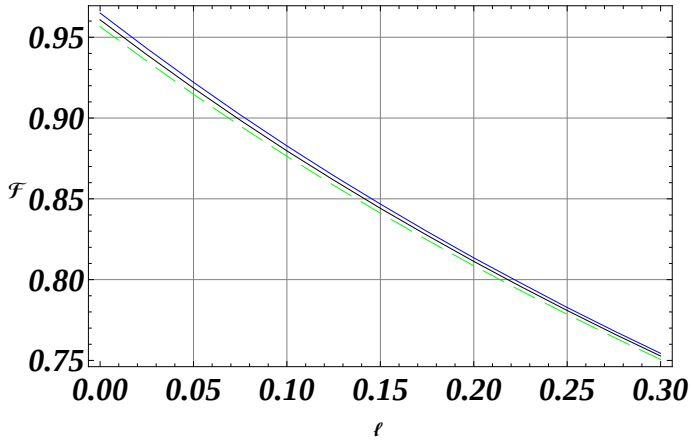

Figure 5.7: (Color online) Optimized fidelity of the states generated in realistic conditions (with $\eta = 0.15$) plotted as a function of the loss parameter ℓ, for $r = 1.6$ (blue full line). The plot is compared with those relative to the fidelity of the PS squezed states ($s = 0$, black full line)) and to the fidelity of the TB ($s = r$, green large–dashed line), both as well generated in realistic conditions with $\eta = 0.15$.

the actual realization of the experimental generation.

CHAPTER 6

EXPERIMENTAL ANALYSIS OF DECOHERENCE OF THE BI-PARTITE GAUSSIAN STATES

The aim of this Chapter is to discuss and experimentally analyse the effects of the transmission, in a lossy channel, over the quantumness of bi-partite Gaussian **CV** optical entangled states [6]. While these effects on **CV** entangled states obtained by above threshold OPOs have been already investigated [77], we focus our analysis on the states generated by a type-II sub–threshold **OPO** [78],[8].

The investigated **CV** entangled state represents one of the possible quantum resources in **CV** teleportation protocols [27]. The experimental data we present extend the analysis of Ref. [79] discussing the behaviour of the **CV** entangled system to the strong decoherence regime (up 99% of loss).

Optical entangled states can be obtained in non–linear processes such as parametric amplifiers that, depending on their operating regime, can prepare either single photon [81] or **CV** Gaussian entangled states [82, 83, 84, 85]. In the latter case the non–linear medium is allocated in a optical cavity and the OPOs, below the oscillation threshold and in a semiclassical approach, are described by bilinear Hamiltonians so realising the paradigm for Gaussian state generation [86]. In particular below threshold a single continuous wave **OPO**, generating squeezing in a fully degenerate operation [87], can give raise to a pair of bright **CV** entangled beams in the non–degenerate case [84, 85, 89, 90, 91]. Both the cases lead to states that represent robust resources for implementing different quantum communication tasks [92].

In this Chapter, we briefly analyze the physics of the source of the Gaussian bi-parite state and the experimental method used for its detection: the homodyne technique. We experimental discuss the behaviour, under strong loss, of a bright bi–partite **CV** Gaussian entangled state outing a sub–threshold type–II **OPO**. In particular, we analyse the trends of different quantumness and entanglement markers in order to discuss the limit at which the examined state can be transmitted before loosing its quantum ability of being employed in quantum communication protocols. More in details, we show: the state purity (seen in Sect. 1.5); three different entanglement criteria (seen in Sect. 2.1.2.4): Peres–Horodechi–Simon, Duan, EPR–Reid; the mutual information (seen in Sect. 2.3), and quantum discord (seen in Sect. 2.3). In addition we relate these criteria to the teleportation fidelity $\mathcal{F}$, i.e. the state ability of overcoming the quantum limit in a teleportation protocol of a coherent state (seen in Sect. 2.2).

6.1 The Experiment

The transmission over a Gaussian channel is described by Eq. (1.46). As already mentioned this evolution is equivalent to a fixed amount of loss introduced by the transmissivity < 1 of a fictitious beam splitter (seen in Sect. 1.5). From the point of view of experimental implementation, instead, the realistic transmission channel can be simulated via a optical variable absorber (attenuator filter).The actual experimental apparatus is made of the **CV** entangled state source, a variable attenuator (mimicking the BS), and a state characterization stage. A block diagram of the experimental setup is presented in Fig. 6.1

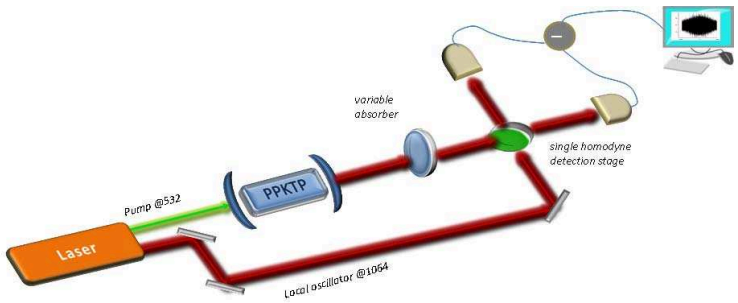

Figure 6.1: *(color online)* Block diagram of the experimental setup. The details on the OPO source are given in Ref. [96], while the characterization stage, based on a single homodyne detector, is fully described in Ref. [99].

The attenuation of a light beam, which passes through a attenuating sample, can be described by the action of the beam splitter matrix, of the type

$$U_{BS} = \begin{pmatrix} t & r \\ -r & t \end{pmatrix}, \tag{6.1}$$

on the input beam. The real coefficients t and r, in Eq. (6.1), represent the Fresnel coefficients of transmission and reflection, respectively. The element t of the matrix U_{BS} can be associated to the transmission coefficient of a attenuator filter. This allows we to describe the filter through the U_{BS} matrix itself. In this sense, it is proposed a description of the filter, that simulates the deteriorating action of decoherence, in terms of BS. We have seen how the covariance matrix $\boldsymbol{\sigma}$, that describes the Gaussian bi-partite state, under the attenuator action of the

environment is transformed as, Eq. (1.48) of Sect.(1.4.4):

$$\begin{aligned}
\boldsymbol{\sigma}_T &= \begin{pmatrix} \mathbf{A}_T & \mathbf{C}_T \\ \mathbf{C}_T^{\intercal} & \mathbf{B}_T \end{pmatrix} && (6.2)\\
&= (1-T)\frac{1}{2}\mathbb{I} + T\boldsymbol{\sigma}_1 && (6.3)\\
&= \begin{pmatrix} \frac{(1-T)}{2}+Tn & 0 & Tc_1 & 0 \\ 0 & \frac{(1-T)}{2}+Tn & 0 & Tc_2 \\ Tc_1 & 0 & \frac{(1-T)}{2}+Tm & 0 \\ 0 & Tc_2 & 0 & \frac{(1-T)}{2}+Tm \end{pmatrix}, && (6.4)
\end{aligned}$$

where $\mathbf{A}_T = diag\,(n_T, n_T)$, $\mathbf{B}_T = diag\,(m_T, m_T)$, $\mathbf{C}_T = diag\,(c_{1,T}, c_{2,T})$, and $T = t^2$.

Consequently the different quantum markers (purity, teleportation fidelity, PHS criterion, Duan criterion, EPR criterion, mutual information and quantum discord) evolve as:

$$\begin{aligned}
\mu_T &= \frac{1}{4\sqrt{\det\left[\boldsymbol{\sigma}_T\right]}}\,,\\
\mathcal{F}_T &= \frac{1}{\sqrt{1+\left(m_T+n_T\right)^2+2\left(c_{2,T}-c_{1,T}\right)\left(1+m_T+n_T\right)+2\left(m_T+n_T-2c_{1,T}c_{2,T}\right)}}\\
w_{PHS,T} &= n_T^2+m_T^2+2\left|c_{1,T}c_{2,T}\right|-4\left(n_Tm_T-c_{1,T}^2\right)\left(n_Tm_T-c_{2,T}^2\right)\\
w_{DUAN,T} &= \sqrt{\left(2n_T-1\right)\left(2m_T-1\right)}-\left(c_{1,T}-c_{2,T}\right)\\
w_{EPR,T} &= n_T^2\left(1-\frac{c_{1,T}^2}{n_Tm_T}\right)\left(1-\frac{c_{2,T}^2}{n_Tm_T}\right)-\frac{1}{4}\\
\mathcal{I}_T &= f\left(n_T\right)+f\left(m_T\right)-f\left(d_{+,T}\right)-f\left(d_{-,T}\right)\\
\mathcal{D}_T &= f(m_T)-f\left(d_{+,T}\right)-f\left(d_{-,T}\right)+f\left(\frac{n_T+2n_Tm_T+2c_1c_2}{1+2m_T}\right) \qquad (6.5)
\end{aligned}$$

where the subscript $_T$ indicates the quantity undergone to a lossy transmission.

We note that the vacuum state obtained for $T = 0$ is a pure one i.e. $\mu_0 = 1$. Moreover, in the ideal case (no loss), the **OPO** would generate a pure state as well. Being $\mu_T < \mu_{0,1}$, for $T \neq 0, 1$, the evolution of μ_T is not monotonic. The purity of the composite system cannot be considered a general entanglement marker [93]. As a matter of fact, any pair of physical systems in a pure state have $\mu = 1$ even if they are disentangled. On the other hand, in our specific case, having a precise hypothesis on the ideal state (a pure twin–beam diagonal state) outing the **OPO** crystal allows us to consider μ as a measure of the total decoherence that has affected the state.

It is easy to see that $\mathcal{F}_T$, $w_{PHS,T}$, and $w_{DUAN,T}$ describe properties very robust under decoherence. Once $\mathcal{F} > 1/2$, $w_{PHS} < 0$ and $w_{DUAN} < 0$ for $T = 1$ they

will keep breaking the respective bounds for every level of loss. Both mutual information and quantum discord show, with respect to loss, the same feature even if decoherence affects their amount. On the contrary a state that show EPR–like correlation ($w_{EPR} < 0$) for $T = 1$ will not keep this property along the propagation so that some particular protocol based on this property cannot be reproduced. Under a total loss greater than 50% any state looses this correlation property.

We see from Eq. (6.4) that the dynamics of the system is described by a single parameter, T. However, it may happen that the damping rates of the two distinguishable beams of a bi-partite system might be much different. For this reason, we want to briefly analyze the case of unbalanced absorption of the modes. In this case, in the Master Equation (1.45),

$$\dot{\rho}_S(t) = \sum_{k=1,2} \frac{\Gamma_k}{2} \mathcal{L}[a_k] \rho_S(0) \ ,$$

we have two different damping rates, Γ_1 and Γ_2, for the modes 1 and 2 corresponding to two different transmission coefficients, T_1 and T_2, respectively. The **CM** (6.2) becomes

$$\boldsymbol{\sigma}_T = \begin{pmatrix} \mathbf{A}_{T_1} & \mathbf{C}_{T_1T_2} \\ \mathbf{C}_{T_1T_2}^{\intercal} & \mathbf{B}_{T_2} \end{pmatrix}. \tag{6.6}$$

The matrices of type (6.4) and (6.6) completely describe the Gaussian bi-partite state (Sect. (1.3.1)) and they can be measured by homodyne detection technique.

6.1.1 Homodyne detection technique

The homodyne technique allows to measure the generalized quadrature $\mathfrak{X}(\theta)$ of the quantum field. In Fig. 6.1 is presented the block diagram. Input 1 impact the beam under analysis, represented by the operator a_1. The second entrance is illuminated by an intense coherent beam $\alpha_{LO} \equiv |\alpha_{LO}| e^{i\theta}$, said local oscillator (LO), with relative phase equal to θ. Outputs 3 and 4 are collected by two detectors that convert the input light intensity in the photocurrents i_3 and i_4, respectively. In a ideal process each incident photon is converted into a photoelectron. In the realistic case, indeed, conversion process occurs with quantum efficiency η non-unitary [94],

$$\eta = \zeta (1 - R_a) \left(1 - e^{-\alpha d}\right),$$

with ζ the fraction of electron-hole pairs which effectively contribute to the photocurrent generated by the photodetection process, R_a is the reflectance of the surface of the photodetector active area, α is the absorption coefficient of the material of which is composed the detector and d is the thickness of the photodetector

active area. From the definition of η it is evident that the quantum efficiency may never exceed unity (corresponding to ideal detectors). For the homodyne technique we use two separate photodetectors with equal quantum efficiencies.

Subsequently, the two photocurrents are subtracted, $i_{34} = i_3 - i_4$. This allows to eliminate the fluctuations correlated. In fact, referring to Appendix, Eq. (9.4), the average number of photons to output 3 is the sum of three terms

$$\begin{aligned} \langle n_3 \rangle &= T \langle n_1 \rangle + (1-T) |\alpha_{LO}|^2 + \sqrt{2T(1-T)} |\alpha_{LO}| \langle \mathfrak{X}(\theta + \pi/2) \rangle \quad (6.7) \\ &\simeq (1-T) |\alpha_{LO}|^2 + \sqrt{2T(1-T)} |\alpha_{LO}| \langle \mathfrak{X}(\theta + \pi/2) \rangle \ , \end{aligned}$$

being the local oscillator much more intense of the mode 1,

$$|\alpha_{LO}|^2 \gg \frac{T}{1-T} \langle n_1 \rangle . \quad (6.8)$$

The first two terms, in Eq.(6.7), depend on the number of photons of the incident light beams on the beam splitter, while the third is a term of interference given by

$$\begin{aligned} 2\sqrt{T(1-T)} \langle I \rangle &= \sqrt{2T(1-T)} |\alpha_{LO}| \left\langle a_1^\dagger e^{i(\theta+\pi/2)} + a_1 e^{-i(\theta+\pi/2)} \right\rangle \\ &= \sqrt{2T(1-T)} |\alpha_{LO}| \langle \mathfrak{X}(\theta + \pi/2) \rangle \ . \end{aligned}$$

Under the approximation Eq. (6.8), we can neglect the variance of the input beam 1, so that the variance of the output signal 3 is linked to the variance of the local oscillator (LO) and of the interference term, being null the covariance between the beam 1 and the LO. We have

$$\left\langle \Delta n_3^2 \right\rangle = (1-T) |\alpha_{LO}|^2 \left[(1-T) + 2T \left\langle \Delta \mathfrak{X}(\theta + \pi/2)^2 \right\rangle \right] \ .$$

In the case of balanced beam splitter ($T = 1/2$), the photocurrent $i_{34} = e\eta (\langle n_3 \rangle - \langle n_4 \rangle)$ and the corresponding variance $\langle \Delta i_{34}^2 \rangle$ are

$$\begin{aligned} i_{34} &= \sqrt{2} e\eta |\alpha_{LO}| \langle \mathfrak{X}(\theta + \pi/2) \rangle , \\ \left\langle \Delta i_{34}^2 \right\rangle &= 2 \left(e\eta |\alpha_{LO}|^2 \right) \left\langle \Delta \mathfrak{X}(\theta + \pi/2)^2 \right\rangle , \end{aligned}$$

where e is the electronic charge. The photocurrent variance is therefore directly linked to the variance of the quadrature, through the intensity of the beam LO. The homodyne detection technique allows, therefore, to measure the quadrature $\langle \mathfrak{X}(\theta + \pi/2) \rangle$ and its variance and to assess whether the signal is squeezed or not [95]. Furthermore, it should be noted that in the expressions of the photocurrent, the amplitude of the beam LO is attenuated by an amount equal quantum efficiency η.

Becouse of the attenuating nature of the quantum efficiency, we can represent a realistic photodiode with quantum efficiency $\eta < 1$, as a ideal photodiode ($\eta = 1$)

preceded by a beam splitter with transmittivity $T = \sqrt{\eta}$. With this assumption, the detected covariance matrix $\boldsymbol{\sigma}_{\eta^2}$ is modified from the covariance matrix of the state $\boldsymbol{\sigma}_1$ before the photodetection. We have

$$\boldsymbol{\sigma}_{\eta^2} = \left(1-\eta^2\right)\frac{1}{2}\mathbb{I} + \eta^2\boldsymbol{\sigma}_1.$$

Combining the attenuating action and the efficiency of the detection system, the evolution of the covariance matrix becomes

$$\begin{aligned}\boldsymbol{\sigma}_{T_{eq}} &= \left(1-\eta^2\right)\frac{1}{2}\mathbb{I} + \eta^2\boldsymbol{\sigma}_T \\ &= \left(1-\eta^2\right)\frac{1}{2}\mathbb{I} + \eta^2\left[(1-T)\frac{1}{2}\mathbb{I} + T\boldsymbol{\sigma}_1\right] \\ &= (1-T_{eq})\frac{1}{2}\mathbb{I} + T_{eq}\boldsymbol{\sigma}_1,\end{aligned}$$

where $T_{eq} = \eta^2 T$.

6.1.2 Non-degenerate optical parametric oscillator (**OPO**)

In this Section, we introduce briefly the optical process of second harmonic which is at the base of each source of squeezed states. A *pump* beam a_p of frequency ω_p is injected into a non-linear cristal. To effect of non-linearity, the input beam produces two beams, *signal* a_s and *idler* a_i, such that $\omega_s + \omega_i = \omega_p$, where $\omega_s(\omega_i)$ is the signal(idler) frequency. The setup used for the experiment is such as, $\omega_s = \omega_i$ and the two generated beams are collinear and distinguishable for the orthogonal polarizations. Generally, the generated fields would be weak without the use of a resonance cavity, which reinforces the two signals. Such a system (non-linear cristal + resonance cavity) takes the name of Optical Parametric Oscillator (**OPO**).

For the sake of simplicity, let us consider a non-linear crystal in the absence of optical cavity and invested by a field a_p with amplitude α_p, frequency ω_p and wavevector $\mathbf{k}_p$. The conservation of energy and momentum ensure that

$$\begin{aligned}\omega_s + \omega_i &= \omega_p, \\ \mathbf{k}_s + \mathbf{k}_i &= \mathbf{k}_p,\end{aligned}$$

where $\mathbf{k}_s(\mathbf{k}_i)$ is the wavevector of the signal(idler) beam. We analyze the case of the non-degenerate **OPO**, in which the two output beams are distinguishable in polarization. The Hamiltonian $\mathfrak{H}$ of the system is

$$\begin{aligned}\mathfrak{H} &= \mathfrak{H}_s + \mathfrak{H}_i + \mathfrak{H}_{NL} &(6.9)\\ &= \hbar\frac{\omega_p}{2}\left(a_s^\dagger a_s + a_i^\dagger a_i\right) - i\hbar\frac{\chi^{(2)}}{2}\alpha_p\left(a_s^\dagger a_i^\dagger + a_s a_i\right), &(6.10)\end{aligned}$$

where $\mathfrak{H}_k$ is the Hamiltonian of the field $k\,(=s,i)$, and α_p is the amplitude of the pump beam. Typically, the pump beam is intense enough to be able to be treated classically. The non-linear Hamiltonian $\mathfrak{H}_{NL}$, proportional to the non-linear susceptibility, generates squezeed states. In fact, the Heisenberg equations of motion for the operators a_s and a_i are

$$\frac{da_s}{dt} = \frac{1}{i\hbar}\left[a_s, \mathfrak{H}\right] = \wp a_i^\dagger, \tag{6.11}$$

$$\frac{da_i}{dt} = \frac{1}{i\hbar}\left[a_i, \mathfrak{H}\right] = \wp a_s^\dagger, \tag{6.12}$$

with $\wp = \chi^{(2)}\alpha_p$. The system of equations (6.11, 6.12) provides the following coupled solutions

$$\begin{aligned} a_s\left(t\right) &= a_s \cosh\left(\wp t\right) + a_i^\dagger \sinh\left(\wp t\right), \\ a_i\left(t\right) &= a_i \cosh\left(\wp t\right) + a_s^\dagger \sinh\left(\wp t\right), \end{aligned}$$

which recall the evolution of the operators under the application of two-mode squeezed operator, Eq.(3.6, 3.7),

$$S_{12}\left(\zeta\right) = \exp\left\{-\zeta a^\dagger b^\dagger + \zeta^* ab\right\},$$

with the substitutions $a \to a_s$, $b \to a_i$, and $\zeta \to i\hbar\chi^{(2)}\alpha_p/2$.

In our detection scheme, we make use of a beam (*local oscillator*) with frequency equal to that of the signal and idler, but with a relative phase θ. Furthermore, one can show that although the modes a and b are not squeezed, a combination of them is squeezed. Introducing, then, the generalized quadrature operator

$$\mathfrak{X}_{c,d}\left(\theta\right) = \frac{1}{\sqrt{2}}\left(\mathfrak{X}_a\left(\theta\right) \pm \mathfrak{X}_b\left(\theta\right)\right),$$

it is possible to show that

$$\left\langle \Delta\mathfrak{X}_{c,d}\left(\theta\right)^2 \right\rangle = \frac{1}{2}\left[\cosh\left(2r\right) \mp \cos\left(2\theta\right)\sinh\left(2r\right)\right],$$

with $r = |\zeta| = \left|i\hbar\chi^{(2)}\alpha_p/2\right|$, so we have

$$\begin{aligned} \left\langle \Delta X_{c,d}^2 \right\rangle &= \frac{1}{2}e^{\pm 2r}, \\ \left\langle \Delta Y_{c,d}^2 \right\rangle &= \frac{1}{2}e^{\mp 2r}. \end{aligned}$$

As a matter of fact, **CV** entangled states produced by type–II **OPO**, show, in view of the symmetry in the interaction Hamiltonian Eq.(6.9, 6.10), $c_1 = -c_2$. This is not true for **CV** entangled states obtained by mixing the outputs of two independent type–I OPOs. In such a case the two fields have disjoint Hamiltonians and the symmetry is broken.

6.1.3 **CV** entangled state source

The state source relies on a CW internally frequency doubled Nd:YAG laser (Innolight Diabolo) whose outputs @532nm and @1064nm are respectively used as the pump for a non degenerate **OPO** and the local oscillator (LO) for the homodyne detector. The **OPO** is set to work below the oscillation threshold and it provides at its output two entangled thermal states (the signal a and the idler b): the aim is indeed to measure the **CM** of these two beams under losses.

The **OPO** is based on an α-cut periodically poled KTP non linear crystal (PPKTP, *Raicol Crystals Ltd.* on custom design) which allows implementing a type II phase matching with frequency degenerate and cross polarized signal and idler beams, for a crystal temperature of $\approx 53°$C. The transmissivity of the cavity output mirror, T_{out}, is chosen in order to guarantee, together with crystal losses (κ) and other losses mechanisms (T_{in}), an output coupling parameter $\eta_{out} = T_{out}/(T_{in} + \kappa)$ @1064 nm of ≈ 0.73, corresponding to an experimental linewidth of 15 MHz @1064 nm. In order to obtain a low oscillation threshold, **OPO** cavity geometry is set to warrant simultaneous resonance on the pump, the signal and the idler [96]. the pump resonance is guaranteed by servo-assisting the **OPO** cavity with a Drever Pound Hall system [97], while the resonance of other beams is induced by exploiting the natural birefringence of the KTP to tune the optical path of each beam inside the cavity, through a fine control of the crystal temperature and tilt [96]. The **OPO** is equipped with a handmade control system able to stabilize the nonlinear crystal temperature up to 0.1 mK. Measured oscillation threshold is around 50 mW; during measurement runs the system has been operated at ≈60% of the threshold power to avoid unwanted non–Gaussian effects [98].

The two beams outing the **OPO** are transmitted through a filter of variable optical density that mimics the BS. The loss level introduced by the filter is polarization independent and can be tuned from a few percent up to more than 99%.

6.1.4 Characterization stage

The signal and idler modes are then sent to the covariance matrix measurement set-up: this consists in a preliminary polarization system, that allows choosing the beam to be detected and a standard homodyne detector. The polarization system is made of an half-wave plate ($\lambda/2$) followed by a polarizing beam splitter (PBS); the different wave-plate orientations allow choosing the beam to be transmitted by the PBS: the signal (a), the idler (b) or their combinations $c = \frac{1}{\sqrt{2}}(a+b)$ or $d = \frac{1}{\sqrt{2}}(a-b)$. Two other combinations, $e = \frac{1}{\sqrt{2}}(ia+b)$ and $f = \frac{1}{\sqrt{2}}(ia-b)$, can be obtained by inserting before the PBS an additional quarter wave plate ($\lambda/4$) [99]. Acquisition times are considerably short thank to pc-driven mechanical actuators that allow setting the $\lambda/2$ and $\lambda/4$ positions in a fast and well calibrated

manner.

Once a beam is selected, it goes to an homodyne detector put downstream the PBS. This exploits, as local oscillator, the laser output @1064 nm, previously filtered and adjusted to match the geometrical properties of the **OPO** output: a typical interferometer visibility is 0.98. The LO phase θ is spanned to obtain a 2π variation in 200 ms. The homodyne photodiodes (PDs) (model Epitaxx ETX300) have both nominal quantum efficiencies of 0.91 and each is matched to a low-noise trans-impedance ac (>few kilohertz) amplifier. The difference photocurrent is eventually further amplified by a low-noise high gainamplifier (MITEQ AU 1442).

In order to avoid low frequency noise the homodyne current is demodulated at Ω=3 MHz and low-pass filtered (B=300 KHz). Then it is sampled by a PCI acquisition board obtaining 10^6pts/run, with 14-bit resolution. The electronic noise floor is 16 dBm below the shot noise level, corresponding to SNR $\approx$40. Data are analysed by a ©Mathematica routine that extract from the six homodyne traces the relevant quadrature variances necessary for reconstructing the whole covariance matrices [99].

6.2 Experimental results

We have performed different sets of measurement under lossy transmission in order to investigate different loss regimes. Each experimental **CM** comes from seven homodyne traces: the shot noise calibration trace, obtained by obscuring the **OPO** output, six traces each for one of the six modes required for a full state characterization. Contrarily to other previous experiments, where quantum tomographic routine were used in order to retrieve experimental **CM**s [78], we have evaluated **CM**s by a simpler ©Mathematica routine that calculates relevant second order moments of homodyne distributions in a faster way without enhancing the experimental indeterminacy on the **CM** elements. We have tested on a few **CM**s that this procedure gives results in all compatible with quantum tomography. We have also checked, with the standard procedure outlined in [100], that the states under scrutiny were effectively Gaussian.

Once a **CM** is obtained the different entanglement witnesses (w_{PHS}, w_{DUAN}, and w_{EPR}), state purity (μ), teleportation fidelity ($\mathcal{F}$), quantum discord ($\mathcal{D}$), and mutual information ($\mathcal{I}$) are calculated (Eqs. (6.5)). Then, the overall decoherence, i.e. the total level of loss that includes **OPO** cavity escape efficiency, propagation loss, filter absorption, homodyne efficiency, is assigned as a label to the measurement [79]. This expected level of decoherence is then compared to the theoretical one obtained by inverting Eq. (6.2) and solving for T under the condition $\det(\boldsymbol{\sigma}_1) = 1/16$; thus requiring that $\boldsymbol{\sigma}_1$ represents a pure state. We have verified that, even if experimental **CM**s do not reproduce exactly *diagonal* states, all of them respect the Duan conditions (2.14) within experimental indeter-

minacies. So that for the analysed matrices the Duan witness w_{DUAN} represents a sufficient and necessary condition for entanglement.

In all the reported plots we have considered the less decohered datum (obtained for $T = 0.63$) as a reference so that all the reported theoretical curves are obtained imposing that Eqs. (6.4) and (6.5) evaluted for $T = 0.63$ give the measured values.

The total losses we have measured span the interval $37 - 99\%$ ($0.01 \leq T \leq 0.63$). We note that $T = 0.63$, in absence of extra loss and having a cavity escape efficiency of ≈ 0.73, implies an overall state detection efficiency of ≈ 0.86 in agreement with an homodyne visibility of 0.98 ± 0.01, a photodiode (nominal) efficiency of 0.90 ± 0.01 and residual transmission loss between the **OPO** output mirror and the detector surface of 0.01 ± 0.01.

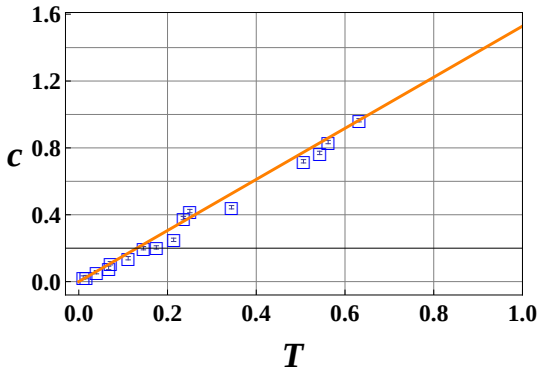

Figure 6.2: *(color online)* behaviour of the averaged correlation term $|c_{1,T}| + |c_{2,T}|/2$ in Eq. (6.2). As expected the correlation reduces linearly with T. The full (*dark orange*) line represents the linear behaviour calculated starting from the first experimental point we have measured ($T = 0.63$). Error bars are smaller than data points and amount to ± 0.01.

In Fig. 6.2 we report the behaviour vs. T of the averaged correlation term $((|c_{1,T}| + |c_{2,T}|)/2$ see Eq. (6.4)). As expected the correlation between the two sub–systems degrades linearly with the total loss ($T \to 0$). The expected behaviour (full *dark orange* line), obtained by considering the less absorbed **CM** ($T = 0.63$) as a reference, follows quite well the reported data. Actually, data refer to acquisition taken on different days so that, the scattering of the point around that line is more due to source long–term dynamics then to actual deviation from the Lindblad model. At the same time the fact that the points are reasonably close to that line proves that the long term stability of the source can be considered quite good.

As already mentioned, w_{PHS} and w_{DUAN} describe a physical property of the state that is strong under decoherence as proved for lower loss (below 90%) in Ref. [79]. They are symptoms of un–separability, in the sense that the system state

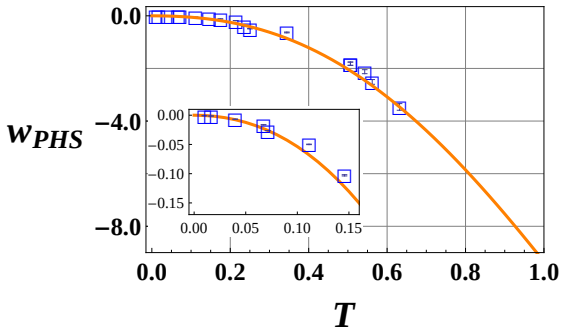

Figure 6.3: *(color online)* w_{PHS} vs. T. The full (*dark orange*) line represents the expected behaviour calculated by the third of Eqs. (6.5) setting the first experimental point at $T = 0.63$ as the intial datum. Error bars, obtained by propagating the experimental indeterminacies in Eq. (2.20a), range between 10^{-4} and 0.1. In the inset we report the high loss regime ($T < 0.15$) for better enlightning the un–separability, as witnessed by w_{PHS}, even in presence of strong decoherence.

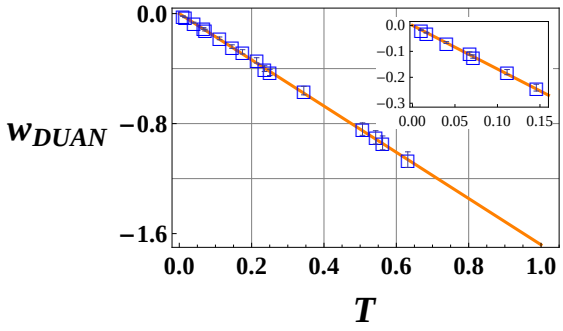

Figure 6.4: *(color online)* w_{DUAN} vs. T. The full (*dark orange*) line represents the expected behaviour calculated by the fourth of Eqs. (6.5) setting the first experimental point at $T = 0.63$ as the intial datum. Error bars, obtained by propagating the experimental indeterminacies in Eq. (2.20b), range between 0.01 and 0.06. In the inset we report the plot for $T < 0.15$ in order to better visualize the persistence of entanglement, as witnessed by w_{DUAN}, even in presence of strong decoherence.

cannot be described by a density matrix in the form of Eq. (2.6) [121]. This can be seen in Figs. 6.3 and 6.4 where w_{PHS} and w_{DUAN} are plotted vs. T. We have also enlarged, in the insets the region for strong loss ($T < 0.15$) to prove that, even if the analysed state is very close to a two mode vacuum (the total average number of photon $((n+m-1)/2)$ reduces to 0.02 ± 0.01) it is still experimentally possible to prove that the state is non–separable. It has to be noted that, while, for $T \to 0$, w_{PHS} approaches its classical limit non–linearly (see the third of Eqs. (6.5)), w_{DUAN} (see the fourth of Eqs. (6.5)) is linear. Thus, in the very high loss regime it becomes more reliable to assess entanglement using the latter than the former.

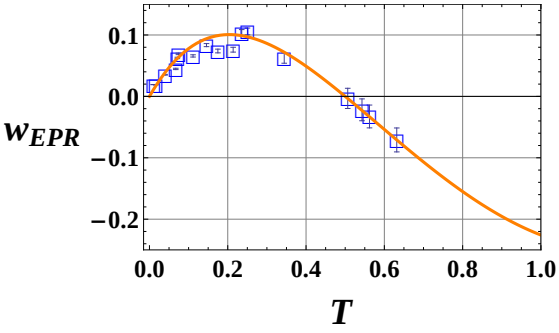

Figure 6.5: *(color online)* w_{EPR} vs. T. The full (*dark orange*) line represents the expected behaviour calculated by the fifth of Eqs. (6.5) setting the first experimental point at $T = 0.63$ as the intial datum. Error bars, obtained by propagating the experimental indeterminacies in Eq. (2.20c), range between 2×10^{-4} and 0.02. They are considerably larger for point at low losses. As expected for total losses larger than 0.5 $w_{EPR} > 0$ and the state does not show *EPR* correlation.

$w_{EPR} < 0$ indicates that the state exhibits EPR–like correlation so that it is possible to gain information on the expectation value of one observable on one sub–system with a precision better than the standard quantum limit once the EPR companion is measured on the other sub–system. This feature is by far the most fragile under decoherence: for $T < 0.5$ no state can keep this quantum feature. This can be understood from the fact that loss, a stochastic process, affects directly the degree of correlation between the two sub–systems while the system representation (i.e. its un–separability) is only smoothed by this process. It is relevant to note that $T = 0.5$ also corresponds to the minimum state purity μ. So that, loosing the EPR character coincides with the maximum mixedness for the state during its propagation. In Fig. 6.5 we report the experimental behaviour found for w_{EPR} for our system. Measured **CM**s for $T < 0.5$ all show $w_{EPR} > 0$. A positive w_{EPR} indicates that, for these states, any attempt to gain information on one sub–system by measuring the other would result less precise than the standard

quantum limit.

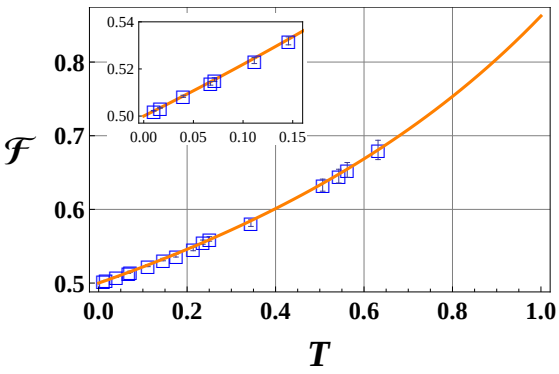

Figure 6.6: *(color online)* $\mathcal{F}$ vs. T. The full (*dark orange*) line represents the expected behaviour calculated by the second of Eqs. (6.5) setting the first experimental point at $T = 0.63$ as the intial datum. Error bars, obtained by propagating the experimental indeterminacies in Eq. (2.25), range between 10^{-4} and 0.01. In the inset we report the plot for $T < 0.15$ in order to underline the persistence of a quantum teleportation regime even in presence of strong decoherence (high loss) thus proving that even for, in principle, infinite distance this class of states would allow to perform the teleportation of a coherent state with a fidelity above 1/2.

An important signature for an entangled **CV** state is its ability of acting as a quantum resource in the **CV** teleportation protocol for coherent state. In Eq. (2.25) we have expressed the fidelity $\mathcal{F}$ as a function of the **CM** elements. $\mathcal{F}$, as w_{PHS} and w_{DUAN}, represents a robust signature of quantum properties for the state undergoing to a lossy transmission. In particular, in Fig. 6.6, we see that even in the high loss regime, $\mathcal{F}$ remains above the classical limit of 0.5 (see the inset for greater details). Thus proving that **CV** entangled state, as the one produced by our source, could be used as resource for realising teleportation protocol of coherent state, in principle, at an infinite distance.

Eventually we have retrieved, from our **CM**s, the value for the quantum mutual information $\mathcal{I}(\boldsymbol{\sigma})$ (Eq. (2.31)) and quantum discord $\mathcal{D}(\boldsymbol{\sigma})$ (Eq. (2.33)).

In Fig. 6.7 we report the experimental data together with the expected behaviours, as usually calculated considering the less decohered matrix as a reference, for $\mathcal{I}$ and $\mathcal{D}$ vs. T. As it can be seen the quantum discord follows very well its *theoretical* line while quantum mutual information is a little more scattered around it. Moreover, our data prove that even in presence of strong decoherence, it is possible to evaluate that $\mathcal{D}$ keeps > 0, within the experimental indeterminacies, all the way down to an highly absorbed state. We note that Gaussian quantum discord is attracting, very recently, a lot of experimental interest [101, 102, 103]. In particular, in Ref. [101], the authors give an operational significance to quantum discord as the possibility of encoding quantum information in separable states.

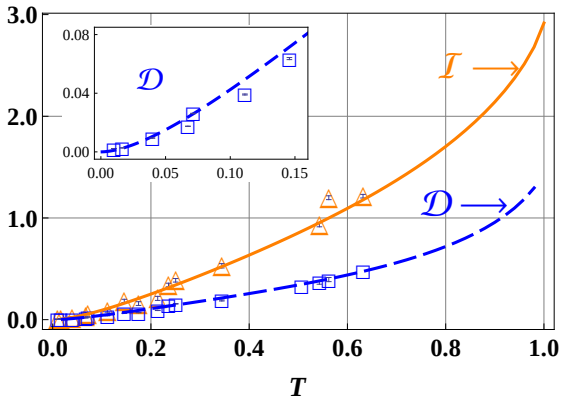

Figure 6.7: *(color online)* $\mathcal{I}$ and $\mathcal{D}$ vs.T. The full (*dark orange*) and dashed (*blue*) lines represent the expected behaviours calculated by the sixth and seventh of Eqs. (6.5) setting the first experimental point at $T = 0.63$ as the intial datum. Error bars, obtained by propagating the experimental indeterminacies in Eqs. (2.31) and (2.33), respectively, range between 3×10^{-3} and 0.02 for $\mathcal{I}$ and 10^{-4} and 0.03 for $\mathcal{D}$. In the inset we report the $\mathcal{D}$ data for $T < 0.15$ in order to underline the persistence of true quantum correlation even in presence of strong decoherence (high loss). Note that the data for $\mathcal{I}$ scatter more from the expected behaviour may be signalling extra classical correlations.

In Ref. [102] the optimal strategy for evaluating $\mathcal{D}(\boldsymbol{\sigma})$ in homodyne measurement is presented. It is interesting to compare our experimental plot with the one reported in Ref. [103] where the authors analyse the quantum discord under the lossy transmission of one of the two sub–systems. We note that in their case the scattering of the experimental points around the theoretical curve is almost equivalent for $\mathcal{I}$ and $\mathcal{D}$ while in our case there is a clear difference.

6.3 Conclusions

Gaussian bi–partite states are one of the most renown resources for implementing **CV** quantum communication protocols such as **CV** teleportation of coherent states. In this chapter we have experimentally analysed how decoherence affects different entanglement criteria and quantum markers for a **CV** bi–partite state outing a sub–threshold type–II **OPO**. The decoherence is experimentally introduced by transmistting the quantum state through a variable attenuator. Before illustrating our experimental results we have discussed in details the relationship between the three different entanglement criteria used in the **CV** framework and linked them to the teleportation fidelity and quantum discord. The latters represent two possible quantum signatures for evaluating the ability of this class of states in quantum communication protocols.

On one hand, our findings prove that the Lindblad approach for describing

lossy transmission is valid all the way down to strongly decohered states. On the other hand, with this chapter, we prove that the particular class of states we have analysed keeps, within the experimental indeterminacies, its main quantum signatures, i.e. the possibility of realizing quantum teleportation of coherent states with a fidelity above 0.5 and a quantum discord above 0 for a total loss of $\approx 99\%$. This proves that the class of **CV** entangled states, we analysed, would allow, in principle, to realize quantum teleportation over an infinitely long Gaussian channel.

In analysing how quantum discord (see Fig. 6.7) and quantum mutual information behave under decoherence we interestingly found that the scattering of the points around the theoretical curve is significantly more evident for the quantum mutual information may be signalling that a key role, in our case, is played by unexpected classical correlations. This point will be subject of further theoretical and experimental investigation.

CHAPTER 7

NON-DEGENERATE TYPE II **OPO** WITH FLUCTUATING PARAMETERS

The fields generated by optical parametric oscillators (**OPO**s) are widely used in quantum communication as resource states for different protocols as the teleportation one. The reason for this lies in the fact that ideal OPOs generate of Gaussian **CV** entangled states. OPOs can be divided into two types depending on the type of interaction realized in the non–linear crystal. Type–I refer to crystals in which the downconverted signal and idler beams have the same polarization, type–II to cross–polarized beams. In the latter case, below threshold and at frequency degeneracy [104] a single type–II **OPO** generates a bi–partite entagled state. In the former a single **OPO** generates a squeezed vacuum state [86] and entagnlement is obtained by mixing at a balanced beam–splitter two independently generated squeezed vacuum field. In the case these two type–I OPOs are pumped by the same field the two generation schemes are completely equivalent and the equations ruling the dynamics of the entangled state are in all equal.

Aim of this chapter is to analyse such a dynamics in presence of noise sources other from the quantum noise entering the **OPO** cavity through different loss mechanisms. In particular, we describe the dynamic of a type–II frequency degenerate **OPO** by a set of Langevin equations by including in the model introduced by Graham and Haken in the late 60s [105] different classical noise sources like pump amplitude fluctuations, laser phase diffusion, cavity resonance fluctuations and fluctuations in the non-linear effective coefficient. The presence of extra noise sources modifies the statistical properties of the state and switches unexpected, in a quite **OPO**, cross–correlations. The effects of fluctuating terms propagates all the way down to the quantum property of the bi–partite state affecting the ability of such a state of being a resource for quantum communication protocols.

As a matter of fact, in recent years, the quest for entangled states sharing an high level of correlation has pushed up the level of measured squeezing. So that starting from a squeezing level of -6.0 dB established by Polzik et al.[106] a breakthrough of -7.2 dB, was brought by Aoki et al. [107] using periodically poled $KTiOPO_4$ crystals. Almost contemporarily Suzuki et al.[108] and Takeno et al.[109] have reported a squeezing of -9 dB. Recently Eberle et al.[110] have reported a squeezing of 12.7 dB. On one hand, this squeezing levels require extremely challenging experimental techniques. On the other hand, these levels can only be obtained getting closer to the oscillation threshold. A regime, as already proved experimentally in a type–I **OPO** [98], where the role of these

fluctuating terms become more evident. As discussed by Chaturvedi et al [111] the fields generated by the **OPO** contribute increasingly to the fluctuations of the pump giving rise to a phase transition. Even if the latter begins for relative distances from the threshold of the order of 10^{-6}, and squeezing above 10 dB, the impact of amplitude fluctuations must be brought into account earlier [112]. Moreover, once a type–II **OPO** or a pair of type–I **OPO** driven by the same laser are considered, the frequency fluctuations of the pump laser and optical modes of the cavity induce a coupling between the quadrature X and Y giving rise to correlations unexpected in ideal systems.

More generally, the output of an **OPO** depends on the fluctuations of the quantum noise entering the system due to the interaction with the continuum of e.m. modes of the outer space. This truly quantum noise adds itself to the fluctuations of the pump and other device parameters as the mechanical stability of the optical cavity and/or the temperature fluctuations of the non-linear medium. The latter ones can be described as classical stochastic processes with correlation times much longer than the quantum one.

As we mentioned in the course of this dissertation, the proper use of the fluctuating parameters of the **OPO** system can adequately be addressed to engineering of non-Gaussian states. In fact, a first consequence of the presence of extra noise terms the generated state looses its Gaussian character so that its Wigner function become slightly non-Gaussian. Moreover, the fidelity of various **CV** teleportation schemes have been evaluated by giving for granted the Gaussian character of the resources provided by physical **OPO** sources. Thus, it is rather intuitive that loosing the Gaussian character the fidelity that the state can provide changes. In particular, we found that the fidelity is increased in presence of extra fluctuations. This is not surprising being well known that, as proved in Ref. [1], that the teleportation fidelity can be increased by using non–Gaussian resource.

In the present chapter, under the guidance of Prof. Salvatore Solimeno and Dott. Alberto Porzio of the Università degli Studi di Napoli "FedericoII", we present an initial discussion on the effects of the presence of extra noise sources onto the characteristic characteristic functions, of the field quadratures, for the quantum state as a function of the pump strength quantified by the relative distance from the oscillation threshold. Due to these influences the state becomes non-Gaussian. Moreover, the introduction of phase dependent noises, as pump frequency and cavity resonance condition, leads to the coupling between the different Langevin equations for the field quadratures so that a certain degree of correlation appear in the out-of-diagonal elements of the quantum state covariance matrix. Once the fluctuating Langevin equations are solved, the net effect on the bi–partite state covariance matrix and on the effective teleportation fidelity are calculated.

The weight of these sources in determining the deviation from the Gaussian statistics was discussed in Ref. [112] where it was shown that the **OPO** is mainly

dependent on the pump amplitude relative fluctuations $\mu(t)$. In view of the prominent role of the pump amplitude fluctuation and in order to properly evaluate the contribution of the different noise sources to the changes in the covariance matrix and the teleportation fidelity, we have solved exactly the equation for what concern the pump fluctuation and treated all the other sources in a perturbative fashion. To clearly indicate this hierarchy in the formulas we have indicated with a bar "" quantities averaged on the pump amplitude noise and with $\langle\rangle_i$ (i a label indicating the noise under consideration) all the other averages.

The chapter is organized as follows. In Sec. 7.1 the **OPO** Langevin system is derived by taking into account the set of four parameters μ_p (relative pump amplitude fluctuation), ϖ_p (pump frequency deviation from the mean value), $\delta\nu$ (deviation of the cavity resonance ferquency), $\delta\chi$ (fluctuation of the non–linear coupling parameter). In Sec. 7.2 the field equations of motion are integrated. The relative covariance matrix $\boldsymbol{\sigma}$ for the field transmitted through a noisy channel and the characteristic function are obtained in Sec. 7.3. In particular for what concerns $\boldsymbol{\sigma}$ it is shown that as a consequence of the fluctuations of ϖ_p, $\delta\nu$ and $\delta\chi$ off-diagonal terms σ_{xy} are generally not zero. On the other hand the characteristic function coincide formally with that relative to Gaussian states with classically fluctuating $\boldsymbol{\sigma}(\tau)$. Eventually the effects of the source parameter fluctuations on the fidelity of a coherent state teleported is analyzed in Sec. 7.4.

7.1 Graham-Haken-Langevin system

Type II OPOs rely on parametric down–conversion: a strong *pump* beam at frequency ω_p interacts in a non–linear crystal with the vacuum fields thus generating two mutually orthogonal beams, *signal* and *idler*, at frequency $\omega_s = \omega_i = \frac{1}{2}\omega_p$ respectively [105],[111]. The three **OPO** cavity modes a_k (a_0 pump at frequency ω_p, a_s and a_i respectively signal and idler) evolve under the action of the Hamiltonian

$$H_{int} = i\hbar 2\chi\left(b_s b_i b_0^\dagger - b_0 b_s^\dagger b_i^\dagger\right) + i\hbar\left(\mathcal{E}^* b_0 - \mathcal{E} b_0^\dagger\right) \tag{7.1}$$

where χ is the coupling parameter proportional to the crystal second order susceptibility $\chi^{(2)}$. The pump field $\mathcal{E} = e^{-i\phi_p}\epsilon\left(1+\mu_p\right)$ is treated in the rotating frame $e^{-i\omega_p t}$ as a complex quantity with a constant amplitude ϵ modulated by a fluctuating factor $1+\mu_p(t)$ ($\langle\mu_p\rangle = 0$) times a phase factor $e^{-i\phi_p}$, where $\phi_p(t)$ is a slowly diffusing phase, i.e. in accordance with the usual laser theory $\left\langle\left(\phi_p(t) - \phi_p(t')\right)\right\rangle^2 = 2\Delta y_\ell |t-t'|$ with Δ_ℓ the laser linewidth [113]. In particular $\frac{d}{dt}\phi_p = \varpi_p$ a stationary Gaussian process with $\langle\varpi_p(t)\,\varpi_p(t')\rangle = 2\Delta_\ell\delta(t-t')$. $\mu_p(t)$ will be treated as a stationary Gaussian process. Analogously a_s, a_i are defined in the frame $e^{-i\omega_p t/2}$.

The cavity modes are characterized by damping factors $\gamma_{j,M}, \gamma_{j,x}$ $\left(\gamma_j = \gamma_{j,M} + \gamma_{j,x}\right)$ due respectively to the output mirror (M) and the other loss mechanisms (x:

crystal absorption and scattering, absorption of the two mirrors, etc.). Modes are assumed to be slightly detuned by $\varpi_k = \frac{\pi c}{L_k}\left[L_k\frac{\omega_k}{\pi c}\right] - \omega_k$, $[x]$ standing for the closest integer to x. $L_k = \bar{L}_k + \delta L_k$ with $\bar{L}_k$ the average **OPO** cavity optical length ($L_k = n_k L$) at frequency ω_k while δL_k is due to the mirror position fluctuations. Moreover, in view of the condition $\omega_s = \omega_i = \frac{1}{2}\omega_0$ we have $\varpi_s = \varpi_i = \frac{1}{2}\varpi_0$.

The evolution of the cavity mode operators is rooted in the theoy of Langevin equations with quantum sources developed by Graham-Haken[105]. Namely it is described by the Graham-Haken Langevin equations (GHLE) :

$$\begin{aligned}\frac{d}{dt}b_j &= -\kappa b_j + 2\chi b_0 b^\dagger_{j'} + R_j \; j = s,i \text{ and } j \neq j' \\ \frac{d}{dt}b_0 &= -\kappa_0 b_0 - 2\chi^* b_s b_i + \mathcal{E} + R_0\end{aligned} \tag{7.2}$$

where $\kappa = \gamma - i\varpi_s, \kappa_0 = \gamma_0 - i2\varpi_s$. The parameter χ is proportional to the crystal susceptibility $\chi^{(2)}$ through the phase–matching factor[114], the focusing parameter and the crystal absorption. Under this assumption χ will be replaced in the following by $\bar{\chi}e^{-i\phi_\chi}(1+\delta\chi)$ with $\bar{\chi}$ depending on the slow variations of T while ϕ_χ is a phase depending on the position of the beam waist with respect to the crystal center. With an accurate alignment ϕ_χ can be set equal to 0.

Besides other the system (7.2) contains the fluctuating forces $R_k(t) = \sqrt{2\gamma_{k,M}}b_{k,M} + \sqrt{2\gamma_{k,x}}b_{k,x}$ which take into account the delta correlated vacuum fluctuation fields, $\left\langle b_{k,M,x}(t)\, b^\dagger_{k,M,x}(t')\right\rangle = \delta(t-t')$, entering the **OPO** cavity.

Next, replacing b_s and b_i with the modes $b_\varsigma = (\varsigma b_s + b_i)/\sqrt{2}$, $\varsigma = +/-1$, Eqs. (7.2-a) transform into

$$\frac{d}{dt}b_\varsigma = -\kappa b_\varsigma + \varsigma 2\chi b_0 b^\dagger_\varsigma + R_\varsigma \tag{7.3}$$

This change in the reference frame for the downconverted modes uncouples the equations for the signal and idler modes. The two equations in b_+ and b_- represent two distinct fully degenerate type–I **OPO** pumped by the same field and working out of phase. Each of these type–I generates a squeezed vacuum state. As a matter of fact, it is possible to obtain an entangled CV system by mixing two independent squeezed vacua on a beam splitter. This operation is in all equivalent to going back to the previous rederence frame. With an accurate tuning the systematic deviation fom resonance can be removed so that ϖ reduce to the contribution of the residual mirror vibrations.

The **OPO** admits a threshold value for the amplitude ϵ

$$\epsilon_{th} = \frac{\gamma_0\gamma}{2|\bar{\chi}|} = \frac{\sqrt{\gamma_0\gamma}}{\sqrt{2}g_{\bar{\chi}}}$$

with

$$g_{\bar{\chi}} = \frac{2|\bar{\chi}|}{\sqrt{2\gamma_0\gamma}}$$

an adimensional parameter, of the order of 10^{-6}, describing the non–linear interaction strength $\bar{\chi}$ of the **OPO** crystal[111].Below threshold, a_0 has a non–zero mean value r_0 proportional to the driving field amplitude ϵ $(= \gamma_0 r_0)$.

Now, it is worth replacing ϵ with the parameter E:

$$E = \frac{\epsilon}{\epsilon_{th}} = \sqrt{2\hat{\gamma}_0} r_0 g_{\bar{\chi}}$$

with the caret labeling hereafter quantities divided by γ. Separating the average part r_0 from the fluctuating one $\delta b_0 = r_0 a_0$ we put $b_0 = e^{-i\phi_p} r_0 (1 + a_0)$ $(a_0 = X_0 + iY_0)$. Conversely the modes b_ς have zero mean value and will be expressed in terms of rescaled operators $b_\varsigma = r_\varsigma a_\varsigma$, with $r_\varsigma = \sqrt{\hat{\gamma}_0} r_0$. Hence, ignoring the contribution of the term proportional to $b_s b_i$ the system (7.2) reduces to

$$\begin{aligned} \dot{a}_\varsigma &= -\hat{\kappa} a_\varsigma + \varsigma E e^{-i\phi_p} (1 + a_0 + \delta\chi) a_\varsigma^\dagger + \frac{\hat{R}_\varsigma}{r_\varsigma} \\ \dot{a}_0 &= -(\hat{\kappa}_0 - i\hat{\varpi}_p) a_0 + \hat{\gamma}_0 \mu_p + i\hat{\varpi} + e^{i\phi_p} \frac{\hat{R}_0}{r_0} , \end{aligned}$$

with $\varpi = 2\varpi_s + \varpi_p$ and a dot indicating the derivative $d/d(\gamma t)$. In particular

$$\frac{\left\langle \hat{R}_\varsigma(\tau) \hat{R}_\varsigma^\dagger(\tau') \right\rangle}{r_\varsigma^2} = \frac{4}{E^2} g_{\bar{\chi}}^2 \delta(\tau - \tau') .$$

Introducing now the vectors

$$\begin{aligned} \dot{X}_0 &= -\hat{\gamma}_0 X_0 - \hat{\varpi} Y_0 + \hat{\gamma}_0 \mu_p + \hat{X}_{R_0}, \\ \dot{Y}_0 &= -\hat{\gamma}_0 Y_0 + \hat{\varpi} X_0 + \hat{\varpi} + \hat{Y}_{R_0}, \end{aligned} \tag{7.4}$$

and

$$\begin{aligned} \dot{X}_\varsigma &= -[\lambda_\varsigma - \varsigma E (X_0 + \delta\chi)] X_\varsigma - \left(\frac{\hat{\varpi}}{2} - \varsigma E Y_0 \right) Y_\varsigma + \hat{X}_{R_\varsigma}, \\ \dot{Y}_\varsigma &= -[\lambda_{-\varsigma} + \varsigma E (X_0 + \delta\chi)] Y_\varsigma + \left(\frac{\hat{\varpi}}{2} + \varsigma E Y_0 \right) X_\varsigma + \hat{Y}_{R_\varsigma}, \end{aligned} \tag{7.5}$$

and defining the vector variables

$$\mathbf{\Psi}_\varsigma = \begin{bmatrix} X_\varsigma(\tau) \\ Y_\varsigma(\tau) \end{bmatrix} , \ \mathbf{N}_\varsigma(\tau) = \begin{bmatrix} \hat{X}_{R_\varsigma}(\tau) \\ \hat{Y}_{R_\varsigma}(\tau) \end{bmatrix}$$

with $X_\varsigma(\tau), Y_\varsigma(\tau)$ signal and idler quadratures, measured by homodyne detectors using $\mathcal{E}_{\rm hom} \propto e^{-i\omega_p t/2 - i\phi_p/2}$ as local oscillator,

$$\begin{aligned} X_\varsigma &= \frac{E}{2\sqrt{2}g_{\bar\chi}}\left(e^{i\phi_p/2}a_\varsigma + e^{-i\phi_p/2}a_\varsigma^\dagger\right) \\ Y_\varsigma &= \frac{E}{2\sqrt{2}g_{\bar\chi}}\left(-ie^{i\phi_p/2}a_\varsigma + ie^{-i\phi_p/2}a_\varsigma^\dagger\right) \end{aligned}$$

and doing the same for the analogous quantities X_0, Y_0 relative to the pump mode and the vacuum fluctuations$\hat X_{R_\varsigma}, \hat Y_{R_\varsigma}, \hat X_{R_0}, \hat Y_{R_0}$,

$$\mathbf{\Psi}_0 = \begin{bmatrix} X_0 \\ Y_0 \end{bmatrix}, \ \mathbf{N}_0 = \begin{bmatrix} \hat\gamma_0\mu_p + \hat X_{R_0} \\ \hat\varpi + \hat Y_{R_0} \end{bmatrix}$$

the system (7.3) can be recast as

$$\begin{aligned} \dot{\mathbf{\Psi}}_\varsigma &= -\mathbf{H}\cdot\mathbf{\Psi}_\varsigma + \mathbf{N}_\varsigma \\ \dot{\mathbf{\Psi}}_0 &= -\mathbf{H}_0\cdot\mathbf{\Psi}_0 + \mathbf{N}_0 \end{aligned} \tag{7.6}$$

where

$$\begin{aligned} \mathbf{H}_\varsigma &= \begin{bmatrix} \lambda_\varsigma & 0 \\ 0 & \lambda_{\bar\varsigma} \end{bmatrix} + \begin{bmatrix} \varsigma E(X_0+\delta\chi) & -\frac{\hat\varpi}{2} - \varsigma E Y_0 \\ \frac{\hat\varpi}{2} - \varsigma E Y_0 & -\varsigma E(X_0+\delta\chi) \end{bmatrix} = \mathbf{H}_\varsigma^{(0)} + \varepsilon\mathbf{W}_\varsigma \\ \mathbf{H}_0 &= -\hat\gamma_0\mathbf{1} + \hat\varpi\begin{bmatrix} 0 & -1 \\ 1 & 0 \end{bmatrix} = \mathbf{H}_\varsigma^{(0)} + \varepsilon\mathbf{W}_0 \end{aligned}$$

with $\hat\varpi = \hat\varpi_s + \hat\varpi_i + \hat\varpi_p = 2\hat\varpi_s + \hat\varpi_p$, $\lambda_\varsigma = 1 - \varsigma E$.

In particular

$$\begin{aligned} \left\langle \hat X_{R_\varsigma}(\tau)\hat X_{R_\varsigma}(\tau')\right\rangle &= \left\langle \hat Y_{R_\varsigma}(\tau)\hat Y_{R_\varsigma}(\tau')\right\rangle = \delta(\tau-\tau'), \\ \left\langle \hat X_{R_0}(\tau)\hat X_{R_0}(\tau')\right\rangle &= \left\langle \hat Y_{R_0}(\tau)\hat Y_{R_0}(\tau')\right\rangle = \hat\gamma_0^2\delta(\tau-\tau'). \end{aligned}$$

In conclusion, the **OPO** analyzed in the following is characterized by classical fluctuating parameters $\mu_p, \varpi_p, \varpi_k$ and $\delta\chi$, all together determining the **OPO** dynamics. For typical operating conditions, ($\sigma_{\mu_p} \simeq 10^{-3} \div 10^{-2}, g_{\bar\chi} \simeq 10^{-6}$, $\gamma \simeq 10 \div 20$ MHz, $\sigma_{\varpi_p} \simeq 1 \div 1000$ Hz, $\sigma_T \simeq 1 \div 10$ mK, $\partial n/\partial T \approx 10^{-6} \div 10^{-4}$ and $\sigma_\chi \approx 10^{-5} \div 10^{-4}$) $\sigma_{\hat\varpi_p}$ and $\sigma_{\hat\nu}$ respectively range in the intervals $10^{-6} \div 10^{-4}$ and $10^{-5} \div 10^{-3}$.

We note that the presence of phase noises (ϖ_p and ϖ_k) implies that the X quadrature is dynamically coupled to Y. As we will see, this circumstance introduces in the downconverted field cross–correlation terms that are absent in an ideal system.

7.2 Integration of the GHL system

Integrating (7.4) yields

$$\begin{aligned} X_0(\tau) &= \int_{-\infty}^{\tau} e^{-\hat{\gamma}_0(\tau-\tau')} \cdot \\ &\quad \left[\cos\varphi(\tau,\tau')\left(\hat{\gamma}_0\mu_p(\tau') + \hat{X}_{R_0}(\tau')\right) - \sin\varphi(\tau,\tau')\left(\hat{\varpi}(\tau') + \hat{Y}_{R_0}(\tau')\right)\right] d\tau' \\ Y_0(\tau) &= \int_{-\infty}^{\tau} e^{-\hat{\gamma}_0(\tau-\tau')} \cdot \\ &\quad \left[\cos\varphi(\tau,\tau')\left(\hat{\varpi}(\tau') + \hat{Y}_{R_0}(\tau')\right) + \sin\varphi(\tau,\tau')\left(\hat{\gamma}_0\mu_p(\tau') + \hat{X}_{R_0}(\tau')\right)\right] d\tau' \end{aligned}$$

with $\varphi(\tau,\tau') = \int_{\tau'}^{\tau} \hat{\varpi} d\tau''$.

Analogously we have

$$\mathbf{\Psi}_\varsigma(\tau) = \int_{-\infty}^{\tau} \mathbf{G}_\varsigma(\tau,\tau') \cdot \mathbf{N}_\varsigma(\tau')$$

with

$$\mathbf{G}_\varsigma(\tau,\tau') = \hat{T} e^{-\int_{\tau'}^{\tau} \mathbf{H}_\varsigma d\tau''} = 1 - \int_{\tau'}^{\tau} \mathbf{H}_\varsigma d\tau'' + \int_{\tau'}^{\tau} \mathbf{H}_\varsigma d\tau'' \int_{\tau'}^{\tau''} \mathbf{H}_\varsigma d\tau''' - \cdots$$

$\hat{T}$ being the time ordering operatorand. Next$\mathbf{G}_\varsigma(\tau,\tau')$ can be expabded in a power series in ε :

$$\mathbf{G}_\varsigma(\tau,\tau') = \mathbf{G}_\varsigma^{(0)}(\tau,\tau') + \varepsilon\mathbf{G}_\varsigma^{(1)}(\tau,\tau') + \varepsilon^2\mathbf{G}_\varsigma^{(2)}(\tau,\tau')$$

where

$$\begin{aligned} \frac{d}{d\tau}\mathbf{G}_\varsigma^{(0)}(\tau,\tau') &= -\mathbf{H}_\varsigma^{(0)} \cdot \mathbf{G}_\varsigma^{(0)} \\ \frac{d}{d\tau}\mathbf{G}_\varsigma^{(1)}(\tau,\tau') &= -\mathbf{H}_\varsigma^{(0)} \cdot \mathbf{G}_\varsigma^{(1)} + \mathbf{W}_\varsigma \cdot \mathbf{G}_\varsigma^{(0)} \\ \frac{d}{d\tau}\mathbf{G}_\varsigma^{(2)}(\tau,\tau') &= -\mathbf{H}_\varsigma^{(0)} \cdot \mathbf{G}_\varsigma^{(2)} + \mathbf{W}_\varsigma \cdot \mathbf{G}_\varsigma^{(1)} \end{aligned}$$

that is

$$\begin{aligned} \mathbf{G}_\varsigma^{(0)}(\tau,\tau') &= e^{-\int_{\tau'}^{\tau} \mathbf{H}_\varsigma^{(0)} d\tau''}, \\ \mathbf{G}_\varsigma^{(1)\prime}(\tau,\tau') &= \int_{\tau'}^{\tau} \mathbf{G}_\varsigma^{(0)}(\tau,\tau'') \cdot \mathbf{W}_\varsigma(\tau'') \cdot \mathbf{G}_\varsigma^{(0)}(\tau'',\tau')\, d\tau'', \\ \mathbf{G}_\varsigma^{(2)\prime}(\tau,\tau') &= \int_{\tau'}^{\tau} \mathbf{G}_\varsigma^{(1)}(\tau,\tau'') \cdot \mathbf{W}_\varsigma(\tau'') \cdot \mathbf{G}_\varsigma^{(1)}(\tau'',\tau')\, d\tau''. \end{aligned}$$

7.3 Covariance matrix and characteristic function

In order to find the covariance matrix, we average the quantity

$$\mathbf{\Psi}_{\varsigma}(\tau)\,\mathbf{\Psi}_{\varsigma}^{T}(\tau)=\int_{-\infty}^{\tau}d\tau'\int_{-\infty}^{\tau}d\tau''\mathbf{G}_{\varsigma}(\tau,\tau')\cdot\mathbf{N}_{\varsigma}(\tau')\,\mathbf{N}_{\varsigma}^{T}\left(\tau'\right)\cdot\mathbf{G}_{\varsigma}^{T}(\tau,\tau'') \quad (7.7)$$

with respect to the quantum noise $\mathbf{N}_{\varsigma}(\tau')$. We obtain

$$\boldsymbol{\sigma}_{\varsigma}(\tau)=\int_{-\infty}^{\tau}\mathbf{G}_{\varsigma}(\tau,\tau')\cdot\rho_{th}\cdot\mathbf{G}_{\varsigma}^{T}(\tau,\tau')$$

with

$$\rho_{th}=\left\langle\mathbf{N}_{\varsigma}(\tau')\,\mathbf{N}_{\varsigma}^{T}(\tau')\right\rangle$$

the density matrix of the quantum noise entering the cavity.

From (7.7) it descends for the covariance matrix [115] $\sigma_{\varsigma ij}$ averaged with respect to the quantum noise sources $\hat{X}_{R_{\varsigma}},\hat{Y}_{R_{\varsigma}}$

$$\begin{aligned}
\sigma_{\varsigma xx}(\tau) &= \left\langle X_{\varsigma}^{2}(\tau)\right\rangle=\sigma_{\bar{\varsigma}yy}(\tau)=\left\langle Y_{\bar{\varsigma}}^{2}(\tau)\right\rangle\\
&= \int_{-\infty}^{\tau}\left[e^{2\lambda_{\varsigma}\tau'}G_{\varsigma xx}^{2}(\tau,\tau')+e^{2\lambda_{\bar{\varsigma}}\tau'}G_{\varsigma xy}^{2}(\tau,\tau')\right]d\tau'\\
\sigma_{\varsigma xy}(\tau) &= \left\langle X_{\varsigma}(\tau)\,Y_{\varsigma}(\tau)\right\rangle=\left\langle Y_{\varsigma}(\tau)\,X_{\varsigma}(\tau)\right\rangle\\
&= \int_{-\infty}^{\tau}\left[-e^{2\lambda_{\varsigma}\tau'}G_{\varsigma xx}(\tau,\tau')\,G_{\bar{\varsigma}xy}(\tau,\tau')+e^{2\lambda_{\bar{\varsigma}}\tau'}G_{\varsigma xy}(\tau,\tau')\,G_{\bar{\varsigma}xx}(\tau,\tau')\right]d\tau'.
\end{aligned}$$

In particular, the variance $\left\langle X_{\theta\varsigma}^{2}\right\rangle=\sigma_{\theta\varsigma}$ of $X_{\theta\varsigma}=X_{\varsigma}\cos\theta+Y_{\varsigma}\sin\theta$ reads

$$\sigma_{\theta\varsigma}(\tau)=\sigma_{\varsigma xx}(\tau)\cos^{2}\theta+2\sigma_{\varsigma xy}(\tau)\sin 2\theta+\sigma_{\varsigma yy}(\tau)\sin^{2}\theta.$$

Depending $X_{\varsigma}(\tau),Y_{\varsigma}(\tau)$ on the Gaussian quantum processes $\hat{X}_{R_{\varsigma}}(\tau'),\hat{Y}_{R_{\varsigma}}(\tau')$ we have more in general

$$\left\langle X_{\theta\varsigma}^{2n}(\tau)\right\rangle=\left\{\begin{array}{c}(2n-1)!!\sigma_{\theta\varsigma}^{n}(\tau)\\ 0\text{ othervise}\end{array}\right. . \quad (7.8)$$

In the following we will neglect the quantum fluctuations of $\hat{X}_{R_0},\hat{Y}_{R_0}$ with respect to $\mu_{p}(\tau')$ and $\hat{\varpi}(\tau')$. In this way the covariance matrix elements can be written as

$$\begin{aligned}
\sigma_{\varsigma xx}(\tau) &= \frac{2g_{\bar{\chi}}}{E^{2}}\frac{2\left\langle n(\tau)\right\rangle+1}{2}\left[\cosh\left(2r(\tau)\right)-\sinh\left(2r(\tau)\right)\cos 2\varphi(\tau)\right],\\
\sigma_{\varsigma yy}(\tau) &= \frac{2g_{\bar{\chi}}}{E^{2}}\frac{2\left\langle n(\tau)\right\rangle+1}{2}\left[\cosh\left(2r(\tau)\right)+\sinh\left(2r(\tau)\right)\cos 2\varphi(\tau)\right],\\
\sigma_{\varsigma xy}(\tau) &= \frac{2g_{\bar{\chi}}}{E^{2}}\frac{2\left\langle n(\tau)\right\rangle+1}{2}\sinh\left(2r(\tau)\right)\sin 2\varphi(\tau).
\end{aligned}$$

The quantum density matrix $\rho(t)$ of the **OPO** modes is asociated to the Weyl characteristic function

$$\chi(u_\varsigma, v_\varsigma) = Tr[\hat{D}(u_\varsigma, v_\varsigma)\rho_\varsigma] = \left\langle \hat{D}(u_\varsigma, v_\varsigma) \right\rangle ,$$

which can be constructed starting from the set of moments $\left\langle a^{\dagger m} a^{\mathrm{n}} \right\rangle$. In view of (7.8) we have

$$\chi(u_\varsigma, v_\varsigma) = \exp\left[-\left(\sigma_{\varsigma xx} u_\varsigma^2 + 2\sigma_{\varsigma xy} u_\varsigma v_\varsigma + \sigma_{\varsigma yy} v_\varsigma^2\right)\right] \tag{7.9}$$

averaged with respect the classical processes ϖ_p, ν, and χ and depending on time through the fluctuation induced by the pump amplitude in $\boldsymbol{\sigma}(\tau)$.

Analogously we have for the Wigner function

$$W(X_\varsigma, Y_\varsigma) = \frac{1}{\det \boldsymbol{\sigma}_\varsigma(\tau)} \left\langle \exp\left[-\left(\frac{X_\varsigma^2}{\sigma_{\varsigma xx}(\tau)} + 2\frac{X_\varsigma Y_\varsigma}{\sigma_{\varsigma xy}(\tau)} + \frac{Y_\varsigma^2}{\sigma_{\varsigma yy}(\tau)}\right)\right] \right\rangle_{\varpi,\chi} .$$

We have seen that the covariance matrix of the mixed state $\boldsymbol{\sigma}_\varsigma$ propagating through a noisy channel is given by

$$\boldsymbol{\sigma}_\varsigma(\tau) = \boldsymbol{\sigma}_\infty\left(1 - e^{-\Gamma\tau}\right) + \boldsymbol{\sigma}_\varsigma(0)\, e^{-\Gamma\tau}$$

with $\boldsymbol{\sigma}_\infty$ the asymptotic covariance matrix

$$\boldsymbol{\sigma}_\infty = \begin{bmatrix} \frac{2N+1+2M_1}{2} & M_2 \\ M_2 & \frac{2N+1-2M_1}{2} \end{bmatrix}$$

being $M = M_1 + iM_2$ the bath correlation function and N a phenomenological parameter related to the purity of the asymptotic state. Hence,

$$\boldsymbol{\sigma}_\varsigma(\tau) = \begin{bmatrix} \frac{2N_{eff}+1+2M_{1eff}}{2} & M_{2eff} \\ M_{2eff} & \frac{2N_{eff}+1-2M_{1eff}}{2} \end{bmatrix}$$

where

$$\begin{aligned} N_{eff} &= N + \frac{\sigma_{\varsigma xx}(0) + \sigma_{\varsigma yy}(0) - 2N - 1}{2} e^{-\Gamma\tau} \\ M_{1eff} &= M_1 + \frac{\sigma_{\varsigma xx}(0) - \sigma_{\varsigma yy}(0) - 2N - 1}{2} e^{-\Gamma\tau} \\ M_{2eff} &= M_2 + (\sigma_{\varsigma xy}(0) - M_2)\, e^{-\Gamma\tau} \end{aligned}$$

Accordingly at zeroth order $\chi(\xi_\varsigma; \tau)$ reduces to

$$\chi(\xi_\varsigma; \tau) = \left\langle \exp\left[-\left(\frac{A_{\bar{\varsigma}}(\tau)}{E_{\bar{\varsigma}}} u_\varsigma^2 + \frac{A_\varsigma(\tau)}{E_\varsigma} v_\varsigma^2\right)\right] \right\rangle_{\mu_p} \tag{7.10}$$

while

$$\begin{aligned}\tanh\left(2r\left(\tau\right)\right) &= \frac{\frac{A_{\varsigma}(\tau)}{E_{\varsigma}}-\frac{A_{\bar{\varsigma}}(\tau)}{E_{\bar{\varsigma}}}}{\frac{A_{\varsigma}(\tau)}{E_{\varsigma}}+\frac{A_{\bar{\varsigma}}(\tau)}{E_{\bar{\varsigma}}}}\\ \left\langle n\left(\tau\right)\right\rangle+\frac{1}{2} &= \frac{E^{2}}{2g_{\bar{\chi}}}\sqrt{\frac{A_{\varsigma}\left(\tau\right)}{E_{\varsigma}}\frac{A_{\bar{\varsigma}}\left(\tau\right)}{E_{\bar{\varsigma}}}}\end{aligned}$$

7.4 Teleportation

The fidelity of the teleportation of a coherent state.$|\beta\rangle$ using a two-mode squeezed vacuum (Gaussian) state as a resource reads [25]

$$\mathcal{F}=\frac{1}{e^{-2r}+1}.$$

where r is the degree of effective squeezing available. So that a perfect fidelity ($\mathcal{F}=1$) can be approached only in the limit of infinite squeezing.

We aim at calculating the fidelity of a teleportation protocol [26] of a coherent state using, as a resource, the two–mode state generated by a type–II **OPO** with fluctuating parameters described in the above sections and compare the result with the fidelity attainable by the same resource in the absence of fluctuations.

In a more general fashion the fidelity can be expressed in terms of the characteristic functions of the input and output state [75, 1]

$$\mathcal{F}=\frac{1}{2\pi}\int du_{2}dv_{2}\chi_{in}\left(u_{2},v_{2}\right)\chi_{out}\left(-u_{2},-v_{2}\right) \tag{7.11}$$

where $\chi_{in}\left(x,v\right)$ is the characteristic function of the input state, in our case coherent state $|\beta\rangle$,

$$\chi_{in}\left(x,v\right)=\exp\left[-\frac{1}{2}\left|\alpha\right|^{2}+\left[\left(x+iv\right)\beta^{*}-\left(x-iv\right)\beta\right]/\sqrt{2}\right]$$

and χ_{out} is the characteristic function of the teleportated state that can be expressed in terms of the resource state characteristc function

$$\chi_{out}\left(u_{2},v_{2}\right)=\chi_{in}\left(u_{2},v_{2}\right)\chi_{res}\left(u_{2},-v_{2};u_{2},v_{2}\right), \tag{7.12}$$

This general approach allows to calculate the fidelity even if the state is non-Gaussian. Moreover, in Ref. [1], the performance of the a non-Gaussian state, used as resources in the teleportation protocol, is proven to be given by a fine interplay among entanglement, non-Gaussianity, and the state affinity to a two–mode squeezed-vacuum. In our case, the balance among these quantities is determined precisely by the amount of fluctuations in phase and amplitude.

As we have shown the presence of fluctuating terms in the equations ruling the **OPO** induces a modification in the characteristic functions of the entangled squeezed state acting as the resource state for the teleportation protocol. So that $\chi_{res}(u_2,-v_2;u_2,v_2)$ in Eq. (7.12) is given by

$$\chi_{res}(u_1,v_1;u_2,v_2)=\chi(u_+,v_+;t)\,\chi(u_-,v_-;t),$$

where $\chi(u_+,v_+;t)$ is given in Eq. (7.9) and

$$\begin{aligned} u_\varsigma &= \frac{\varsigma u_1+u_2}{\sqrt{2}}, \\ v_\varsigma &= \frac{\varsigma v_1+v_2}{\sqrt{2}}, \end{aligned} \tag{7.13}$$

So the characteristic function (7.12) becomes

$$\chi_{out}(u_2,v_2;\tau)=\chi_{in}(u_2,v_2)\exp\left[-\frac{E^2}{4g_{\bar{\chi}}}\left(\sigma_{+xx}(\tau)\,u_2^2+\sigma_{-yy}(\tau)\,v_2^2\right)\right].$$

Therefore, the fidelity $\mathcal{F}$, Eq.(7.11), is given by averaging on the time-dependent quantities

$$\mathcal{F}\equiv\overline{f(\tau)},$$

where

$$\begin{aligned} f(\tau) &= \frac{1}{2\pi}\int du_2dv_2\chi_{in}(u_2,v_2;\tau)\,\chi_{out}(-u_2,-v_2;\tau) \\ &= \frac{1}{\sqrt{\left(\frac{E^2}{2g_{\bar{\chi}}}\sigma_{+xx}(\tau)+1\right)\left(\frac{E^2}{2g_{\bar{\chi}}}\sigma_{-yy}(\tau)+1\right)}} \end{aligned} \tag{7.14}$$

Expanding in terms of the fluctuating quantities $\sigma_{+xx}(\tau)$ and $\sigma_{-yy}(\tau)$, and retaining only even non–zero moments, we have

$$\mathcal{F}=\sum_{k=0}^{\infty}\mathcal{F}^{(k)}$$

with

$$\begin{aligned} \mathcal{F}^{(k)} &= \sum_{\substack{n:\\ n+m=k}}\frac{\delta_{k,0}}{\sqrt{\left(\frac{E^2}{2g_{\bar{\chi}}}\overline{\sigma_{+xx}}+1\right)\left(\frac{E^2}{2g_{\bar{\chi}}}\overline{\sigma_{-yy}}+1\right)}} \\ &\quad+\frac{\delta_{m,0}\Sigma_{+xx}^{(n-1)}}{\sqrt{\frac{E^2}{2g_{\bar{\chi}}}\overline{\sigma_{-yy}}+1}}+\frac{\delta_{n,0}\Sigma_{-yy}^{(m-1)}}{\sqrt{\frac{E^2}{2g_{\bar{\chi}}}\overline{\sigma_{+xx}}+1}}+\Sigma_{+xx}^{(n-1)}\Sigma_{-yy}^{(m-1)} \end{aligned}$$

where

$$\Sigma_{\varsigma qq}^{(\ell)} = \Theta\left[\ell\right] \frac{(2\ell)!!\,(4\ell+3)!!}{(4\ell+4)!!} \frac{\left(\frac{E^2}{2g_{\bar{\chi}}}\right)^{2(\ell+1)} \left(\overline{\sigma_{\varsigma qq}^2\left(\tau\right)} - \overline{\sigma_{\varsigma qq}}^2\right)^{\ell+1}}{\left(\frac{E^2}{2g_{\bar{\chi}}}\overline{\sigma_{\varsigma qq}} + 1\right)^{(4\ell+5)/2}}.$$

The parameters $\Sigma_{\varsigma qq}^{(\ell)}$ are the averages of the fluctuating quantities $\sigma_{\varsigma qq}^2\left(\tau\right)$. In particular, we have

$$\mathcal{F}^{(0)} = \frac{1}{\sqrt{\left(\frac{E^2}{2g_{\bar{\chi}}}\overline{\sigma_{+xx}} + 1\right)\left(\frac{E^2}{2g_{\bar{\chi}}}\overline{\sigma_{-yy}} + 1\right)}}\,, \tag{7.15}$$

$$\begin{aligned}\mathcal{F}^{(1)} &= \frac{\Sigma_{+xx}^{(0)}}{\sqrt{\frac{E^2}{2g_{\bar{\chi}}}\overline{\sigma_{-yy}} + 1}} + \frac{\Sigma_{-yy}^{(0)}}{\sqrt{\frac{E^2}{2g_{\bar{\chi}}}\overline{\sigma_{+xx}} + 1}} \qquad (7.16)\\ &= \frac{3}{8}\mathcal{F}^{(0)}\left(\frac{\left(\overline{\sigma_{+xx}^2\left(\tau\right)} - \overline{\sigma_{+xx}}^2\right)}{\left(\overline{\sigma_{+xx}} + \frac{2g_{\bar{\chi}}}{E^2}\right)^2} + \frac{\left(\overline{\sigma_{-yy}^2\left(\tau\right)} - \overline{\sigma_{-yy}}^2\right)}{\left(\overline{\sigma_{-yy}} + \frac{2g_{\bar{\chi}}}{E^2}\right)^2}\right)\end{aligned}$$

$$\begin{aligned}\mathcal{F}^{(2)} &= \frac{\Sigma_{+xx}^{(1)}}{\sqrt{\frac{E^2}{2g_{\bar{\chi}}}\overline{\sigma_{-yy}} + 1}} + \frac{\Sigma_{-yy}^{(1)}}{\sqrt{\frac{E^2}{2g_{\bar{\chi}}}\overline{\sigma_{+xx}} + 1}} + \Sigma_{+xx}^{(0)}\Sigma_{-yy}^{(0)} \qquad (7.17)\\ &= \frac{35}{64}\mathcal{F}^{(0)}\left(\frac{\left(\overline{\sigma_{+xx}^2\left(\tau\right)} - \overline{\sigma_{+xx}}^2\right)^2}{\left(\overline{\sigma_{+xx}} + \frac{2g_{\bar{\chi}}}{E^2}\right)^4} + \frac{\left(\overline{\sigma_{-yy}^2\left(\tau\right)} - \overline{\sigma_{-yy}}^2\right)^2}{\left(\overline{\sigma_{-yy}} + \frac{2g_{\bar{\chi}}}{E^2}\right)^4}\right.\\ &\quad \left. + \frac{9}{64}\frac{\left(\overline{\sigma_{+xx}^2\left(\tau\right)} - \overline{\sigma_{+xx}}^2\right)^2\left(\overline{\sigma_{-yy}^2\left(\tau\right)} - \overline{\sigma_{-yy}}^2\right)^2}{\left(\overline{\sigma_{+xx}} + \frac{2g_{\bar{\chi}}}{E^2}\right)^4\left(\overline{\sigma_{-yy}} + \frac{2g_{\bar{\chi}}}{E^2}\right)^4}\right). \qquad (7.18)\end{aligned}$$

It is worth noting that the even moments all have positive coefficients so that any fluctuation of $\sigma_{+xx}\left(\tau\right)$ and $\sigma_{-yy}\left(\tau\right)$ will improve the overall fidelity.

At zeroth order in $\varpi_p, \delta\chi$, *i.e.* considering pump amplitude fluctuation only, the resource characteristic function χ_{res} reduces to

$$\chi_{out}\left(u_2, v_2; \tau\right) = \chi_{in}\left(u_2, v_2\right) \exp\left[-\frac{E^2}{4g_{\bar{\chi}}}\frac{A_{\bar{\varsigma}}\left(\tau\right)}{E_{\bar{\varsigma}}}\left(u_2^2 + v_2^2\right)\right].$$

So that, the fluctuating fidelity $f\left(\tau\right)$ Eq. (7.14) becomes

$$f\left(\tau\right) = \frac{1}{\frac{E^2}{2g_{\bar{\chi}}}\frac{A_{\bar{\varsigma}}(\tau)}{E_{\bar{\varsigma}}} + 1}.$$

Expanding in terms of the fluctuating quantity $A_{\overline{\varsigma}}(\tau)$ and retaining only even non–zero moments, gives

$$\begin{aligned}\mathcal{F} &= \sum_{n=0}^{\infty}\mathcal{F}^{(n)} \\ \mathcal{F}^{(n)} &= \frac{\left(\frac{E^2}{2g_{\bar{\chi}}E_{\overline{\varsigma}}}\right)^{2n}\left(\overline{A_{\overline{\varsigma}}^2(\tau)}-\overline{A_{\overline{\varsigma}}}^2\right)^{2n}}{\left(\frac{E^2}{2g_{\bar{\chi}}}\frac{\overline{A_{\overline{\varsigma}}}}{E_{\overline{\varsigma}}}+1\right)^{2n+1}}\end{aligned}$$

with

$$\begin{aligned}\mathcal{F}^{(0)} &= \frac{1}{\frac{E^2}{2g_{\bar{\chi}}}\frac{\overline{A_{\overline{\varsigma}}}}{E_{\overline{\varsigma}}}+1}\ , \\ \mathcal{F}^{(1)} &= \mathcal{F}^{(0)}\frac{\left(\overline{A_{\overline{\varsigma}}^2(\tau)}-\overline{A_{\overline{\varsigma}}}^2\right)^2}{\left(\overline{A_{\overline{\varsigma}}}+\frac{2g_{\bar{\chi}}}{E^2}E_{\overline{\varsigma}}\right)^2}\ , \\ \mathcal{F}^{(2)} &= \mathcal{F}^{(0)}\frac{\left(\overline{A_{\overline{\varsigma}}^2(\tau)}-\overline{A_{\overline{\varsigma}}}^2\right)^4}{\left(\overline{A_{\overline{\varsigma}}}+\frac{2g_{\bar{\chi}}}{E^2}E_{\overline{\varsigma}}\right)^4}\ .\end{aligned}$$

It is worth noting that the even moments all have positive coefficients so that any fluctuation of $A_{\overline{\varsigma}}(\tau)$ will improve the overall fidelity.

CHAPTER 8

CONCLUSION

We have developed some important aspects of quantum information, often using the characteristic function formalism, particularly suitable for the study of non-Gaussian quantum states. For example, in the Chapter 1, we have used the formalism of the characteristic function for calculating the action of the conditional measurements on multipartite systems in very general circumstances. This description is found to be very useful in Chapter 5 , where we have introduced a suitable generation scheme capable to produce a class of non-Gaussian tunable states which well approximates the class of **SB** states proposed in [1]. A preliminary analysis showed that the state generated by our scheme, used as a resource, provides the maximum fidelity of teleportation of a coherent state in the most interesting range of the experimentally accessible values of squeezing r at present. The obtained performance is better both of generated **TB** and of generated **PS** squeezed states (these last representing the best resources till now experimentally obtained). This result is given in both ideal and realistic conditions. In particular, in ideal conditions of generation (no losses, perfect photon-resolving detection), for $r > 0.5$ the performance of the proposed optimal states lies very near to that of the optimized theoretical **SB** state. In realistic conditions (presence of losses, only on/off measurements allowed), obviously, the fidelities sensibly deteriorate, but, as remarked, the optimal generated state provides again, in a large zone of interesting values of r, the best performance with respect to **TB** and **PS** squeezed states.

It is interesting to note that the performance can be even further improved with a slight improvement in reducing the level of losses and in increasing the detection efficiency. Regarding the problem of increasing the efficiency in photon-resolving it can be solved by the implementation of superconducting wires at very high efficiency. If these improvements are achieved, the optimal realistic tunable state will approach ideal instance.

In any case, our preliminary analysis shows that our scheme can generate non-Gaussian states which perform better than other generated states, including the **PS** squeezed states. In a forthcoming work we will design in details the experimental set up needed to realize our scheme. To this aim, we will consider the two possible instances: continuous wave and pulsed regime. In the same work we will show how we will reconstruct the generated states by performing suitable homodyne detections.

Obviously, at the end of this route we aim to obtain our most ambitious

goal, the actual realization of the experimental generation. The realization of this states is very important for the development of the new technologies in Quantum Information. We have found also that the **SB** states were found to be the best resources for protocol Swapping too. In fact, in the Chapter 4 we have studied the efficiency of the vLB **CV** quantum swapping protocol for the transmission of quantum states and entanglement. As a preliminary task, we have expressed the entanglement swapping protocol in the characteristic function representation. In order to evaluate the performance of the swapping protocol the teleportation fidelity of a coherent state has been assumed as convenient indicator to quantify the performance levels, using the swapped states as entangled resource. We have shown that the optimization procedures of the squeezed Bell resource allow to have high values of the fidelities both in the ideal and the realistic instances.

Also for the violation of Bell's inequality, the **SB** states offer the best performance in respect with all the other considered states. In particular, in the Chapter 3 we have used two different approaches for evaluating the entity of inequality violation: that of psudo-spin and that of the Wigner function. In both cases, the **SB** states maximize the violation of inequality with respect to other non-Gaussian and Gaussian states. This supports the project of an experimental scheme of generation of this important class of non-Gaussian quantum states (Chapter 5).

Another important non-Gaussian quantum state, that can be generated easily, is produced by **OPO** with fluctuating pump. Squeezed beams generated by parametric oscillators operating under threshold are widely used as resources for the teleportation of quantum states. From the moment that the fidelity of these processes increases with the degree of squeezing these devices are designed in such a way as to bring the amplitude of the pump to the oscillation threshold. As it approaches the component antisqueezed the field suffers from increasingly of the fluctuations of the pump, the oscillation frequency of the optical cavity and effective coupling parameter of nonlinear crystal used. In the chapter 7 we have got an expression of the correlation matrix of the field by introducing three stochastic mutually correlated functions. These are obtained the moments to the various orders by assuming that the noise of the amplitude of the pump is uniform in a given band. It is also shown that the fluctuations of the pump frequency and the resonance of the cavities have the effect of coupling the two quadratures X and Y. Due to the presence of these fluctuating factors the characteritic function looses its Gaussian character. Such non-Gaussianity leads to an increase in fidelity of teleportation of a cohrent state.

Finally, in the Chapter 6, we have experimentally analysed how decoherence affects different entanglement criteria and quantum markers for a **CV** bi–partite state outing a sub–threshold type–II **OPO**. The decoherence is experimentally introduced by transmistting the quantum state through a variable attenuator. Before illustrating our experimental results we have discussed in details the rela-

tionship between the three different entanglement criteria used in the **CV** framework and linked them to the fidelity of teleportation and quantum discord. The latters represent two possible quantum signatures for evaluating the ability of this class of states in quantum communication protocols.

On one hand, our findings prove that the Lindblad approach for describing lossy transmission is valid all the way down to strongly decohered states. On the other hand, we have proved that the particular class of states we have analysed keeps, within the experimental indeterminacies retains, its main quantum signatures, i.e. the possibility of realizing quantum teleportation of coherent states with a fidelity above 0.5 and a quantum discord above 0 for a total loss of $\approx 99\%$. This proves that the class of **CV** entangled states, we analysed, would allow, in principle, to realize quantum teleportation over an infinitely long Gaussian channel.

In analysing how quantum discord (see Fig. 6.7) and quantum mutual information behave under decoherence we interestingly found that the scattering of the points around the theoretical curve is significantly more evident for the quantum mutual information may be signalling that a key role, in our case, is played by unexpected classical correlations. This point will be subject of further theoretical and experimental investigation.

CHAPTER 9

APPENDIX A: BEAM SPLITTER

The beam splitter (BS) has an important role in the study of quantum aspects of the light radiation and is the main component of homodyne detection. It is an optical device with two inputs and two outputs (see Fig. 9.1).

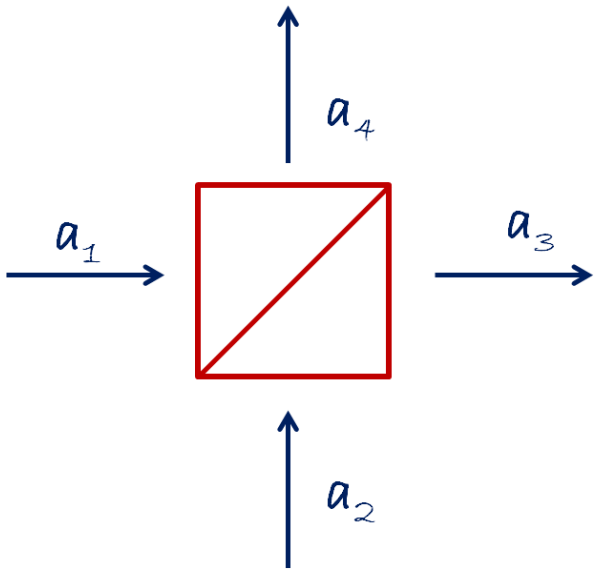

Figure 9.1: Schematic representation of a Beam Splitter.

Recalling that the electromagnetic fields can be expressed through the operators of annihilation and creation, the output fields a_3 and a_4 of the BS are related to the input fields a_1 and a_2 by linear relations of the type:

$$\begin{pmatrix} a_3 \\ a_4 \end{pmatrix} = \mathbf{S} \begin{pmatrix} a_1 \\ a_2 \end{pmatrix} = \begin{pmatrix} S_{11} & S_{12} \\ S_{21} & S_{22} \end{pmatrix} \begin{pmatrix} a_1 \\ a_2 \end{pmatrix},$$

where $\mathbf{S}$ is the BS matrix. The element $S_{11}\,(S_{22})$ is interpretable as the transmission coefficient for the beam that enters in the port $1\,(2)$, and emerges from $3\,(4)$. The terms off-diagonal of $\mathbf{S}$, indeed, represent the reflection coefficients. We assume the BS lossless. In general, the elements of the matrix $\mathbf{S}$ are complex and may be expressed in terms of amplitude $|S_{ij}|$, and phase ϕ_{ij}, *i.e.*

$$S_{ij} = |S_{ij}|\, e^{i\phi_{ij}}.$$

We note that it is necessary that the operators a_3 and a_4 verify the commutation relations. So that they may actually represent the fields if

$$\begin{aligned}\left[a_j, a_j^\dagger\right] &= 1, \quad \text{for } j = 3, 4,\\ [a_j, a_{j'}] &= \left[a_j^\dagger, a_{j'}^\dagger\right] = 0.\end{aligned}$$

Such commutation relations impose a restriction to the elements of the matrix,

$$|S_{11}|\,|S_{21}| = |S_{12}|\,|S_{22}|\,, \tag{9.1}$$
$$\phi_{11} - \phi_{12} = \phi_{21} - \phi_{22} \pm \pi, \tag{9.2}$$

from which we obtain the following relations

$$\begin{aligned}|S_{11}|^2 &= |S_{22}|^2 = T = \cos^2\theta,\\ |S_{21}|^2 &= |S_{12}|^2 = R = \sin^2\theta,\end{aligned}$$

T and R being the transmittance and reflectance, respectively, of the beam splitter, such that $T + R = 1$. The above relations show that the dynamics of the BS is established by a single parameter

$$\theta = \arctan\sqrt{\frac{1-T}{T}}.$$

Starting from (9.2) it is convenient to define the phases

$$\begin{aligned}\phi_T &\equiv (\phi_{11} - \phi_{22})/2,\\ \phi_R &\equiv (\phi_{12} - \phi_{21} \mp \pi)/2,\\ \phi_0 &\equiv (\phi_{11} + \phi_{22})/2,\end{aligned}$$

so that we have the most general form of the matrix $\mathbf{S}$

$$\begin{aligned}\mathbf{S} &= e^{i\phi_0}\begin{pmatrix} e^{i\phi_T}\cos\theta & e^{i\phi_R}\sin\theta\\ -e^{-i\phi_R}\sin\theta & e^{-i\phi_T}\cos\theta\end{pmatrix}\\ &= e^{i\phi_0}\begin{pmatrix} t & r\\ -r^* & t^*\end{pmatrix},\end{aligned}$$

where $t = e^{i\phi_T}\sqrt{T}$, and $r = e^{i\phi_R}\sqrt{R}$. Its determinant is

$$\det[\mathbf{S}] = e^{2i\phi_0},$$

and the transformation is unitary. The number of photons, between the input modes and output modes, is conserved,

$$n_3 + n_4 = n_1 + n_2. \tag{9.3}$$

It is clear that imposing energy conservation (9.3) does not determine uniquely the transformation realized by the BS. There are three independent phases: ϕ_T, ϕ_R, and ϕ_0, that remain indeterminate, as well as the transmissivity T. The presence of many degrees of freedom makes possible to build different types of beam splitter:

- BS with real coeffiients: $\phi_T = \phi_R = 0$. In this case, the incident fields are not out of phase, with the consequent conservation of the polarization;
- symmtric BS: we have $S_{11} \in \text{Re}$ and $S_{12} \in \text{Im}$, *i.e.* $\phi_T = 0$ and $\phi_R = \pi/2$;
- balanced BS: it is a symmetric BS with $T = R = 1/2$.

Moreover, without loss of generality, we can set the phase factor global ϕ_0 equal to zero. This is justified if the input beams of the BS propagate in the same plane.

Now, we want to evaluate the number of photons and the variance of the output fields. Combining the results obtained for the matrix $\mathbf{S}$, we obtain

$$\begin{aligned} a_3 &= \sqrt{T}e^{i\phi_T}a_1 + \sqrt{1-T}e^{i\phi_R}a_2, \\ a_4 &= -\sqrt{1-T}e^{-i\phi_R}a_1 + \sqrt{T}e^{i\phi_T}a_1, \end{aligned}$$

so the photon number operator of the two modes is

$$\begin{aligned} n_3 &= Tn_1 + (1-T)\,n_2 + 2\sqrt{T\,(1-T)}\hat{I}, \\ n_4 &= (1-T)\,n_1 + Tn_2 - 2\sqrt{T\,(1-T)}\hat{I}, \end{aligned}$$

where $\hat{I}$ is the interference operator

$$\hat{I} = \frac{1}{2}a_1^\dagger a_2 e^{-i(\phi_T - \phi_R)} + h.c.$$

The expectation values of the number of photons are

$$\langle n_3 \rangle = T\,\langle n_1 \rangle + (1-T)\,\langle n_2 \rangle + 2\sqrt{T\,(1-T)}\left\langle \hat{I} \right\rangle, \tag{9.4}$$

$$\langle n_4 \rangle = (1-T)\,\langle n_1 \rangle + T\,\langle n_2 \rangle - 2\sqrt{T\,(1-T)}\left\langle \hat{I} \right\rangle. \tag{9.5}$$

For the coherent states $|\alpha_i\rangle$ such that $\alpha_i = |\alpha_i|\,e^{i\phi_i}$, with $i = 1, 2$, the expectation value of the interference operator is

$$\begin{aligned} \left\langle \hat{I} \right\rangle_{|\alpha_1,\alpha_2\rangle} &= \left\langle \alpha_1, \alpha_2 \left| \hat{I} \right| \alpha_1, \alpha_2 \right\rangle \\ &= |\alpha_1|\,|\alpha_2| \cos\left(\phi_1 - \phi_2 + \phi_T - \phi_R\right), \end{aligned}$$

and it corresponds to the interference pattern for classical state. We can see that $\left\langle \hat{I} \right\rangle_{|n_1,n_2\rangle} = 0$ for the Fock states $|n_1, n_2\rangle$.

In order to calculate the variances, we denote the covariance classical with the symbol

$$\mathrm{cov}\left(A, B\right) \equiv \langle A, B\rangle - \langle A\rangle \langle B\rangle ,$$

and the quantum one as

$$\Xi\left(A, B\right) = \frac{1}{2}\left[\mathrm{cov}\left(A, B\right) + \mathrm{cov}\left(B, A\right)\right]$$

so that if $[A, B] = 0$ then $\Xi\left(A, B\right)$ =cov(A, B). The variance of the sum of two generic operators can be, thus, expressed distinguishing the classical contribution from the quantum one,

$$\begin{aligned} \left\langle \Delta\left(A+B\right)^2 \right\rangle &= \left\langle \left(A+B\right)^2 \right\rangle - \left\langle A+B\right\rangle^2 \\ &= \left\langle \Delta A^2 \right\rangle + \left\langle \Delta B^2 \right\rangle + \Xi\left(A, B\right). \end{aligned}$$

In this notation the variances of photon number of the output modes become [142]

$$\begin{aligned} \left\langle \Delta n_3^2 \right\rangle &= T^2\left\langle \Delta n_1^2 \right\rangle + \left(1-T\right)^2\left\langle \Delta n_2^2 \right\rangle + 2T\mathrm{cov}\left(n_1, n_2\right) \\ &\quad +4T\left(1-T\right)\left\langle \Delta \hat{I}^2 \right\rangle + T^{3/2}\left(1-T\right)^{1/2}\Xi\left(n_1, \hat{I}\right) \\ &\quad +\left(1-T\right)^{3/2}T^{1/2}\Xi\left(n_2, \hat{I}\right), \end{aligned}$$

$$\begin{aligned} \left\langle \Delta n_4^2 \right\rangle &= \left(1-T\right)^2\left\langle \Delta n_1^2 \right\rangle + T^2\left\langle \Delta n_2^2 \right\rangle + 2T\mathrm{cov}\left(n_1, n_2\right) \\ &\quad +4T\left(1-T\right)\left\langle \Delta \hat{I}^2 \right\rangle - \left(1-T\right)^{3/2}T^{1/2}\Xi\left(n_1, \hat{I}\right) \\ &\quad -T^{3/2}\left(1-T\right)^{1/2}\Xi\left(n_2, \hat{I}\right), \end{aligned}$$

The first three terms depend on the fluctuations of the input fields. The other three terms, instead, are are proportional to the fluctuations introduced by the beam splitter.

BIBLIOGRAPHY

[1] Dell'Anno, S De Siena, L. Albano, and F. Illuminati, *Continuous-variable quantum teleportation with non-Gaussian resources*, Phys. Rev A 76, 022301.

[2] F. Dell'Anno, D. Buono, G. Nocerino, S. De Siena, and F. Illuminati, *Realistic entanglement swapping with non-Gaussian resources* (*next submission*).

[3] D. Buono, G. Nocerino, F. Dell'Anno, S. De Siena, and F. Illuminati (*in preparation*).

[4] D. Buono, G. Nocerino, F. Dell'Anno, S. De Siena, F. Illuminati, and A. Porzio, *Tunable non Guassian resources by ancillary squeezing and conditioning. I. Basic scheme of generation and preliminary analysis* (*next submission*).

[5] D. Buono, G. Nocerino, A. Porzio, and S. Solimeno (*in preparation*).

[6] D. Buono, G. Nocerino, A. Porzio, and S. Solimeno, *Experimental analysis of decoherence in continuous-variable bi-partite systems*, Phys. Rev. A 86, 042308 (2012).

[7] D. Buono, G. Nocerino, A. Porzio, and S. Solimeno (*next submission*).

[8] D. Buono, G. Nocerino, V. D'Auria, A. Porzio, S. Olivares, and M. G. A. Paris, *Quantum characterization of bi-partite Gaussian states*, J. Opt. Soc. Am. B, **27**, A110 (2010).

[9] D. Buono, G. Nocerino, A. Porzio, and S. Solimeno, *Survival of continuous variable entanglement over long distances*, Physica Scipta (*submitted and accepted*).

[10] J. J. Sakurai, *Modern Quantum Mechanics*, Addison Wesley (1992).

[11] Gregg Jaeger, *Quantum Information*, Springer, 2007.

[12] E. Schrödinger, Proc. Camb. Philos. Soc. **31**, 555 (1935).

[13] Wolfgang P. Schleich, *Quantum Optics in Phase Space*, Wiley-VCH, 2001.

[14] A. Ferraro, S. Olivares, and M. G. A. Paris, *Gaussian States in Quantum Information*, Bibliopolis, Napoli (2005).

[15] P. Caldirola, R. Cirelli, G.M. Prosperi, *Introduzione alla Fisica Teorica*, UTET, 1982.

[16] R. Loudon, P.L. Knight, *Squeezed light*, Journal of modern optics **34**, 709 (1987).

[17] H. P. Robertson, *The Uncertainty Principle*, Phys. Rev. **34**, 163 (1929).

[18] A. Serafini, F. Illuminati, M. Paris, S. De Siena, *Entanglement and Purity of Two-Mode Gaussian States in Noisy Channels*, Phys. Rev. A 69, 022318 (2004); A. Serafini, M.G.A. Paris, F.Illuminati and S. De Siena, *Quantifyng decoherence in continuous variable systems*, J. Opt. B. **7**, R19 (2005).

[19] J. Williamson, *On the Algebraic Problem Concerning the Normal Forms of Linear Dynamical Systems*, Am. J. Math. **58**, 141 (1936).

[20] L. Mandel, E. Wolf, *Optical coherence and quantum optics*, Cambridge University Press, 1995.

[21] Stephen M. Barnett and Paul M. Radmore, *Methods in Theoretical Quantum Optics*, Clerendon Press - Oxford 1997.

[22] F. Dell'Anno, S. De Siena, and F. Illuminati, *Realistic continuous-variable quantum teleportation with non-Gaussian resources*, Phys. Rev. A **81**, 012333 (2010).

[23] Q.F. Walls, G.J. Milburn *Quantum Optics*, Springer-Verlag 1995.

[24] H.-P. Breur and F. Petruccione, *The Theory of Open Quantum Systems* (Oxford University Press, Oxford, 2002).

[25] S. Pirandola and S. Mancini, *Quantum Teleportation with Continuous variables: a survey*, Laser Physics **16**, 1418 (2006).

[26] S.L. Braunstein and H.J. Kimble, *Teleportation of Continuous Quantum Variables*, Phys. Rev. Lett. 80, 869 (1998).

[27] L. Vaidman, *Teleportation of quantum states*, Phys. Rev. A **49**, 1473 (1994); S. L. Braunstein, H. J. Kimble, *Teleportation of Continuous Quantum Variables*, Phys. Rev. Lett. **80**, 869 (1998).

[28] Ingemar Bengtosson and Karol Zyczkowski, *Geometry of Quantum State*, Cambridge University Press, 2000.

[29] S. Popescu adn D. Rohrlich, *Thermodynamics and the measure of entanglement*, Phys. Rev. A **56**, R3319 (1997).

[30] Michael A. Nielsen and Isaac L. Chuang, *Quantum Computation and Quantum Information*, Cambridge University Press, 2000.

[31] R. Simon, *Peres-Horodecki Separability Criterion for Coninuous Variable Systems*, Phys. Rev. Lett. 84, 2726 (2000).

[32] Lu-Ming Duan, G. Giedke, J.I. Cirac, adn P. Zoller, *Inseparability Criterion for Continuous Variable Systems*, Phys. Rev. Lett. **84**, 2722 (2000).

[33] M. D. Reid, *Demonstration of the Einstein-Podolsky-Rosen paradox using nondegenerate parametric amplification*, Phys. Rev. **A 40**, 913 (1989).

[34] A. Einstein, B. Podolsky, and Rosen, *Can Quantum-Mechanical Description of Physical Reality Be Considered Complete?*,Phys. Rev. **47**, 777 (1935).

[35] William Hall, *Constructions of indecomposable positive maps based on a new criterion for indecomposability*, arXiv:quant-ph/0607035 (2006).

[36] Dariusz Chru sci nski and Andrzej Kossakowski, *Spectral conditions for positive maps and entanglement witnesses*, Journal of Physics: Conference Series 284, 012017 (2011).

[37] V. Vedral and M. B. Plenio, *Entanglement measures and purification procedures*, Phys. Rev. A **57**, 1619 (1998).

[38] S. L. Braunstein and H. J. Kimble, *Teleportation of Continuous Quantum Variables*, Phys. Rev. Lett. **80**, 869 (1998); A. Furusawa et al., Science **282**, 706 (1998).

[39] F. A. S. Barbosa, A. J. de Faria, A. S. Coelho, K. N. Cassemiro, A. S. Villar, P. Nussenzveig, and M. Martinelli, *Disentanglement in bipartite continuous-variable systems*, Phys. Rev. A **84**, 052330 (2011).

[40] J. Wenger, R. Tualle-Brouri, and P. Grangier, *Non-Gaussian Statistics from Individual Pulses of Squeezed Light*, Phys. Rev. Lett. **92**, 153601 (2004).

[41] K. Wakui, H. Takahashi, Optics express **5**, 3568 (2007).

[42] A. Ourjoumtsev, A. Dantan, R. Tualle-Brouri, and P. Grangier, *Increasing Entanglement between Gaussian States by Coherent Photon Subtraction*, Phys. Rev. Lett. **98**, 030502 (2007).

[43] B. P. Lanyon, M. Barbieri, M. P. Almeida, and A. G. White, *Experimental Quantum Computing without Entanglement*, Phys. Rev. Lett. **101,**.200501 (2008).

[44] Paolo Giorda and Matteo G. A. Paris, *Gaussian Quantum Discord*, Phys. Rev. Lett., **105**, 020503 (2010).

[45] Gerardo Adesso and Animesh Datta, *Quantum versus Classical Correlations in Gaussian States*, Phys. Rev. Lett., **105**, 030501 (2010).

[46] Harold Ollivier and Wojciech H. Zurek, *Quantum Discord: A Measure of the Quantumness of Correlations*, Phys. Rev. Lett. **88**, 017901 (2001).

[47] K. Modi, A. Brodutch, H. Cable, T. Paterek, and V. Vedral, *Quantum discord and other meause of quantum correlation*, (2011), arXiv:1112.6238.

[48] A. Wehrl, *General properties of entropy*, Rev. Mod. Phys. **50** (2), 221, (1978).

[49] N. Bohr, *Can quantum-mechanical description of physical reality be considered complete?*, Phys. Rev 48, 696 (1935);

[50] D. Bohm, and Y. Aharonov, *Discussion of the experimental proof for the paradoz of Einstein, podolsky, and Rosen*, Phys. Rev. **108**, 1070 (1957).

[51] J. S. Bell, *Speakable and Unspeakable in Quantum Mechanics*, Cambridge (1987).

[52] J. Jarrett, *On the Physical Significance of the Locality Conditions in the Bell Arguments*, Nous 18, 569 (1984).

[53] J. F. Clauser, M. A. Horne, A. Shimony, and R.A. Holt, *Proposed experiment to test hidden-variable theories*, Phys. rev Lett. **23**, 880 (1969).

[54] F. Laloë, *Do we really understand quantum mechanics? Strange correlations, paradoxes, and theorems*, Am. J. Phys. **69**, 655 (2001).

[55] Karl Popper, *Quantum Theory and the Schism in Physics: From the Postscript to The Logic of Scientific Discovery* (1989).

[56] Raimon Panikkar, *La porta stretta della conoscenza*, Rizzoli (2005).

[57] E. G. Cavalcanti, S. J. Jones, H. M. Wiseman, and M. D. Reid, *Experimental criteria for steering and the Einstein-Podolsky-Rosen paradox*, Phys. Rev A **80**, 032112 (2009).

[58] Zeng-Bing Chen, Jian-Wei Pan, Guang Hou, and Yong-De Zhanh, *Maximal Violation of Bell's Inequality for Continuous Variable Systems*, Phy. Rev. Lett. **88**, 040406 (2002).

[59] N. Gisin, and A. Peres, *Maximal violation of Bell's inequality for arbitrarily large spin*, Phys. Rev. A **162**, 15 (1998).

[60] Konrad Banaszek and Krzysztof Wodkiezicz, *Testing Quantum Nonlocality in Phase Space*, Phys. Rev. Lett. **82**, 2009(1999).

[61] Konrad Banaszek and Krzysztof Wodkiezicz, *Non locality of the Einstein-Podolsky-Rosen state in the Wigner representation*, Phys. Rev. A **58**, 4345(1998).

[62] Hyunseok Jeong, Jinhyoung Lee, and M. S. Kim, *Dynamics of nonlocality*

for a two-mode squeezed state in a thermal environment, Phys. Rev. A **61**, 052101 (2000).

[63] N. Gisin, G. Ribordy, W. Tittel, and H. Zbinden, Rev. Mod. Phys. **74**, 145 (2002).

[64] H.-J. Briegel, W. Dur, J.I. Cirac, and P. Zoller, *Quantum Repeaters: The Role of Imperfect Local Operations in Quantum Communication*, Phys. Rev. Lett. **81**, 5932 (1998).

[65] S. L. Braunstein and P. van Loock, *Quantum information with continuous variables*, Rev. Mod. Phys. **77**, 513 (2005).

[66] P. van Loock and S.L. Braunstein, *Unconditional teleportation of continuous-variable entanglement*, Phys. Rev. A **61**, 010302 (1999).

[67] X. Jia, X. Su, Q. Pan, J. Gao, C. Xie, and K. Peng, *Experimental Demonstration of Unconditional Entanglement Swapping for Continuous Variables*, Phys. Rev. Lett. **93**, 250503 (2004).

[68] T. Yang, Q. Zhang, T.-Y. Chen, S. Lu, J. Yin, J.-W. Pan, Z.-Y. Wei, J.-R. Tian, and J. Zhang, *Experimental Synchronization of Independent Entangled Photon Sources*, Phys. Rev. Lett. **96**, 110501 (2006).

[69] J. Hoelscher-Obermaier and P. van Loock, *Optimal Gaussian entanglement swapping*, Phys. Rev. A **83**, 012319 (2011).

[70] U. Leonhardt and H. Paul, *Realistic optical homodyne measurements and quasiprobability distributions*, Phys. Rev. A **48**, 4598 (1993).

[71] S. L. Braunstein and P. Van Loock, *Quantum information with continuous variables*, Rev. Mod. Phys. **77**, 513 (2005).

[72] Virginia D'Auria, Antonino Chiummo, Martina De Laurentis, Alberto Porzio, and Salvatore Solimeno, *Tomographic characterization of OPO sources close to threshold*, Opt. Express **13**, 948 (2005).

[73] V D'Auria, C de Lisio, A. Porzio, S. Solimeno and Matteo G A Paris, *Transmittivity measurements by means of squeezed vacuum light*, J. Phys. B **39**, 1187 (2006).

[74] ShengLi Zhang and Peter van Loock, *Local Gaussian operations can enhance continuous-variable entanglement distillation*, Phys. Rev. A **84**, 062309 (2011).

[75] P. Marian and T. A. Marian, *Continuous-variable teleportation in the characteristic-function description*, Phys. Rev. A **74**, 042306 2006 .

[76] Sebastian Steinlechner, Jöran Bauchrowitz, Tobias Eberle, Roman Schnabel, *Strong continuous variable EPR-steering with a detection efficiency above 96%* arXiv:1112.0461 (2011).

[77] F. A. S. Barbosa, A. S. Coelho, A. J. de Faria, K. N. Cassemiro, A. S. Villar, P. Nussenzveig, and M. Martinelli, Nat. Photonics **4**, 858 (2010).

[78] V. D'Auria, S. Fornaro, A. Porzio, S. Solimeno, S. Olivares, and M.G.A. Paris, *Full Characterization of Gaussian Bipartite Entangled States by a Single Homodyne Detector*, Phys. Rev. Lett. **102**, 020502 (2009).

[79] W. P. Bowen, R. Schnabel, P. K. Lam, and T.C. Ralph, *Experimental Investigation of Criteria for Continuous Variable Entanglement*, Phys. Rev. Lett. **90**, 043601, (2003); *Experimental characterization of continuous-variable entanglement*, Phys. Rev. A **69**, 012304 (2004).

[80] W. P. Bowen, N. Treps, B.C. Buchler, R. Schnabel, T. C. Ralph, T. Symul, and P.K. Lam, IEEE J.Sel. Top. Quant. **9**,1519 (2003).

[81] Paul G. Kwiat, Klaus Mattle, Harald Weinfurter, Anton Zeilinger, Alexander V. Sergienko and, Yanhua Shih, *New High-Intensity Source of Polarization-Entangled Photon Pairs*, Phys. Rev. Lett. **75**, 4337 (1995).

[82] Z.Y. Ou, S.F. Pereira, H.J. Kimble, and K.C. Peng, *Realization of the Einstein-Podolsky-Rosen paradox for continuous variables*, Phys. Rev. Lett. **68**, 3663, (1992).

[83] Warwick P. Bowen, Nicolas Treps, Roman Schnabel, and Ping Koy Lam, *Experimental Demonstration of Continuous Variable Polarization Entanglement*, Phys. Rev. Lett. **89**, 253601 (2002).

[84] J. Laurat, G. Keller, J. A. Oliveira-Huguenin, C. Fabre, T. Coudreau, A. Serafini, G. Adesso, and F. Illuminati, J. Opt. B: Quantum Semiclassical Opt. **7**, S577–S587 (2005).

[85] A. S. Villar, L. S. Cruz, K. N. Cassemiro, M. Martinelli, and P. Nussenzveig, *Generation of Bright Two-Color Continuous Variable Entanglement*, Phys. Rev. Lett. **95**, 243603 (2005).

[86] M.J. Collett and C.W. Gardiner, *Squeezing of intracavity and traveling-wave light fields produced in parametric amplification*, Phys. Rev. A **30**, 1386 (1984).

[87] Ling-An Wu, H. J. Kimble, J. L. Hall, and Huifa Wu, *Generation of Squeezed States by Parametric Down Conversion*, Phys. Rev. Lett. **57**, 2520 (1986).

[88] Stefano Olivares and Matteo G A Paris, *Photon subtracted states and enhancement of nonlocality in the presence of noise*, J. Opt. B **7**, S392 (2005).

[89] Xiaolong Su, Aihong Tan, Xiaojun Jia, Qing Pan, Changde Xie, and Kunchi Peng, Optics Letters **31**, 1133 (2006).

[90] Jietai Jing, Sheng Feng, Russell Bloomer, and Olivier Pfister, *Experimen-*

tal continuous-variable entanglement from a phase-difference-locked optical parametric oscillator, Phys. Rev. A **74**, 041804(R) (2006).

[91] G. Keller, V. D'Auria, N. Treps, T. Coudreau, J. Laurat, and C. Fabre, Opt. Expr. **16**, 9351, (2008).

[92] Christian Weedbrook, Stefano Pirandola, Raúl García-Patrón, Nicolas J. Cerf, Timothy C. Ralph, Jeffrey H. Shapiro, and Seth Lloyd, *Guassian Quantum Information*, Rev. Mod. Phys. **84**, 621 (2012).

[93] Gerardo Adesso, Alessio Serafini, and Fabrizio Illuminati, Phys. Rev. Lett. **92**, 087901 (2004).

[94] B. E. A. Saleh, M. C. Teich, *Fondamentals of Photonics*, John Wiley & Sons, Inc., 1991.

[95] M. O. Scully and M. S. Zubairy, *Quantum Optics*, Cambridge University Press (1997).

[96] V. D'auria, S. Fornaro, A. Porzio, E.A. Sete, and S. Solimeno, Appl. Phys. B **91**, 309 (2008).

[97] R. W. P. Drever, J. L. Hall, F. V. Kowalski, J. Hough, G. M. Ford, A. J. Munley, and H. Ward, "Laser phase and frequency stabilization using an optical resonator," Appl. Phys. B **31**, 97–105 (1983).

[98] Virginia D'Auria, Antonino Chiummo, Martina De Laurentis, Alberto Porzio, and Salvatore Solimeno, Opt. Express **13**, 948 (2005); V. D'Auria, C. de Lisio, A. Porzio, S. Solimeno, Javaid Anwar, and M. G. A. Paris, *Non-Gaussian states produced by close-to-threshold optical parametric oscillators: Role of classical and quantum fluctuations*, Phys. Rev. A **81**, 033846 (2010).

[99] Virginia D'Auria, Alberto Porzio, Salvatore Solimeno, Stefano Olivares, and

Matteo G A Paris, *Characterization of bi-partite states using a single homodyne detector*, J. Opt. B: Quantum Semiclass. Opt. **7** S750 (2005); Alberto Porzio, Virginia D'Auria, Salvatore Solimeno, Stefano Olivares, and Matteo G.A. Paris, *Homodyne characterization of continuous variable bi-partite states*, Int. J. .Quantum Information, **5**, 63 (2007).

[100] J. Řeháček, S. Olivares, D. Mogilevtsev, Z. Hradil, M. G. A. Paris, S. Fornaro, V. D'Auria, A. Porzio, and S. Solimeno, *Effective method to estimate multidimensional Gaussian states*, Phys. Rev A **79**, 032111 (2009).

[101] Mile Gu, Helen M. Chrzanowski, Syed M. Assad, Thomas Symul, Kavan Modi, Timothy C. Ralph, Vlatko Vedral, and Ping Koy Lam, Nat. Physics **8**, 671 (2012).

[102] Rémi Blandino, Marco G. Genoni, Jean Etesse, Marco Barbieri, Matteo G.A. Paris, Philippe Grangier, and Rosa Tualle-Brouri, arXiv:1203.1127v3 [quant-ph] 11 Jun 2012.

[103] Lars S. Madsen, Adriano Berni, Mikael Lassen, and Ulrik L. Andersen, *Experimental Investigation of the Evolution of Gaussian Quantum Discord in an Open System*, Phys. Rev. Lett. **109**, 030402 (2012).

[104] P. D. Drummond and M. D. Reid, Phys. Rev. A **41**, 3930 (1990).

[105] R. Graham and H. Haken, *The quantum fluctuations of the optical parametric oscillator I*, Z. Phys. **210**, 276 (1968); R. Graham, *The quantum fluctuations of the optical parametric oscillator II*, Z. Phys. **210**, 319 (1968).

[106] E.S. Polzik, J. Carri, and K.J. Kimble, Appl. Phys. B **55**, 279 (1992).

[107] T. Aoki, G. Takahashi, and G. Furusawa, Opt. Express, **14**, 6930 (2006).

[108] S. Suzuki, H. Yonezawa, F. Kannari, M. Sasaki, and A. Furusawa, Appl. Phys. Lett. **89**, 061116 (2006).

[109] Y. Takeno, M. Yukawa, H. Yonezawa and A. Furusawa, Opt. Express 15, 432 (2007).

[110] T. Eberle, S. Steinlechner, J. Bauchrowitz, V. Handchen, H. Vahlbruch, M. Mehmet, H. Mulle-Ebhardt and R. Schnabel, Phys. Rev. Lett., 104, 251102 (2010).

[111] S. Chaturwedi, K. Dechoum and P. D. Drummond, *Limits to squeezing in the degenerate optcal parametric oscillator*, Phys. Rev. A **65**, 033805 (2002); P. D. Drummond, K. Dechoum, S. Chaturwedi, *Critical quantum fluctuations in the degenerate parametric oscillator,* Phys. Rev. A **65**, 033806 (2002); K. Dechoum, P. D. Drummond, S. Chaturvedi, M. D. Reid, *Critical quantum fluctuations and entanglement in the nondegenerate parametric oscillator,* Phys. Rev. A **70**, 053807 (2004).

[112] V. D'Auria, C. de Lisio, A. Porzio, S. Solimeno, J. Anwar, and M. G. A. Paris, *Non-Gaussian state produced by close to threshold optical parametric oscillators: rule of classical quantum fluctuations*, Phys. Rev. A **81**, 33846 (2010).

[113] M. D. Reid and P. D. Drummond, Phys. Rev. Lett. **60**, 2731 (1988); M. D. Reid and P. D. Drummond, *Correlations in the nondegenerate paramentric oscillation: squeezing in the presence of phase diffusion*, Phys. Rev. A **40**, 4493 (1989); P. D. Drummond and M. D. Reid, *Correlations in the nondegenerate paramentric oscillation. II. Below threshold results,* Phys. Rev. A **41**, 3930 (1990).

[114] G. D. Boyd and D. A. Kleinman, J. Appl. Phys. **39**, 3597 (1968); Y. F. Chen and Y. C. Chen, Appl. Phys. B **76**, 645 (2003).

[115] M. G. A. Paris, F. Illuminati, A. Serafini and S. De Siena, *Purity of Gaussian states: measurement schemes and time evolution in noisy channels*, Phys. Rev. A **68**, 0123144 (2003).

[116] G. Adesso and F. Illuminati, in N. J. Cerf, G. Leuchs, E. S. Polzik, *Quan-*

tum Information with Continuous Variables of Atoms and Light, Chap 1, Imperial College Press, 2007.

[117] A. Serafini, Phys. Rev. Lett. **96**, 110402 (2006).

[118] R.R. Puri, *Mathematical Methods of Quantum Optics*, Sprinder, 2001.

[119] A. Peres, *Separability Criterion for Density Matrices*, Phys. Rev. Lett. **77**, 1413 (1996).

[120] Pawel Horodecki, *Separability criterion and inseparable mixed states with positive partial transposition*, Physics Letters A **232**, 333 (1997).

[121] Reinhard F. Werner, *Quantum states with Einstein-Podolsky-Rosen correlations admitting a hidden-variable model*, Phys. Rev. A **40**, 4277 (1989).

[122] B.M. Terhal, *Bell inequalities and the separability criterion*, Phys. Lett. A 271, 319 (2000) quant-ph/9911057.

[123] S. M. Barnett and S. J. D. Phoenix, *Entropy as a measure of quantum optical correlation*, Phys. Rev. A 40, 2404 (1989).

[124] B.L. Schumaker, C.M. Caves, *New formalism for two-photon quantum optics. II. Mathematical foundation and compact notation*, Phys. Rev. A **31**, 3093 (1985).

[125] S. Chaturwedi and P. D. Drummond, Eur. Phys. J. B. **8**, 251 (1999).

[126] J. Eisert, S. Scheel, and M. B. Plenio, *Distilling Gaussian States with Gaussian Operations is Impossible*, Phys. Rev. Lett. **89,** 137903 (2002).

[127] J. Fiurášek, *Gaussian Transformations and Distillation of Entangled Gaussian States*, Phys.Rev. Lett. **89** 137904 (2002).

[128] Hiroki Takahashi, Jonas S. Neergaard-Nielsen, Makoto Takeuchi, Masahiro Takeoka, Kazuhiro Hayasaka, Akira Furusawa, Masahide Sasaki, *Non-Gaussian entanglement distillation for continuous variables*, arXiv:0907.2159 (2009).

[129] T. Opatrný, G. Kurizki, and D.-G. Welsch, Phys.Rev. A **61**, 032302 (2000).

[130] P. T. Cochrane, T. C. Ralph, and G. J. Milburn, Phys Rev. A **65**, 062306 (2002).

[131] N. J. Cerf, O. Krüger, P. Navez, R. F. Werner, and M. M. Wolf, Phys. Rev. Lett. **95**, 070501 (2005).

[132] P. D. Drummond and P. Kinsler, Q. Opt. **7**, 727 (1995). P. Kinsler, P. D. Drummond, Phys. Rev. A **52**, 783 (1995).

[133] S. F. Pereira, Z. Y. Ou, H. J. Kimble, *Quantum communication with correlated nonclassical states*, Phys. Rev. A **62** 042311 (2000).

[134] M. J. Collett, C. W. Gardiner, *Squeezing of intracavity and traveling-wave light fields produced in parametric amplification*, Phys. Rev. A **30**, 1386 (1984); C. W. Gardiner, M. J. Collett, *Input and output in damped quantum systems: Quantum stochastic differential equations and the master equation*, Phys. Rev. A **31**, 3761 (1985); M. J. Collett, D. F. Walls, *Squeezing spectra for nonlinear optical systems*, Phys. Rev. A **32**, 2887 (1985).

[135] M. S. Kim, E. Park,P. L. Knight, and H. Jeo ll, and D.-G. Welsch, Phys. Rev. A **55** (1997).

[136] M. Yukawa et al, H. Benichi and A. Furusawa, *High-fidelity continuous-*

variable quantum teleportation toward multistep quantum operations, Phys. Rev. A, **77**, 022314 (2008).

[137] T. Ide, H. F. Hofmann, T. Kobayashi,and A. Furusawa, *Continuous-variable teleportation of single-photon states*, Phys. Rev. A **65**, 012313 (2001).

[138] H.F. Hofmann, T. Ide, T. Kobayashi, and A. Furusawa, *Fidelity and information in the quantum teleportation of continuous variables*, Phys. Rev. A **62**, 062304, (2000).

[139] A. Furusawa, J. L. Sorensen, S. J. Braunstein, C. A. Fuchs, H. J. Kimble, and E. S. Polzik, *Unconditional Quantum Teleportation*, Science **282**, 706 (1998).

[140] T. C. Zhang, K. W. Goh, C. W. Chou, P. Lodahl and H. J. Kimble, *Quantum teleportation of light beams*, Phys. Rev. A **67**, 033802 (2003).

[141] P. K. Lam, T. C. Ralph, B. C. Buchler, D. E. McClelland, H. A. Bachor and J. Gao, J. Opt. B **1**, 469 (1999).

[142] R.A. Campos, B.E.A. Saleh, M.C. Teich, *Quantum-mechanics lossless beam splitter: SU(2) symmetry and photon statistisc*, Phys. Rev. A **40**, 1271 (1989).